Durham E-Theses

Theoretical modelling of the m.i.s.s structure in one and two dimensions

Lavelle, Stephen William

How to cite:

Lavelle, Stephen William (1989) *Theoretical modelling of the m.i.s.s structure in one and two dimensions*, Durham theses, Durham University. Available at Durham E-Theses Online: http://etheses.dur.ac.uk/6744/

Use policy

The full-text may be used and/or reproduced, and given to third parties in any format or medium, without prior permission or charge, for personal research or study, educational, or not-for-profit purposes provided that:

- a full bibliographic reference is made to the original source
- a link is made to the metadata record in Durham E-Theses
- the full-text is not changed in any way

The full-text must not be sold in any format or medium without the formal permission of the copyright holders.

Please consult the full Durham E-Theses policy for further details.

Academic Support Office, Durham University, University Office, Old Elvet, Durham DH1 3HP
e-mail: e-theses.admin@dur.ac.uk Tel: +44 0191 334 6107
http://etheses.dur.ac.uk

THEORETICAL MODELLING OF THE M.I.S.S STRUCTURE IN ONE AND TWO DIMENSIONS

by

Stephen William Lavelle

B.Sc., A.R.C.S., M.Sc.

The copyright of this thesis rests with the author. No quotation from it should be published without his prior written consent and information derived from it should be acknowledged.

This thesis is submitted to the University of Durham in candidature for the degree of Doctor of Philosophy

School of Engineering and Applied Science

University of Durham

August 1989

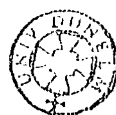

2 AUG 1990

Theories are nets to catch what we call 'the world': to rationalize, to explain, and to master it. We endeavour to make the mesh ever finer and finer.

Karl Raimund Popper.

DECLARATION

I hereby declare that the work reported in this thesis has not been previously submitted for any degree. All material in this thesis is original except where indicated by reference to other work.

ABSTRACT

In this thesis, a 1-D computer model of MISS operation is described. This is then used to characterise the qualitative behaviour of the MISS for changes in its structural parameters. The modelled device is assumed to have a four layer $MInp$ structure, commonly used by both theorists and experimentalists. Derived from this 1-D model is a quantitative description of switching in the three layer MIS diode, using a heavily doped ($10^{17}cm^{-3}$) n-type substrate. Results are then presented describing its behaviour for changes in fabrication parameters.

The computer model of MISS functioning is extended into quasi 2-D by incorporating current spreading in the pn region of the device. Using this, the effect of changes in metal top contact area on device behaviour are explained, with the model providing an accurate quantitative description of these effects for thick oxide ($30\AA$) devices.

The stability of the MISS as a circuit element is examined in its negative impedance region. A simple equivalent circuit model is produced, and calculated values for negative differential capacitance and negative differential resistances from the quasi 2-D MISS and MIS diode models are used to characterise device behaviour in this region.

Within the work a number of accepted terms and ideas are challenged, with their uses being either redefined or discarded. This has been found to be necessary because of the scope of the work presented, which covers such a large range of device parameters.

ACKNOWLEDGEMENTS

I would like to thank my supervisor Dr Martin Morant, for his help throughout this work, and his careful reading of the text.

Thanks are also due to Mary Bartlett for her support and encouragement, and my father for his financial help.

This work was supported in part by a three year S.E.R.C studentship.

LIST OF CONTENTS

CHAPTER ONE:

INTRODUCTION TO THE M.I.S.S DEVICE

1.1 Introduction 1

1.2 The MISS Device Structure 2

1.3 The MISS I-V Characteristic 2

1.4 Computer Modelling 3

1.5 Thesis Outline 4

1.6 Thesis Objectives 5

References 7

CHAPTER TWO:

A REVIEW OF THE CURRENT THEORETICAL

UNDERSTANDING OF TWO TERMINAL M.I.S.S BEHAVIOUR

2.1 Introduction 9

2.2 Historical Perspective 10

2.3 The Punchthrough Model 13

2.3.1. Regenerative Feedback For The Punchthrough Device 16

2.4 The Avalanche Model 17

2.4.1 Regenerative Feedback For The Avalanche Device 18

2.5 The Device Switching Criterion 19

2.6 Other Work 21

2.7 Discussion 27

References 32

CHAPTER THREE:

IMPROVED THEORY OF M.I.S.S BEHAVIOUR

3.1 Introduction 35

3.2 Basic Device Equations 36

3.2.1 Model Assumptions 37

3.3 The Model of the *MIS* Structure 38

3.3.1 The Depletion Region 38

3.3.2 The Tunnelling Currents 40

3.4 The Model of the *pn* Junction Region 42

3.4.1 Electron Recombination Currents 42

3.4.2 The Hole Injected Current 43

3.5 Lightly Doped *n*-Type Layers - Method of Solution 44

3.6 Heavily Doped *n*-Type Layers - Method of Solution 46

3.7 The Computational Technique 47

3.8 The Current Voltage Characteristic 50

3.8.1 The Lightly Doped Device 52

3.8.1.1 The High Impedance OFF State 53

3.8.1.2 The Vicinity of the Switching Point 55

3.8.1.3 The Negative Impedance Region 56

3.8.1.4 The Holding Point and Low Impedance ON State 57

3.8.2 The Heavily Doped Device 58

3.8.2.1 The High Impedance OFF State 59

3.8.2.2 The Vicinity of the Switching Point 60

3.8.2.3 The Negative Impedance Region 62

3.8.2.4 The Holding Point and Low Impedance ON State 63

3.9 A Qualitative Interpretation of MISS Operation 63

3.10 Discussion 65

References 67

CHAPTER FOUR:

RESULTS OF M.I.S.S BEHAVIOUR IN ONE DIMENSION.

4.1 Introduction 68

4.2 Effect of n-Type Layer Doping Density 69

4.3 Effect of Work Function 73

4.3.1 Lightly Doped n-Type Layer 74

4.3.2 Heavily Doped n-Type Layer 75

4.4 Effect of Oxide Thickness 78

4.4.1 Lightly Doped n-Type Layer 78

4.4.2 Heavily Doped n-Type Layer 79

4.5 Effect of n-type Layer Thickness 80

4.5.1 Lightly Doped n-Type layer 80

4.5.2 Heavily Doped n-Type Layer 82

4.6 MIS Switching Characteristics 83

4.7 Discussion 85

References 89

CHAPTER FIVE:

TWO-DIMENSIONAL MODELLING OF THE M.I.S.S DEVICE

5.1 Introduction 90

5.2 Modelling 91

5.2.1 Other Assumptions 93

5.2.2 Current Spreading Equation 94

5.3 Method of Solution for the Two-Dimensional Model 97

5.4 Results 99

5.4.1 Effect of Oxide Thickness 100

5.4.2 Effect of Top Contact Radius 102

5.4.2.1 The Thin Oxide MISS 102

5.4.2.2 The Thick Oxide MISS 104

5.4.3 Effect of Work Function 105

5.4.3.1 The Thin Oxide MISS 105

5.4.3.2 The Thick Oxide MISS 106

5.5 Discussion 107

References 109

CHAPTER SIX:

STEADY STATE NEGATIVE IMPEDANCE

6.1 Introduction 110

6.2 The MISS Device as a Circuit Element 111

6.2.1 MISS Circuit Analysis 112

6.3 Results 114

6.3.1 Calculated Values for r_{nd} and c_{nd} from

the 2-D MISS model 115

6.3.1.1 Effect of Oxide Thickness 115

6.3.1.2 Effect of Top Contact Radius 117

6.3.1.3 Effect of Work Function 118

6.3.2 Calculated Values for r_{nd} and c_{nd} from the MIS device Model 119

6.3.2.1 Effect of Oxide Thickness 119

6.3.2.2 Effect of Work Function 120

6.3.3 Stability of the Two Dimensional MISS as a Circuit 120

6.4 Discussion 122

References 124

CHAPTER SEVEN:

SUMMARY DISCUSSION AND SUGGESTIONS FOR FURTHER WORK

7.1 Summary and Discussion 125

7.2 Further work 128

References 130

APPENDIX A:

TUNNELLING IN THIN SILICON DIOXIDE

A.1 Introduction 131

A.2 Tunnelling Current Expressions 131

A.3 Tunnelling Attenuation Factor η 135

A.4 A Tunnelling Comparison 138

References 140

APPENDIX B:

ELECTRIC FIELD IN THE MIS DEPLETION REGION

B.1 Introduction 141

B.2 General Theory 141

B.3 Further Approximation 143

References 145

APPENDIX C:

AVALANCHE MULTIPLICATION

C.1 Introduction 146

C.2 Multiplication Coefficients 146

References 149

APPENDIX D:

GENERATION CURRENT

D.1 Introduction 150

D.1 The Generation Current Equation 150

References 153

APPENDIX E:

MISS CIRCUIT THEORY

E.1 Introduction 154

E.2 Circuit Analysis 154

References 157

APPENDIX F:

NUMERICAL CONSTANTS AND EXPRESSIONS 158

References 160

APPENDIX G:

MODELLING PROGRAMS 161

Abbreviations

AFL - Avalanche Feedback Loop

CIFL - Controlled Inversion Feedback Loop

ICS - Inversion Controlled Switch

IS - Insulator Semiconductor

MIS - Metal-Insulator-Semiconductor Diode (Switching Device)

MIS - Metal Insulator Semiconductor (Structure)

MISS - Metal Insulator Semiconductor Switch

RFM - Regenerative Feedback Mechanism

Notation

The symbols used are given together with a brief explanation and units:

$A_{e[h]}$ - Richardson's constant for electrons[holes]. $(A/cm^2/K^2)$

A_T - Area of top contact. (cm^{-2}).

c_{nd} - Negative differential capacitance. (F).

$D_{n[p]}$ - Diffusion constant for electrons[holes] in $p[n]$ type material. (cm^2/s).

d_{ox} - Oxide thickness. (cms).

E_b - Gap between the Silicon and SiO_2 conduction bands. (eV).

E_c - Energy of the silicon conduction band. (eV).

E_v - Energy of the silicon valence band. (eV).

E_g - Silicon band gap. (eV).

E_{gi} - Insulator band gap. (eV).

E_{fm} - Metal Fermi Level. (eV).

E_{fn} - Electron Quasi-Fermi level. (eV).

E_{fp} - Hole Quasi-Fermi level. (eV).

$\mathcal{E}_s$ - Electric field in the silicon at the IS interface. (V/cm).

$\mathcal{E}_{ox}$ - Electric field in the oxide. (V/cm).

$\mathcal{E}_{dep}$ - Electric field in the oxide due to depletion. (V/cm).

$\mathcal{E}_{inv}$ - Electric field in the oxide due to inversion. (V/cm).

$E\psi_s$ - Band bending in the MIS depletion region measured from the conduction band at the edge of the neutral region to the conduction band at the the IS interface. (eV).

g_j - pn junction small signal gain.

g_s - MIS small signal gain.

G_j - pn junction large signal gain.

G_j - MIS large signal gain.

g_T - Small signal gain product

I_{tot} - Total current flow through the device. (A)

$I_S[I_H]$ - Current at switching[holding] point. (A).

I_{sp} - Electron spreading current away from the top contact. (A).

$J_S[J_H]$ - Current density at switching[holding] point. (A/cm^2).

J_{tn} - Electron tunnelling current through the insulator. (A/cm^2).

J_{tp} - Reverse hole tunnelling current through the insulator. (A/cm^2).

$J_{tp(f)}$ - Forward hole tunnelling current through the insulator. (A/cm^2).

$J_{tp(r)}$ - Hole tunnelling current through the insulator. (A/cm^2).

J_g - Generation current in the MIS depletion region. (A/cm^2).

J_{pj} - Hole injected current into the MIS depletion region. (A/cm^2).

$J_{pj(f)}$ - Forward hole injected current into the MIS depletion region. (A/cm^2).

$J_{pj(r)}$ - Reverse hole injected current into the MIS depletion region. (A/cm^2).

J_{rec} - Recombination current in the neutral region between the MIS and pn depletion regions. (A/cm^2).

J_{rj} - Recombination current in the pn depletion region. (A/cm^2).

J_{ns} - Substrate diffusion current. (A/cm^2).

J_{re} - Total electron recombination current in the pn region. (A/cm^2).

k - Boltzmann constant. (eV/K).

L - Parasitic inductance. (H).

L_d - Debye length. (cms).

$L_{n[p]}$ - Diffusion length for electrons[holes] in $p[n]$ type material. (cms).

m_0 - Free electron mass. (Kg).

m_{hh} - Heavy hole effective mass. (Kg).

m_{lh} - Light hole effective mass. (Kg).

m_t - Transverse electron effective mass. (Kg).

m_l - Longtitudinal electron effective mass. (Kg).

$M_{n[p]}$ - Avalanche multiplication coefficient for electrons[holes].

N_a - Acceptor doping density. (cm^{-3})

N_d - Donor doping density. (cm^{-3}).

n_i - Intrinsic carrier concentration. (cm^{-3}).

N_c - Effective density of states in the conduction band. (cm^{-3}).

N_v - Effective density of states in the valence band. (cm^{-3}).

Q_{ss} - Interface charge density. (cm^{-2}).

r_{nd} - Negative differential resistance. (Ω).

r_0 - Radius of the top contact. (cms).

r_1 - Value for radius at which current and junction potential are effectively zero. (cms).

t_c - Equilibrium time. (S).

T - Temperature. (K).

U_{ox} - Energy drop across the oxide measured from the semiconductor to the metal. (eV).

U_f - Energy drop across the pn junction due to a forward voltage V_f.[B (eV).

V_a - Avalanche Voltage. (V).

V_{ox} - Potential drop across the oxide measured from the semiconductor to the metal. (V).

V_{bi} - Built in potential of the pn junction. (V).

V_f - Potential drop across the pn junction measured from the n-type semiconductor to the p type semiconductor. (V).

V_H - Holding voltage for the $MISS$ device. (V).

$V_S[V_H]$ - Switching [Holding] voltage for the MISS. (V).

V_{tot} - Total potential drop across the device. (V)

W_{mis} - Width of the MIS depletion region (cms)

W_{epi} - Width of the n-type layer (cms)

W_f - Work function for the metal. (V)

W_{pn} - Width of the pn junction depletion region (cms)

W_n - Width of the pn junction depletion region on the n-type side. (cms)

W_p - Width of the pn junction depletion region on the p-type side. (cms).

W_{neut} - Width of the neutral region between the pn and MIS depletion regions (cms)

Greek Symbols

ϵ_0 - Permittivity of free space. (F/cm).

ϵ_{ox} - Permittivity of SiO_2. (F/cm).

ϵ_{si} - Permittivity of Silicon. (F/cm).

τ_n - Lifetime of electrons in p type material (s)

τ_p - Lifetime of holes in n type material. (s).

ψ_s - Potential drop across the MIS depletion region. (V).

$\mu_{n[p]}$ - Electron[Hole] Mobility. ($cm^2/V - s$).

Φ_m - Metal work function. (V).

χ_s - Electron affinity of silicon. (V).

ξ - Quasi-Fermi level splitting at the IS interface $E_{fp} - E_{fn}$. (eV).

$\eta_{e[h]}$ - Electron[Hole] tunnelling attenuation factor (cm^{-1})

CHAPTER ONE

INTRODUCTION TO THE M.I.S.S. DEVICE

1.1 Introduction

The MISS device (Metal Insulator Semiconductor Switch) was first reported by Yamamoto and Morimoto [1]. They described its fabrication as an n-type epitaxial layer of 2-5μm thickness grown on a p-type silicon substrate. The surface was oxidised to produce a thin layer of SiO_2 ($< 100\mathring{A}$), and evaporated on to this was a gold top contact. An examination of the current-voltage characteristic showed the structure to switch from a high impedance, low current 'OFF' state, to a low impedance, high current, 'ON' state. Between these states a current controlled negative impedance region was found.

A number of different acronyms have been adopted by investigators to describe the device. The term ICS (Inversion Controlled Switch) was used by Kroger and Wegener [2,3] to indicate something of device behaviour, but throughout this thesis the structure will be referred to as a MISS; the term having first been used by Simmons and El-Badry, and now generally accepted [4,5]. This term should not be confused with the MIS acronym used for describing the Metal Insulator Semiconductor structure.

1.2 The MISS Device Structure

The structure of the MISS generally includes a thin n-type layer on a heavily doped p-type substrate. On top of the n-type layer a film of an insulating or semi-insulating material is grown which impedes the flow of electrons and holes through it, but does not stop carrier flow altogether. A metal top contact is then evaporated on to the surface, and an ohmic contact is made to the substrate. The ideal one-dimensional device structure is shown in Fig 1.1. The MISS itself has been fabricated by many investigators using a variety of doping levels, insulators, and metals. $MIpn^+$ as well as $MInp^+$ devices have been produced, using insulators of SiO_2 [1], Si_3N_4 [2], and polysilicon [3]. Top contact metals have included aluminium [1,6], gold, platinum, nickel [7], molybdenum [2,8] and chromium [3,8]. The device has also been fabricated from gallium arsenide using a Langmuir Blodgett film as the semi-insulating layer [13]. The range of materials from which the MISS has been made appears to show a quite general switching mechanism, and this should become evident from the modelling of the device.

1.3 The MISS I-V Characteristic

The ideal MISS $I-V$ characteristic can be drawn in the form shown in Fig 1.2, where it can be seen that only one value of the total current applies for each point on the curve, making the device current controlled. The point at which the MISS moves into its negative impedance region as current increases is termed the switching point. Here the device potential V_S is at a local maximum. At the end

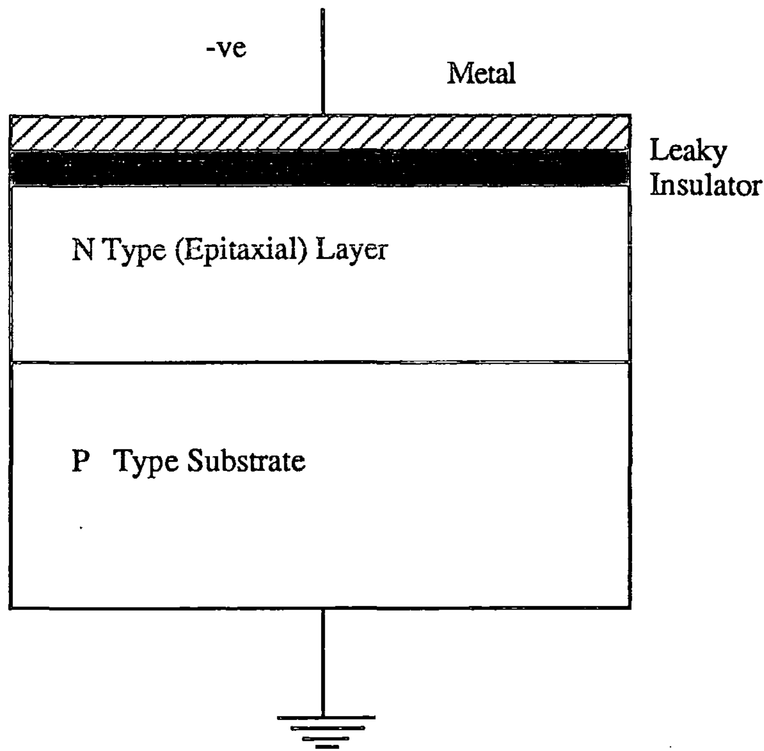

Fig 1.1: General 1-D Device Structure

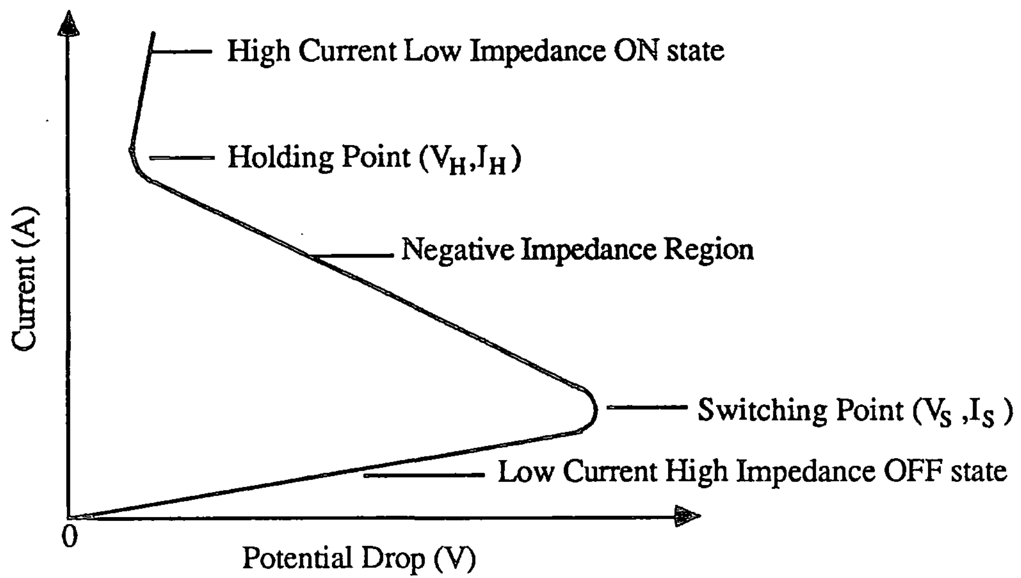

Fig 1.2: The Ideal Current Voltage Curve

of its passage through the negative impedance region the total potential across the device stops decreasing, reaching a local minimum V_H called the holding point. It is this switching from the end of the OFF state (V_S, I_S), to the start of the ON state (V_H, I_H), that gives rise to the name Metal Insulator Semiconductor Switch.

When thinking about the device it is necessary to bear in mind the feature of charge storage at the n-type layer - leaky insulator interface. This capacitive effect is very important when trying to understand the dynamic behaviour of the device.

1.4 Computer Modelling

Computer modelling is becoming increasingly common in all fields of science and engineering; the reasons for this are not difficult to find; for the MISS the reasons can be summarised as follows:

i) Ease of modelling compared with experimental investigation requiring device fabrication

ii) Low cost

iii) Ability to produce results that would be difficult to obtain from experiment.

With (i), once a computer model has been developed, the effect of a variety of physical parameters can be investigated and results compared. Obviously a fabrication facility would be hard pressed to produce a MISS with five different metal top contact work functions. This leads naturally into ii). A computer model

is far cheaper than fabrication of a whole spectrum of devices once its accuracy has been verified. For (iii), a variety of results can be provided from a computer model which are almost impossible to obtain from experiment. It is the provision of this kind of data that is one of the main thrusts for the present work. For example the ability to separate the electron and hole currents in chapter 3, and the evaluation of the separate contributions to the oxide electric field in chapter 4. This is continued in chapter 5 where electron current spreading is dealt with for a two-dimensional device structure.

1.5 Thesis Outline

In chapter 2, an examination of present theories for describing the behaviour of the MISS is undertaken. This is done from a historical perspective, and attempts to show how ideas about the MISS have developed from the initial work of Yamamoto *et al.*

In chapter 3, a new complete one-dimensional computer model is produced. This involves a description of the device physics together with the computational procedures used to solve the equations. The computer model was developed on a large main-frame machine which avoided the use of many of the approximations seen in other work. After describing the model, a number of results are presented for two 'ideal' devices to illustrate certain important aspects of the behaviour of the MISS.

In chapter 4, a large number of computed results are given showing the effects of variations in structural parameters on the MISS $I-V$ characteristic. Also, the

1-D MISS model is adapted to allow the MIS diode switching device [11] to be modelled. This is an original model which allows a close quantitative analysis of the MIS diode to be achieved.

Chapter 5 deals with the limitations of the 1-D model, and develops a 2-D computer model based upon current spreading in the n-type and substrate layers away from the top contact. Results for different device parameters are then given.

Chapter 6 deals with the stability of the device in the negative impedance region and analyses both the negative differential resistance (NDR), and the negative differential capacitance (NDC) of the MISS in this region. It evaluates the magnitudes for NDR and NDC from the model, and then goes on to examine the functioning of the device as a circuit element using these values.

Chapter 7 provides a discussion and summary of the most important ideas presented in the thesis.

1.6 Thesis Objectives

One of the main aims of this thesis is to examine the present understanding of MISS operation in one-dimension, and to challenge the validity of certain accepted ideas about device behaviour. This includes the important effect of generation current in the MIS depletion region on the shape of the $I - V$ characteristic for a lightly doped n-type layer device, and its effect on the $I - V$ curve at the switching point [9]. Also, the behaviour of the device with a heavily doped n-type layer is examined, and switching is shown to be dominated by the effect of ionised donors rather than avalanche multiplication as suggested by some authors [10].

As a natural extension to the 1-D MISS model, an original description of the MIS diode switching device is presented [11]. The structure consists of a thin oxide, grown on a heavily doped n-type substrate with a metal top contact. It has only three layers, yet still displays negative impedance. The results presented are an accurate quantitative analysis of its behaviour, and as far as is known it is the first computer model for this structure.

There are a number of major problems with the 1-D MISS model when it is used to provide a quantitative description of device behaviour. Predicted currents at the switching and holding points are smaller than those found from experiment, [5], and the holding voltage remains constant at only one volt [10,11], regardless of the modelled oxide thickness. Also, experimentally there is found to be a marked affect on the $I - V$ characteristic with changes in top contact area. The three difficulties with the 1-D model mentioned above are related; all being due to the greater area of the pn junction compared with the top contact. An original two-dimensional model has therefore been developed to provide a better quantitative fit of theory with experiment. It has been produced by using electron and hole tunnelling expressions for the oxide suitable for high current densities, and by extending the model into 2-D to deal with current spreading. This provides a much closer fit with experiment, especially for the thicker oxide devices ($> 25\AA$).

The negative impedance region of the device was found to be stable under certain conditions from work in Durham [12]. This is a surprising result, and by ignoring the accepted explanation of switching by regenerative feedback, the device can be shown to behave as a stable circuit element. This has also been given detailed treatment.

References

1. Yamamoto, T. and Morimoto, M., 'Thin-MIS-Structure Si Negative Resistance diode', *Appl. Phys. Lett.*, **20**, pp. 269-270, (1972).
2. Kroger, H., and Wegener, H. A. R.,, 'Bistable impedance states in m.i.s structures through controlled inversion', *Appl. Phys. Lett.*, **23**, pp. 397-399, (1973).
3. Kroger, H., and Wegener, H.A.R., 'Controlled Inversion Transistors', *Appl. Phys. Lett.*, **27**, pp. 303-304, (1975).
4. Simmons, J. G. and El-Badry, A., 'Theory of Switching Phenomena in Metal Semi-Insulator $n-p^+$ Silicon Devices', *Solid St Electron.*, **20**, pp. 955-961, (1977).
5. Simmons, J. G. and El-Badry, A., 'Experimental Studies of Switching in Metal Semi-Insulating $n-p^+$ Silicon Devices, *Solid St Electron.*, **20**, pp. 963-966, (1977).
6. Buxo, J., Owen, A. E., Sarrabayrouse, G., and Sebaa, J. P., 'The characterisation of metal thin insulator $n-p^+$ silicon switching devices', *Rev. Phys. Appl.*, **17**, pp. 767-770, (1978).
7. Yamamoto, T., Kawamura, K., and Shimizu, H., 'Silicon $p-n$ insulator-metal ($p-n$-I-M) devices', *Solid St. Electron.*, **19**, pp. 701-706, (1976).
8. Kroger, H., and Wegener, H.A.R., 'Steady-State Characteristics of Two Terminal Inversion-Controlled Switches', *Solid St Electron.*, **21**, pp. 643-654, (1978).
9. Habib, S. E-D. and Simmons, J. G., 'Theory of Switching in $p-n$ Insula-

tor(Tunnel) Metal Devices Part 1, Punchthrough Mode', *Solid St Electron.*, **22**, pp. 181-192, (1979).

10. Habib, S. E-D. and Simmons, J. G., 'Theory of Switching in $p-n$ Insulator(Tunnel) Metal Devices Part 2, Avalanche Mode', *Solid St Electron.*, **23**, pp. 497-505, (1980).

11. Hayashi, Y., 'Switching Phenomena in Thin-Insulator Metal Insulator Semiconductor Diodes', *Appl. Phys Lett.*, **37(4)**, pp. 407-408, (1980).

12. Majlis, B. Y., 'Ph.D Thesis', *Durham University*, (1988).

13. Thomas, N. J., 'Ph.D Thesis', *Durham University*, (1986).

CHAPTER TWO

A REVIEW OF THE CURRENT THEORETICAL UNDERSTANDING OF TWO TERMINAL M.I.S.S BEHAVIOUR

2.1 Introduction

This chapter describes past theoretical work on the behaviour of the MISS device. Initially it proceeds in a historical manner, before examining in detail in sections 2.3 and 2.4 the more comprehensive model of 1-D device operation due to Habib and Simmons [7,8]. In their work, two switching mechanisms were developed: the punchthrough and avalanche modes. They discussed their methods for the calculation of the $I-V$ characteristic, together with the general concept of regenerative feedback for explaining switching. The theoretical $I-V$ curve for the device was produced from the solution of coupled time-independent current and potential equations using standard semiconductor theory.

Section 2.5 carries on the discussion of regenerative feedback, drawing on the work of Mattos [11] and Board [23]. In section 2.6 other work associated with the behaviour of the MISS is then described. This includes two-dimensional effects, together with a description of related device structures which also demonstrate an S-shaped current voltage characteristic. Finally, in section 2.7 the theories described are subjected to critical scrutiny to outline areas where problems lie, and further work is necessary. For consistency, the notation in papers referenced

has been adapted to the common notation used throughout this thesis to prevent any confusion.

Unless explicitly stated otherwise, the terms insulator and oxide are used interchangeably; most work having been done using silicon, and an oxide being the most convenient form of insulator when dealing with this semiconductor. Carrier transport through the oxide is assumed to be via quantum mechanical tunnelling, where each carrier tunnels independently, and carrier energy and transverse momentum are conserved.

2.2 Historical Perspective

As described above, the first reported instance of a negative impedance switching characteristic for a four layer $MInp$ device was by Yamamoto *et al* in 1972 [1]. When first fabricated the device was thought to have a three layer, Mnp structure, in which the metal made a good contact to the n-type epitaxial layer, and the negative impedance was due to avalanching at the edge of the gold (M) - silicon contact. However, once the existence of a thin interfacial layer of SiO_2 had been demonstrated, the investigators began to deliberately fabricate the structures using thin films of oxide to separate the metal top contact from the $n-p$ structure. In this initial paper no comprehensive explanation was given for the switching mechanism of the device, although the importance of hole injection from the $n-p$ junction on the degree of inversion at the IS (Insulator Semiconductor) interface was appreciated. The current flow through the oxide was seen as the sum of electrons tunnelling from the metal through the insulator into the conduction

band of the semiconductor, together with electron tunnelling into interface states at the IS surface where recombination took place with holes from the valence band.

In 1973, Kroger and Wegener [2] grew silicon nitride films with thicknesses of $20 - 200\AA$ on the n-type epitaxial layer of an $n - p$ junction, and then used a molybdenum top contact to complete the device. They explained the switching characteristic as being controlled by the MIS (Metal Insulator Semiconductor) depletion layer. In the high impedance state, the formation of an inversion layer at the IS interface was thought to be thwarted by a small but finite hole tunnel current, causing the growth of a deep depletion layer with a concomitant large potential drop across it. In the low impedance state, where the potential drop across the device was far smaller, a strongly inverted layer was thought to be present at the IS surface. They emphasised the need for the $n - p$ junction to be sufficiently forward biased in the ON state to maintain a hole inversion layer, injecting enough carriers to compensate for the flow of holes through the insulator. In 1975, Kroger and Wegener[3] went on to describe the control of the switching point for the device via an injecting third terminal based on their theory outlined above.

In 1977, El-Badry and Simmons, drawing on the results of their experimental work [5], developed more quantitative descriptions of switching in the $MInp^+$ device for lightly and heavily doped n-type epitaxial layers [6]. They divided the $I - V$ characteristic into three parts: the high impedance OFF state, the switching state, and the low impedance ON state, Fig 1.2. The devices described were assumed to have highly doped p^+ substrates. They also assumed a thickness

of oxide which allowed quantum mechanical tunnelling of carriers between the metal and the silicon. This structure has since been adopted by most investigators when modelling the behaviour of the thin oxide MISS. For the lightly doped n-type layer device ($< 10^{16} cm^{-3}$), they described the MIS depletion region under the insulator as reaching the p^+n junction at the switching point; this they termed the punchthrough mode. At punchthrough, almost all of the applied potential V_S is assumed to be dropped across the depletion layer at the switching point, so by ignoring the potentials across the oxide and the p^+n junction, the switching voltage V_S could then be given the simple form:

$$V_S = qN_d \frac{(W_{epi} - W_{pn})^2}{2\epsilon_s} \qquad 2.2.1.$$

where W_{epi} is the width of the n-type epitaxial layer, and W_{pn} the width of the p^+n depletion region using the one sided abrupt junction approximation. In this model, the build-up of holes at the IS interface produces two interacting effects. The n-type epitaxial layer under the insulator moves from deep depletion towards inversion, and the build up of holes at the interface causes a greater potential drop across the insulator, and hence an increase in the conduction current. With the build up of an inversion layer, the width of the MIS depletion layer, and hence the potential dropped across it, decrease. The decrease in the depletion layer voltage can be greater than the increase in the insulator voltage so that the total voltage falls while the current increases. These two interacting effects produced the switching state (or negative resistance region) of the current voltage curve. Finally the low impedance state of the device is reached when the reduction in the potential drop across the MIS depletion region is outweighed by the increase in the sum of the oxide and p^+n junction potentials. This produces a net increase

in the total voltage across the device while the current flow through the device is still increasing.

The second type of switching mechanism was described as being seen for heavily doped n-type layer devices ($> 10^{16} cm^{-3}$). With these structures the increase in hole flow towards the IS interface at the switching point is caused by avalanche multiplication in the MIS depletion region rather than hole injection from the p^+n junction. This was termed the avalanche mode of switching. Because the switching point was described as being controlled by the onset of avalanching, the approximate switching voltage could be expressed as

$$V_a = 60(E_g/1.1)^{3/2}(N_d/10^{16})^{-3/4} \qquad 2.2.2.$$

where N_d is the epitaxial layer donor doping density, and E_g the energy gap of the silicon; expression (2.2.2) being generally used for determining the onset of avalanche multiplication in silicon.

2.3 The Punchthrough Model

Habib and Simmons published two papers in 1977, [7,8], dealing in far more detail with the punchthrough and avalanche modes of switching. The papers were based around a computer model of device behaviour which used electron and hole current continuity equations to produce the current-voltage curve.

For the $MInp^+$ structure, they used a band diagram of the form given in Fig 2.1. The symbols for the currents utilised in the model are shown together with the band bending necessary for describing the device behaviour. In the punchthrough model, recombination currents in the neutral epitaxial layer and the substrate

were neglected, as was the generation current in the MIS depletion region. The continuity equations used in the model were

$$J_{tn} = J_{rj} \quad \text{and} \quad J_{tp} = J_{pj} \qquad 2.3.1$$

for electron and hole currents respectively, where J_{tn} and J_{tp} are the electron and hole tunnelling currents, and J_{rj} and J_{pj} are the pn depletion region recombination current, and hole injected current into the MIS depletion region respectively.

In this paper the basic theory was regarded as being applicable to other forms of leaky insulator provided modifications were made for electron and hole conduction. Switching from the OFF to the ON state was ascribed to a regenerative feedback mechanism (described in the next section).

The assumptions made in the punchthrough model were as follows;

i) Current transport through the oxide is dominated by tunnelling.

ii) Hot carrier and space charge effects are neglected due to the low electric fields and carrier densities respectively.

iii) The abrupt junction approximation is used for the pn junction and the MIS depletion region.

iv) Dynamic IS surface state effects are ignored apart from a constant bias independent charge, and a trapezoidal tunnelling barrier is assumed.

v) The electron recombination currents in the neutral n-type epitaxial layer and p-type substrate, together with the generation current in the MIS depletion region are neglected.

vi) The effect of variations in the tunnelling transmission coefficient with oxide potential drop, and degeneracy effects at the IS interface, are ignored when calculating the electron and hole tunnel currents.

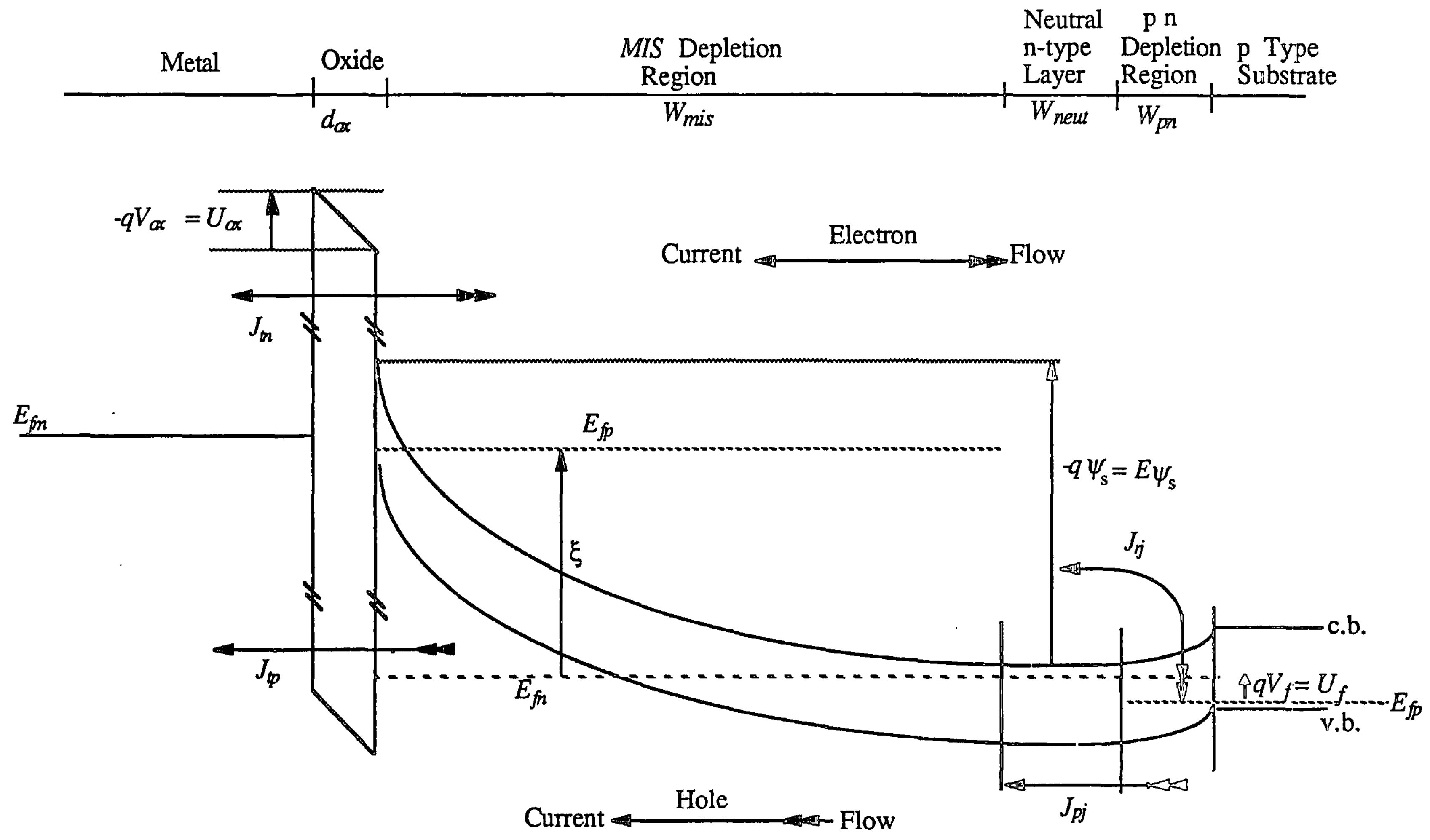

Fig 2.1: Current Components for the Punchthrough MISS Model. Habib and Simmons [7].

In describing the device behaviour, three distinct states were recognised for the $I - V$ curve, based upon the hole current expression

$$J_{tp} = J_{tp(f)} - J_{tp(r)} = J_{pj(f)} - J_{pj(r)} = J_{pj} \qquad 2.3.2$$

where J_{tp}, $J_{tp(f)}$ and $J_{tp(r)}$ are the total, forward and reverse components of the hole tunnel current respectively, and similarly J_{pj}, $J_{pj(f)}$ and $J_{pj(r)}$ are the total, forward and reverse components of the hole injected current from the pn junction into the MIS depletion region respectively. The sum of the two forward and reverse components are equal to the actual total hole tunnel current and hole injected current. Using these expressions the three states recognised were the semiconductor limited state, the tunnel limited state and the intermediate state.

In the semiconductor limited state the forward hole diffusion current, $J_{pj(f)}$, is much smaller than the reverse tunnel current $J_{tp(r)}$. Because $J_{pj(f)} > J_{pj(r)}$ this implies that $J_{tp(r)} \approx J_{tp(f)}$. With this being the case, to prevent an excess hole tunnel current, the hole quasi Fermi level is pinned to the metal Fermi level at the IS interface.

In the tunnel limited state, the forward tunnel current $J_{tp(f)}$, is much smaller than the reverse diffusion current $J_{pj(r)}$. This is caused by the high hole density at the IS interface and the very small MIS depletion layer width. With $J_{tp(f)} > J_{tp(r)}$ this implies $J_{pj(f)} \approx J_{pj(r)}$ and to prevent excess hole flow the hole quasi Fermi level in the MIS depletion must be pinned to the hole quasi Fermi level of the p substrate in this case.

The intermediate state was described as lying between the semiconductor and tunnel limited states. For this case the forward tunnel current is much greater than the reverse hole injected current, and the forward hole injected current is

much greater than the reverse tunnel current. It is only in this state that the device can display negative resistance.

By applying these equations to the device behaviour, a neat qualitative description was obtained for the current-voltage curve. The terms ' semiconductor limited' and 'tunnel limited' have been adopted by other investigators.

2.3.1. Regenerative Feedback For The Punchthrough Device

In an attempt to describe the current-voltage characteristic between the switching and holding points a feedback loop was described in the following cause and effect form.

The forward voltage across the p^+n junction is incremented by a small amount, increasing the recombination current in the p^+n depletion region J_{rj}, and causing extra holes to be injected from the p^+ substrate towards the metal so increasing J_{pj}, the hole current injected into the MIS depletion region. If the hole current is tunnel limited, a build up of holes takes place at the IS interface causing an increase in V_{ox}, the potential drop across the oxide, and hence an increase in the electron tunnel current J_{tn}. This increased electron tunnel current flows towards the p^+n junction, increasing J_{rj} and hence turning the p^+n junction even harder on. In [7], this was termed the *Controlled Inversion Feedback Loop* (CIFL) and could be described in symbols as

$$\Delta J_{rj} \rightarrow \Delta J_{pj} \rightarrow \Delta V_{ox} \rightarrow \Delta J_{tn} \rightarrow \Delta J_{rj} \qquad 2.3.3.$$

All Δ changes in the expression above for currents and potentials are positive, with the final change in J_{rj} being greater than the initial change for the device

when in the negative impedance region. The actual criterion for switching was the point at which the open-loop gain of the feedback path was equal to unity making the initial and final changes in J_{rj} the same.

2.4 The Avalanche Model

For the heavily doped n-type layer MISS model [8], current continuity for the device was again used for determining the $I - V$ characteristic. The feedback mechanism was demonstrated in two parts, with the switching characteristic close to the switching point dominated by the *Avalanche Feedback Loop*, AFL as opposed to the *Controlled Inversion Feedback Loop* CIFL.

The complete current continuity expression for electrons was given by

$$M_n J_{tn} + M_n f_n J_g + (M_p - 1) J_{pj} = J_{rj} + J_{ns} \qquad 2.4.1$$

and for holes

$$J_{tp} = M_p f_p J_g + M_p J_{pj} + (M_n - 1) J_{tn} \qquad 2.4.2.$$

M_n and M_p are the avalanche multiplication coefficients, and $M_n f_n$ incorporates the avalanching of the generation current in the MIS depletion region. This model included the substrate diffusion current J_{ns}, and the generation current in the depletion region J_g. The avalanche multiplication coefficients M_n and M_p, only become accountable when the electric field at the IS interface due to ionised donors in the n-type layer is $> 10^5 V/cm$. For fields lower than this, the carrier currents entering the MIS depletion region do not produce impact ionisation, producing values for M_n and M_p of unity. In this case the avalanche mode current

continuity equations, minus the substrate current and generation current, have the same form as in the punchthrough model. The electron and hole currents for the device are demonstrated in Fig 2.2.

2.4.1 Regenerative Feedback For The Avalanche Device

Two regenerative feedback loops were identified in [8] for the heavily doped device, the Controlled Inversion Feedback Loop already identified for the punchthrough model, and the Avalanche Feedback Loop. The CIFL has the same form as for the punchthrough mode and can be written as

$$\Delta J_{rj} \rightarrow \Delta J_{pj} \rightarrow \Delta V_{ox} \rightarrow \Delta J_{tn} \rightarrow \Delta J_{rj} \qquad 2.4.3.$$

with all symbols having the same meaning.

However, by setting the electron tunnel current equal to zero, a second feedback loop, the AFL, was identified as

$$\Delta V_j \rightarrow \Delta J_{pj} \rightarrow \Delta(M_p - 1)J_{pj} \rightarrow \Delta J_{rj} \rightarrow \Delta V_j \qquad 2.4.4$$

For this feedback loop, incrementing the forward voltage across the p^+n junction, V_f, produces an increase in the hole injected current J_{pj}. The epitaxial layer has a high doping density, and at the switching point the device has a large enough potential drop across the MIS depletion region for avalanche multiplication to occur. The injected hole current produces an avalanched electron current $(M_p - 1)J_{pj}$ which flows back to the p^+n junction turning it further on.

Both feedback loops were assumed to be present for a heavily doped n-type layer structure, with one strengthening the regenerative behaviour of the other.

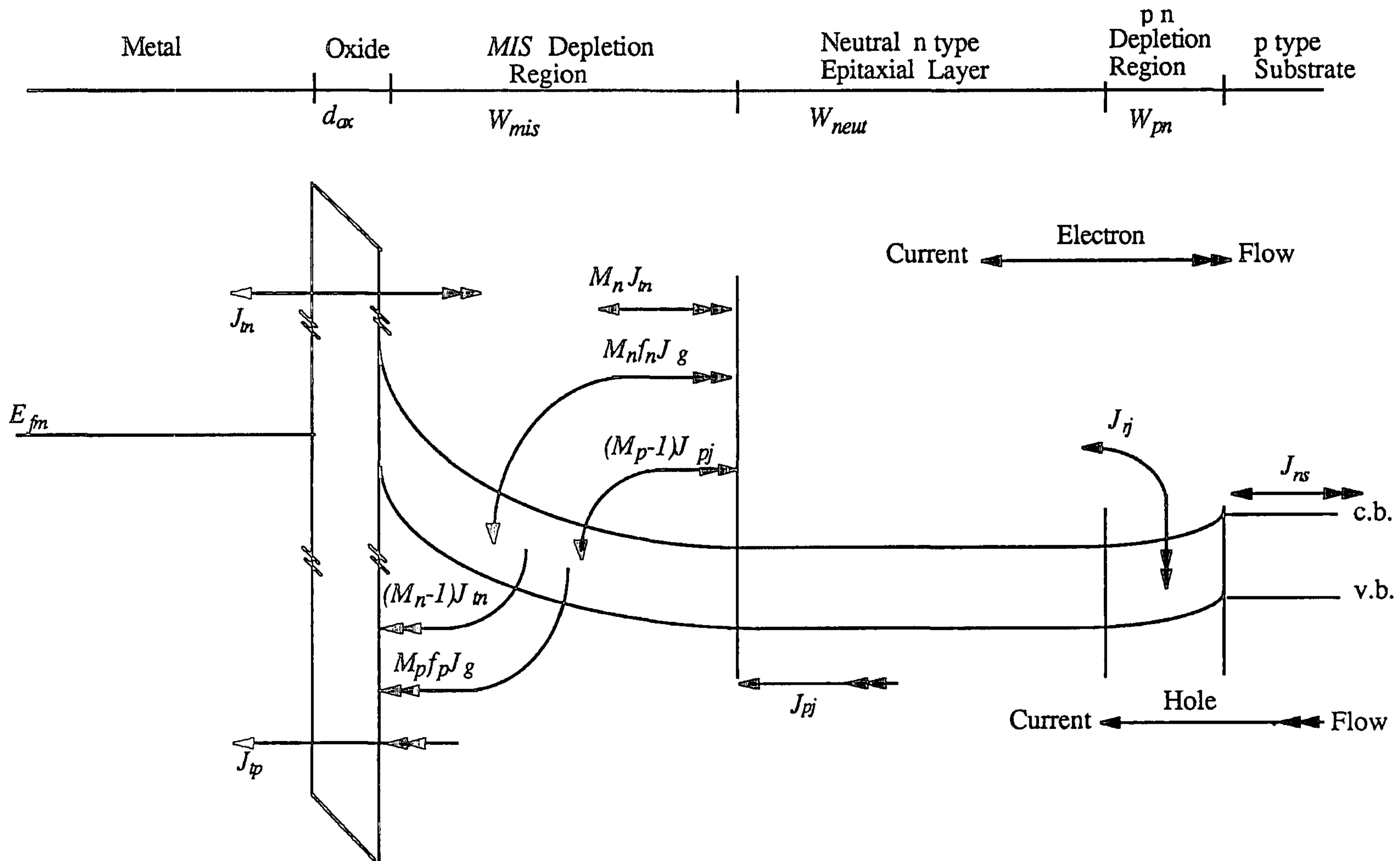

Fig 2.2: Current Components for the Avalanche MISS Model. Habib and Simmons [8].

The term 'avalanche mode' was given to devices whose switching voltage was determined by the AFL as opposed to the CIFL.

The avalanche model identified two possible forms of switching characteristic, the two-state form and the three-state form see Figs 2.3 and 2.4. Both forms were initiated by the AFL, but the shape of the curves was due to the type of interaction of the two feedback loops.

For the two-state form the AFL and CIFL were assumed to interact. This meant the CIFL reached unity gain while the device was in its negative resistance region due to the AFL. For the three state $I - V$ characteristic, the AFL and CIFL were regarded as non interacting which produced the three-state form for the switching characteristic shown in Fig 2.4.

2.5 The Device Switching Criterion

Following Habib and Simmons [7,8], Sarrabayrouse *et al* [9,10] performed an experimental and theoretical investigation of the behaviour of the $MISS$. They attempted to construct a general model for the device which could deal with a range of epitaxial layer doping densities. A similar current continuity model as described by Habib *et al* was used, and switching was again ascribed to regenerative feedback.

More recently, Mattos and Sarrabayrouse [11] constructed a model which dealt with the $MIpn$ device structure, (as opposed to the $MInp$ discussed by most investigators). The essential features of this model are similar to those of their $MInp$ model, but with a more quantitative examination of the current feedback

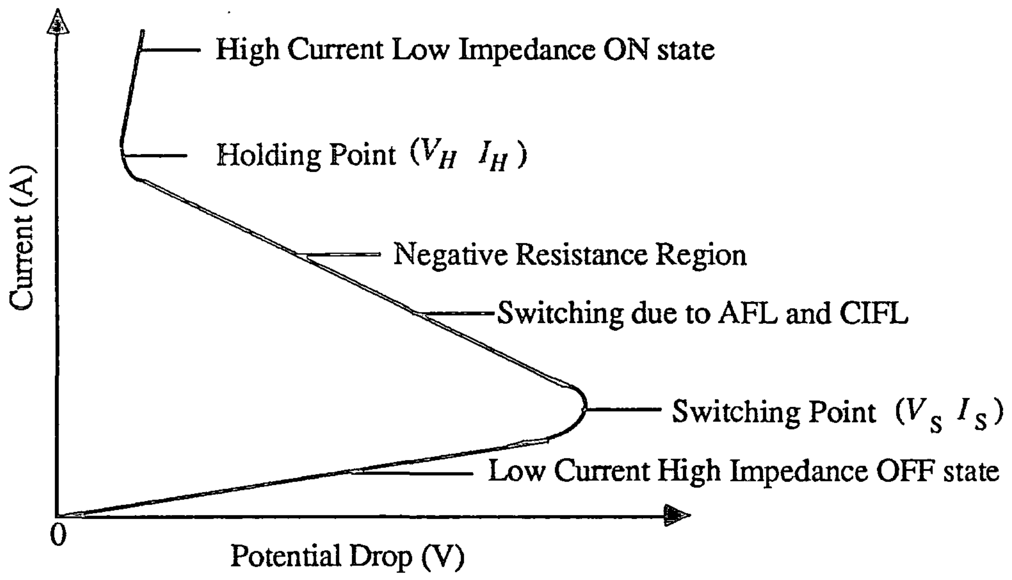

Fig 2.3: Ideal Two State Current Voltage Curve

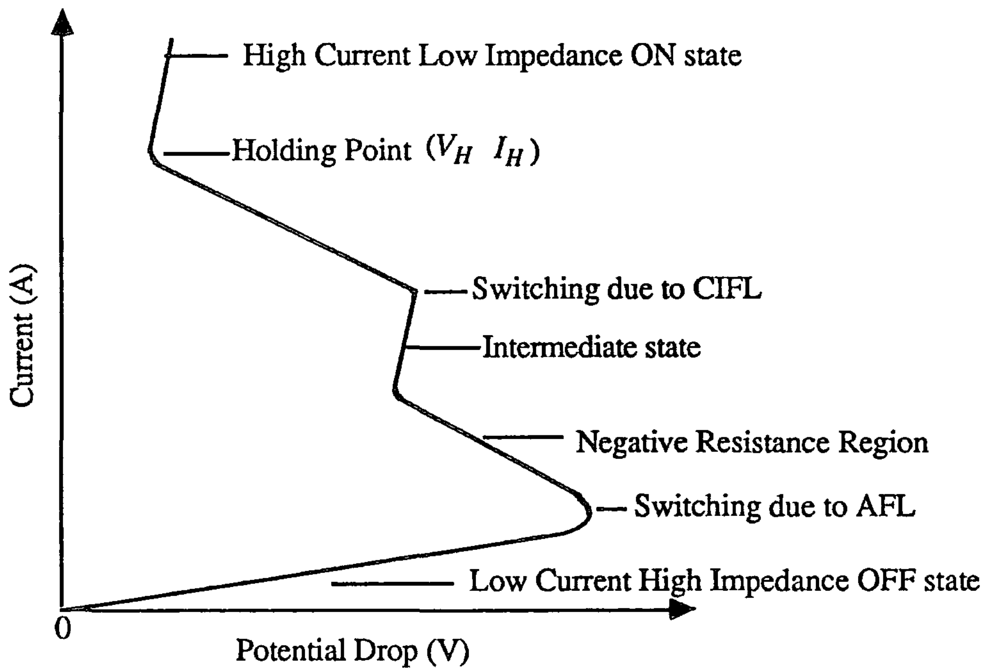

Fig 2.4: Ideal Three State Current Voltage Curve

mechanism through the device. The new features of their model are described here, but with the results modified to apply to the $MInp$ structure, which is dealt with in the thesis.

Two large-signal current gains were defined, one for the $p-n$ junction, and one for the insulator. The $p-n$ junction plus neutral region gain, G_j was defined to be

$$G_j(\psi_s, \xi, V_f) = \frac{J_{pj}}{J_{ns} + J_{rj} + J_{rec}} \qquad 2.5.1.$$

with J_{pj} the hole injected current into the MIS depletion region, J_{ns} the substrate electron current, J_{rj} the electron recombination current in the space charge region of the $p-n$ junction, and J_{rec} the electron recombination current in the neutral epitaxial region between the MIS and $p-n$ junction depletion regions. This gain is actually defined for the electron and hole currents at the interface between the MIS and the neutral n-type region. The gain is regarded as a function of three variables: ψ_s, the total potential-drop in the MIS depletion region, ξ, the quasi Fermi level splitting in the MIS depletion region, and V_f the forward voltage across the $p-n$ junction.

The large signal MIS gain G_s was defined to be

$$G_s(\psi_s, \xi, V_{ox}) = \frac{J_{tn}}{J_{tp}} \qquad 2.5.2.$$

the ratio of the electron tunnelling current J_{tn} to the hole tunnelling current J_{tp}. ψ_s and ξ have the same meanings as above, with V_{ox} the voltage drop across the oxide.

By ignoring any avalanche multiplication in the MIS depletion region, the switching condition was written explicitly in the form of a large signal gain product

as

$$G_j.G_s = 1 \qquad 2.5.3.$$

Expression (2.5.3) was derived from a more general expression for the switching criterion making divisions of device behaviour into punchthrough and avalanche modes unnecessary.

In a review of 'New Unorthodox Semiconductor Devices', Board [22] gave an explicit small signal expression for the open loop gain g_T and from this outlined the switching criterion

$$g_T = \frac{dI_{pj}}{dI_{tn}} \frac{dQ_h}{dI_{pj}} \frac{dV_f}{dQ_h} \frac{dI'_{tn}}{dV_f} \qquad 2.5.4$$

where Q_h is the hole charge stored at the IS interface and all other symbols have their usual meanings. The term dI'_{tn} is the final change in I_{tn} given an initial change dI_{tn} having passed around the feedback loop. In Board's analysis the conditions for stability were given as $g_T < 1$ stable, and $g_T > 1$ unstable.

2.6 Other Work

After construction of the basic 1-D MISS model, Habib and co-workers went on to deal with two further aspects of device behaviour: the effect of a thick tunnel oxide, and the effect of surface states on the switching characteristics of the device [13].

For a thick oxide device, the calculations of Habib and Simmons [12] showed that for a sufficiently large value of metal work function, and with the tunnelling attenuation factors for carriers adjusted to deal with very high potentials across the oxide, a switching characteristic could be generated for a MISS with an oxide

thickness of $70\AA$. For this device, Fowler-Nordheim tunnelling of carriers through the oxide was expected, and the tunnelling attenuation factors were calculated accordingly. With this thick oxide structure, the hole current was tunnel limited for small current bias, in contrast to the thin oxide MISS where it is semiconductor limited in the OFF state. No quasi-Fermi level splitting was present for this region of the $I - V$ curve. As the applied voltage increased, a deep depletion mode was entered with the hole tunnelling current being supplied by generation in the MIS depletion region. For a large enough current the regenerative feedback mechanism [7] was assumed to come into operation, producing a negative impedance region leading to the low impedance ON state. From the model, for a $70\AA$ device the current densities at the switching and holding points were calculated to be $2.10^{-5}A/cm^2$ and $6.10^{-5}A/cm^2$ respectively.

In the same paper, by changing the fixed tunnelling attenuation factor for electrons, curves were generated for thin oxide devices with silicon of $< 111 >$ orientation, as opposed to the $< 100 >$ normally used in modelling the device.

In the paper of Habib and Eltoukhy [13], an analysis of the effect of surface states was made on the switching current and voltage of the device; this switching mechanism was termed 'the surface states mode', as opposed to the earlier punchthrough and avalanche modes of device behaviour. It was able to describe the effect of single-level traps in the silicon forbidden band at the IS interface on the switching current and voltage. The traps performed three functions; As tunnelling sites for carriers from the metal through the oxide, as charge storage centres for carriers so affecting the total oxide potential drop, and as recombination centres for carriers from the conduction and valence bands. The results of the

investigation showed that for a sufficiently large interface state density, switching took place as soon as the hole quasi-Fermi level crossed the energy level of the interface states in the forbidden band and hence the switching voltage could be limited by this process.

In two related papers, Duncan *et al* [24] and Faraone *et al* [16] described experimental results for the two dimensional effects of device geometry on the switching characteristic of the MISS. In [23], it was shown experimentally that for a large metal top contact radius, the device appeared to be in its ON state for all currents with no negative impedance region. As the top contact radius decreased the device began to exhibit a well defined OFF state, moving into a negative impedance region and then the ON state. For the very small top contact radius device, it seemed to remain in its semiconductor limited OFF state so exhibiting no switching characteristic. For the thicker oxide structure it was seen that the device became semiconductor limited throughout its $I-V$ curve for larger values of top contact radius than for the thinner oxide devices. These effects were ascribed to the perimeter to area ratio (PAR) for the different devices, with the larger top contact radii having a smaller PAR so being affected less by any current spreading in the device.

Zolomy [14], set out a method of incorporating the experimentally prominent two dimensional effects in the behaviour of the two terminal MISS device. He pointed out that the previous theory needed separate equations to describe the MISS before and after punchthrough, and also that the holding currents produced by the theory are smaller than experimental values, especially for thicker oxides. His model takes into consideration two effects: the existence of pin-holes in the

oxide, and the ratio of the areas of the $p-n$ junction and the MIS depletion region. The paper also dealt with the effect of a fixed density of interface states in a similar manner to the treatment of the same case by Habib and Eltoukhy [13].

The separate description given to the punchthrough region of the $I-V$ curve was ignored in this model, in contrast to Habib and Simmons, so using the same current continuity equations for the whole $I-V$ characteristic. In the pin-hole model, [14], the oxide grown on the epitaxial layer is recognised as being non-uniform, having a number of small regions of oxide far thinner than the average. These oxide thicknesses are still greater than $10\AA$. The small regions of thin oxide provide far more conductive paths for current flow through the oxide, but though they cause a greater current flow through the device, they do not alter the growth of the MIS depletion layer under the insulator. They therefore alter the switching and holding currents, but not the switching or holding voltage. The current fringing effect was modelled by Zolomy by adjusting the active collecting area of the MIS depletion region relative to the $p-n$ junction area. This was achieved by the use of a suitable multiplying constant.

A model of device operation using a conductive SIPOS (Semi-Insulating Polycrystalline Silicon) film as the insulator, as opposed to a thin oxide, was developed by Bolt *et al* [16], producing a current voltage curve qualitatively similar to that from the standard MISS models. The current equations for the $p-n$ region of the device were the same as those for the thin oxide MISS. The conductive mechanism for carriers through the SIPOS was assumed to be dependent upon the density of silicon grains within the layer. The metal Fermi level was also assumed to be pinned at the metal-SIPOS interface making the supply of electrons through the

SIPOS independent of the electrical state of the device. Because of the thickness of the SIPOS layer the electron current was assumed to comprise a drift-diffusion component together with a recombination current. For holes, conduction was dependent amongst other things on the hole density at the SIPOS-semiconductor interface. With both the hole and electron currents, the theoretical expressions were based upon experimental work.

There has also been investigation of MISM (Metal Insulator Semiconductor Metal) and MISIM (Metal Insulator Semiconductor Insulator Metal) devices whose current-voltage curves are qualitatively similar to those of the MISS [17-19]. They have a high impedance OFF region followed by a negative impedance region leading to the low impedance high current ON state. For these devices as with the MISS, the high switching voltage is caused by the growth of a deep depletion layer in the semiconductor.

For the MISM device, the *pn* junction of the MISS is replaced by a Schottky barrier in forward bias, the reverse biased MIS remains unchanged. The Schottky barrier provides a sink for electrons injected from the MIS and provides a minority carrier hole current towards the IS interface. The Schottky barrier is usually regarded as a majority carrier device, though minority carrier injection does occur under certain circumstances. Reference [17] describes this device in which punchthrough of the reverse biased MIS to the Schottky barrier occurs. As the Schottky barrier minority carrier injection increases, the device switches into its ON state.

As described in [19], it is only needs a small extension of the idea to produce the MISIM structure. Schottky barriers often have a very thin layer of oxide

between the metal and the semiconductor in practice, and by allowing the oxide thickness to be increased this produces another MIS structure, this time in forward bias as the injector of holes towards the reverse biased MIS. Because of the existence of two MIS regions, the device was shown to display a bidirectional switching characteristic. Hayashi [24] demonstrated a negative impedance characteristic for an MIS structure with no p-type substrate, so demonstrating again that the negative impedance characteristic is not confined to the MISS structure.

In attempting to understand the similarity of the S-type negative resistance current-voltage curves for the three types of device MISS, MISM and MISIM, Zolomy [20] described the need for two amplifying mechanisms within a device structure to produce the switching characteristic, Fig 2.5. The switching was again ascribed to a positive feedback mechanism in which switching is produced when the open loop gain is greater than unity. The output of each amplifying structure is connected to the input of the other and the controlling input currents for each are of opposite sign i.e. an input electron current produces an output hole current, and for the other amplifying structure an input hole current produces an output electron current. Using this method of analysis for the device switching, other negative resistance devices were envisaged.

Another general attempt at describing S-type negative resistance in devices was given by Board [22]. Unlike Zolomy he viewed the device as consisting of a storage element and an injecting element (as opposed to the two amplifying elements of Zolomy) placed within a minority carrier diffusion length of each other so that interaction could take place, Fig 2.6. For the MISS device the injecting element can be identified as the $p-n$ junction, and the storage element as the

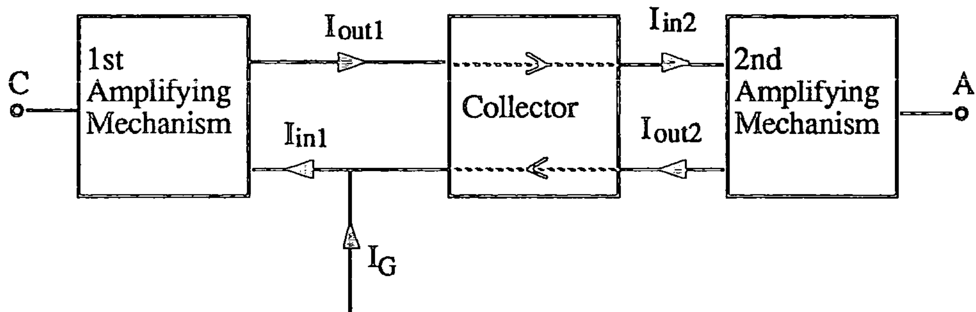

Fig 2.5: Basic Concept of a Negative Resistance Bipolar Device with Two Amplifying and One Collecting Elements Resulting in a Positive Feedback Loop. Zolomy [22]

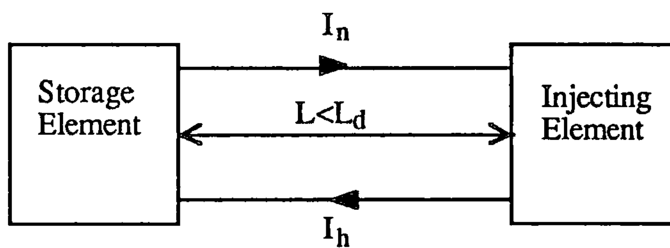

Fig 2.6: The Regenerative Switching Device. Identification of the Storage and Injecting Elements. Board[23]

MIS, with charge storage of holes at the IS interface. He also described the device as having three states (in the same manner as other researchers), a stable low-current high-voltage OFF state, an unstable region, and a low-voltage high-current ON state. The unstable region was described as having 'no operating point that is stable with time, unless imposed by external circuit conditions'

The most recent work by Zolomy [25] attempts to provide a simple calculation of the switching voltage for the MISS based upon a thyristor analogy. The p-type substrate is viewed as being the emitter for a *pnp* transistor, with the neutral region of the n-type layer becoming the base, and the MIS depletion region the collector. The common-base current amplification factor α_{pnp} for this analysis is then defined. An amplification factor α_{MIS} for the MIS region of the device is also defined as the ratio of the electron tunnel current over the total current flow through the device. The threshold (or switching voltage) was then given by analogy with thyristor work to be

$$V_S = U_B(1 - \alpha_{pnp} - \alpha_{MIS}) \qquad 2.6.1$$

where U_B is the breakdown voltage for the MIS determined from the n-type layer doping concentration.

2.7 Discussion

The more general features of MISS behaviour from previous work can be summarised as follows. The magnitude of the switching voltage is due to the growth of a deep depletion layer in the MIS region in the OFF state, which collapses through the negative impedance region until a point is attained at which

the decrease in the potential drop across the depletion region is less than the sum of the increases in the oxide potential and the pn junction potential. For the $MInp$ structure, holes collect at the IS interface giving rise to an inversion layer as the device moves from its OFF state towards its ON state. The actual switching mechanism has been described as a regenerative feedback mechanism between the $p-n$ and MIS regions of the device.

The first point to note about the regenerative feedback model is that it provides a simple picture for demonstrating why the device is unstable within its negative impedance region producing switching from the high impedance OFF state to the low impedance ON state. However, its limitations can be understood if the small signal changes in currents and voltages used for description in standard modelling are viewed as being time-dependent. For instance, a change in the forward recombination current of the pn junction ΔJ_{rj} (expression 2.3.3) will cause not only an increase in the hole injected current ΔJ_{pj}, but also changes in the neutral region recombination current, the substrate current, and the potential drop across the MIS depletion region. Similarly, the increase in J_{pj} will cause not only an increase in V_{ox}, but a change in the depletion layer width and hence the generation current. With these limitations, although the feedback concept shows the instability of the negative impedance region it cannot be used for any quantitative analysis of the instability given the steady state form of device equations used in current models. In the the steady state punchthrough model of Habib and Simmons only the two tunnelling currents J_{tn} and J_{tp}, the recombination current J_{rj} and the hole injected current J_{pj} are used. In the description above however, other currents have been incorporated in discussing the feedback. This is because

the steady state currents are large signal, whereas for small signal changes, other currents could dominate for different regions of the $I - V$ curve, making a more complete description of current contributions necessary.

For the regenerative feedback analysis of Mattos *et al*, a large signal gain was defined (as opposed to the small signal gain of Habib and Simmons) giving a switching condition for the punchthrough device of $G_j.G_s = 1$. This analysis is incorrect because by using the electron and hole current continuity equations (2.3.1) it can be seen that this product will always be equal to unity. Hence

$$G_j.G_s = \frac{J_{tn}}{J_{tp}}.\frac{J_{pj}}{J_{rj}} = \frac{J_{tn}}{J_{tp}}.\frac{J_{tp}}{J_{tn}} = 1 \qquad 2.7.1$$

Therefore the large signal analysis provides no information about the switching characteristic of the device.

A continuous model for device behaviour was described by Zolomy [21] who kept the standard semiconductor equations through the switching point so allowing a complete $I - V$ characteristic to be calculated without resorting to a separate description of the device physics at punchthrough. However this did not allow the whole range of device structures to be analysed. With the MISS model described in chapter three, $I - V$ curves for both the punchthrough and avalanche devices together with thin and thick oxide structures can be calculated using a single computer model.

In the two-dimensional modelling of MISS behaviour, the discrepancy between the one dimensional modelling and actual experimental results (which give a greater device current and potential drop especially for the holding point) is ascribed to pin-hole conduction paths through the insulator, and current spreading in the n-type layer and substrate. For the latter, no quantitative analysis was

given apart from provision of a multiplicative factor in the device equations for current flow in the-n-type layer based upon the Debye length. In chapter five, this deficiency is remedied by calculation of the current spreading in an infinite n-type layer and p-type substrate and its effect on the resulting MISS $I-V$ characteristic.

Hayashi's work [25] showed that given an n-type layer doping density great enough for avalanche multiplication to occur, an MIS structure with no hole injection from a p-type substrate was capable of producing an S-type current voltage characteristic. This was not explained apart from a qualitative description of the effect of avalanche multiplication in the MIS depletion region. The actual quantitative analysis for this device's behaviour is described in chapter 5 and its relationship to the heavily doped n-type layer MISS structure is demonstrated.

All computer models of MISS behaviour use steady state semiconductor equations which produce a calculated total potential drop given a specific current through the device. If the MISS was regarded as a circuit element, this modelling would be analogous to having a flat load line parallel to the voltage axis cutting the device's $I-V$ curve at one and only one point. This is the equivalent to having an infinite load resistor. However, in analysing the switching of the device, the standard regenerative feedback model assumes that once the open loop gain has reached unity the device will switch from its high impedance OFF state to its low impedance ON state. Again, viewing the device as a circuit element this is equivalent to having a load line for the device which cuts the device's $I-V$ curve in both its OFF and ON states together with the negative impedance region. There has been no published attempt to understand the device as a circuit element with a real load line that intersects the $I-V$ characteristic in the negative

impedance region only, so holding it in the intermediate state. In chapter six a simple equivalent circuit model is constructed for the device which demonstrates that the device can have a stable negative impedance under certain circumstances. Regenerative feedback can therefore be viewed as necessary for switching, but not for the existence of a stable negative impedance region.

It must be stressed that the regenerative feedback model discussed by many investigators is a useful method of visualising switching behaviour, but switching is a dynamic process and hence cannot be modelled using the steady state device equations. Therefore though it is a much simpler method of conveying information about switching than a complete time-dependent model would be, it can provide no quantitative information about dynamic device behaviour. The misunderstanding that arises about stability is due to the static device equations being used for visualising a dynamic process.

The thyristor analogy of Zolomy [25], provides an approximate value for the switching voltage of the device. However, as doping levels increase, current flow through the device is affected more by ionised donors in the MIS depletion region than by avalanching, making the analogy inappropriate for the more heavily doped devices. Also, with the MISS there is no sudden redistribution in the potential drop across the device in contrast to the thyristor in which a pn junction moves from reverse to forward bias at switching. Therefore the thyristor analogy should be regarded as possibly useful for the description of the lightly doped n-type layer devices, but it is information which is also immediately available from a simple calculation of the punchthrough voltage.

References

1. Yamamoto, T. and Morimoto, M., 'Thin-MIS-Structure Si Negative Resistance diode', *Appl. Phys. Lett.*, **20**, pp. 269-270, (1972).

2. Kroger, H. and Wegener, H.A.R., 'Bistable Impedance States in MIS Structures through Controlled Inversion', *Appl. Phys. Lett.*, **23**, pp. 397-399, (1973).

3. Kroger, H. and Wegener, H.A.R., 'Controlled Inversion Transistors', *Appl. Phys. Lett.*, **27**, pp. 303-304, (1975).

4. Kroger, H. and Wegener, H.A.R., 'Steady-State Characteristics of Two Terminal Inversion-Controlled Switches', *Solid-St Electron.*, **21**, pp. 643-654, (1978).

5. Simmons, J. G. and El-Badry, A., 'Experimental Studies of Switching in Metal Semi-Insulating $n - p^+$ Silicon Devices', *Solid-St Electron.*, **20**, pp. 963-966, (1977).

6. Simmons, J. G. and El-Badry, A., 'Theory of Switching Phenomena in Metal Semi-Insulator $n - p^+$ Silicon Devices', *Solid-St Electron.*, **20**, pp. 955-961, (1977).

7. Habib, S. E-D. and Simmons, J. G., 'Theory of Switching in $p - n$ Insulator(Tunnel) Metal Devices Part 1, Punchthrough Mode', *Solid-St Electron.*, **22**, pp. 181-192, (1979).

8. Habib, S. E-D. and Simmons, J. G., 'Theory of Switching in $p - n$ Insulator(Tunnel) Metal Devices Part 2, Avalanche Mode', *Solid-St Electron.*, **23**, pp. 497-505, (1980).

9. Sarrabayrouse, G. , Buxo, J., Owen, A. E., Munoz-Yague, A. and Sabaa. J-P., 'Inversion-Controlled Switching Mechanism of MISS Devices', *IEE. PROC*, **127**, pp. 119-125, (1980).

10. Sarrabayrouse, G. , Buxo, J., Sabaa, J-P., and Essaid, A., 'Switching Properties of Inversion-Controlled Metal-Thin Insulator -Si(n)-Si(p^+) Devices', *IEE. PROC.*, **128**, pp. 53-57, (1981).

11. Fiore De-Mattos, A. C. and Sarrabayrouse, G., 'The MISS Device Modelling and Influence of Critical Parameters', *Phys. Stat. Sol.*, **87**, pp. 699-707, (1985).

12. Habib, S. E-D. and Simmons, J. G., 'Theory of Switching in $p-n$ Insulator(Tunnel) Metal Devices. Thick-Tunnel Oxides and Indirect Tunnel Effects', *IEE PROC.*, **127, Pt I, No. 3**, pp. 111-118, (1980).

13. Habib, S. E-D. and Eltoukhy, A. A., 'A New Surface-States Mode of Switching in M-Thin Insulator-n-p^+ Devices', *J. Appl. Phys.*, **52(4)**, pp. 3027-3031, (1981).

14. Zolomy, I., 'Modified Theory of $MISS$, $MIST$, and $OMIST$ Devices', *Solid St-Electron.*, **26, No 7**, pp. 643-651, (1983).

15. Duncan, K. A., Tonner, P. D., Simmons, J. G., and Faraone, L., 'Characteristics of Metal/Tunnel-Oxide/n/p^+/ Silicon Switching Devices-I. Effects of Device Geometry and Fabrication Processes', *Solid St-Electron.*, **24, No 10**, pp. 941-948, (1981).

16. Bolt, M. J. B., Simmons, J. G., Taylor, G. W. and Zimmerman, C., 'Experimental and Theoretical Electrical Characteristics of Metal-SIPOS-n-p^+ Structures', *Semicond. Sci. Technol.*, **2**, pp. 666-674, (1987).

17. Darwish, M., and Board, K., 'Switching in m.i.s.m Structures', IEE Proc. I, *Solid-State & Electron Devices,* **127**, No **6**, pp 317-322, (1980).

18. Darwish, M. and Board, K., 'Experimental Observation of Switching in MISM and MISIM Structures', *IEE Proc. I, Solid-State & Electron Devices*, **128**, No **5**, pp 161-164, (1981).

19. Darwish, M. and Board, K., 'Theory of Switching in MISIM Structures', IEE Proc. I, *Solid-State & Electron Devices*, **128**, No **5**, pp 165-173, (1981).

20. Zolomy, I., 'A Survey of New Bipolar Amplifying and Negative-Resistance Devices', *Solid St-Electron.*, **28**, No **6**, pp. 537-547, (1985).

21. Zolomy, I., 'A Comprehensive Theory of MISS Devices Including Punch-Through and Avalanche-Induced Switchings Negative-Resistance Devices', *Phys. Stat. Sol.*, **100**, pp. 693-699, (1987).

22. Board, K., 'New Unorthodox Semiconductor Devices', *Rep. Prog. Phys.*, **48**, pp. 1595-1635, (1985).

23. Faraone, L., Simmons, J. G., Hsueh, F-L., and Mishra, U. K., 'Characteristics of Metal/Tunnel-Oxide/n/p^+/ Silicon Switching Devices-II. Low Dimensional Effects in Oxide Isolated Structures', *Solid St-Electron.*, **25**, **No 5**, pp. 335-344, (1982).

24. Hayashi, Y., 'Switching Phenomena in Thin Insulator Metal Insulator Semiconductor Diodes', *Appl. Phys Lett.*, **37(4)**, pp. 407-408, (1980).

25. Zolomy, I., 'Approximate Calculation of the Switching Voltage of MISS', *Phys. Stat. Sol.(a)*, **111**, pp. 371-375, (1989).

CHAPTER THREE

IMPROVED THEORY OF M.I.S.S BEHAVIOUR USING A ONE-DIMENSIONAL MODEL

3.1 Introduction

This chapter deals with the semiconductor theory and computational techniques involved in the steady state modelling of an $MInp$ MISS, fabricated from silicon with a tunnelling thickness SiO_2 insulator. Using this device structure the most important features of two terminal MISS operation in one dimension can be calculated.

The device description is divided into two parts: the first deals with devices whose n-type epitaxial layer doping densities are small, $<= 10^{16}cm^{-3}$, and the second deals with devices whose n-type layer doping densities are high, $>= 10^{16}cm^{-3}$. The separation between 'light' and 'heavy' doping is at approximately the same doping density as the distinction between the punchthrough and avalanche models of Habib and Simmons [1,2]; although in the present model the physics of the highly doped n-type layer MISS has been found to be markedly different. Furthermore, the computer model developed can incorporate all values of n-type doping in a continuous way, and it is only in the following description of the device physics that a separation is made.

After the physics of the new device model has been described, an analysis of

the current-voltage characteristics for two ideal devices is made: one with a lightly doped n-type layer, and the other with a heavily doped n-type layer. The discussion divides the current voltage curve into four regions: the high impedance low current OFF state, the vicinity of the switching point, the negative impedance region, and the low impedance high current ON state. In chapter four a more complete examination has been made of the effects of changing structural parameters on device behaviour, but in this chapter these two ideal MISS structures are used to show aspects of behaviour that are common to their two classes of device.

In some respects the 1-D computer model described is similar to that produced by Habib [10], and a comparison between the two models is made at the end of this chapter.

3.2 Basic Device Equations

Analysis of the basic device equations for the $MInp$ structure has been divided into two sections. The first deals with the behaviour of the MIS part of the device; it examines the physics of the depletion region with its electric field $\mathcal{E}$, and the oxide potential V_{ox}. Also the three currents associated with the region are considered: these are the generation current in the depletion region J_g, and the two oxide tunnelling currents due to electrons and holes, J_{tn} and J_{tp} respectively. The second section looks at the the pn diode structure, and covers the three electron recombination currents. These are in the depletion region of the pn junction J_{rj}, the neutral n-type layer J_{rec}, and the p-type substrate J_{ns}. It also deals with the hole current injected into the MIS depletion region under the metal, J_{pj}.

In all, seven separate currents are dealt with in this first order model. Three are assigned to the MIS part of the device, and four to the pn structure. Once the assumptions for the model have been given and the basic equations have been discussed, the method of solution for the model will be outlined.

3.2.1 Model Assumptions

1.) The dominant mechanism for carrier transport through the oxide is assumed to be quantum mechanical tunnelling in which energy and transverse momenta are conserved for carriers in tunnelling transitions, and the carriers tunnel independently. (see Appendix A).

2.) Current densities for all regions of the current voltage curve are assumed to be small enough for standard low current semiconductor equations to hold, with space charge effects due to carrier flow being negligible $< 10^2 A/cm^2$, [3].

3.) Surface states at the IS interface are only included as a bias independent charge, and any effect on generation and recombination in the MIS depletion region, or as a pathway for carrier tunnelling has been neglected. (Habib [10]).

4.) The quasi-Fermi levels across the MIS depletion region and the pn junction are assumed to be flat. The term 'quasi-Fermi level' is to be understood as that quantity which when substituted in place of the Fermi level gives the concentration of that carrier under non-equilibrium conditions. (Grove [11]).

5.) The abrupt junction approximation applies to the pn junction, and all doping levels are assumed to be uniform.

6.) This model only describes the time independent steady state.

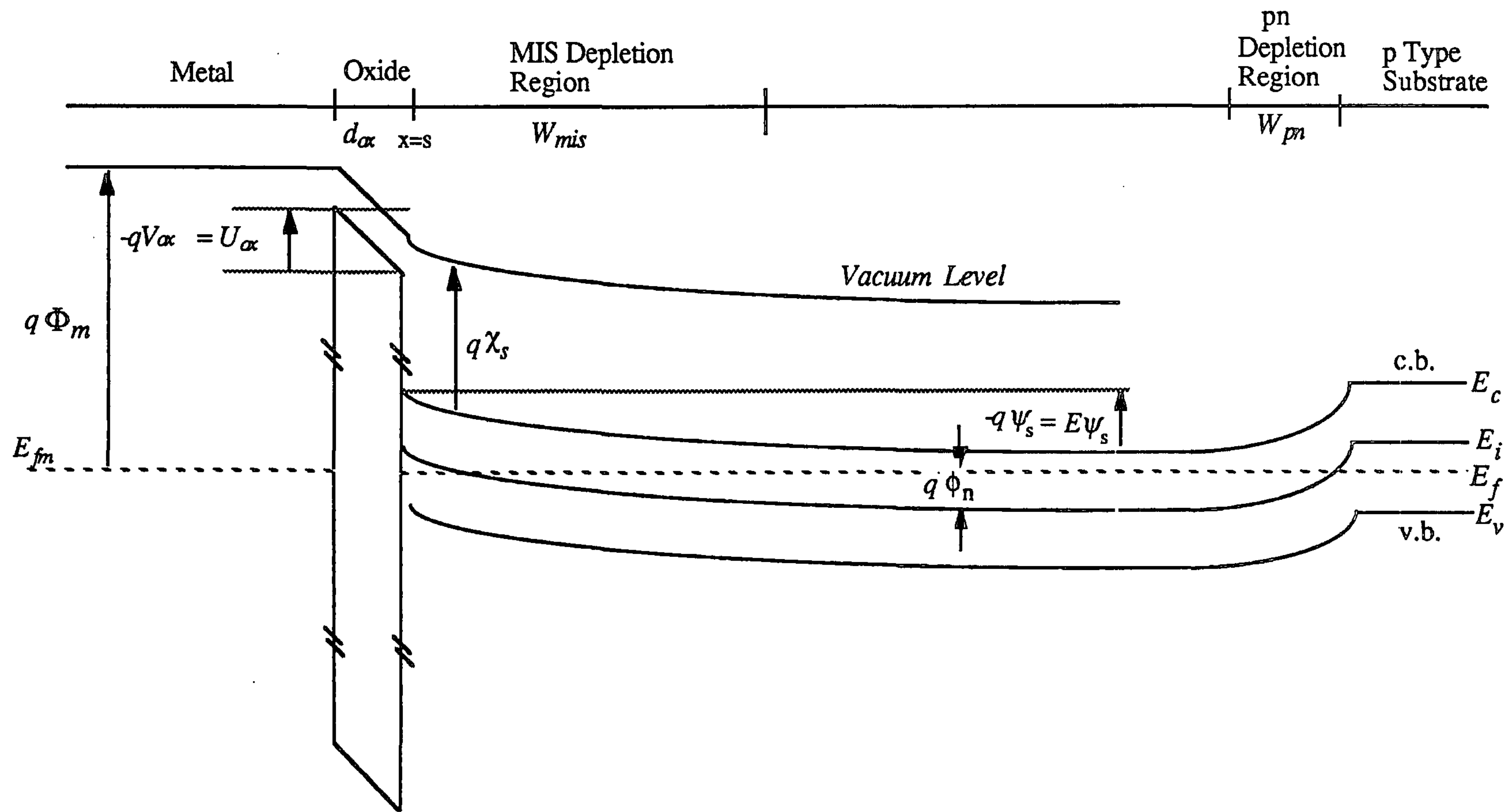

Fig 3.1 Energy values used in modelling the MISS.

3.3 The Model of the MIS Structure

3.3.1 The Depletion Region

In the MIS depletion region, the ionised dopant atoms together with the free electrons and holes give rise to an electric field $\mathcal{E}_s$ in the n-type semiconductor at the IS interface. For a non-degenerate semiconductor, donor impurities are almost completely ionised at room temperature. By assuming complete ionisation, Poisson's equation can be written in the form

$$\frac{d\mathcal{E}}{dx} = \frac{q}{\epsilon_s}\left[p(x) - n(x) + N_d\right] \qquad 3.3.1$$

where $\mathcal{E}$ is the electric field, N_d the donor dopant density, and $n(x)$ and $p(x)$ are the free electron and hole carrier densities at the point x respectively. The values for $n(x)$ and $p(x)$ are determined using Fermi-Dirac statistics giving

$$n = N_c F_{1/2}\left[\frac{(E_{fn}(x) - E_c(x))}{kT}\right] \quad \text{and} \quad p = N_v F_{1/2}\left[\frac{(E_v(x) - E_{fp}(x))}{kT}\right] \qquad 3.3.2$$

$E_c(x)$ and $E_v(x)$ are the energies of the conduction and valence band edges at a position x in the depletion region, Fig 3.1, and E_{fn} and E_{fp} are the energies of the electron and hole quasi-Fermi levels respectively. N_c and N_v are the effective densities of states in the conduction and valence bands of the silicon. $F_{1/2}$ is the Fermi integral of order 1/2. The general expression for a Fermi integral of order j has the form

$$F_j(z) = \frac{1}{\Gamma(j+1)} \int_0^\infty \frac{x^j\, dx}{1 + exp(x - z)} \qquad 3.3.3$$

where $\Gamma(j+1)$ is the gamma function. Poisson's equation can then be integrated to give an expression for the electric field at the IS interface of the form (see

Appendix B)

$$\frac{\mathcal{E}_s^2}{2} = \frac{kT}{\epsilon_s}\left\{N_c F_{3/2}\left[\frac{E_{fn}(0) - E_c(x)}{kT}\right]\Big|_0^s + N_v F_{3/2}\left[\frac{E_v(x) - E_{fp}(s)}{kT}\right]\Big|_0^s\right\} - \frac{q}{\epsilon_s} N_d \psi_s \qquad 3.3.4$$

where $\mathcal{E}_s$ is the electric field at the semiconductor insulator interface, and $x = s$ and $x = 0$ are the limits over which the expression in brackets is evaluated, $x = s$ being the semiconductor insulator interface, and $x = 0$ the edge of the MIS depletion region juxtaposed to the neutral region of the n-type layer as shown in Fig 3.2(a). N_d is the donor dopant density of the n-type layer, and ψ_s is the potential drop measured from the conduction band in the neutral region of the n-type layer to the conduction band at the IS interface. From this expression for $\mathcal{E}_s$, the potential drop across the oxide can be found from Gauss' Law to be

$$\epsilon_{ox}\mathcal{E}_{ox} = \epsilon_s \mathcal{E}_s + qQ_{ss} \qquad 3.3.5$$

where qQ_{ss} is the charge stored in interface states. The potential drop across the oxide is then

$$V_{ox} = -\mathcal{E}_{ox} d_{ox} \qquad 3.3.6$$

The generation current density in the MIS depletion region can be expressed (see Appendix D) as

$$J_g = \frac{q n_i L_d}{\sqrt{2}\tau_0} \frac{1 - e^{-\xi/kT}}{1 + e^{-\xi/2kT}} \left\{[M(\phi_s, \xi)]^{1/2} - (q\phi_n/kT - 1)\right\} \qquad 3.3.7$$

where $M(\psi_s, \xi)$ is the minimum of $(E\psi_s/kT - 1)$ and $((q\phi_n + \xi)/kT - 1)$, n_i is the intrinsic carrier density for silicon, L_d the intrinsic Debye length, ξ the quasi-Fermi level splitting at the IS interface, $q\phi_n$ equal to $E_{fn} - E_i$ in the neutral n-type layer, and $\tau_0 = \tau_p$ the hole lifetime in the n-type layer.

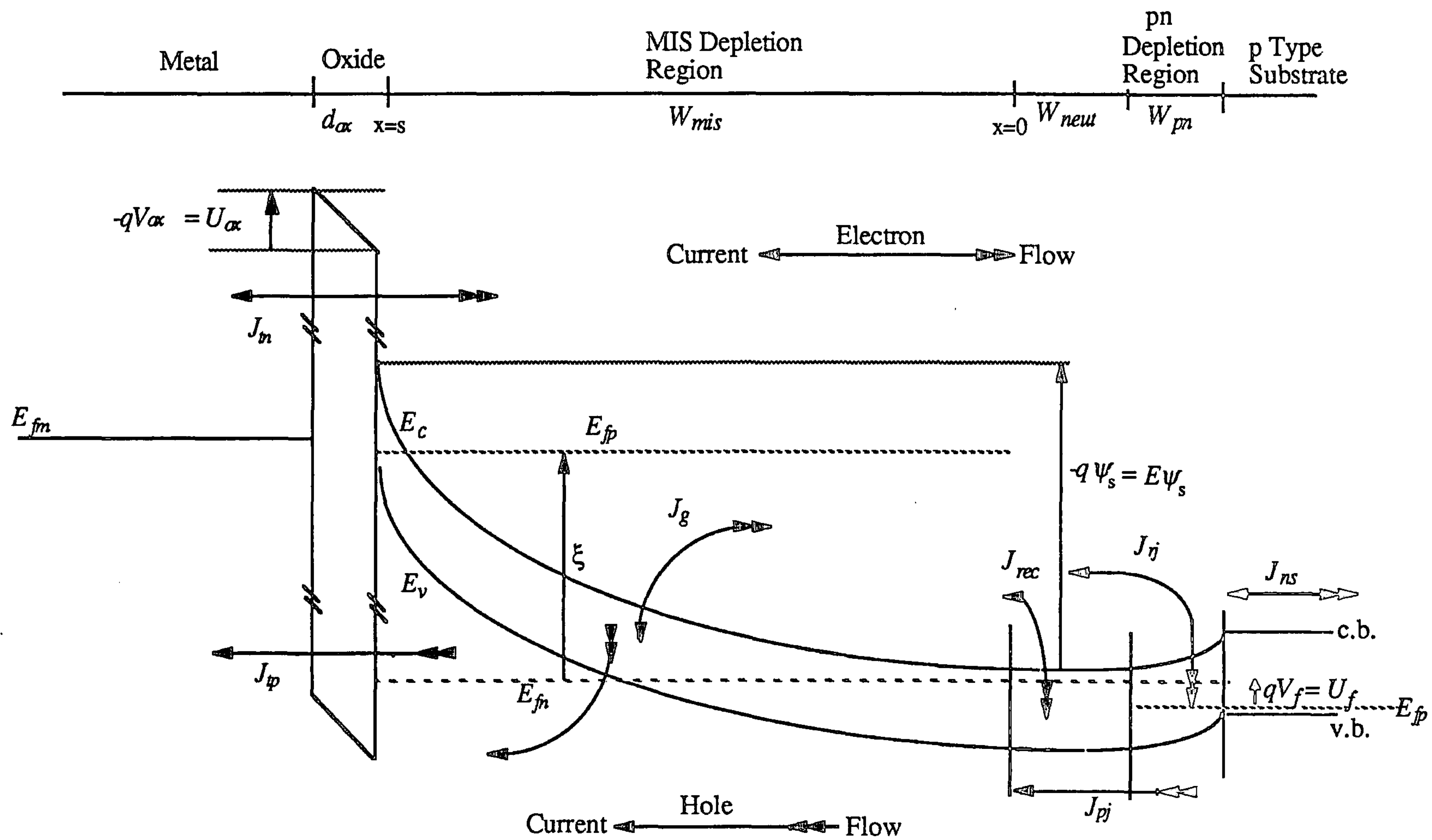

Fig 3.2(a): Current Components for the Lightly Doped n-type Layer MISS Model.

3.3.2 The Tunnelling Currents

As has been demonstrated above, the potential drop across the thin oxide can be easily determined from Gauss' Law. The tunnelling current for electrons through the insulator [Appendix A] can be written in the form

$$J_{tn} = A_e T^2 e^{\eta_{e0}} \left\{ F_1 \left[\frac{E_{fm} - E_c(s)}{kT} \right] - F_1 \left[\frac{E_{fn} - E_c(s)}{kT} \right] \right\} \qquad 3.3.8$$

where

$$E_{fm} - E_c(s) = U_{ox} + q\chi_s - q\Phi_m \qquad 3.3.9$$

$E_{fm} - E_c(s)$ is the difference between the metal Fermi level and the semiconductor conduction band across the oxide. U_{ox}, χ_s, and Φ_m, are the energy drop across the oxide, the silicon electron affinity, and the metal work function respectively.

$$E_{fn} - E_c(s) = q\phi_n - E_g/2 - E\psi_s \qquad 3.3.10$$

where $E_{fn} - E_c(s)$ is the energy difference between the electron quasi Fermi and the semiconductor conduction band at the IS interface, and ϕ_n, E_g, and $E\psi_s$, are the electron quasi Fermi potential, the silicon energy gap, and the energy change from the semiconductor conduction band in the neutral region to the semiconductor conduction band at the IS interface. η_{e0} is the value for the tunnelling attenuation factor at the energy $E = E_c(0)$. This tunnelling current expression is only suitable for a small potential drop across the oxide, and it is only accurate when the metal Fermi level lies opposite, or very close to the semiconductor forbidden band.

A similar expression holds for the hole tunnelling current.

$$J_{tp} = A_h T^2 e^{\eta_{h0}} \left\{ F_1 \left[\frac{E_v(s) - E_{fp}(s)}{kT} \right] - F_1 \left[\frac{E_v(s) - E_{fm}}{kT} \right] \right\} \qquad 3.3.11$$

where

$$E_v(s) - E_{fp} = E\psi_s - \xi - q\phi_n - E_g/2 \qquad 3.3.12$$

where $E_v(s) - E_{fp}$ is the energy difference between the semiconductor valence band and the hole quasi-Fermi level at the IS interface, and ξ is the energy difference between the hole and electron quasi-Fermi levels measured from the electron quasi-Fermi level at the same point.

$$E_v(s) - E_{fm} = q\Phi_m - E_g - q\chi_s - U_{ox} \qquad 3.3.13$$

$E_v(s) - E_{fm}$ is the energy difference between the semiconductor valence band, and the metal Fermi level across the oxide. η_{h_0} is the value of the tunnelling attenuation factor at the energy $E = E_v(0)$

For large potential drops across the insulator, the more general expression due to Green and Shewchun [3] is used.

$$J_{tn} = \frac{4\pi q m_{ti}}{h^3} \int_0^{E_{max}} (f_m - f_s) e^{-\eta(E,0)} \left[\left(1 - exp\left(\frac{-\partial\eta}{\partial E_T} E \frac{m_{ts}}{m_{ti}}\right)\right) \Big/ \left(\frac{\partial\eta}{\partial E_T}\right)\right]\Big|_{E_T=0} dE \qquad 3.3.14$$

where m_{ts}, and m_{ti} are the transverse effective masses of a carrier in the semiconductor and insulator respectively as described in Appendix A. This more accurate expression is necessary for any condition in which the metal Fermi level is raised more than a few $eV's$ above the semiconductor conduction band at the IS interface. It is valid for both types of carrier, with the integral taken over the energy range from the silicon conduction band edge at the IS interface for electrons, and from the silicon valence band edge at the IS interface for holes.

The expression for the tunnelling attenuation factor $\eta(E, E_T)$ is treated as a function of the two energy parameters for a carrier: the total energy E, and the

transverse energy E_T. The expression for η and its first derivative are both evaluated at $E_T = 0$. These values are then substituted to provide a final expression for the total carrier currents through the oxide.

3.4 The Model of the *pn* Junction Region

3.4.1 Electron Recombination Currents

As has been mentioned in Section 3.1, the *pn* region of the device is modelled using four currents, three of which are the electron recombination currents J_{rj}, J_{rec}, and J_{ns}. The recombination current in the depletion region of the *pn* junction is modelled using the standard expression for an abrupt junction as in Grove [11]:

$$J_{rj} = \frac{qn_iW_{pn}}{\tau_0}\left[\frac{e^{qV_f/kT} - 1}{e^{qV_f/2kT} + 1}\right] \qquad 3.4.1$$

where V_f the forward potential across the *pn* junction, $\tau_0 = \tau_p$ is the carrier lifetime and W_{pn} is the width of the *pn* junction depletion region. W_{pn} is given by

$$W_{pn} = \sqrt{\frac{2\epsilon_s}{q}\left(\frac{N_a + N_d}{N_aN_d}\right)(V_{bi} - V_f)} \qquad 3.4.2$$

where N_a and N_d are the acceptor and donor doping densities, and V_{bi} is the built-in potential of the junction. The recombination current in the neutral region has the form

$$J_{rec} = \frac{qD_p}{L_p sinh(W_{neut}/L_p)}(p_j' + p_m')sinh^2(W_{neut}/2L_p) \qquad 3.4.3$$

where

$$p_j' = p_j - p_{n0} = \frac{n_i^2}{N_d}(e^{qV_f/kT} - 1) \qquad 3.4.4$$

is the excess hole density at the edge of the pn depletion region, and

$$p'_m = n_i e^{-(q\varphi_n + \xi)/kT} \qquad 3.4.5$$

is the hole density at the edge of the MIS depletion layer at $x = 0$. W_{neut} is the width of the neutral region between the MIS, and the pn junction depletion regions, and is given by

$$W_{neut} = W_{epi} - W_n - W_{mis} \qquad 3.4.6$$

where W_{epi}, W_n, and W_{mis}, are the widths of the n-type epitaxial layer, the pn depletion region on the n-type side, and the MIS depletion region respectively.

The substrate diffusion current is given by the standard expression

$$J_{ns} = \frac{qD_n n_i^2}{L_n N_a}\left(e^{qV_f/kT} - 1\right) \qquad 3.4.7$$

where D_n and L_n, are the diffusion coefficient and diffusion length for electrons in the p-type semiconductor respectively.

3.4.2 The Hole Injected Current

At the edge of the pn junction depletion region on the n-type layer side, the excess hole density is given by p'_j and at the edge of the depletion region of the MIS, the hole density is given by p'_m. By solving the diffusion equation, and using these boundary conditions, the hole current injected into the MIS depletion region is found to be

$$J_{pj} = \frac{qD_p}{L_p sinh(W_{neut}/L_p)}\left[p'_j - p'_m cosh(W_{neut}/L_p)\right] \qquad 3.4.8$$

Currents for the lightly doped device are shown in Fig 3.2(a). This is similar to Fig 2.1, the most important additions being the inclusion of the generation current J_g, and the two electron recombination currents J_{rec} and J_{ns}. The currents described are necessary for both the lightly and heavily doped n-type layer current continuity equations described in the next two sections.

3.5 Lightly Doped n-Type Layers - Method of Solution

In the previous sections the seven major current contributions in this first order model have been outlined. To determine the $I - V$ curve for the MISS from these expressions, electron and hole current continuity is assumed throughout the device.

For electron flow there must be current continuity at the interface between the MIS depletion region of the device and the neutral region of the n-type layer, giving the equation for electron current continuity:

$$J_{tn} + J_g = J_{rj} + J_{rec} + J_{ns} \qquad 3.5.1$$

where the symbols have their previously defined meanings. For the hole current, continuity occurs at the interface between the MIS depletion region and the insulator giving an expression of the form

$$J_{tp} = J_{pj} + J_g \qquad 3.5.2$$

With these two current continuity equations, two dependent variables can be obtained from their solution. Rather than use total current through the device as the controlling independent variable, the forward voltage across the pn junction,

V_f was chosen, with the implicit assumption that it is a monotonic function of the total device current. For a chosen forward voltage V_f, the two dependent variables determined were the total potential drop across the MIS depletion region ψ_s, and the quasi-Fermi level splitting in the MIS depletion region ξ, which gives a measure of the hole accumulation at the IS interface.

Examining the form of the seven current equations and noting that

$$U_{ox} = -qV_{ox} = -qV_{ox}(\xi, \psi_s) = U_{ox}(\xi, \psi_s) \qquad 3.5.3$$

allows the current continuity equations, with their explicit dependence upon ξ, ψ_s and V_f to be written in the form

$$J_{tn}(\xi, \psi_s) + J_g(\xi, \psi_s) = J_{rj}(V_f) + J_{rec}(\xi, \psi_s, V_f) + J_{ns}(V_f) \qquad 3.5.4$$

for electrons and

$$J_{tp}(\xi, \psi_s) = J_g(\xi, \psi_s) + J_{pj}(\xi, \psi_s) \qquad 3.5.5$$

for holes.

Once this system of equations has been solved giving ξ and ψ_s for a given value of V_f, the total current flow through the device J_{tot}, and total potential drop V_{tot}, determined from the difference between the metal Fermi level and the hole substrate Fermi level can be found giving the total MISS current as

$$J_{tot} = J_{tn} + J_{tp} = J_{rj} + J_{pj} + J_{rec} + J_{ns} \qquad 3.5.6$$

and the total potential drop V_{tot} as

$$-qV_{tot} = (E_{fm} - E_{fp}|_{substrate}) = q\Phi_m - U_{ox} - q\chi_s - E\psi_s - E_g/2 + q\phi_{fn} - qV_f \qquad 3.5.7$$

The system of equations above is therefore sufficient to determine a unique operating point for the device in the steady state.

3.6 Heavily Doped n-Type Layers - Method of Solution

The heavily doped n-type layer MISS behaves differently to the lightly doped device. Ionised donors in the MIS depletion layer make a greater contribution to the oxide electric field, and for certain parameters and epitaxial layer thicknesses the avalanching mechanism in the MIS depletion region also becomes important. The device equations for the heavily doped MISS remain the same as those for the lightly doped case, apart from the inclusion of multiplication factors in the current continuity equations.

At high electric field strengths in a semiconductor, a carrier can attain enough kinetic energy between scattering events for it to shatter silicon to silicon bonds so creating an electron-hole pair. This process is termed collision ionisation. For the electron and hole carrier currents in the MIS depletion layer, this can give rise to an increase in the injected electron and hole components by factors of M_n and M_p respectively, as shown in Fig 3.2. This is similar to Fig 2.2 except that avalanching of the generation current has been ignored. The theory of the multiplication coefficients M_n and M_p is given in Appendix D. The following current continuity equations result,

$$M_n J_{tn} + (M_p - 1)J_{pj} + J_g = J_{rj} + J_{rec} + J_{ns} \qquad 3.6.1$$

for electrons, and

$$M_p J_{pj} + (M_n - 1)J_{tn} + J_g = J_{tp} \qquad 3.6.2$$

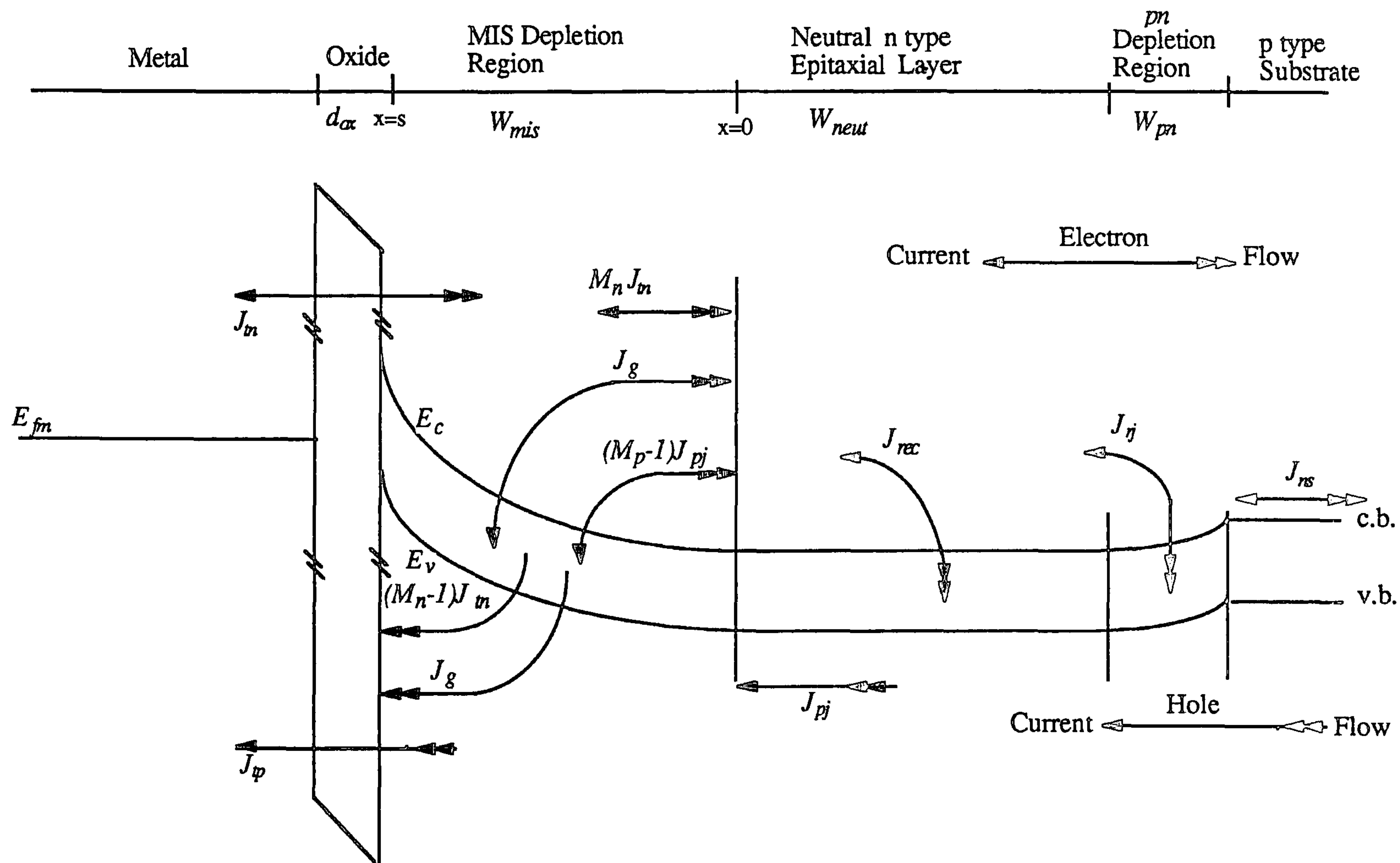

Fig 3.2(b): Current Components for the Heavily Doped n-type Layer MISS Model .

for holes. The $(M_n - 1)$ and $(M_p - 1)$ terms appear because of the creation of a pair of carriers at every ionising impact. Hence for every electron created in an impact ionisation, a hole is also produced; similarly for holes and electrons. Avalanching of the generation current itself has been neglected because its magnitude is much less than that from avalanching of injected carriers due to J_{tn} and J_{tp} in the MIS depletion region. The width of the MIS depletion region is so small for the heavily doped devices that the generation current is negligible compared to either the electron tunnelling current J_{tn} or the hole injected current J_{pj}. The total current flow through the device is again given by

$$J_{tot} = J_{tn} + J_{tp} = J_{rj} + J_{pj} + J_{rec} + J_{ns} \qquad 3.6.3$$

and the total potential drop is given, as in the lightly doped case by

$$-qV_{tot} = (E_{fm} - E_{fp}|_{substrate}) = q\Phi_m - U_{ox} - q\chi_s - E\psi_s - E_g/2 + q\phi_{fn} - qV_f \qquad 3.6.4$$

3.7 The Computational Technique

The computer program for calculating device behaviour was written in a mixture of Pascal and Fortran. At the outset a decision was made to use Pascal because of its better logical structure and greater legibility. In the initial stages of program development external calls to numerical algorithms were not required, due to simple approximations being used in describing the device physics; the self consistent solutions from the current continuity equations were produced from a very simple algorithm. However, as the model developed in complexity, the need arose to utilise the NAG library for the more complex and accurate semiconductor

device equations, and also as a more efficient method for solving the two non-linear equations for electron and hole current continuity. Because the Pascal compiler used did not enable calls directly to the NAG library, a number of subsidiary Fortran subroutines had to be written which were called from the main Pascal body. This is the reason for the length and complexity of the code seen in Appendix G.

In the program, material constants such as ϵ_s and μ_n were declared as constants at the start of the program. These were passed to Pascal procedures globally and given in the parameter lists for the Fortran subroutines. Device structure parameters such as W_f and d_{ox} were declared as variables and initialised at the start of the main Pascal program body. These values were also passed globally to other program sections. The program was very modular in design, with each major physical description of the device such as individual electron and hole current components, and the MIS depletion region electric field expression being written as procedures.

As shown in equations (3.5.4) and (3.5.5), the current continuity expressions for electrons and holes can be regarded as functions of three variables: the quasi-Fermi level splitting in the MIS depletion region ξ, the potential drop across the MIS depletion region ψ_s, and the forward voltage across the pn junction V_f. The same is true for the avalanche current expressions (3.6.1) and (3.6.2). In solving these equations, a specific value was chosen for V_f together with initial estimates of ξ and ψ_s. The two current continuity expressions were rewritten as

$$M_n J_{tn}(\xi, \psi_s) + (M_p - 1) J_{pj}(\xi, \psi_s) + J_g(\xi, \psi_s) - J_{rj}(V_f) - J_{rec}(\xi, \psi_s, V_f) - J_{ns}(V_f) = 0 \quad 3.7.1$$

for electrons, and

$$M_pJ_{pj}(\xi, \psi_s) + (M_n - 1)J_{tn}(\xi, \psi_s) + J_g(\xi, \psi_s) - J_{tp}(\xi, \psi_s) = 0 \qquad 3.7.2$$

for holes. These equations were then passed to a subroutine which calculated the values for ξ and ψ_s to make the continuity equations consistent. When the error in the continuity equations was below a specific value, another value for V_f was chosen. This process was repeated until the complete $I - V$ curve had been generated. A flow diagram of the computational procedure is given in Fig 3.3.

The NAG library was used to solve the two non-linear current continuity equations (3.7.1) and (3.7.2) in ξ and ψ_s. This was achieved using ' Powell's hybrid method' in subroutine C05NBF [6]. For integrals of one variable with non-standard integrands the library subroutine D01AHF was used, based upon a method described by Patterson [7]. Two library functions were also used to evaluate the error function $erf(x)$ and Dawson's integral. These were S15AEF [8] and S15AFF [9] respectively.

The independent variable V_f was incremented for every $10^{-3}V$. It was begun for a *pn* junction forward voltage of $10^{-3}V$, and stopped after fifty points of the ON region had been determined. Depending upon the structural parameters chosen this could result in up to 600 points being calculated. Graphical results were produced using the GHOST80 plotting package, with annotation for the graphs and other diagrams produced using an Apple Macintosh.

The program was run on an Amdahl 58/60 with 32MBytes of main store. Because of the power of the Amdahl, the more precise device equations described could be used. It also allowed a large number of $I - V$ curves to be determined providing a detailed systematic analysis of the changes in 1-D device behaviour

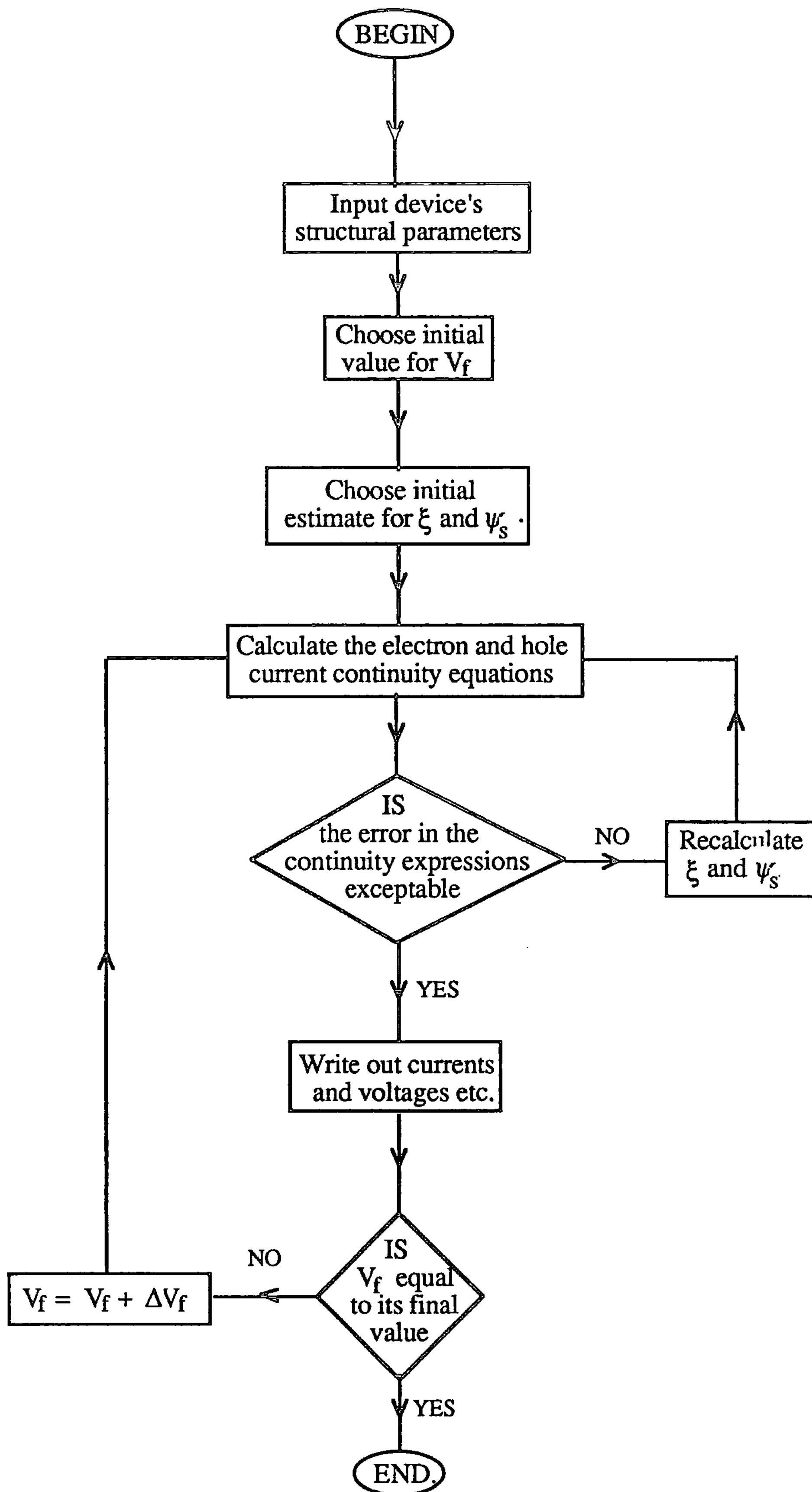

Fig 3.3: Flow Diagram of the Main Computational Steps for Calculation of the MISS I-V Characteristic.

with various structural parameters.

3.8 The Current Voltage Characteristic

Solution of the non-linear device equations (3.6.1) and (3.6.2) enables the overall $I - V$ characteristic to be calculated, together with the individual current and voltage components, so allowing the physical operation of the device to be closely examined. This analysis is performed using the computed results for the lightly and heavily doped devices in this section. The current-voltage curve is divided into four parts. The high impedance low current OFF state, the vicinity of the switching point, the negative impedance region, and the low impedance high current ON state.

The different regions of the calculated $I - V$ curve are discussed with regard to the form of interaction of the MIS and pn regions, but the switching mechanism is not described in terms of a regenerative feedback loop. Using steady state, time independent semiconductor equations, the $I - V$ curve can be evaluated throughout the negative impedance region. The computer model can be visualised as providing a measurement of the device using a perfect current source with a flat load-line.

The devices are discussed together to compare and contrast their $I - V$ characteristics; to demonstrate common features, and to show the relative importance of different current and voltage terms on the $I - V$ curves. The common structural values for both devices are:

Substrate acceptor doping density - $N_a = 10^{19} cm^{-3}$,

Oxide thickness - $d_{ox} = 25\AA$

Work function - $\Phi_M = 4.4eV$

n-type epitaxial layer width - $W_{epi} = 5\mu m$.

n-type layer doping for the lightly doped device - $N_d = 10^{15}cm^{-3}$

n-type layer doping for the heavily doped device - $N_d = 10^{17}cm^{-3}$

Other physical constants are given in Appendix F.

The differences in the $I - V$ characteristics for the two devices are shown clearly in Fig 3.4. At the switching point, the current and potential drop are greater for the lightly doped device. At the holding point, the potential drop is the same for both devices but the heavily doped MISS has a much greater holding current. Comparing the two $I - V$ curves shows the heavily doped MISS to have a lower negative differential impedance which extends across a greater current range.

In discussion, together with absolute values of the various calculated current and voltage components, use is made of what are termed the 'pn multiplication factor' g_j, and the 'MIS multiplication factor' g_s. These are used to demonstrate the differential changes in the relative electron and hole current magnitudes between consecutive calculated operating points for the pn junction and MIS regions of the device. They are defined as follows:

$$g_s = \frac{dJ_{tn}}{dJ_{tp}} \qquad 3.8.1$$

for the MIS multiplication factor and

$$g_j = \frac{dJ_{pj}}{d(J_{rj} + J_{rec} + J_{ns})} \qquad 3.8.2$$

for the pn multiplication factor. These were termed small signal gains by Habib

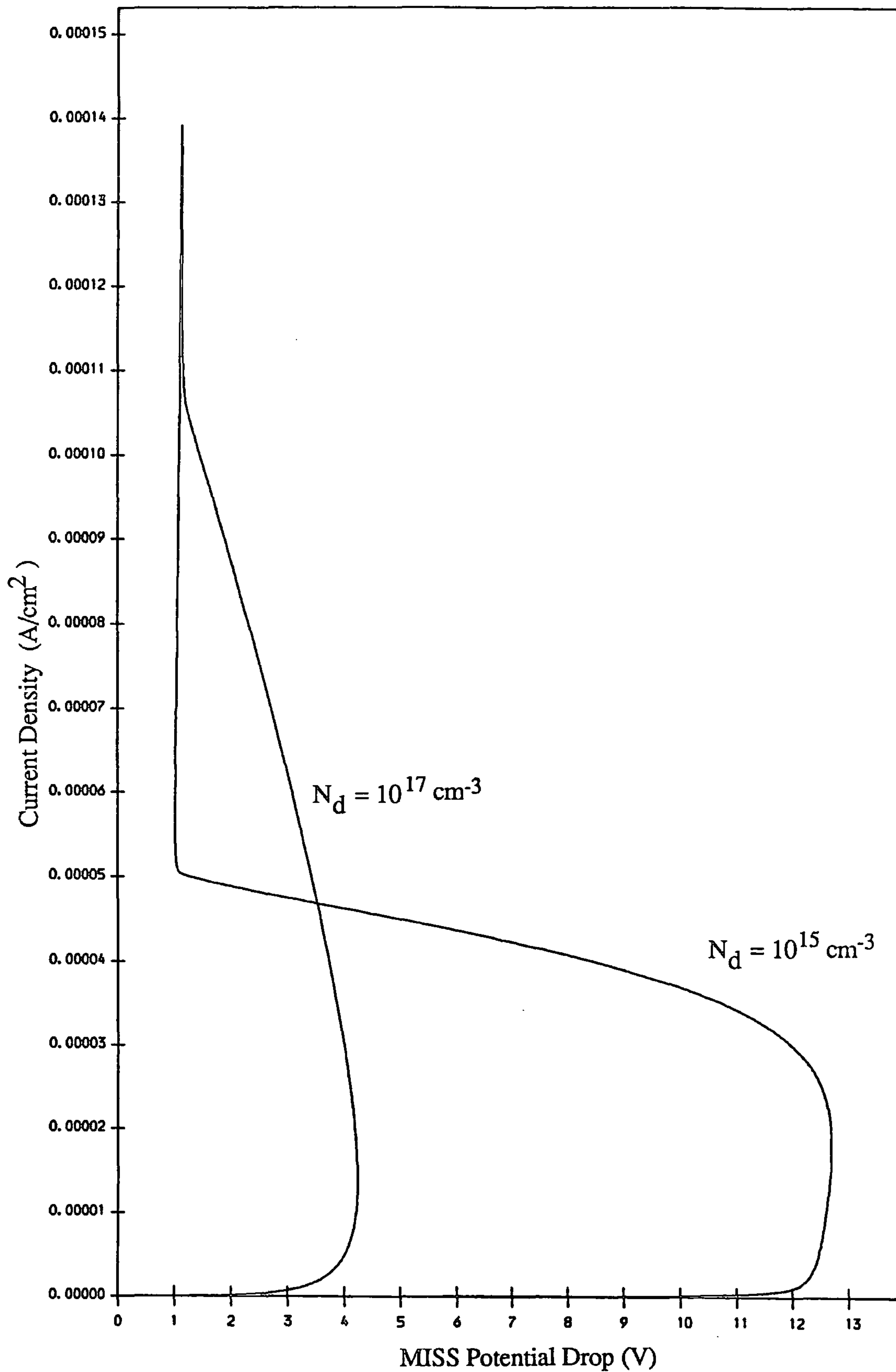

Fig 3.4: I-V Characteristics for the Lightly and Heavily Doped n-type Layer Devices.

[10].

On examining equations (3.6.1) and (3.6.2) it can be seen that

$$M_n dJ_{tn} + (M_p - 1)dJ_{pj} + dJ_g = dJ_{rj} + dJ_{rec} + dJ_{ns} \qquad 3.8.3$$

for electrons, and

$$M_p dJ_{pj} + (M_n - 1)dJ_{tn} + dJ_g = dJ_{tp} \qquad 3.8.4$$

for holes, where it is assumed that the values for the multiplication factors M_n and M_p are constant between two successive calculated operating points. By setting $M_n = M_p = 1$, and $dJ_g = 0$, it can be seen that $g_s = g_j^{-1}$, or alternatively, $g_s g_j = 1$. Therefore any move away from this relation demonstrates the effect of the generation current and/or avalanching on the current voltage characteristic of a particular device.

When discussing the computed $I - V$ characteristics, references to changes in current or voltage components is always w.r.t. stable operating points. Arrows on any computed curves follow the increasing total device current J_{tot}.

3.8.1 The Lightly Doped Device

To allow a closer examination of the lightly doped device using g_j and g_s, it is necessary to produce an expression in which (3.8.3) and (3.8.4) are combined. For the lightly doped device, avalanching is not expected in the MIS depletion region, therefore by setting $M_n = M_p = 1$ in (3.8.3) and (3.8.4), rearranging, and introducing the symbol $dJ_{re} = dJ_{rj} + dJ_{rec} + dJ_{ns}$ gives

$$dJ_{tn} = dJ_{re} - dJ_g \qquad \text{and} \qquad dJ_{tp} = dJ_{pj} + dJ_g \qquad 3.8.5$$

By dividing these expressions, the two differential current continuity equations for the lightly doped device can be expressed in the form

$$g_s g_j + g_s \frac{dJ_g}{dJ_{re}} = 1 - \frac{dJ_g}{dJ_{re}} \qquad 3.8.6$$

Putting $dJ_g = 0$ in (3.8.6) gives $g_j g_s = 1$, and shows (3.8.6) to be consistent with the multiplication factor definitions (3.8.1) and (3.8.2).

3.8.1.1 The High Impedance OFF State

With the lightly doped device structure, the electron current in the MIS depletion layer throughout most of the OFF region (from the point of zero applied potential across the device $V_{tot} = 0$, up to the switching point ($V_{tot} = V_S$) is dominated by the generation current J_g, as shown in Fig 3.5. For the pn region, the dominant electron current is J_{rj}, the pn depletion region recombination current, with the recombination currents in the neutral n-type epitaxial layer J_{rec}, and the substrate, J_{ns}, being negligible, Fig 3.6. The already small recombination current in the neutral region J_{rec} actually falls as the total potential drop increases towards the switching point, because the neutral region width is reduced by the growth of the MIS depletion layer.

In the OFF region, the electron tunnelling current J_{tn} is very small compared with the recombination current J_{rj}. To produce an electron current from the MIS region of the device equal to J_{rj}, the MIS depletion width increases so producing the generation current J_g which is equal to J_{rj} up until close to the switching point. Only as the switching point is approached does J_{tn} begin to dominate the electron current from the MIS region. For the lightly doped device,

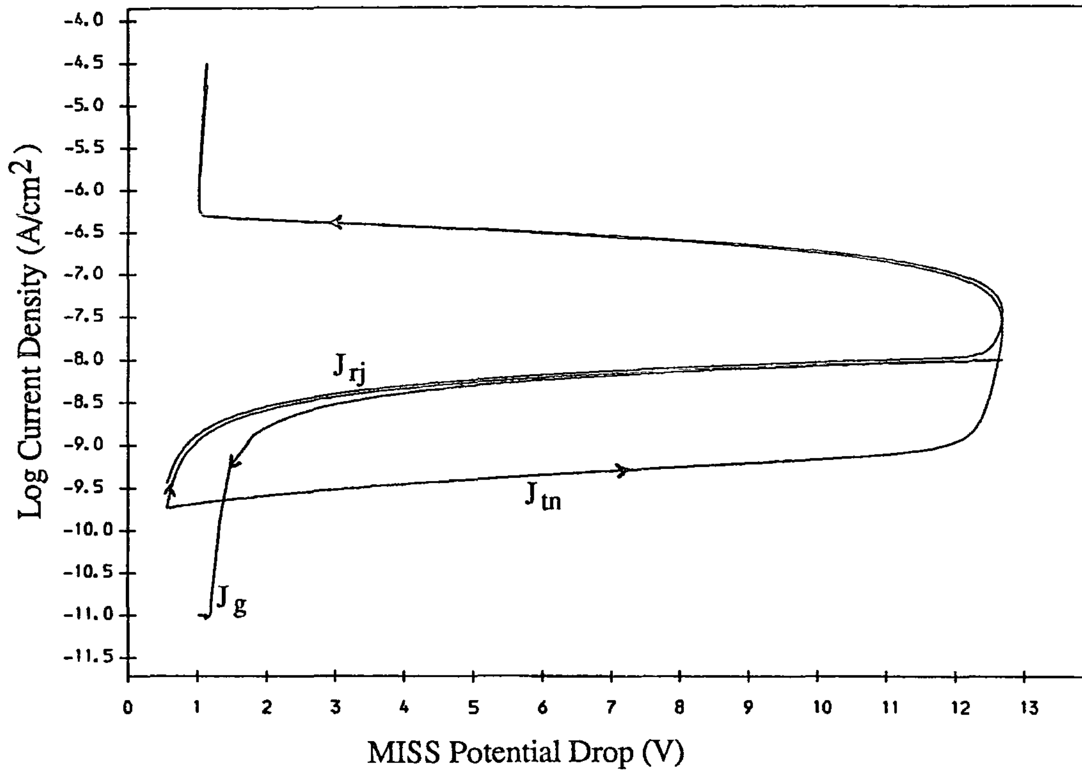

Fig 3.5: Electron Current Densities J_{tn}, J_{rj} and J_g for the Lightly Doped n-type Layer MISS.

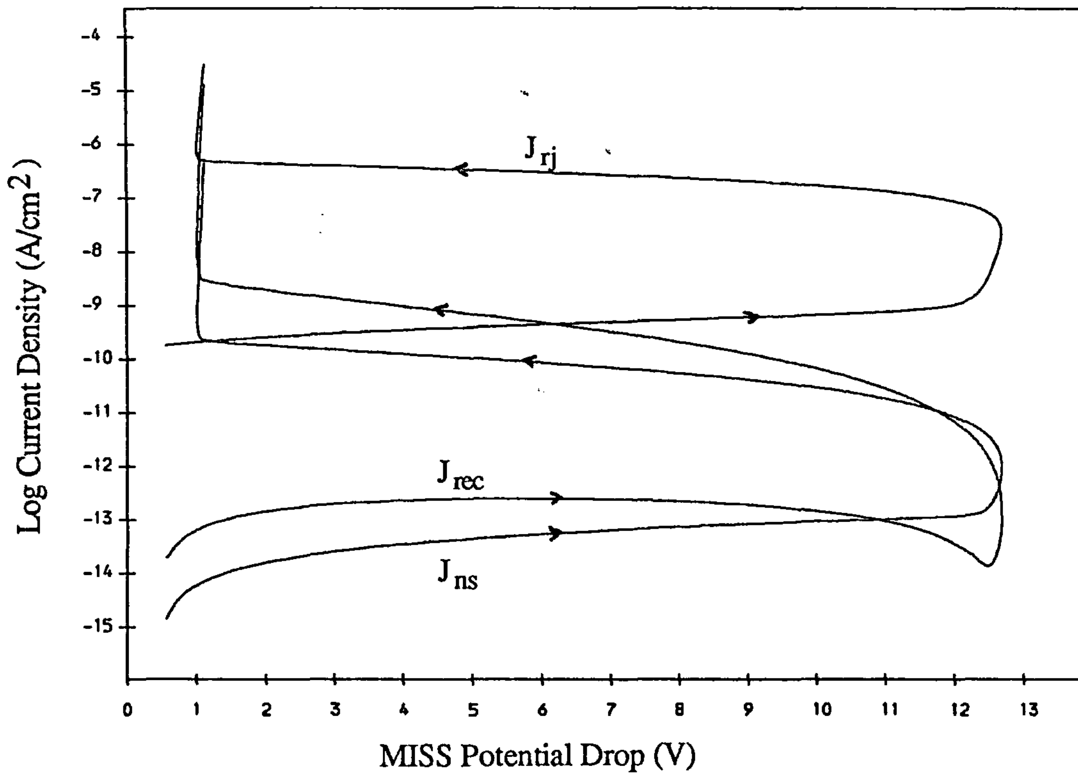

Fig 3.6: Electron Current Densities J_{rj}, J_{rec} and J_{ns} for the Lightly Doped n-type Layer MISS.

the OFF region would pass scarcely any electron current without this generation component, and the device would appear to be almost immediately in its ON state.

Total tunnelling current through the oxide in the OFF state is dominated by the hole tunnelling current, J_{tp}, as shown in Fig 3.7. The hole tunnel current is almost equal to the hole injected current J_{pj} from the *pn* junction throughout the OFF region except very close to the point where $V_{tot} = 0$, Fig 3.8. The hole tunnelling current is much larger than the electron tunnelling current J_{tn} in the OFF region, due to the metal Fermi level E_{fm} being opposite the semiconductor forbidden band, so restricting electron tunnelling into the semiconductor conduction band.

The growth of the MIS depletion region increases the injected hole flow into the MIS from the *pn* junction due to the closer proximity of the two depletion regions. This is in addition to the increase caused by the increasing forward potential V_f across the *pn* junction. Both these processes increase the hole concentration at the IS interface, and so increase both the hole tunnelling current and the oxide potential drop V_{ox}. However J_{tp} still dominates the total tunnel current even with the increase in V_{ox}, because it is only close to the switching point that the metal Fermi level is close enough to the silicon conduction band to allow significant electron tunnelling to occur.

In Fig 3.9, the multiplication factor product $g_j g_s$, and the total MISS potential drop V_{tot}, are plotted against the total device current J_{tot}. The effect of the generation current can be seen immediately by viewing the the shape of the multiplication product against the form of the expression (3.8.6). The value for g_s is

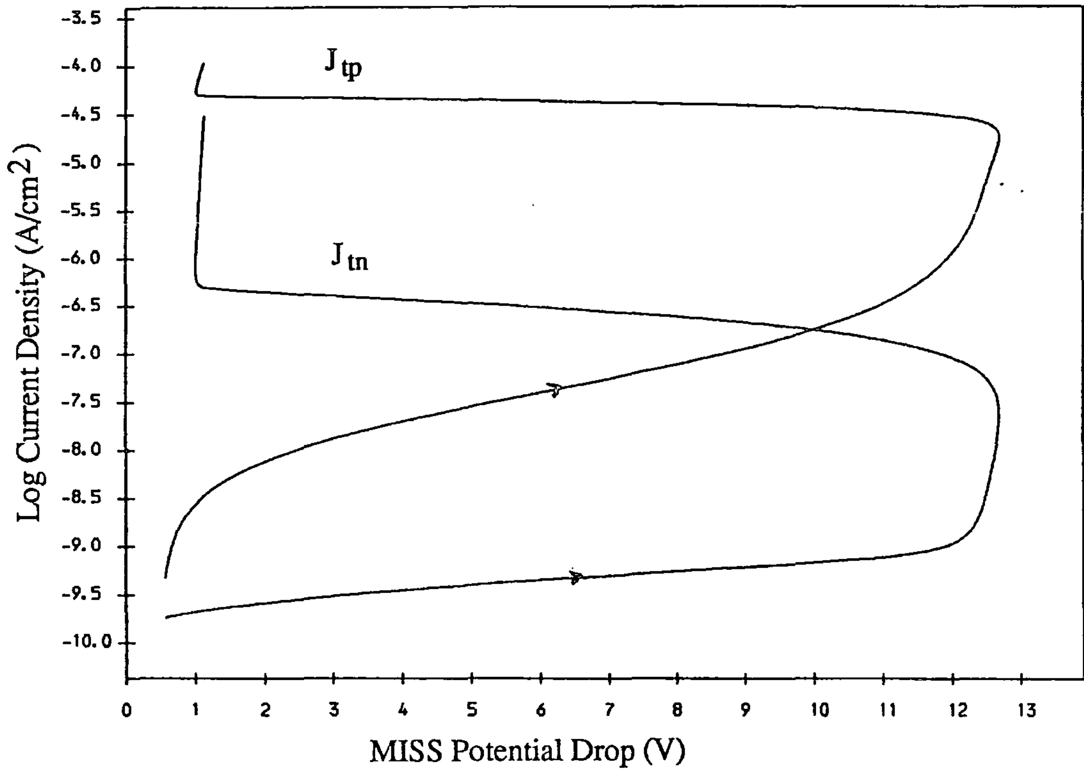

Fig 3.7: Electron and Hole Tunnel Currents, J_{tn} and J_{tp} for the Lightly Doped n-type Layer MISS.

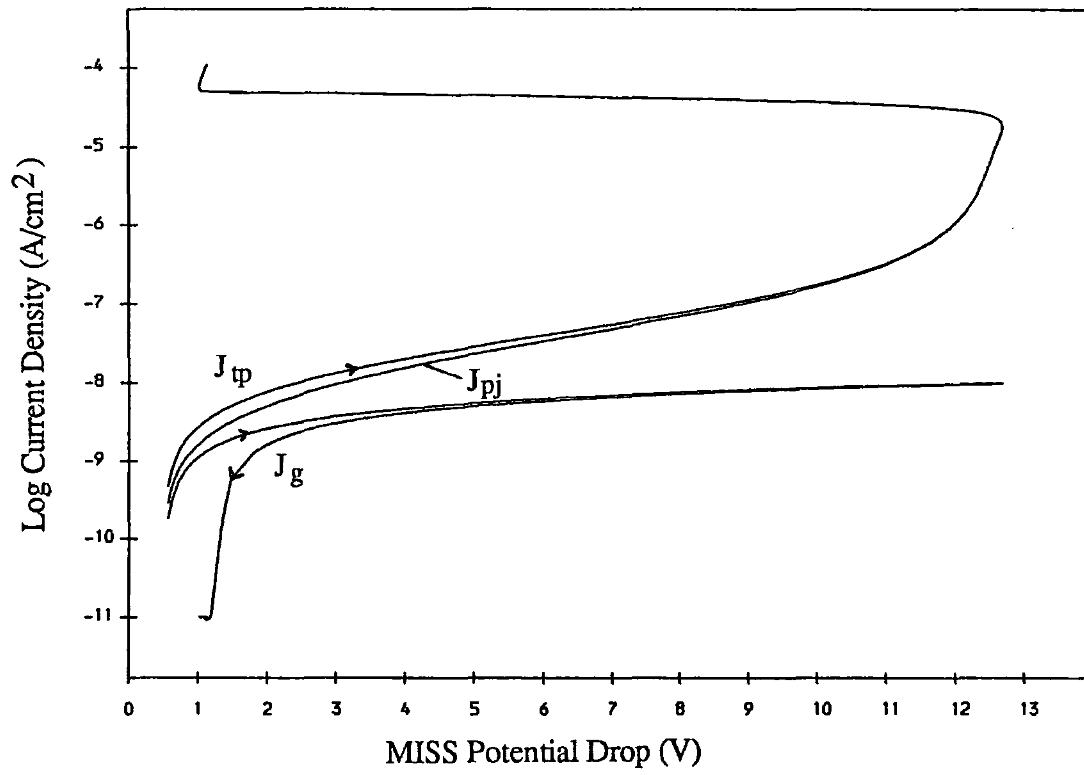

Fig 3.8: Hole Current Densities J_{tp}, J_{pj} and J_g for the Lightly Doped n-type Layer MISS.

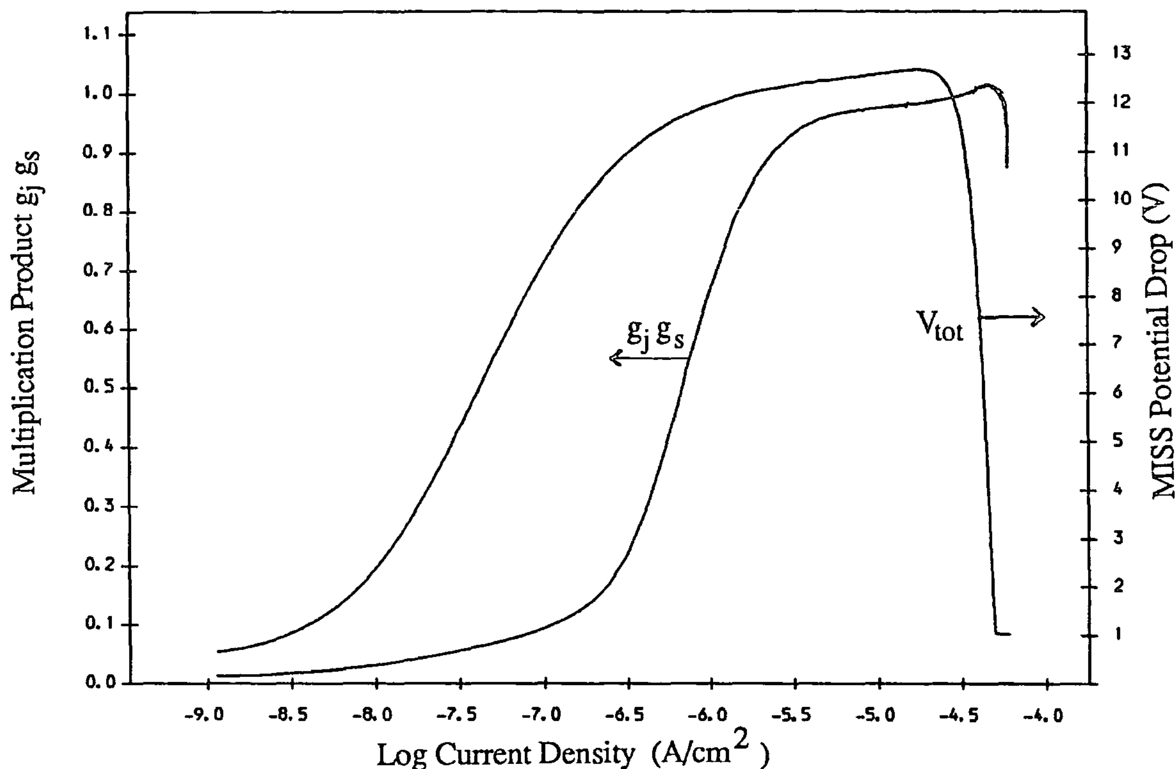

Fig 3.9: Multiplication Factor Product and Total Potential Drop against Current Density for the Lightly Doped n-type Layer MISS

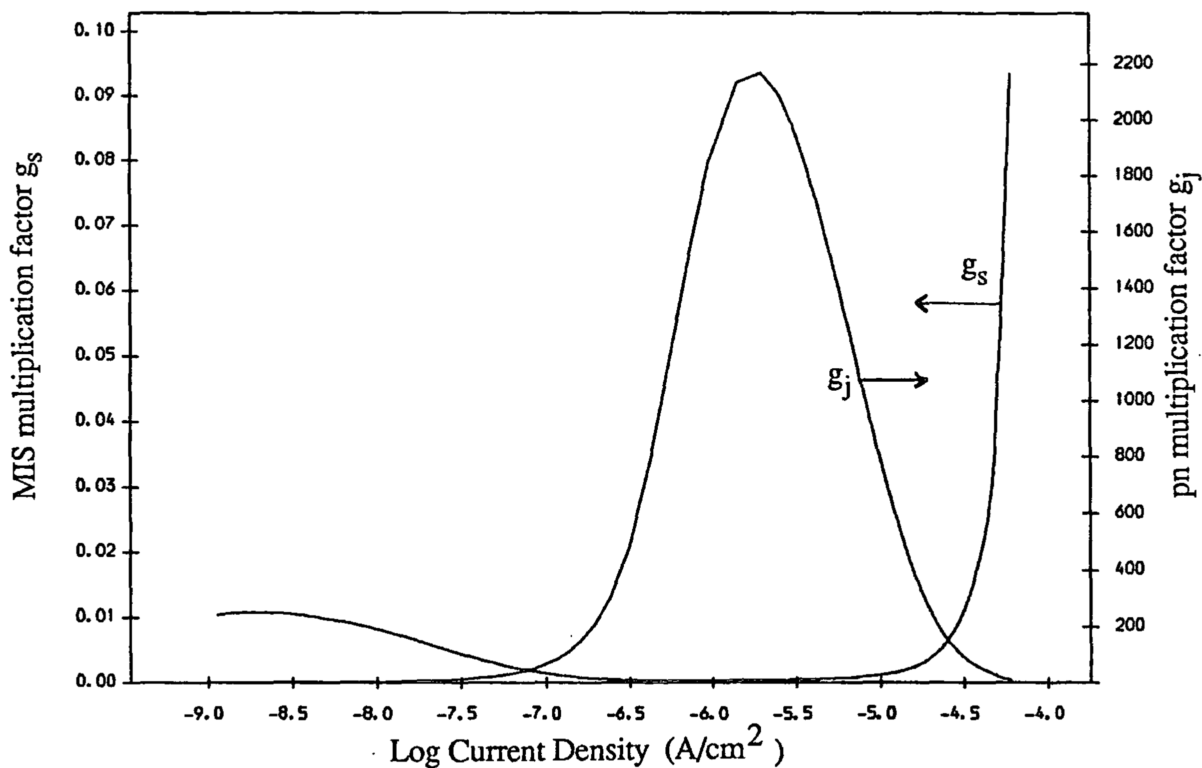

Fig 3.10: MIS and pn Multiplication Factors against Current Density for the Lightly Doped n-type Layer MISS.

negligible until very close to the switching point because of the very small changes in J_{tn} relative to J_{tp} Fig 3.10. Because the electron recombination current in the pn region J_{re} is provided almost totally by the generation current J_g, the right hand side of (3.8.6) is almost zero accounting for the very small value of $g_j g_s$ until close to the switching point. In Fig 3.10 it can be seen that the pn multiplication factor g_j rises very rapidly as the switching point is approached, and this is due to the rapidly increasing hole injected current as the two depletion regions approach each other.

3.8.1.2 The Vicinity of the Switching Point

At the switching point, the potential drop across the MISS reaches a local maximum. As can be seen in Fig 3.4, the device has a potential drop across it which is almost constant as the current increases up to the actual switching point, where the device moves into its negative impedance region. This form of switching is termed punchthrough, and occurs due to the MIS depletion region reaching the pn depletion region which stops any further growth. The small increase in the device potential drop seen in the $I - V$ characteristic is now due to the increases in forward voltage across the pn junction and the oxide potential.

In Fig 3.5 it can be seen that the electron tunnelling current rapidly increases, overtaking the MIS generation current as the main contributory factor to the electron recombination currents in the pn region. The neutral region recombination current J_{rec} reaches a local minimum in the vicinity of the switching point due to the almost negligible width of the neutral region between the two depletion

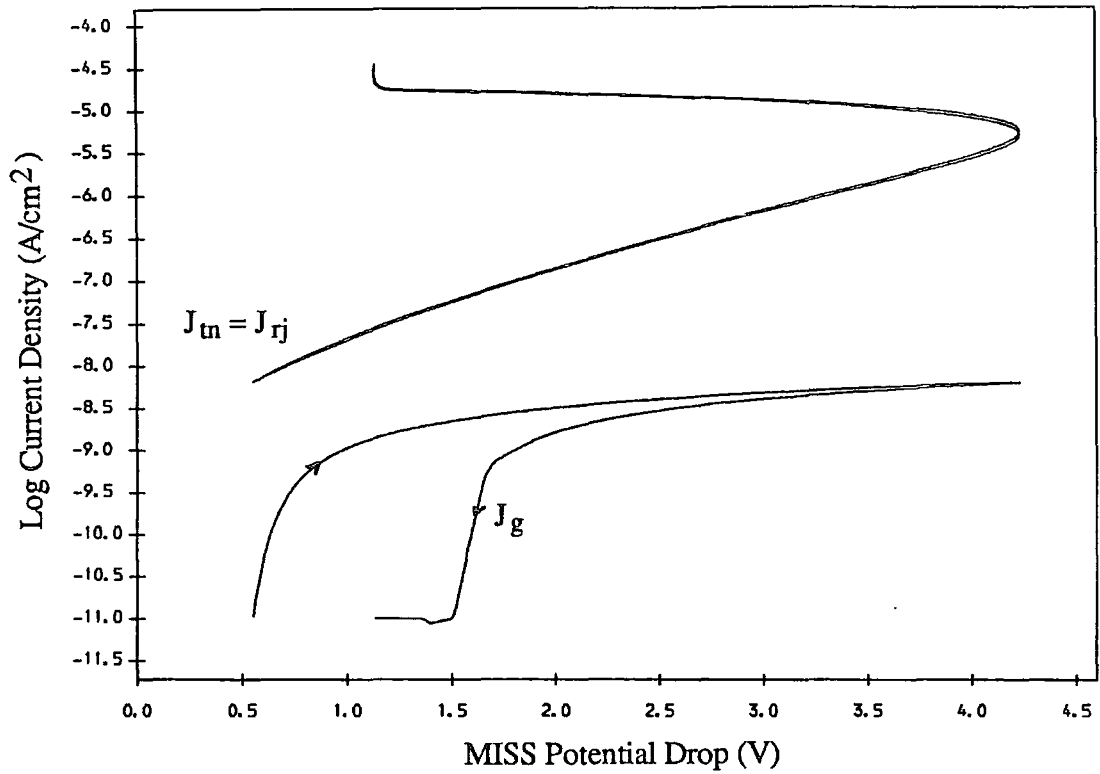

Fig 3.11: Electron Current Densities J_{tn}, J_{rj} and J_g for the Heavily Doped n-type Layer MISS.

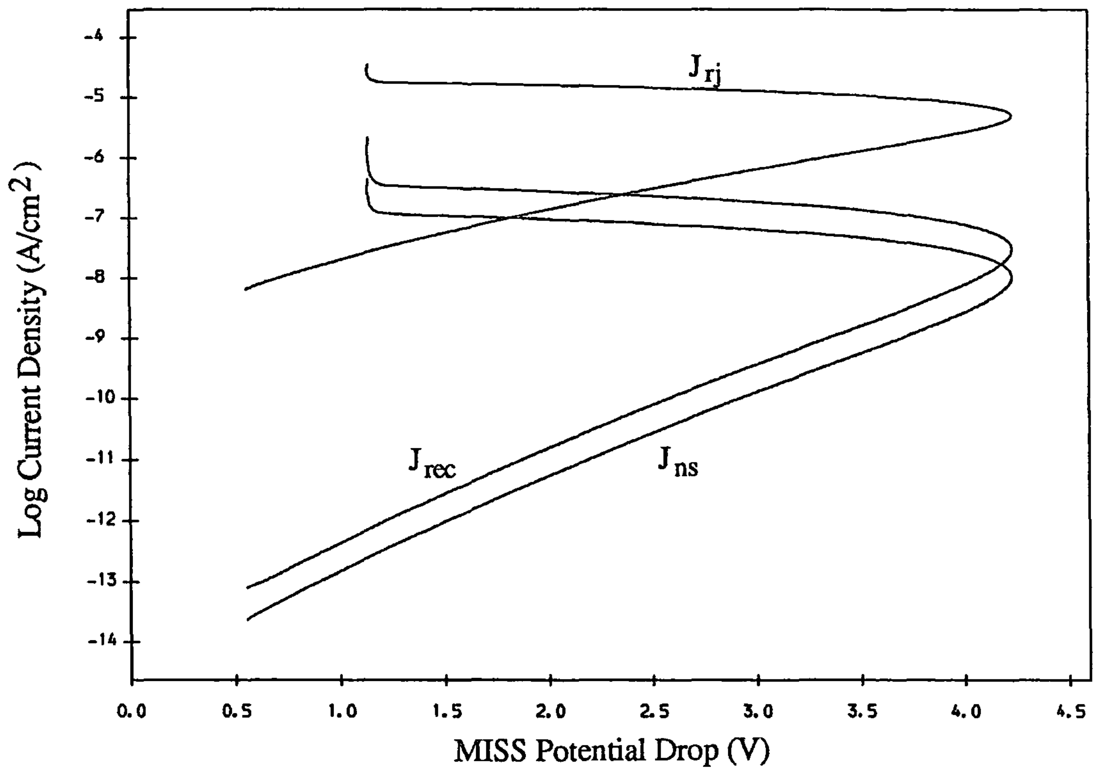

Fig 3.12: Electron Current Densities J_{rj}, J_{rec} and J_{ns} for the Heavily Doped n-type Layer MISS.

regions. Fig 3.6.

With E_{fm} close to the silicon conduction band, the effect of an increase in the hole concentration at the IS interface is now greater on J_{tn} through its effect on the oxide potential, than on J_{tp} through its effect on the tunnelling hole density. See Fig 3.7. This is in contrast to the OFF region where the reverse is the case. The hole injected current J_{pj} is now almost equal to the hole tunnel current, with the effect of the generation current being very small, even though it does reach a maximum with the MIS depletion width.

The multiplication product reaches unity at the switching point, with the generation current having reached a maximum causing $dJ_g = 0$, see Fig 3.9. The pn junction gain reaches a maximum in the vicinity of the switching point with very large changes in dJ_{pj} due to the closeness of the depletion regions. After a rapid increase, g_j declines again due to the MIS depletion region having reached its maximum width, after which it does not influence the increase in J_{pj} at the switching point; dJ_{pj} now being influenced solely by changes in the forward voltage across the pn junction.

3.8.1.3 The Negative Impedance Region

The MIS deep depletion layer begins to collapse in the negative impedance region so reducing the total potential drop across the device. As the current rises the hole injected current J_{pj} still increases even though the depletion regions are becoming further apart, because the potential across the pn junction, V_f, is also still increasing.

The increasing hole current J_{pj} causes a continuous increase in the hole concentration at the IS interface so increasing the electron tunnelling current through the oxide, J_{tn}. The two tunnelling currents, J_{tn}, and J_{tp}, the forward voltage V_f across the pn junction, the hole injected current J_{pj}, the pn junction depletion region recombination current J_{rj}, and the potential drop across the oxide V_{ox}, are all monotonically increasing functions of the total current flow J_{tot} through the device as shown in Figs 3.5-3.8. With the collapse of the MIS depletion region, but the continued increase in the major components of the current and hence in total current flow, the negative impedance characteristic is described.

For the lightly doped device, the pn junction multiplication factor g_j is reduced by three orders of magnitude between its maximum value close to the switching point, and the holding point Fig 3.10. This is caused by a fall in the relative increase of J_{pj} due to the increasing width of the n-type neutral region. The recombination current J_{rj} still dominates the total electron current in the pn part of the device, and increases exponentially with the forward voltage across the pn junction.

3.8.1.4 The Holding Point and Low Impedance ON State

At the holding point the device resumes its positive impedance. The MIS depletion region is still collapsing as the current increases in the ON state, but the sum of the increases in V_f and V_{ox} is now greater than the decrease in ψ_s. Because of the resulting very small change in total potential as the device current increases, the differential impedance of the device in the ON state is very low.

The pn multiplication factor, g_j, still decreases as the total current rises in the ON state while the electron recombination currents rise exponentially as V_f increases Fig 3.6. There is a smaller increase J_{pj} due to the decreasing width of the neutral region, and a far greater hole density at the edge of the MIS depletion region adjacent to the neutral region. In contrast, the MIS multiplication factor g_s increases rapidly in the ON state as the increasing oxide potential moves the metal Fermi level towards the semiconductor conduction band, producing the rapid current multiplication described by Green and Shewchun [3] for MIS diodes. This is demonstrated in Fig 3.10 where the MIS multiplication factor increases rapidly as the absolute electron tunnel current approaches that of the hole tunnel current.

3.8.2 The Heavily Doped Device

The MISS with a heavily doped ($10^{17} cm^{-3}$) n-type layer has a doping density two orders of magnitude greater than that for the lightly doped device. Ionised donors in the MIS depletion region now make a significant contribution to the oxide potential drop, in contrast to the lightly doped case. This can be seen immediately from a simple integration of Poisson's equation for the depletion layer taking into account only the effect of ionised donors. From the expression

$$\frac{d^2\psi}{dx^2} = -\frac{d\psi}{dx}\frac{d\mathcal{E}}{d\psi} = \mathcal{E}\frac{d\mathcal{E}}{d\psi} = -\frac{qN_d}{\epsilon_s} \qquad 3.8.7$$

the electric field at the IS interface due to a potential drop ψ_s in an MIS depletion

region is found to be

$$\mathcal{E}_s = \sqrt{\frac{2q}{\epsilon_s}(N_d|\psi_s|)} \qquad 3.8.8$$

This demonstrates that the IS interface electric field $\mathcal{E}_s$, due to a specified MIS depletion region potential drop will increase as the square root of the doping density, so increasing the influence of ionised donors for a more heavily doped n-type layers on V_{ox}. This is different from the lightly doped case in which V_{ox} is dominated by hole collection at the IS interface.

Again, it is useful to express (3.8.3) and (3.8.4) in terms of g_j and g_s. For this case, by setting $dJ_g = 0$, which is a reasonable assumption close to the switching point, and as the device enters its ON region, the equations

$$M_n dJ_{tn} = dJ_{re} - (M_p - 1)dJ_{pj} \quad \text{and} \quad dJ_{tp} - (M_n - 1)dJ_{tn} = M_p dJ_{pj} \quad 3.8.9$$

result, and by dividing and rearranging these produces an expression of the form

$$(M_n + M_p - 1)g_j g_s + (M_n - 1)g_s + (M_p - 1)g_j = 1 \qquad 3.8.10$$

This expression is not applicable to the OFF state due to the relative magnitude of the generation current. However it can be used in the negative impedance region and the ON state, where J_g is negligible relative to other electron and hole currents.

3.8.2.1 The High Impedance OFF State

The MIS depletion layer is again the main source of potential drop across the device in the OFF state, but the electron tunnelling current is now the dominant

electron current in the MIS region, as opposed to generation for the lightly doped device. This is because the width of the MIS depletion region is an order of magnitude smaller for a specific value of ψ_s in the heavily doped device. The pn depletion region recombination current J_{rj}, is provided almost totally by the electron tunnelling current J_{tn}.

The importance of ionised donors in the MIS depletion region on the oxide electric field can be appreciated by looking at the MIS multiplication factor, g_s, in Fig 3.16. For this device in the OFF region, the electron tunnelling current J_{tn} dominates both the recombination current in the pn depletion region, J_{rj}, and the total current through the device J_{tot} as shown in Fig 3.11. Due to its dominance in the OFF state, g_s, is at its maximum near $V_{tot} = 0$. As the MIS depletion region begins to grow, g_s moves towards a local minimum before increasing and then decreasing as the switching point is reached. The decrease is due to an increase in the hole injected current towards the IS interface so increasing the hole tunnelling current J_{tp}. The four major currents in the heavily doped device are the the two tunnelling currents, J_{tn}, and J_{tp}, the hole injection current J_{pj}, and the pn depletion region recombination current J_{rj}. Apart from J_g which dominates J_{tp} at very small device potentials, the currents which dictate how the device behaves in the OFF state are those mentioned above. See Figs 3.11-3.14.

3.8.2.2 The Vicinity of the Switching Point

At the switching point, hole collection at the IS interface results in an electric field of a comparable magnitude to that due to the ionised donors in the

MIS depletion region. As the injected hole current increases, the MIS depletion region begins to shrink so producing a switching characteristic. The effect of hole inversion can also be seen in Fig 3.13, in which the hole tunnelling current overtakes the electron tunnelling current as the hole density at the IS interface increases. With the more heavily doped n-type layer, avalanche multiplication can occur for a high potential drop across the MIS depletion region. However, for the device described, this does not have a significant effect on the computed $I - V$ characteristic.

The form of the multiplication product $g_j g_s$, is markedly different to that for the lightly doped device. With avalanche multiplication present $g_j g_s$ is less than one prior to switching and only reaches one in the negative impedance region Fig 3.15. This is in contrast to the lightly doped case in which $g_j g_s$ reaches one at the switching point due to the generation current reaching a maximum. The multiplication factors g_j and g_s must not be confused with the avalanche multiplication factors M_n and M_p described in Appendix D.

For the heavily doped device at the switching point, the pn junction multiplication factor g_j is beginning to increase, reaching its maximum after switching. The MIS multiplication factor, g_s, is still decreasing slowly, almost reaching a minimum at the switching point, Fig.3.16.

In Fig 3.17 calculations were made to determine the $I - V$ characteristic for two MISS devices, both with the same physical parameters, but one exhibiting avalanche multiplication, and the other with the avalanche multiplication coefficients set to one. As can be seen, the effect of avalanching is only to reduce the switching voltage by $0.2V$ which suggests that it is the effect of the resultant

electric field due to ionised donors, rather than avalanching, which is the main factor determining the device switching voltage for this doping density and work function.

3.8.2.3 The Negative Impedance Region

For the heavily doped device, g_j and g_s behave in a markedly different manner to those calculated for the lightly doped structure. The *pn* junction multiplication factor g_j still moves towards a minimum as the holding point is approached, but part of the way through the negative impedance region it reaches a maximum. This is due to the increasing hole current injected into the MIS depletion region as the forward potential across the *pn* junction increases, but with the width of the depletion region decreasing slowly, so allowing the injected current to reach a relative maximum.

The MIS multiplication factor, g_s, becomes less than one as the hole inversion layer increases at the IS interface, before beginning to increase again as the holding point is reached. This is also due to the increase in the inversion layer having less effect on the hole tunnelling than on the electron tunnelling current through its effect upon the oxide potential drop.

In the negative impedance region, J_{tp} is the dominant tunnelling current. The hole concentration at the IS interface increases as the $I - V$ characteristic moves through the negative impedance region. The increase in V_{ox} due to holes is offset by a decrease in the electric field contribution from ionised donors.

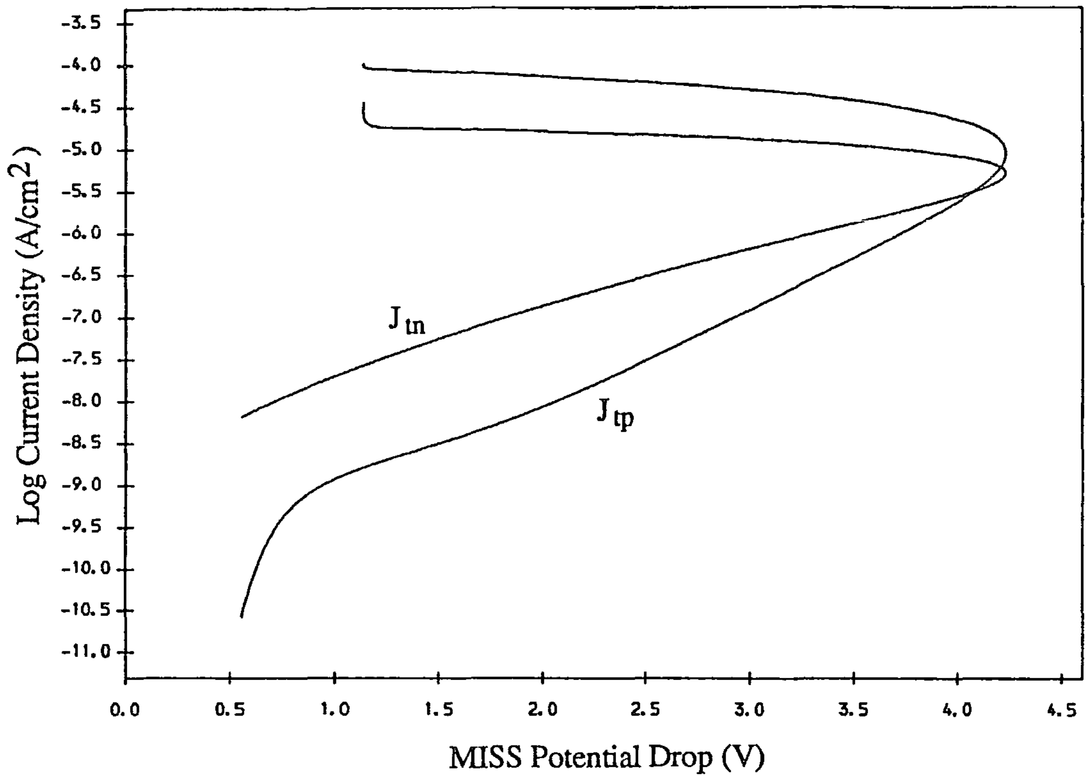

Fig 3.13: Electron and Hole Tunnel Currents J_{tn} and J_{tp} for the Heavily Doped n-type Layer MISS.

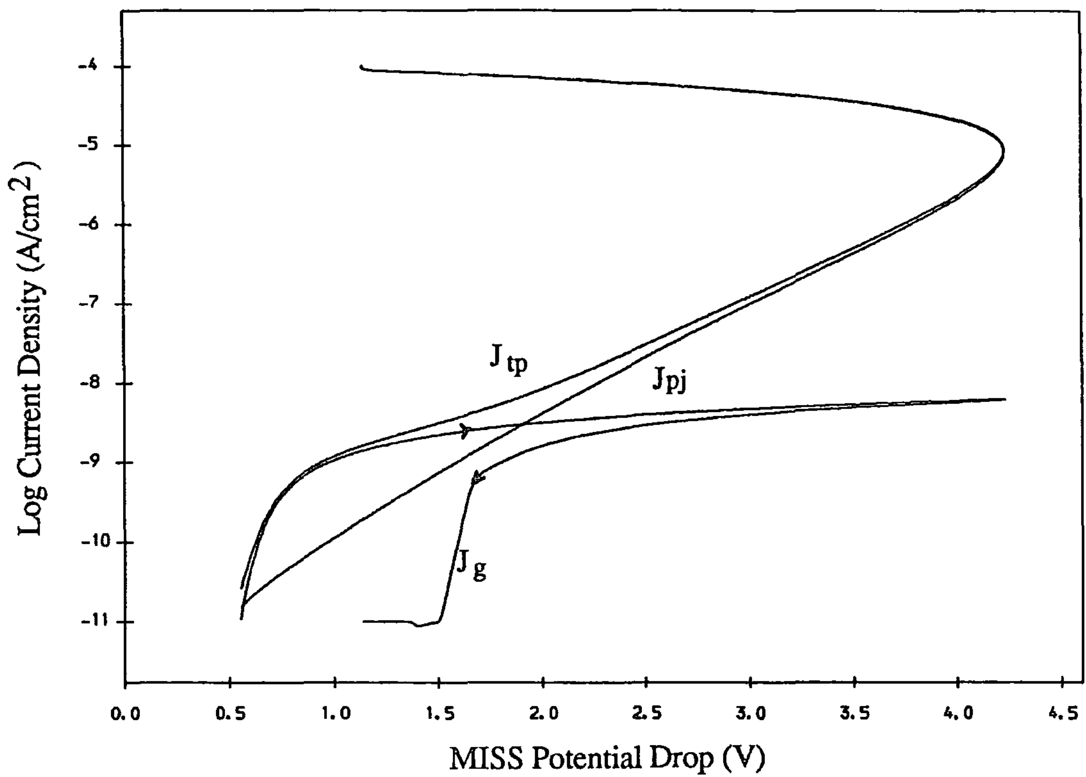

Fig 3.14: Hole Currents Densities J_{tp}, J_{pj} and J_g for the Heavily Doped n-type Layer MISS.

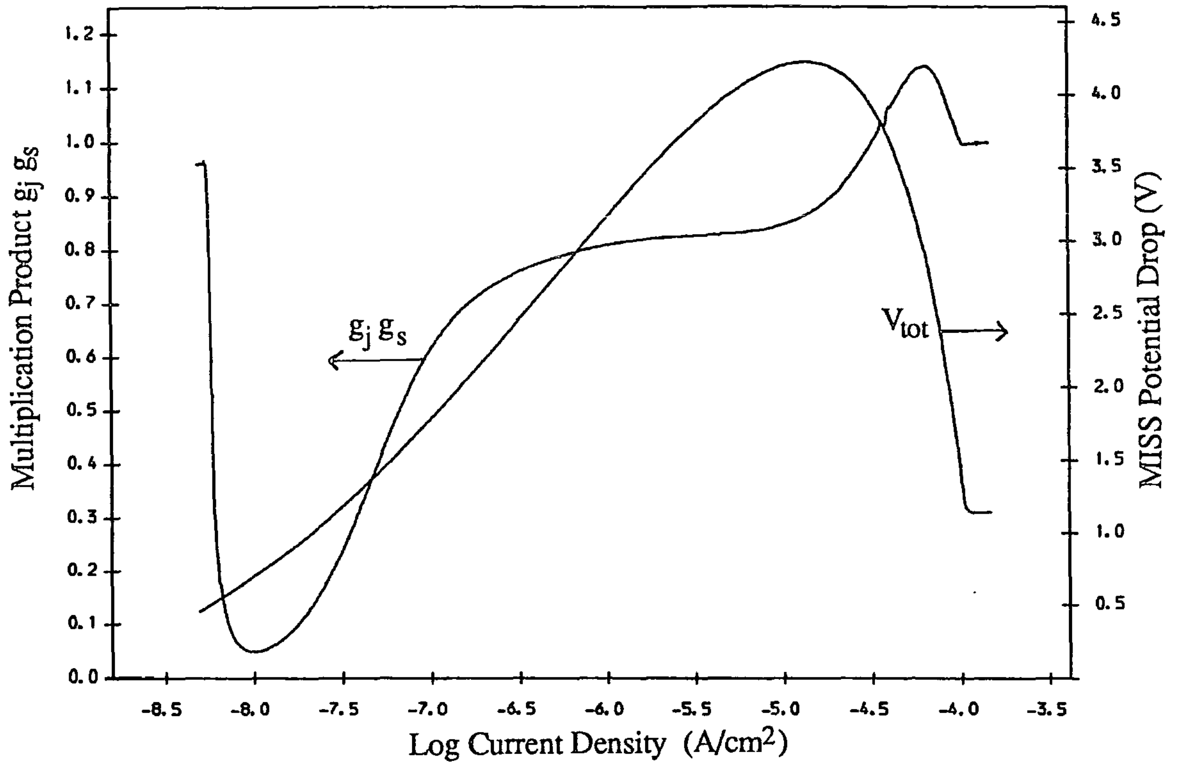

Fig 3.15: Multiplication Factor Product and Total Potential Drop against Current Density for the Heavily Doped n-type Layer MISS.

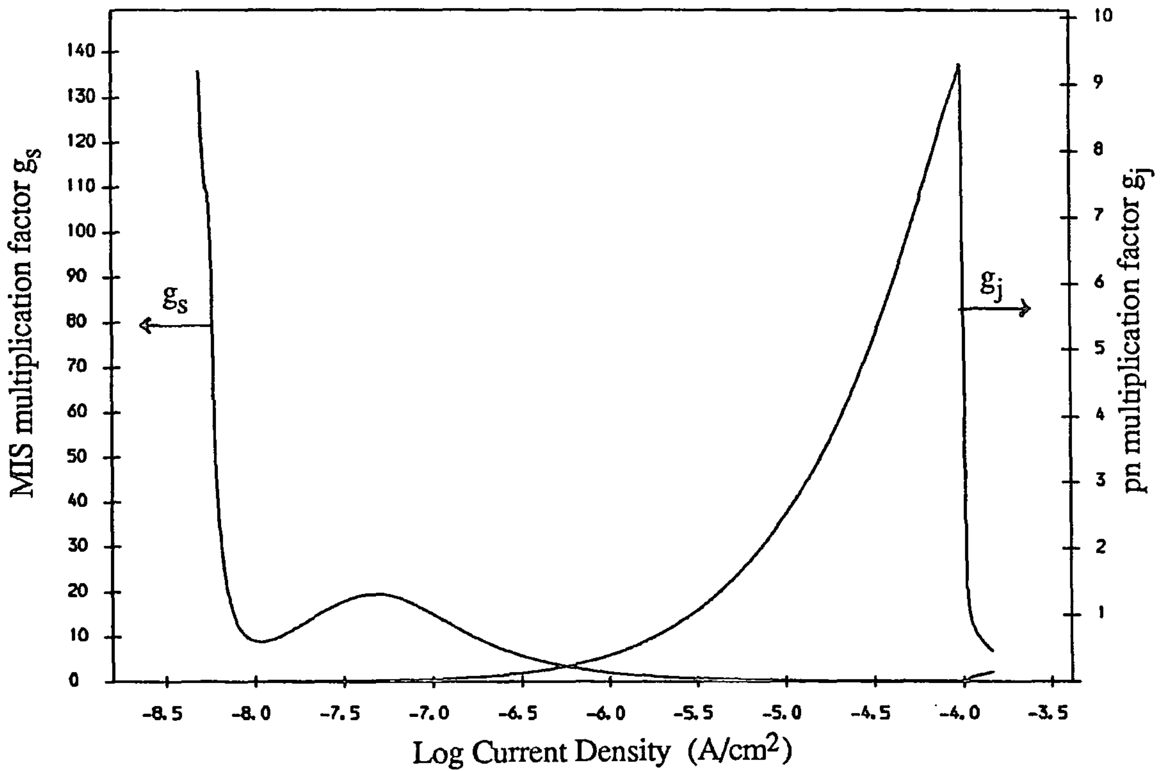

Fig 3.16: MIS and pn Multiplication Factors against Current Density for the Heavily Doped n-type Layer MISS.

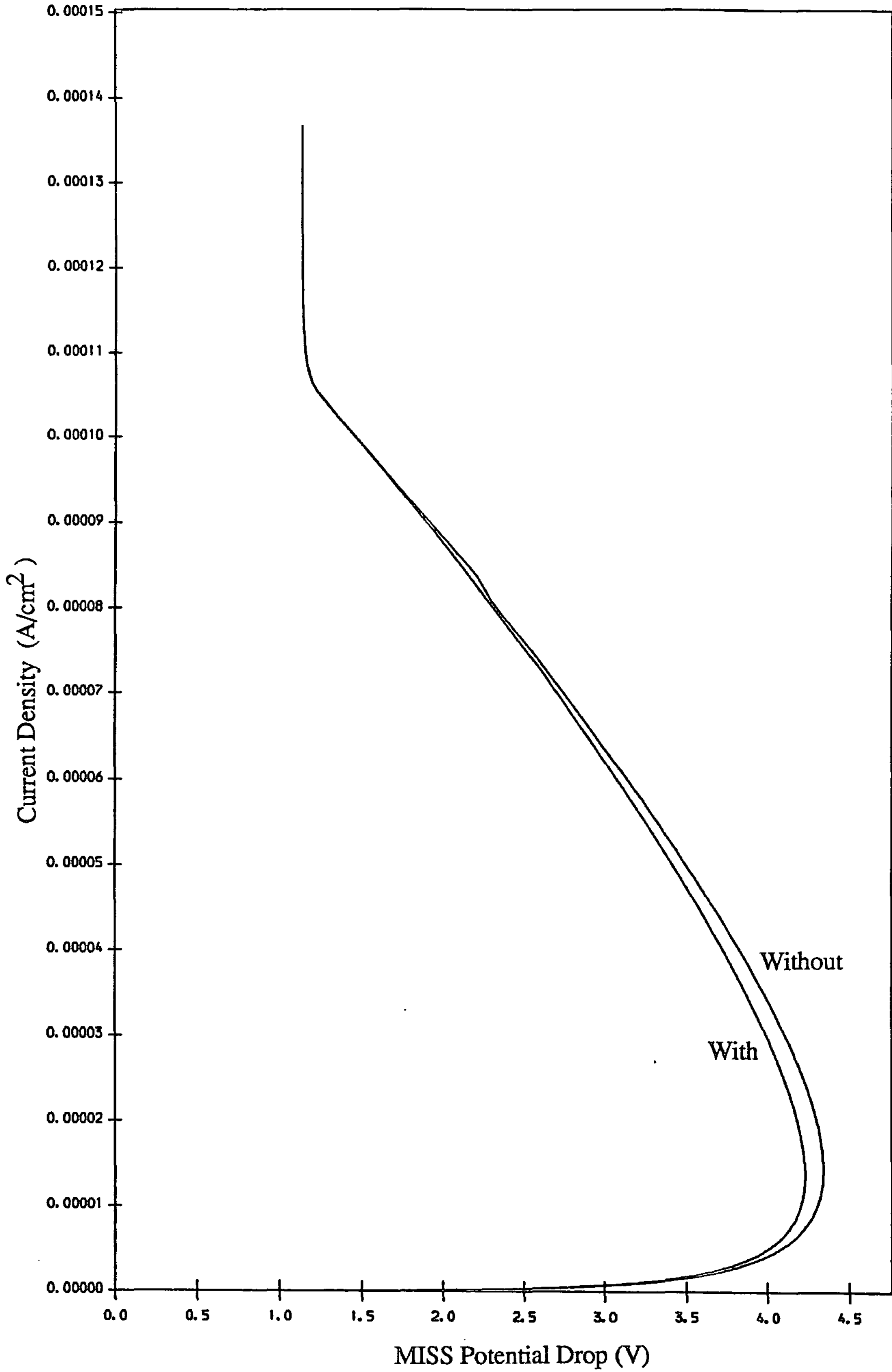

Fig 3.17: I-V Characteristics for the Heavily Doped n-type Layer MISS Calculated With and Without Avalanche Multiplication.

3.8.2.4 The Holding Point and Low Impedance ON State

For the heavily doped device at the holding point, J_{pj}, J_{rj}, J_{tp} and J_{tn} dominate the pn region and MIS region current components. As can be seen in Fig 3.13, J_{tp} is greater than J_{tn} at the holding point and moving into the ON state. However, this is not an essential feature of device operation, and for devices with metal electrodes of lower work functions it is not the case as will be shown in chapter five. The pn multiplication factor also decreases in the ON region for the same reason as for the lightly doped device. In this case, the MIS multiplication factor having reached a minimum begins to increase rapidly again as the hole inversion layer at the IS interface develops, producing a sharp increase in the electron tunnelling current Fig 3.16.

3.9 A Qualitative Interpretation of MISS Operation

An alternative approach to understanding the functioning of the two carrier currents in the MISS, is to handle each individually through indulgence in a gedanken experiment. This involves seperating the electron and hole current components to assess how each would find an equilibrium operating point for fixed values of ψ_s and V_{ox}.

Initially, consider the device with its electron current set to zero, and suppose that a fixed hole current is injected into the MIS depletion region. This hole current causes an increase in hole concentration at the IS interface, and possibly inversion. The hole concentration settles down to allow the hole tunnel current

to become equal to the hole injected current. If the width of the depletion region is changed, so altering the electric field in the oxide, or hypothetically an oxide potential drop was imposed, the hole current can still settle down to an equilibrium value. The hole density would effect the oxide potential but this effect is a consequence of the accumulation of holes and is not itself necessary to promote hole tunnelling. The important point to note is that because hole collection is possible at the IS interface, the quantity of stored charge changes to allow an equilibrium point to be reached.

For electrons, the effect of a change in the potential drop across the MIS depletion region or the oxide is very different. Suppose a fixed electron current is flowing in the pn part of the device, for convenience expressed as J_{rj}. This needs to be equal to the sum of the electron tunnelling current and the generation current from the MIS depletion region, J_{tn} and J_g. Now the electron tunnel current is dependent upon oxide potential drop which in turn depends upon the depletion and inversion layer conditions. The generation current depends most importantly upon the width of the MIS depletion region. As can be seen, the electron current continuity is critically dependent upon ψ_s and V_{ox} Only one value of the oxide potential, and one value of the MIS depletion potential can be found to satisfy the condition for electron continuity, so that it is the electron current which really determines the potential drop through the device.

The two arguments can be summarised as follows: For hole continuity, though holes effect the potential across the device, a particular current can find an equilibrium point for many values of V_{ox}, and ψ_s. There is however only one pair of values for ψ_s and V_{ox} which allows a specified electron current to flow. Hence it is

the electron current that has the dominant controlling influence on the potential across the device.

3.10 Discussion

The MISS has been examined theoretically in one dimension using standard low current density semiconductor equations, and a well documented description of independent particle tunnelling for carrier transport through the oxide. The model has been constructed with as few approximations as possible, and uses the same equations for all parts of the current-voltage curve. By taking a fixed value of V_f, and assuming electron and hole current continuity, the $I - V$ curve has been computed.

In this chapter the behaviour of two typical devices has been examined to demonstrate the effects of lightly and heavily doped n-type layers on the device characteristics. Some of the more important points can be summarised as follows.

For the lightly doped device in the OFF region, the MIS region electron current is dominated by generation J_g. As the hole concentration increases at the IS interface, the change produced in J_{tp} is much greater than that in J_{tn}; the metal Fermi level E_{fm} being opposite the silicon forbidden band. At the switching point, hole collection now produces a much greater change in J_{tn} through its effect on V_{ox}, than on J_{tp} due to the hole density at the IS interface. In the negative impedance region, the MIS depletion region collapses to reduce the rate of increase in hole collection at the IS interface due to an increasing V_f. In the ON region, J_{tn} finally comes to dominate J_{tp}.

For the heavily doped device, the tunnelling current and total MIS region current are dominated by J_{tn} in the OFF region. Ionised donors in the MIS depletion region make the major contribution to the electric field at the IS interface, $\mathcal{E}_s$, with hole collection only becoming important close to the switching point. In the negative impedance region, hole collection becomes the dominant contributor to $\mathcal{E}_s$ with the decline in the MIS depletion region width. In the ON region, J_{tn} increases more rapidly than J_{tp}. Another important point to not for the heavily doped device is that avalanche multiplication is not necessary to cause switching. Therefore an expression for the switching voltage based upon avalanche multiplication is not an accurate description of the switching point [2].

In the computer model of Habib [10], the physical parameters chosen were markedly different to those used throughout this thesis. However a comparison has been made by utilising the initial conditions and constants used by Habib. This is shown in Fig 3.18. It can be seen that the two models are in quite close agreement for the calculated current-voltage curve of a lightly doped n-type layer device.

The ideas presented in this chapter are used throughout the text to analyse the behaviour of related device structures. When similar physical behaviour is encountered, the discussion will be a little more cursory than it has been here. The reader can however return to this chapter to clarify any details.

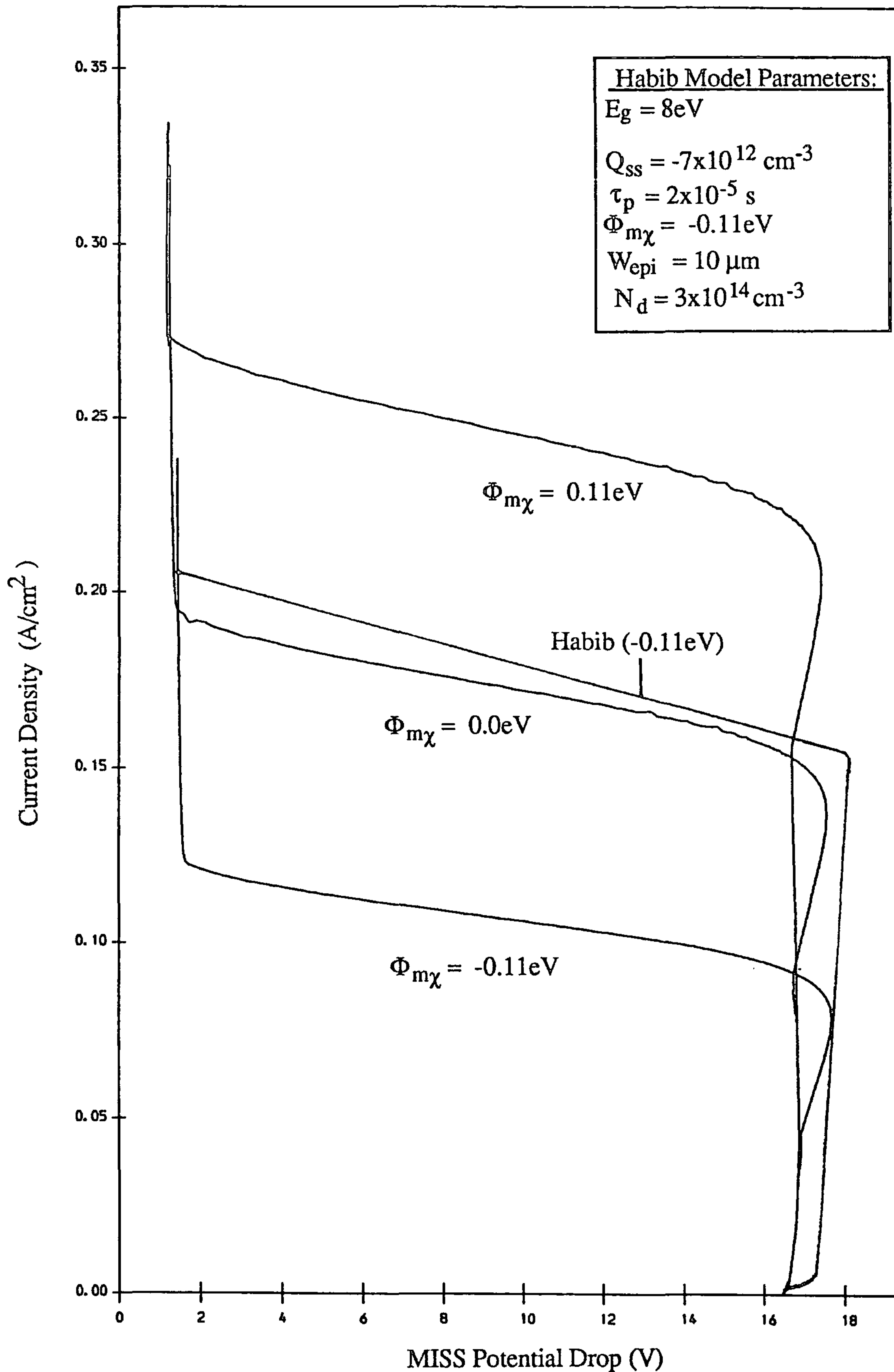

Fig 3.18: A Comparison of the Described MISS model with that due to Habib and Simmons using Similar Physical Parameters.

References

1. Habib, S. E-D. and Simmons, J. G., 'Theory of Switching in $p - n$ Insulator(Tunnel) Metal Devices Part 1, Punchthrough Mode', *Solid-St Electron.*, **22**, pp. 181-192, (1979).
2. Habib, S. E-D. and Simmons, J. G., 'Theory of Switching in $p - n$ Insulator(Tunnel) Metal Devices Part 2, Avalanche Mode', *Solid-St Electron.*, **23**, pp. 497-505, (1980).
3. Green, M. A. and Shewchun, J., 'Current Multiplication in Metal-Insulator-Semiconductor (MIS) Tunnel Diodes', *Solid-St. Electron.*, **17**, pp. 349-365, (1974).
4. Sze, S. M., *Physics of Semiconductor Devices*, Wiley, (1981).
5. Fiore De Mattos, A. C. and Sarrabayrouse, G., 'The MISS Device Modelling and Influence of Critical Parameters', *Phys. Stat. Sol.*, **87**, pp. 699-707, (1985).
6. 'A Hybrid Method for Non-Linear Equations', *Numerical Methods for Non-Linear Algebraic Equations*, Ed. Rabinowitz, P., Gordon and Breach, (1970).
7. Patterson, *Math. Comp*, **22**, pp 847-856, (1968).
8. Abramowitz, M., and Stegun, I. A., *Handbook of Mathematical Functions*, Dover Publications., p. 228, (1968).
9. Abramowitz, M., and Stegun, I. A., *Handbook of Mathematical Functions*, Dover Publications., p. 298, (1968).
10. Habib, S. E-D., *Ph.D. Thesis* , University of Toronto, (1980).
11. Grove, A. S., *Physics and Technology of Semiconductor Devices*, Wiley, (1967).

CHAPTER FOUR

RESULTS FOR THE ONE DIMENSIONAL M.I.S.S MODEL

4.1 Introduction

In this chapter the 1-D computer model is used to determine device behaviour for differing values of n-type layer doping density, metal work function, and oxide and n-type layer thicknesses. By examining the results obtained, further predictions can be made about behaviour for many other structural parameters, and the limitations of the one dimensional computer model can be explored. In the previous chapter, the functioning of two ideal devices was discussed: one with a lightly doped n-type layer ($10^{15} cm^{-3}$), the other with a heavily doped n-type layer ($10^{17} cm^{-3}$). Using these two structures some general ideas about MISS functioning were developed. In this chapter, these ideas are referred to in describing the different MISS structures. This is done either explicitly by name, or through a chapter reference. However, there is still a need for repetition of certain ideas to retain clarity.

The basic structural parameters for the devices modelled here are the same as for chapter 3:

i) Oxide Thickness, $d_{ox} = 25\mathring{A}$

ii) n-type layer thickness, $W_{epi} = 5\mu m$

iii) Work function, $W_f = 4.4eV$

The results discussed have been computed by varying each of the structural parameters individually, whilst keeping all others with their default magnitudes given above.

4.2 Effects of n-Type Layer Doping Density

The current-voltage curve changes considerably as the n-type layer doping density is altered, Figs 4.1(a) and 4.1(b). With the lightly doped n-type layer MISS, switching occurs at punchthrough. This is seen for doping densities of $5.10^{14}cm^{-3}$ and $10^{15}cm^{-3}$. There is a large increase in device current for an almost fixed potential at the switching point, compared to devices with greater n-type layer doping levels. This is due to the IS electric field $\mathcal{E}_s$ being totally dominated by the effect of hole collection at the IS interface. The switching voltage is strongly influenced by the width of the n-type layer, and the width of the pn junction depletion region, through their effect on the hole injected current J_{pj}.

With a more heavily doped n-type layer, the computed $I - V$ curve follows a steeper trajectory through the negative impedance region, and does not show the sharp increase in current for an almost fixed device potential seen for the lightly doped MISS at the switching point. This is because punchthrough does not take place. The $I - V$ characteristic for these intermediate doped devices with doping densities of $5.10^{15}cm^{-3}$, $10^{16}cm^{-3}$ and $5.10^{16}cm^{-3}$, can be seen in Figs 4.1(a) and 4.1(b). Ionised donor atoms in the MIS depletion region, in addition to hole collection, contribute to the oxide potential drop through their

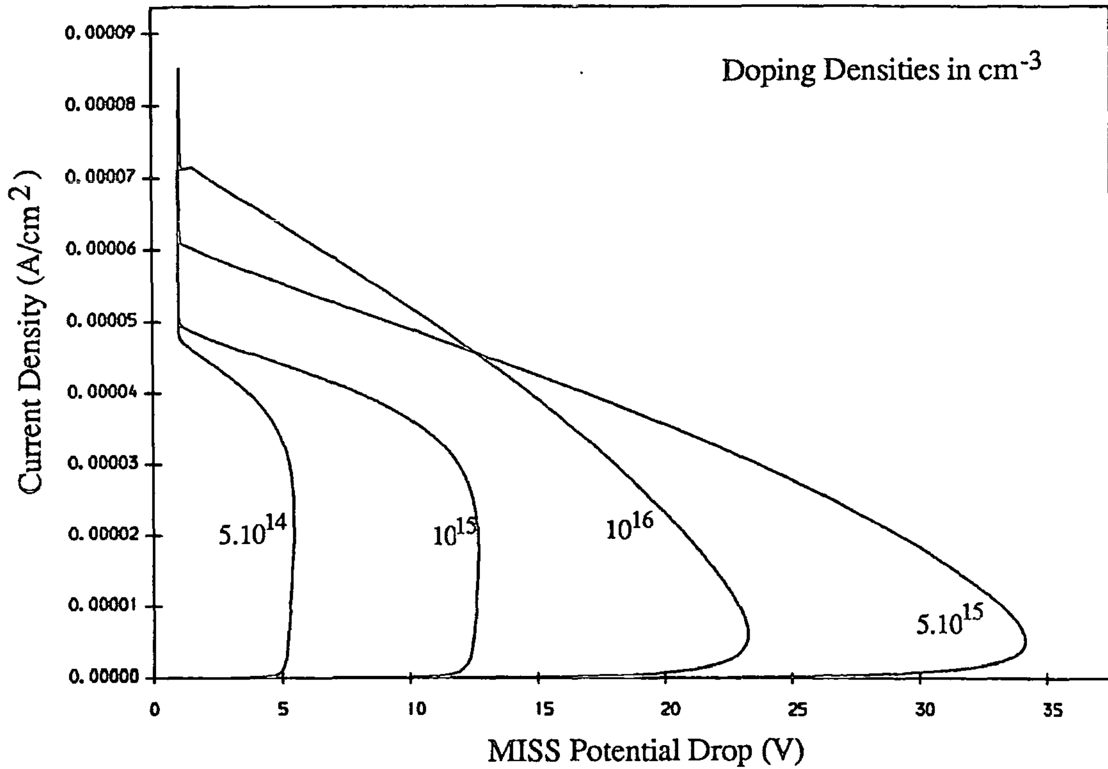

Fig 4.1(a): I-V Characteristics for Lightly Doped n-type Layer Devices.

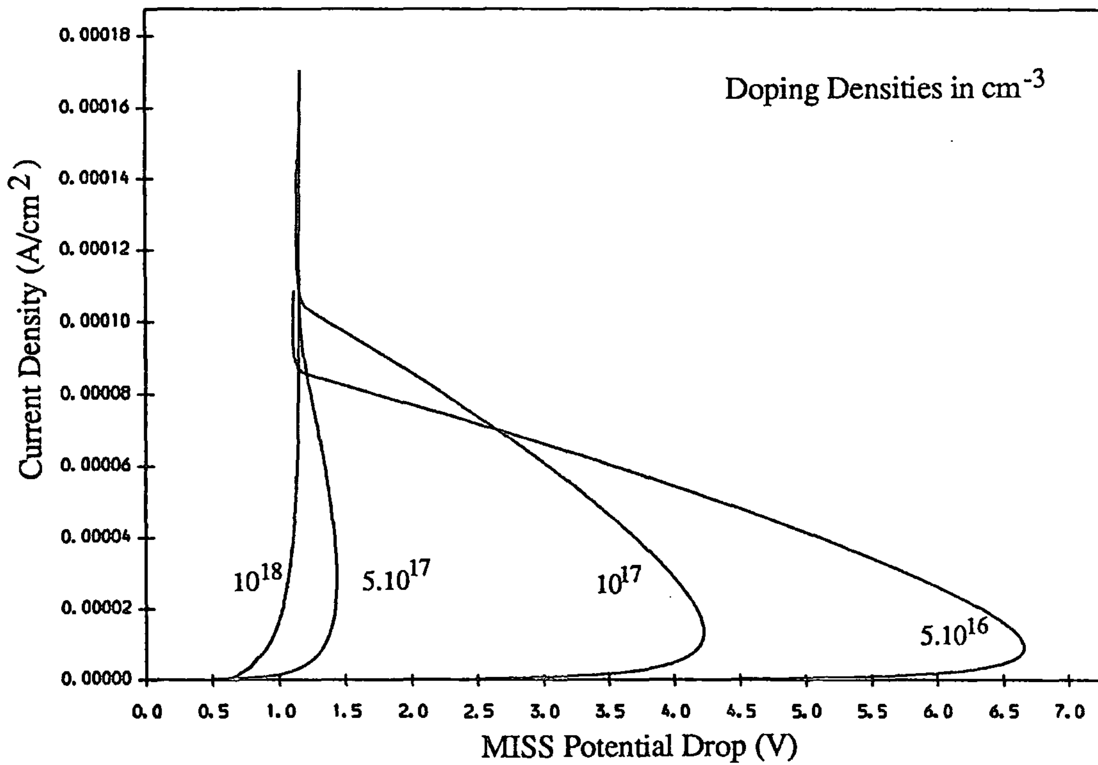

Fig 4.1(b): I-V Characteristics for Heavily Doped n-type Layer Devices.

effect on the electric field at the IS interface. The switching behaviour is similar to that described for the heavily doped MISS in chapter three.

The switching potential reaches a maximum for devices with an n-type layer doping level of $5.10^{15}cm^{-3}$, because the lower doping level makes the ionised donor contribution to $\mathcal{E}_s$ less than for the more heavily doped devices. This results in a wider depletion layer to provide both a greater ionised donor electric field together with a greater injected hole current J_{pj}. However, unlike the lightly doped case the MIS depletion region does not reach the pn depletion region. The switching voltage declines rapidly with increasing n-type layer doping density, because of the increasing influence of ionised donors.

For very high doping levels, the device displays hardly any switching characteristic. This can be seen for doping levels of $5.10^{17}cm^{-3}$ and $10^{18}cm^{-3}$, Fig 4.1(b), and can be understood from an examination of the expression for electric field produced by ionised donors. From the expression for the electric field due to ionised donors with a potential drop ψ_s,

$$\mathcal{E}_s = \sqrt{2q/\epsilon_s}\sqrt{N_d|\psi_s|} \qquad 4.2.1$$

it can be seen that at high doping levels, the contribution to $\mathcal{E}_s$ from the ionised donors is so great as to prevent the growth of a wider depletion region. This results in a diode type characteristic for very large n-type layer doping levels. From (4.2.1) it can be seen that the electric field in the MIS depletion region at the IS interface due to a potential drop ψ_s increases as the square root of the n-type layer doping density.

In Figs 4.1(a) and 4.1(b), the $I-V$ characteristics for a range of n-type layer doping values are demonstrated. However with the difference in scales on both

axes, it is difficult to make certain comparisons between the two sets of curves. In Figs 4.2(a) and 4.2(b) this is remedied by plotting the switching voltages and currents against doping density for about twenty device structures. The carrier lifetimes for differing n-type layer doping densities were obtained from Wolf [1], where the information was presented graphically. The lack of smoothness in the curves is attributable to the difficulty in reading the lifetimes from these curves.

The most important feature to note from these curves is that as functions of doping density, the switching voltage reaches a maximum at the same point as the switching current reaches a minimum. However, the holding current is a monotonic increasing function of n-type layer doping density.

For all devices, the total electric field in the oxide is the sum of two contributory factors: the electric field in the oxide due to ionised donors in the MIS depletion region, $\mathcal{E}_{dep}$, and the electric field in the oxide due to the hole inversion layer $\mathcal{E}_{inv}$. Together these provide the total oxide electric field $\mathcal{E}_{ox}$. Hence in terms of the depletion and inversion contributions, the oxide electric field can be written as

$$\mathcal{E}_{ox} = \mathcal{E}_{dep} + \mathcal{E}_{inv} = -V_{ox}/d_{ox} \qquad 4.2.2$$

These electric field contributions are resolved in Figs 4.3-4.6 for doping densities of $5.10^{14}cm^{-3}$, $5.10^{15}cm^{-3}$, $5.10^{16}cm^{-3}$ and $5.10^{17}cm^{-3}$. Arrows on the curves follow the increasing device current. These curves show the importance of ionised donors on $\mathcal{E}_{ox}$ at the switching point as the doping density increases. At the holding point the inversion layer dominates the oxide potential except for very heavily doped devices where switching is hardly seen.

With the lightly doped device, $< 5.10^{15}cm^{-3}$, the hole current dominates the

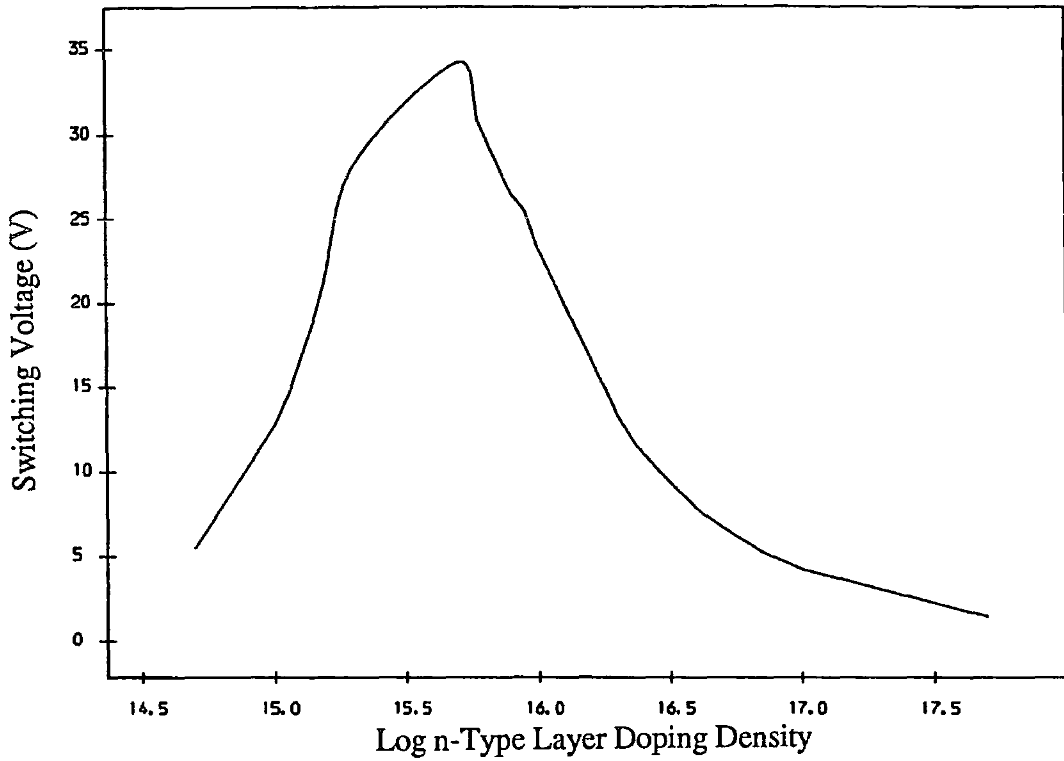

Fig 4.2(a): MISS Switching Voltage Against n-Type Layer Doping Density

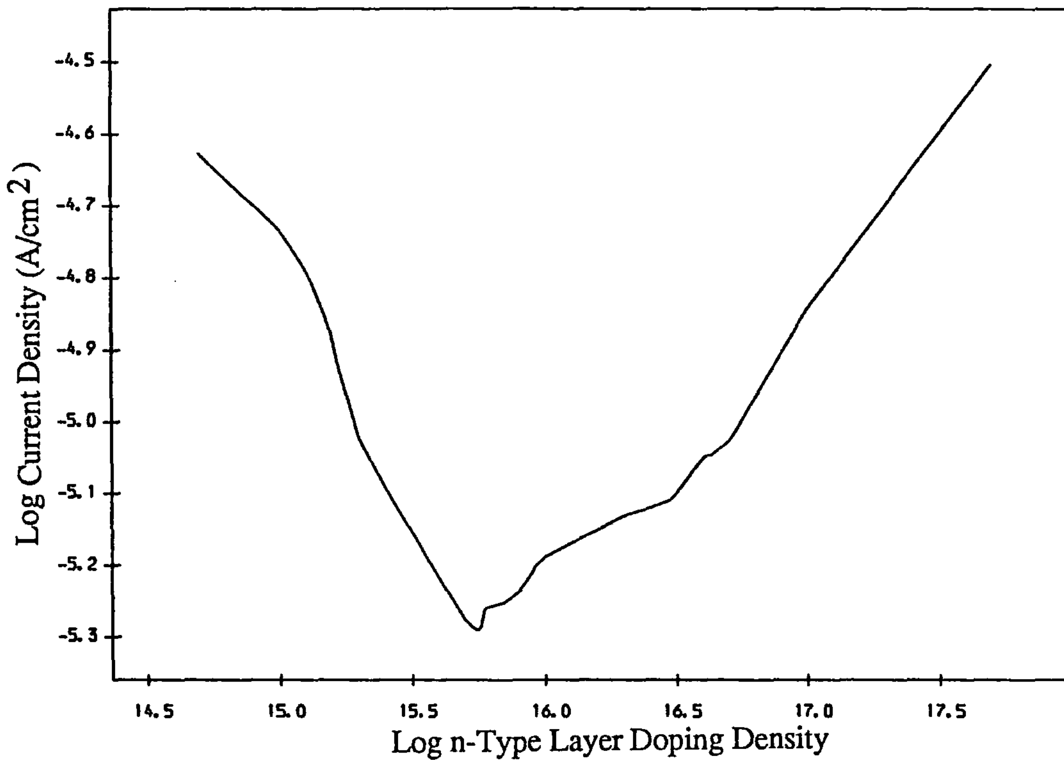

Fig 4.2(b): MISS Switching Current Against n-Type Layer Doping Density

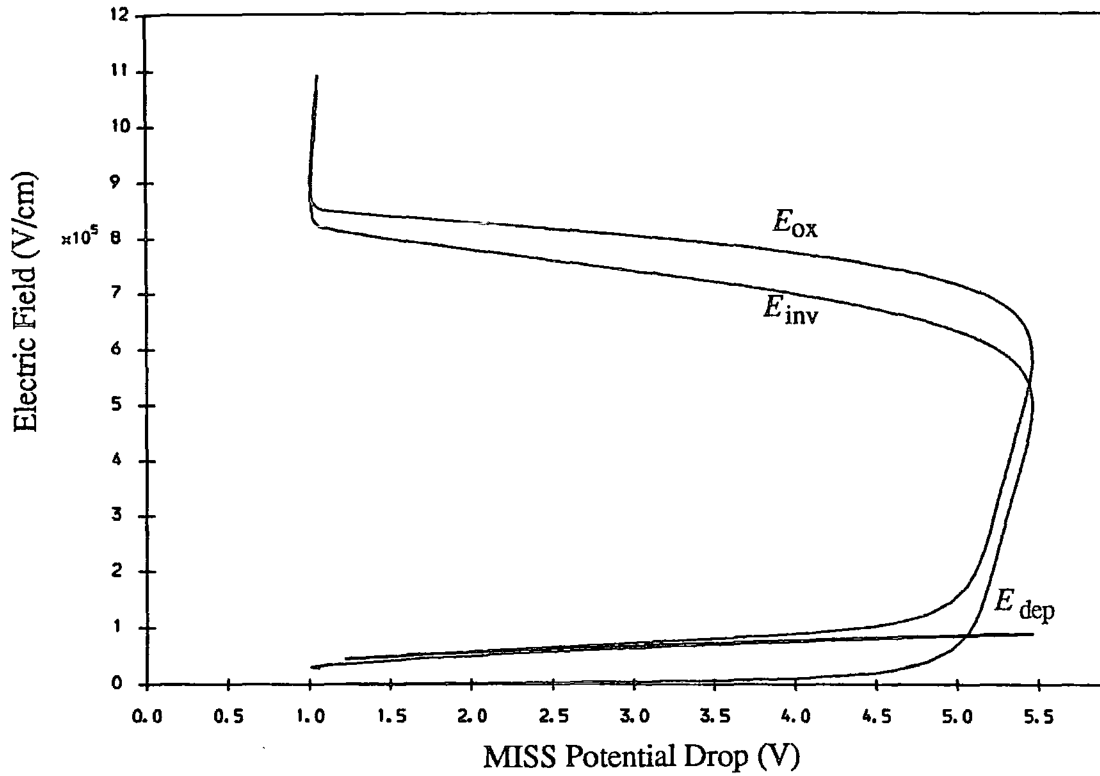

Fig 4.3: Oxide Electric Field Components for the 5.10^{14}cm^{-3} n-type Layer Doped MISS.

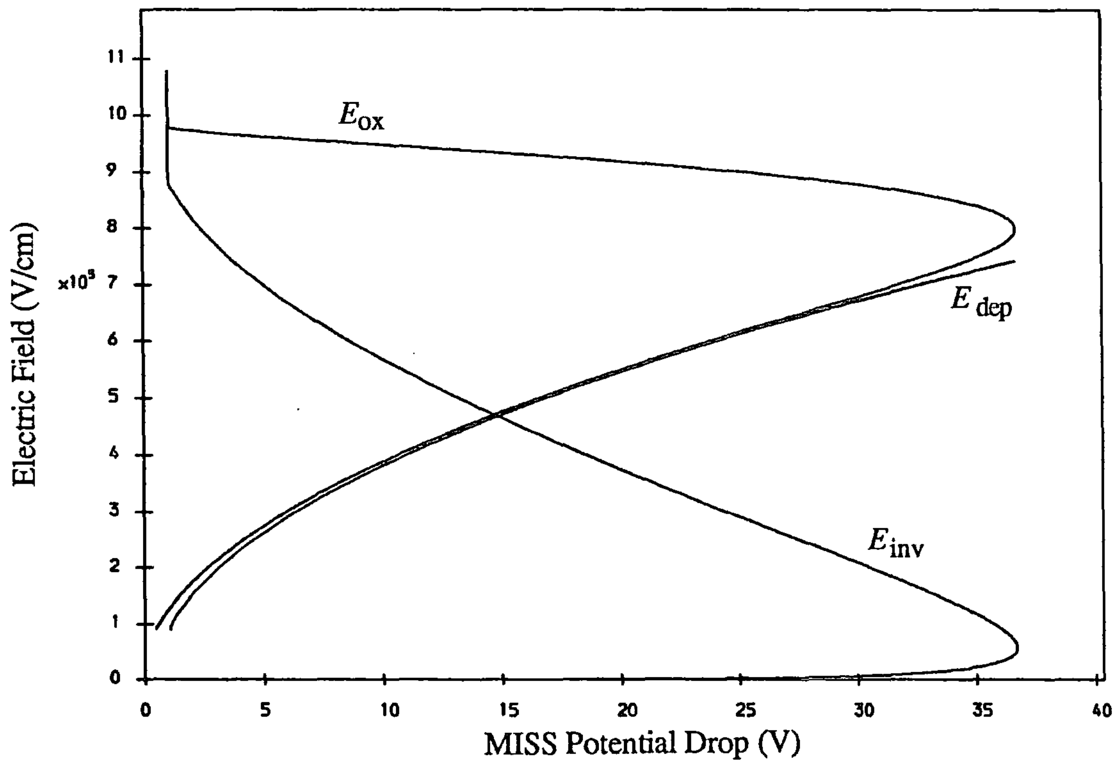

Fig 4.4: Oxide Electric Field Contributions for the 5.10^{15}cm^{-3} n-type Layer Doped MISS.

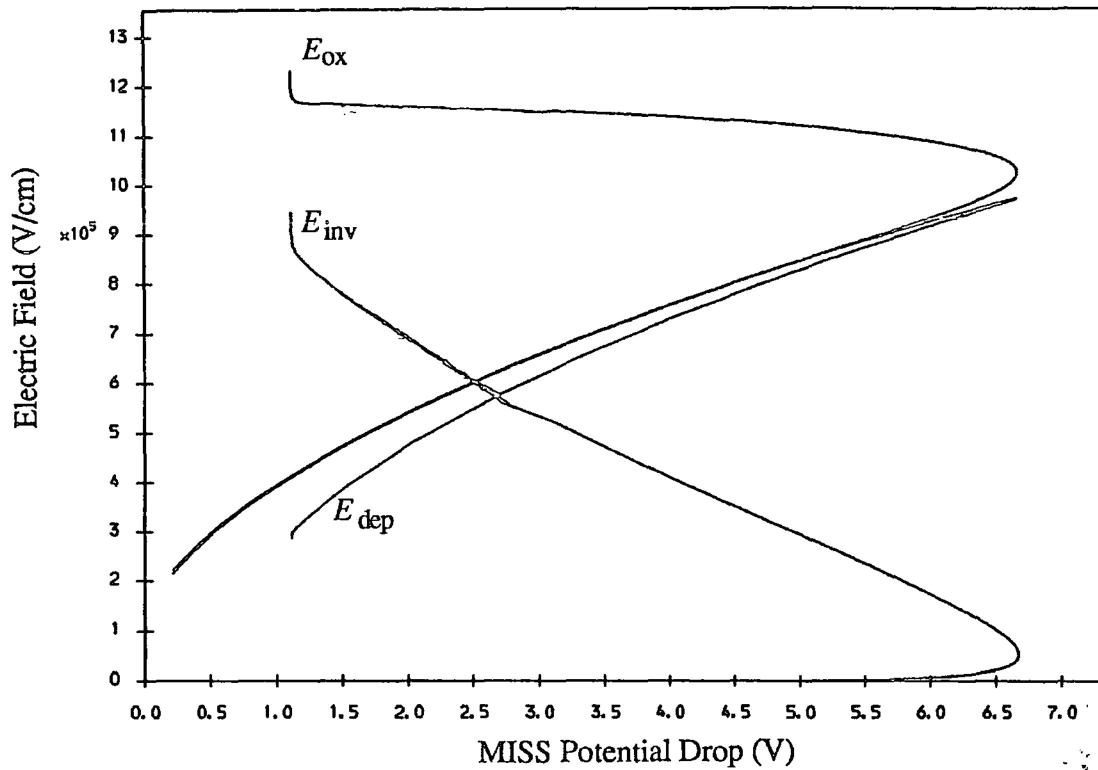

Fig 4.5: Oxide Electric Field Contributions for the $5.10^{16}cm^{-3}$ n-type Layer Doped MISS

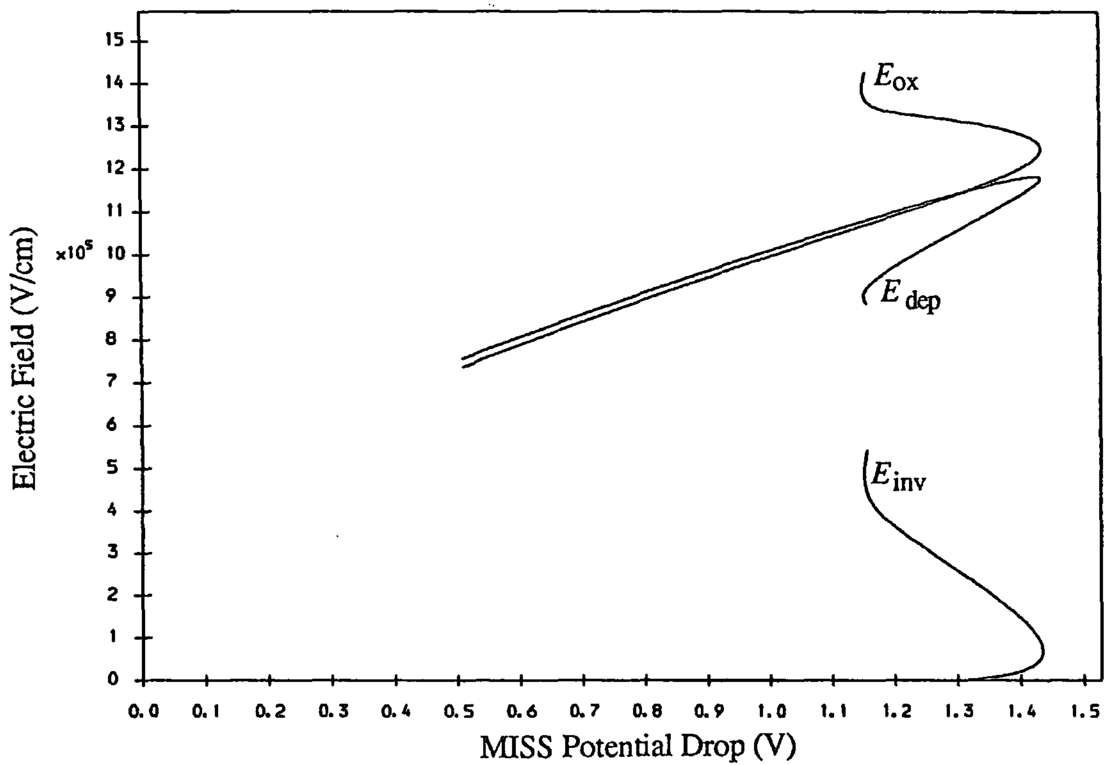

Fig 4.6: Oxide Electric Field Contributions for the $5.10^{17}cm^{-3}$ n-type Layer Doped MISS.

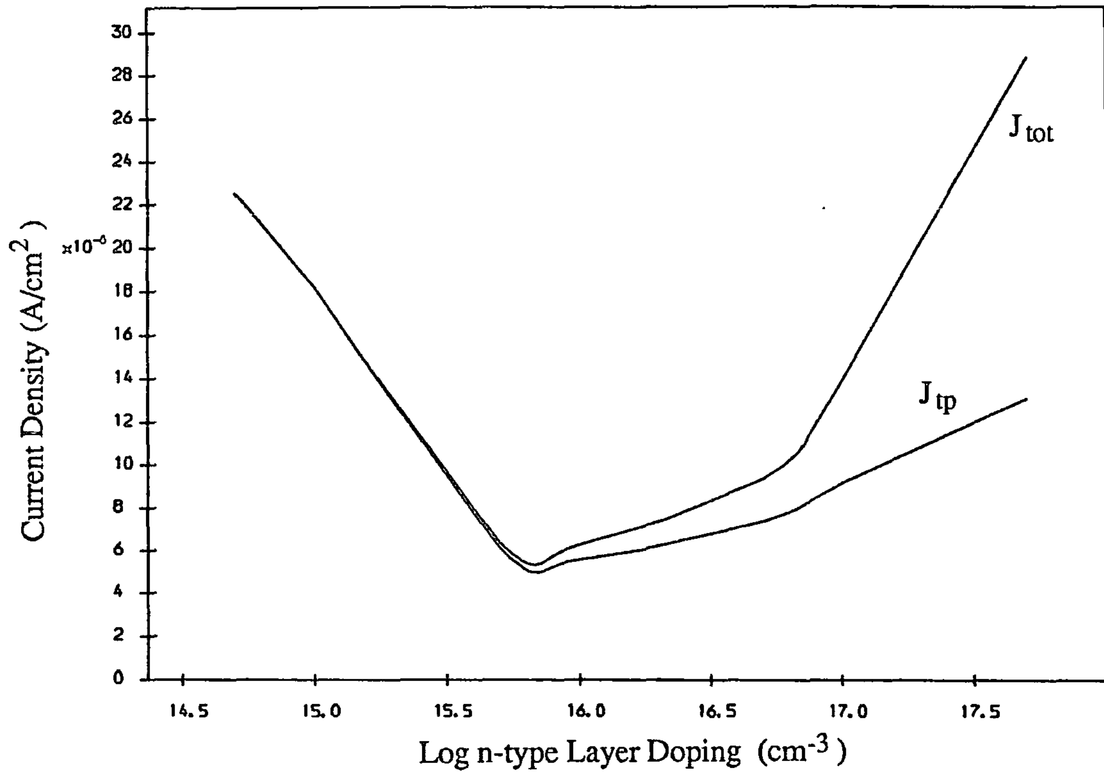

Fig 4.7: Total Current and Hole Tunnelling Current vs n-type Layer Doping at the Switching Point.

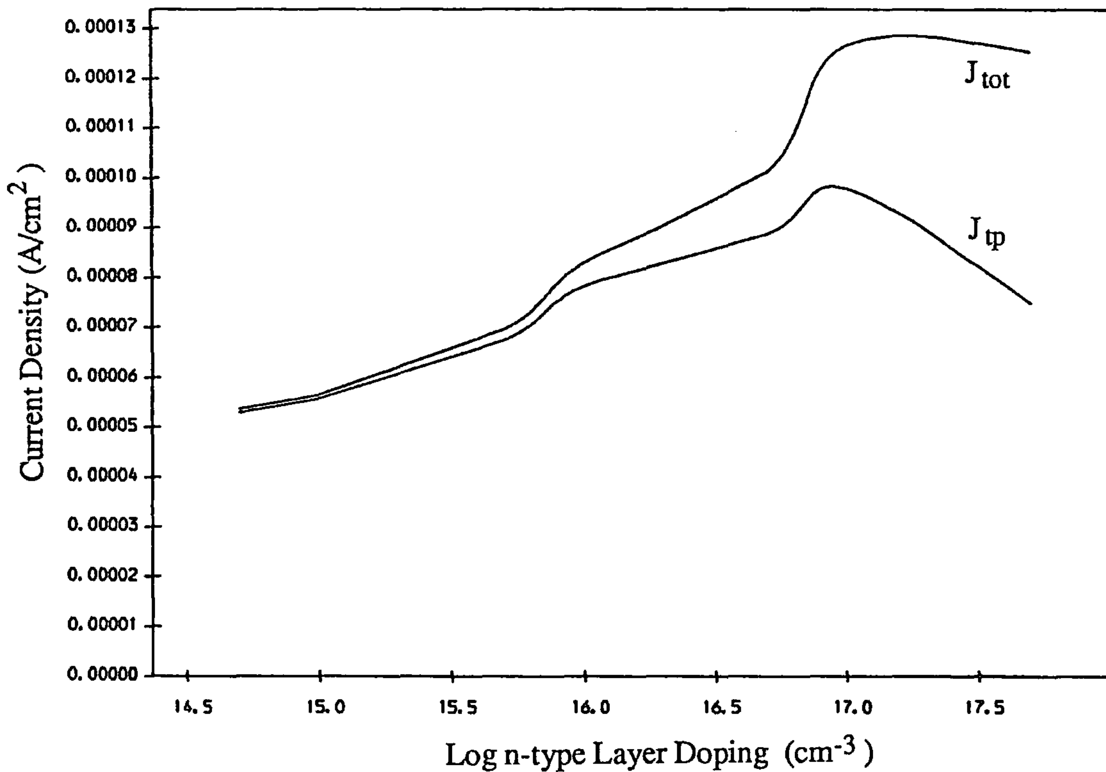

Fig 4.8: Total Current and Hole Tunnelling Current vs n-type Layer Doping at the Holding Point.

total tunnelling current throughout the OFF region and well into the ON region, before the electron current becomes dominant. This is due to the electron tunnelling current J_{tn} through the oxide being heavily dependent upon hole collection at the IS interface, and, for a work function of $4.4eV$, the necessity for an inversion layer at switching, so providing a large hole tunnelling current J_{tp}.

With an intermediate doped n-type layer, 5.10^{15} - $10^{17}cm^{-3}$, holes do not need to collect as quickly because of ionised donors, to provide the oxide potential drop and hence the electron current through the oxide. The hole inversion layer contribution to the oxide electric field only begins to dominate in the negative impedance region. Again, in the ON state, the electron tunnelling current becomes dominant, and the electric field in the oxide is due almost entirely to hole inversion at the IS interface.

For the very heavily doped device, ($> 1.10^{17}cm^{-3}$), the effect of ionised donors is so great as to dominate the contribution to the electric field in the oxide. The hole current always remains at a lower level than the electron current, and the device displays almost no switching characteristic. The total electron recombination current in the pn region of the device is also greater for a specified forward potential V_f across the pn junction, since the shorter lifetime in the n-type layer gives a greater neutral region recombination current J_{rec} for a particular neutral region width W_{neut}. It must be remembered that the hole tunnel current J_{tp} in the MISS is attributable to the hole density at the IS interface which in turn controls the potential drop across the oxide for the lightly doped device. It remains fairly constant while the electron tunnelling current changes because even a small change in hole density affects the oxide voltage so much at the holding

point. At very high densities, the n-type layer itself provides a large contribution to the oxide potential drop through the ionised donor charge, even for very small MIS depletion region potential drops, and the hole tunnelling current due to this decrease in the degree of inversion at the surface, begins to decline. This can be seen in Figs 4.7 and 4.8 where the switching and holding hole currents, and total currents are plotted against doping density.

4.3 Effect of Work Function

Increasing the work function for both lightly and heavily doped n-type layer devices changes the switching and holding currents, together with the switching voltage. Very little effect is seen in the one dimensional model on the holding voltage.

By altering the work function, two contributions to the electron current in the MIS part of the device can be seen: the generation current J_g, and the electron tunnel current J_{tn}. Using the n-type layer doping densities $10^{15} cm^{-3}$, and $10^{17} cm^{-3}$, the effect of avalanche multiplication on the switching behaviour as the work function is increased can also be examined, with the lightly doped device exhibiting no avalanche multiplication, but the more heavily doped device showing avalanche multiplication for the greater metal work function values. Also, by varying the metal work function, the relative effect of ionised donors and the hole inversion layer on the oxide potential drop, and hence on the electron tunnel current J_{tn} can be seen.

One of the assumptions in the computer model is that interface states have no

dynamic effect on current flow, and can be regarded as a bias independent charge of fixed magnitude residing at the IS interface. The effect of interface charge on the oxide potential drop can be calculated simply as

$$-V_{ox} = \mathcal{E}_{ox} d_{ox} = \frac{qQ_{ss}}{\epsilon_{ox}} d_{ox} \tag{4.3.1}$$

The charge is fixed and can therefore be regarded as having the same effect as changing the metal-semiconductor work function difference for a specified oxide thickness. For an oxide of 25Å, every increase in interface state density of $10^{12} cm^{-2}$ is equivalent to a decrease in metal work function of $0.12eV$. Therefore the results presented here can be used by analogy to predict the effect of changes in interface state densities on the calculated $I - V$ characteristic.

4.3.1 Lightly Doped n-Type Layer

For the lightly doped device with a low work function ($< 4.2eV$), switching is not seen at all. The device can be regarded as already being in its ON state, with the metal Fermi level close enough to the semiconductor conduction band for the total pn recombination current J_{rn}, to be supplied by the electron tunnelling current J_{tn} without the need for an increase in oxide potential drop due to enhanced hole collection at the IS interface. The effect of a changing work function on the $I - V$ characteristic of the lightly doped device can be seen in Fig 4.9.

As the work function is increased, the device rapidly attains its punchthrough characteristic for a work function of about $4.3eV$. As the work function increases beyond this, the switching voltage V_S remains virtually constant, although the switching current I_S continues to get larger. The switching voltage remains almost

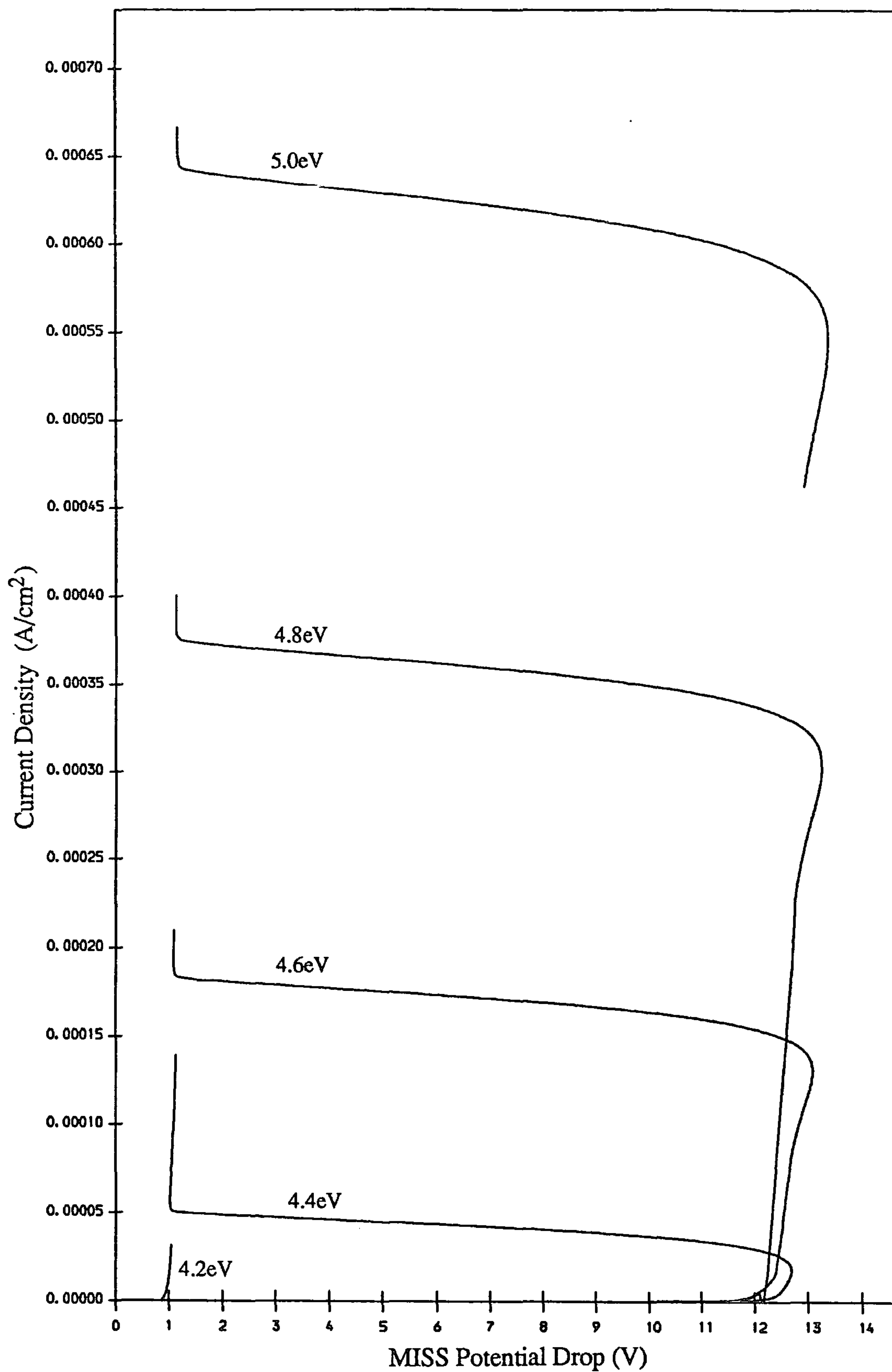

Fig 4.9: I-V Characteristics Using Various Work Functions
for the Lightly Doped n-type Layer MISS.

constant for the higher work functions because most of the applied potential is dropped across the MIS depletion region which reaches its maximum extent at the switching point due to punchthrough.

The increase in switching current is seen for higher work functions because total current through the device is dominated by holes for the lightly doped device, and a larger potential is needed across the oxide to provide the electron tunnel current J_{tn} equal to the recombination current in the pn region. This requires a greater degree of inversion at the IS interface, and therefore provides a greater hole current J_{tp}. The total current for the higher work function devices is increased at the holding point for the same reason.

4.3.2 Heavily Doped n-Type Layer

For the heavily doped MISS, work function changes have an even more marked effect on the $I-V$ characteristic than for the lightly doped device.

The switching voltage increases rapidly as the metal work function is increased, and for very large work functions, $> 4.6eV$, a hump develops in the negative impedance characteristic due to the onset of avalanche multiplication. This is because of the high electric field due to the large potential drop across the MIS depletion region. The holding current increases with metal work function for the same reason as for the lightly doped device.

The large increase in switching voltage with work function is due to both the MIS depletion region, and the hole charge at the IS interface affecting the oxide potential and hence the electron tunnelling current. For the higher work

functions, a greater oxide potential is needed to move the metal Fermi level close to the silicon conduction band, so requiring a wider MIS depletion region to provide the necessary field. The ionised donors in the MIS depletion region provide most of the electric field contribution in the oxide at the switching point for the heavily doped device, Figs 4.5 and 4.6. The doping level in the n-type layer is too great to allow punchthrough to occur for the device parameters described, but the hole density also increases as the depletion region grows, not just due to the increasing forward voltage across the pn junction V_f, but also because the growth of the MIS depletion region brings it closer to the pn depletion region.

The switching current remains almost constant for the heavily doped device as the work function is increased, in contrast to the lightly doped device. See Fig 4.10. This is because the injected hole current is almost the same for the different work function devices for a particular forward voltage across the pn junction. The width of the neutral region W_{neut} is independent of the different work function, because of the much higher doping levels, so that the forward voltage across the pn junction is also similar to provide the same degree of hole injection. Together these conditions make the switching current fairly constant.

For very high work functions values, the switching current becomes smaller as the hole injected current J_{pj} is now augmented by avalanche multiplication of carriers. Hence for a particular value of V_f, a greater degree of hole collection at the IS interface is attained. This increase in avalanche multiplication current is due to a greater MIS depletion width for the higher work function devices. In contrast to the work of Habib and Simmons [2], the switching voltage is partly determined by the electric field in the MIS depletion region, and it is not solely

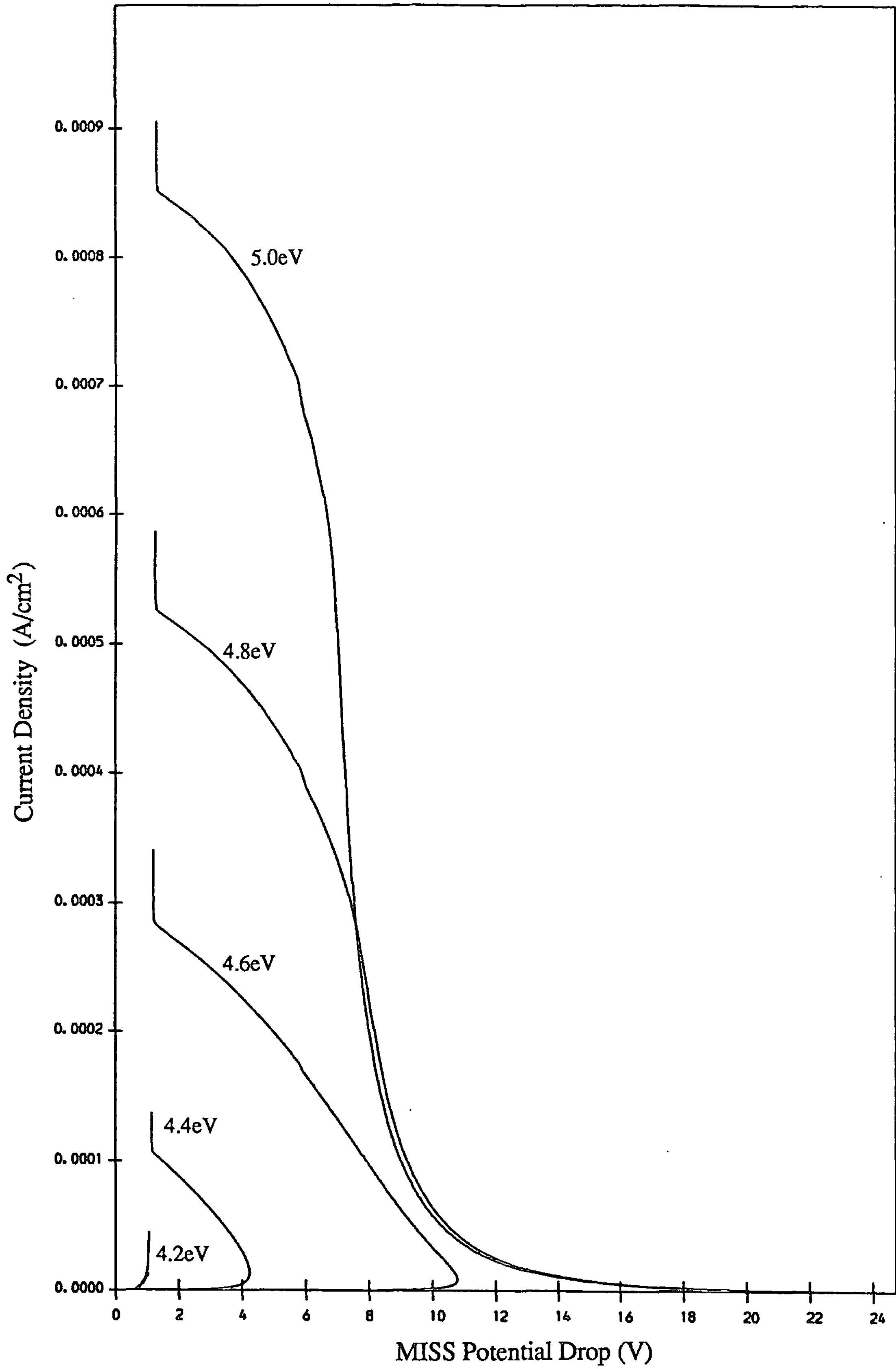

Fig 4.10: I-V Characteristics Using Various Work Functions for the Heavily Doped n-type Layer MISS.

due to the onset of avalanche multiplication. Though avalanche multiplication affects the shape of the $I - V$ characteristic in the negative impedance region, it cannot be used on its own to calculate the switching voltage.

For work function values greater than $4.6eV$, the negative impedance region of the $I - V$ characteristic becomes curved into a half bell shape. This can be understood in terms of avalanche multiplication of carriers. With a very large potential across the device at the switching point, carrier multiplication becomes important. In the negative impedance region, the device moves from a point at which most of the electric field in the oxide is provided by ionised donors, to the major contribution coming from an inversion charge at the IS surface. At the start of the negative impedance region, the decline in total potential across the device is sharp because the hole inversion layer grows rapidly, with increased hole currrent due to avalanche multiplication, as well as an increasing hole current due to the increasing forward potential across the pn junction. This counterbalances the reduction in the oxide electric field contribution from ionised donors more effectively, so producing a sharper switching point than otherwise expected. As the potential across the MIS depletion region declines, the multiplication becomes less marked, so reducing the rate of increase of the hole inversion layer and hence reducing the rate of collapse of the MIS depletion region. This causes a very steep rise in current for only a small drop in device potential. Eventually the point is reached at which the hole injection from the pn junction is great enough for the inversion charge to predominantly control the oxide electric field, moving the metal Fermi level close to the silicon conduction band, and the MISS into its ON state.

For the heavily doped device the holding current increases with work function, since in the one dimensional MISS model, especially for devices with higher work functions, the device current at the start of the ON region is dominated by holes. At the holding point, the main contribution to the electric field comes from hole inversion at the IS interface. This has a direct effect on the hole tunnelling current which is a monotonically increasing function of hole density at the surface, and with the higher work function the hole charge has to be greater to support the oxide potential drop needed to move the metal Fermi level close to the silicon conduction band. Both the lightly and heavily doped devices display this increase in holding current.

4.4 Effect of Oxide Thickness

For the lightly and heavily doped devices, variations in oxide thickness produce marked changes in the $I - V$ characteristics. With both devices there is an oxide thickness window of approximately $10 - 40\AA$ for which a switching characteristic can be obtained. Devices with thinner oxides than these behave like a pn junction attached to Schottky barrier, and for the thicker oxide devices, the current flow through the insulator is too small to allow switching producing the $I - V$ curve of a large value resistor.

4.4.1 Lightly Doped n-Type Layer

A lightly doped device with an oxide of $35\AA$ has almost no switching char-

acteristic. A strong inversion layer forms at the IS interface for a very small potential and the device can be regarded as behaving almost immediately in its ON state, See Fig 4.11. The electron recombination current in the pn depletion region is provided almost immediately by the electron tunnelling current because of the rapid development of the hole inversion layer at the IS interface.

Devices with oxide thicknesses of between $20\AA$ and $28\AA$ behave with the punchthrough switching mechanism. The switching voltage for these devices is nearly constant although the switching current increases as the oxide thickness is reduced.

For very thin oxides, current flow through the device can be regarded as being virtually unimpeded by the oxide, with carriers passing almost freely through the insulator. The switching voltage therefore declines until no switching is observed for devices with thicknesses less than $10\AA$. This limit as the oxide thickness tends to zero is recognisable as a Schottky barrier.

4.4.2 Heavily Doped n-Type Layer

The heavily doped device displays a relatively constant switching voltage through an oxide window of between 20 and $30\AA$, see Fig 4.12.

For the thinner oxide devices, electrons flow more readily through the insulator and the potential drop across the oxide does not need to be as great for a substantial electron current. The MIS depletion layer therefore does not need to grow as wide as in devices with less conductive oxides.

For the thicker oxide device, $35\AA$, the switching and holding points tend to

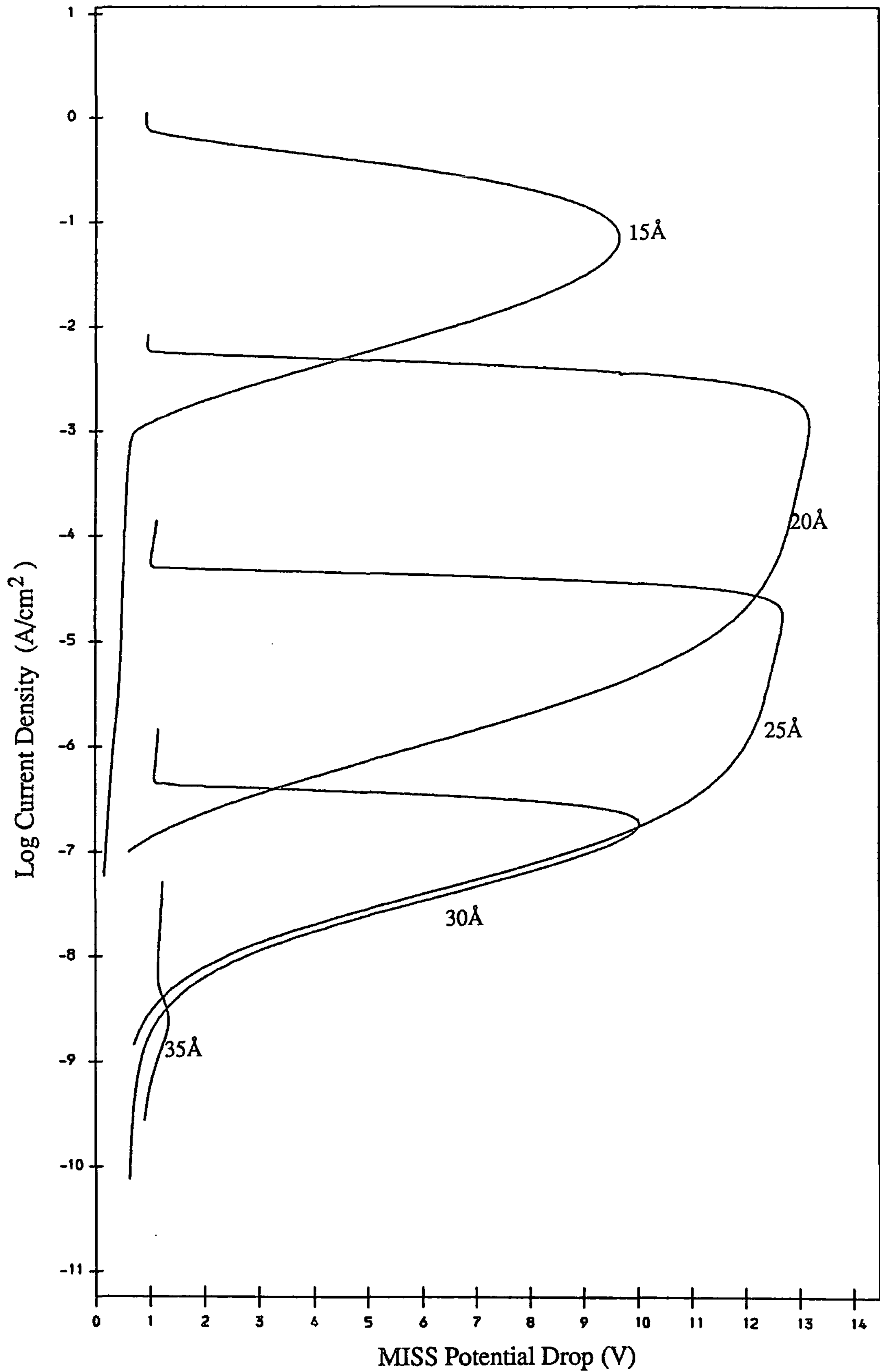

Fig 4.11: I-V Characteristics Using Various Oxide Thicknesses for the Lightly Doped n-type Layer MISS.

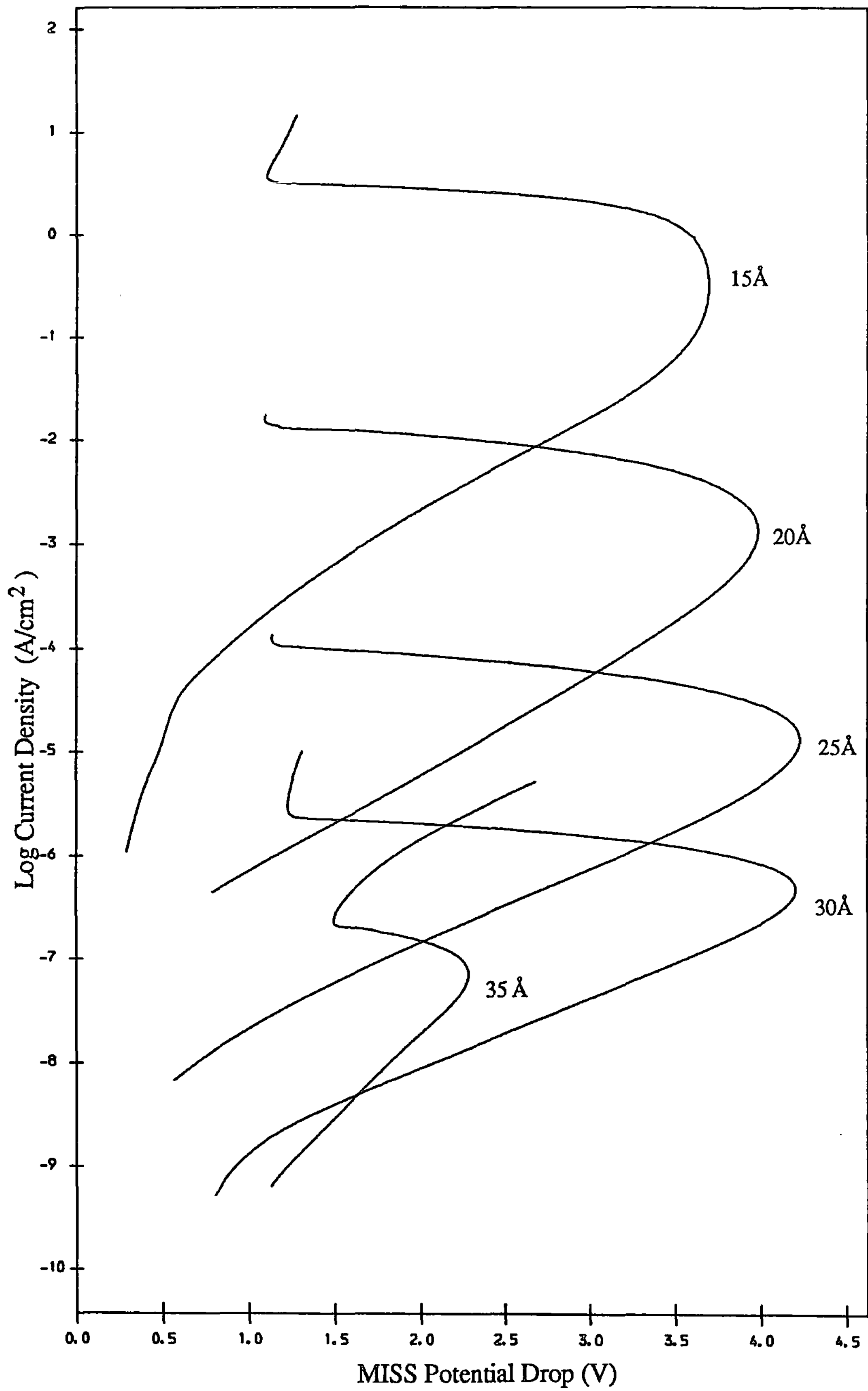

Fig 4.12. I-V Characteristics Using Various Oxide Thicknesses for the Heavily Doped n-type Layer MISS.

move together, eventually squeezing out the negative impedance region altogether. A high potential then needs to be produced across the oxide to allow electron carrier flow. The electron carrier current is very dependent upon a large density of electrons opposite the silicon conduction band. This causes a very steep increase in the oxide potential drop, creating a far less steep $I - V$ characteristic for the device in the ON region. Devices with oxides too thick for switching can be regarded as remaining in the high impedance state.

4.5 Effect of n-type Layer Thickness

There is a marked difference in behaviour between the lightly and heavily doped devices when the n-type layer width is altered. The standard parameters used for the one dimensional model have been chosen to reflect this difference in behaviour.

4.5.1 Lightly Doped n-Type Layer

With the lightly doped device, the effect of ionised donors on the oxide potential drop, V_{ox}, is so small that for a wide range of n-type layer thicknesses the device still punches through to the pn depletion region. Eventually a limit is reached at which the increased charge of the ionised donors in the deep depletion layer, its increased generation current together with the hole injected current is great enough to turn the device ON before the punchthrough condition is reached, See Fig 4.13.

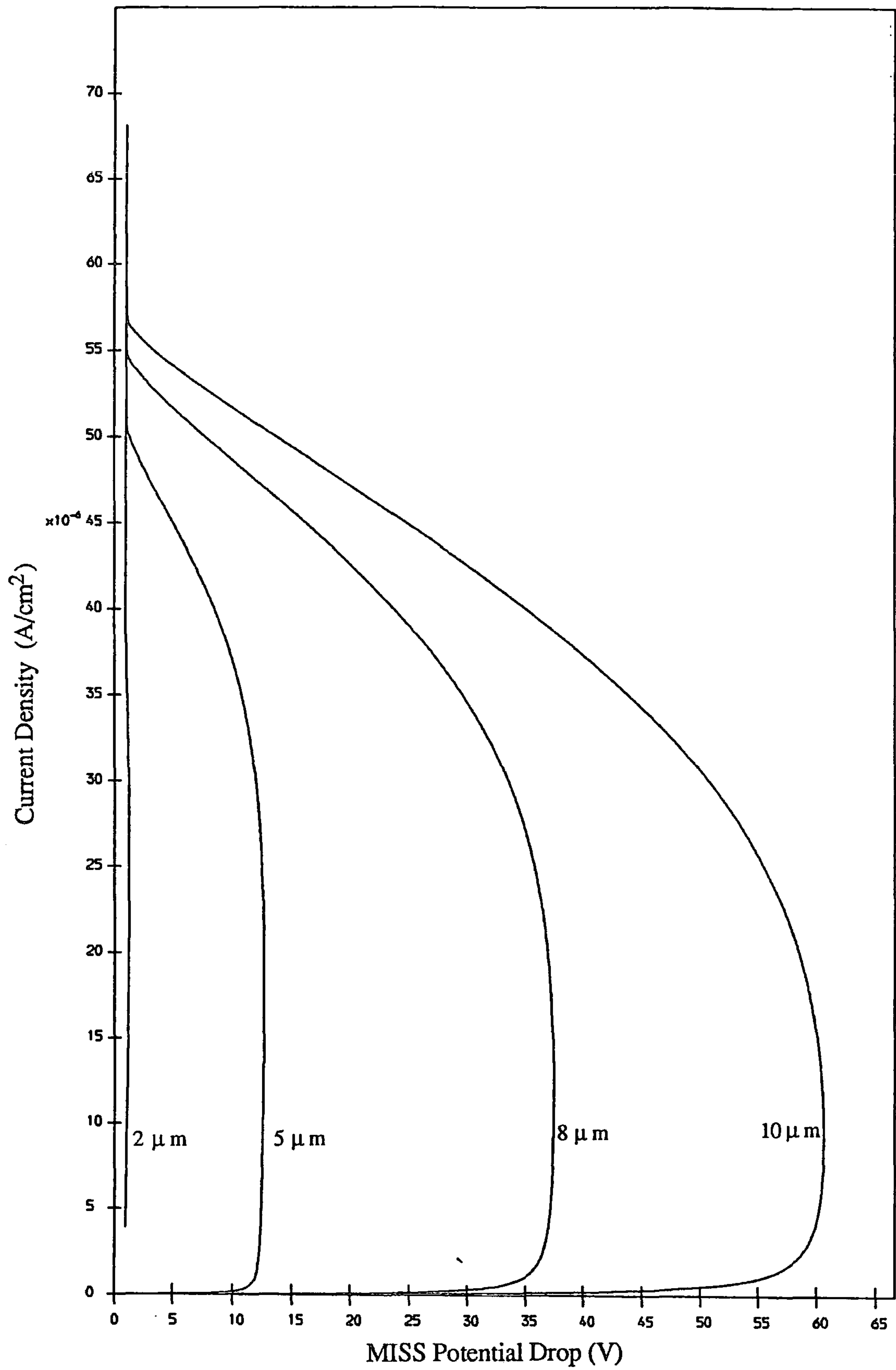

Fig 4.13: I-V Characteristics Using Various n-type Layer Thicknesses for the Lightly Doped n-type Layer MISS.

For the lightly doped device an integration of Poisson's equation, can give an approximate value of the punchthrough switching voltage:

$$V_S = \frac{qN_d(W_{epi} - W_{pn})^2}{2\epsilon_s} \qquad 4.5.1$$

where N_d is the donor doping density of the n-type layer, W_{epi} is the width of the n-type layer, and W_{pn} is the width of the pn depletion layer using the abrupt junction approximation. The expression predicts a switching voltage of 13.4 for the $5\mu m$ device, $39.4V$ for the $8\mu m$ device, and $64V$ for the $10\mu m$ structure. These are reasonable values when compared with the full model. Hence for the lightly doped device, assuming punchthrough, the switching voltage increases as the square of the n-type layer thickness.

As the thickness of the n-type layer is increased, the switching current almost imperceptibly declines for a device with a $25\AA$ oxide. This is due to the greater contribution to the device current from the generation current, J_g, in the wider MIS depletion region. It provides sufficient holes to the IS interface to increase the oxide potential without requiring the pn junction to become so forward biased. This can be seen from the expression for hole current continuity

$$J_{tp} = J_g + J_{pj} \qquad 4.5.2$$

The generation current J_g also provides a contribution to the electron recombination current in the pn section of the device.

The holding current is a monotonically increasing function of the n-type layer thickness. This is due to greater electron recombination current in the neutral region of the n-type layer, needing a greater electron current, and hence a greater hole current to provide the oxide potential drop in the ON region. For the thicker

n-type layer the neutral width W_{neut} is greater causing both the electron and hole currents to be increased at the holding point.

4.5.2 Heavily Doped n-Type Layer

For the heavily doped device there is a far smaller change in switching voltage with n-type layer thickness than for the lightly doped case, Fig 4.14. This is a consequence of the far greater contribution to the oxide electric field by ionised donors of the MIS depletion region.

The small increase in the switching voltage with epilayer thickness is due to the greater neutral recombination current, J_{rec} than for the thinner layers. Also the wider neutral region, W_{neut}, reduces the injected hole current into the MIS depletion region. Both effects increase the switching voltage, giving a greater electron tunnelling current J_{tn} to equal the larger recombination current in the wider depletion layer. This is also the case at the switching point where the hole inversion charge at the IS interface has a larger effect on the electric field in the oxide as the epilayer thickness increases.

The small increase in holding voltage with n-type layer thickness is caused by the greater oxide potential and forward voltage across the pn junction for the reasons explained above. The holding current is also increased by the greater electron recombination current in the neutral region, so that increased hole injection is needed to provide a larger hole inversion charge.

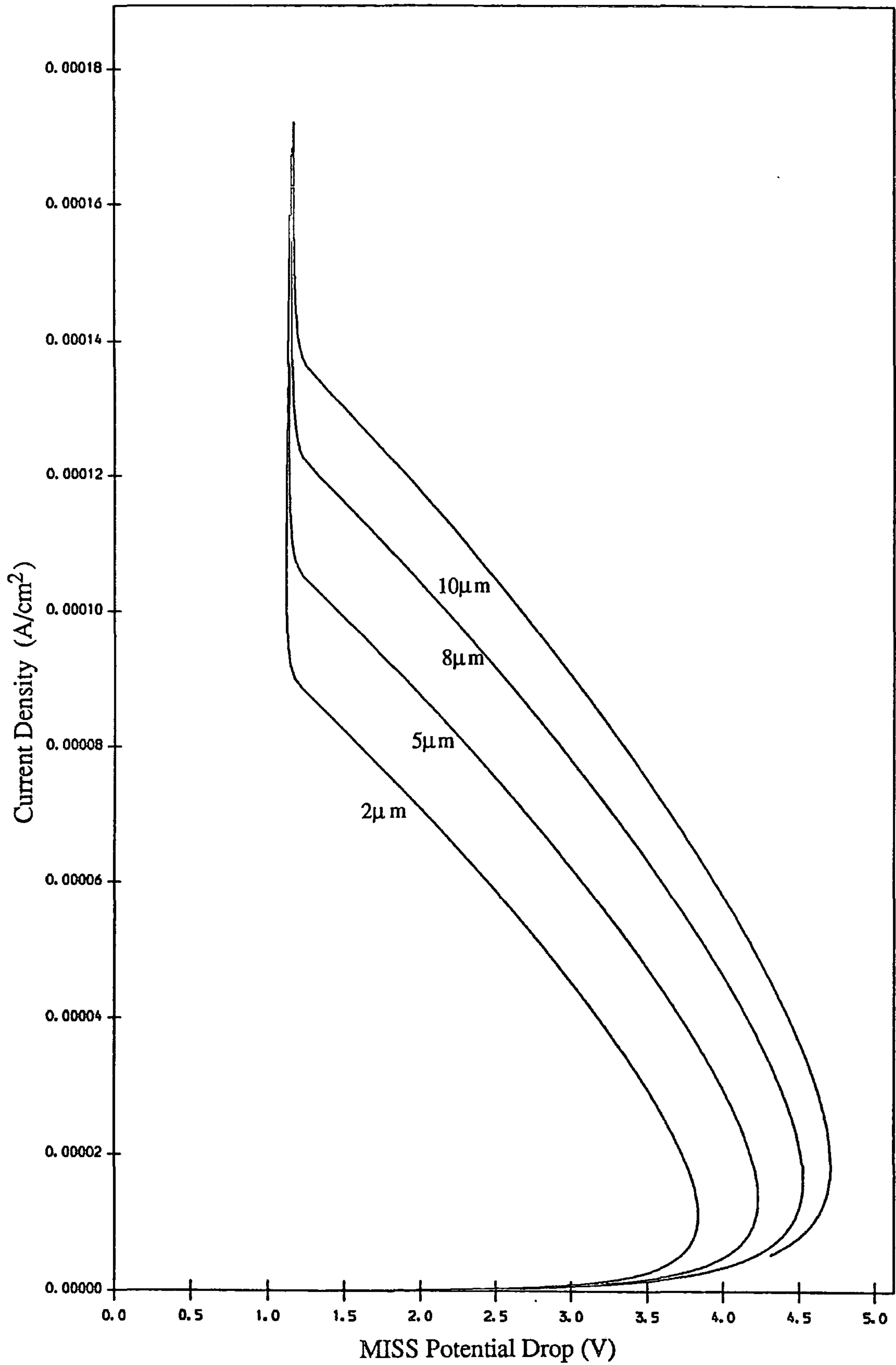

Fig 4.14: I-V Characteristics Using Various n-type Layer Thicknesses for the Heavily Doped n-type Layer MISS.

4.6 MIS Diode Switching Characteristics

The experimental work of Hayashi [3], Fig 4.15(c), showed that thin insulator metal-insulator-semiconductor diodes made with heavily doped n-type substrates could display current controlled negative impedance.

The computer model for the MISS was adapted to deal with this case by increasing the width of the n-type layer W_{epi} to $1cm$, so making J_{pj} negligible ($< 10^{-40} A/cm^2$). By examining the computed results for the heavily doped MISS, Fig 4.14, it can be seen that as the n-type layer thickness is increased, the MISS continues to display a switching characteristic suggesting that for suitable values of doping, the heavily doped MIS diode structure should produce a switching characteristic.

Figs 4.15(a) and 4.15(b) show the computed $I - V$ characteristics of a simple MIS structure with a doping density of $10^{17} cm^{-3}$, a thin $25\AA$ oxide, and three different metal work functions values: 4.4, 4.6, and $4.8eV$

As can be seen, the device has an S-type negative impedance characteristic. This is due to the electron recombination current in the substrate being supplied by electron tunnelling through the oxide, with the oxide potential being controlled by the ionised donors in the depletion region under the insulator. As the electron current grows, so does the potential drop across the n-type layer giving rise to avalanche multiplication of carriers. This begins to supply a hole flux towards the oxide-semiconductor interface producing both a hole tunnelling current, and a contribution to the oxide potential drop.

The greater the electron tunnelling current, the greater the hole multipli-

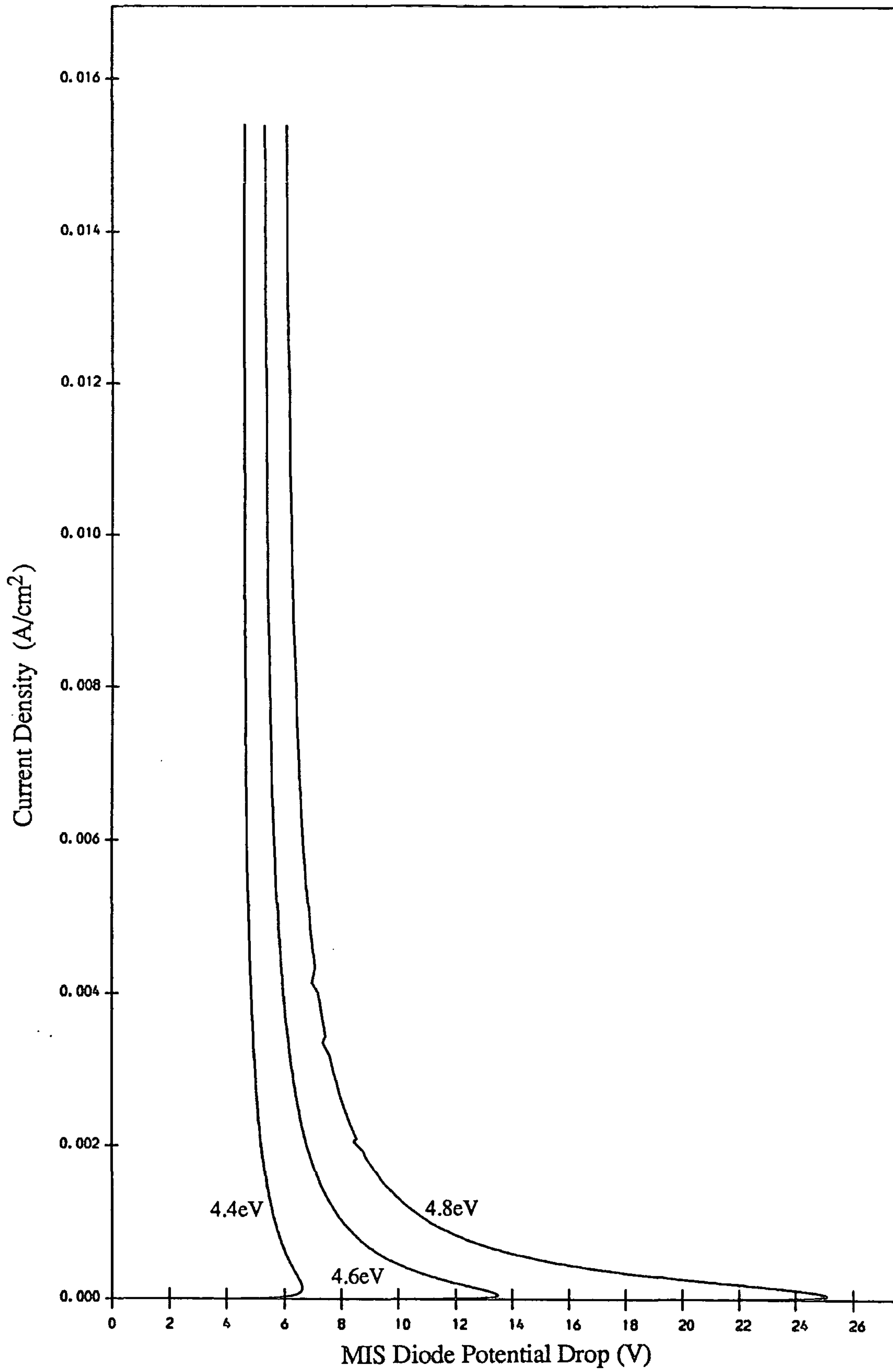

Fig 4.15: I-V Characteristics for the MIS Diode Switching Device Using Various Work Functions.

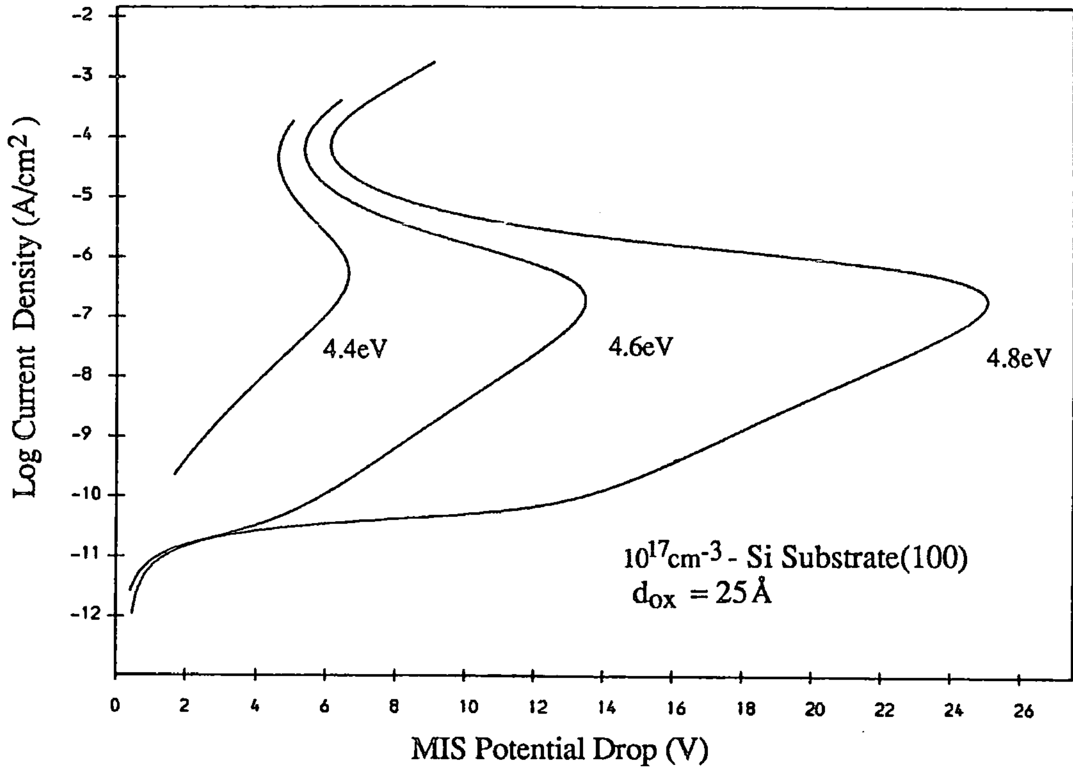

Fig 4.15(b): I-V Characteristics for The MIS Diode Device Using Various Work Functions. (Log)

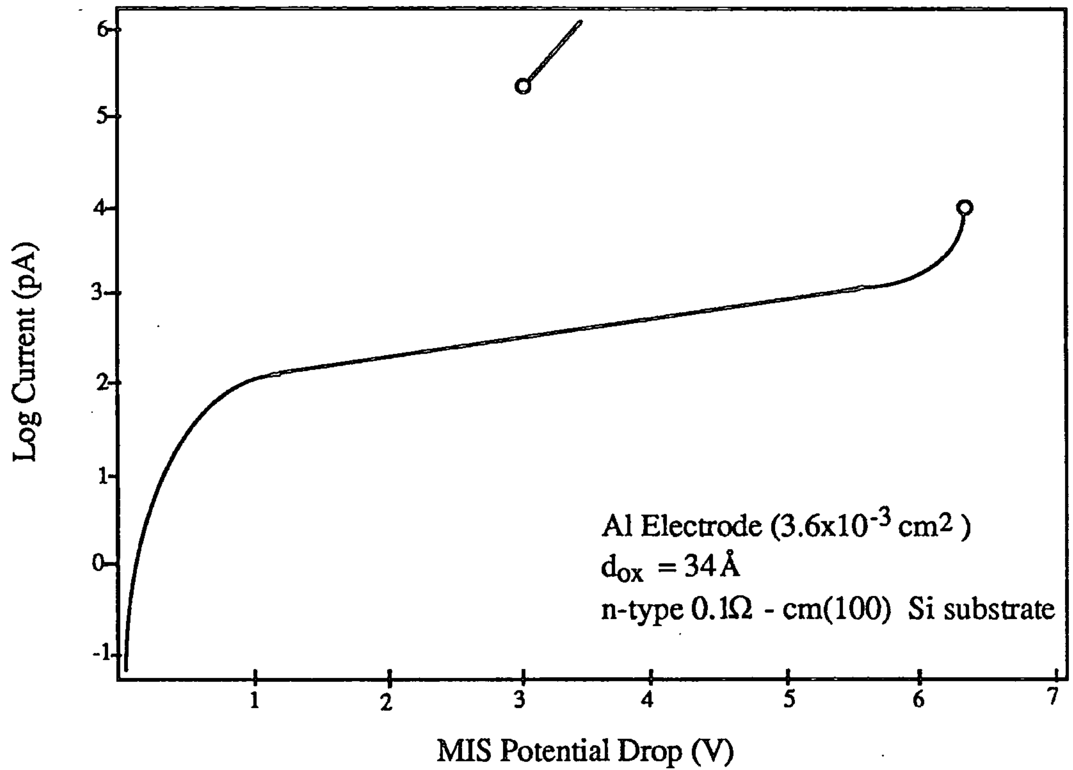

Fig 4.15(c): I-V Characteristic as Given by Hayashi for the The MIS Diode Swiching Device.

cation until a point is reached at which further increases in electron tunnelling current can be provided by very small increases in oxide potential. This causes the MIS depletion layer to decrease slowly in width, although the hole current due to multiplication continues to increase because of the continuing increase in the electron tunnelling current. It is this hole multiplication which causes the continuing increase in the oxide potential. Finally a point is reached at which hole multiplication is just able to sustain the increase in electron tunnel current with no further decrease in the total potential across the device, and the device enters the ON region.

Because the device relies upon avalanche multiplication of carriers to provide the hole inversion layer at the oxide-semiconductor interface, a minimum potential has to be maintained across the depletion region for avalanche multiplication to occur. This accounts for the much higher holding voltages for the MIS diode devices as compared to the other 1-D MISS structures.

The current continuity equations for the MIS structure can be written in the form

$$M_n J_{tn} + J_g = J_{rn} \tag{4.6.1}$$

for electrons, and

$$(M_n - 1)J_{tn} + J_g = J_{tp} \tag{4.6.2}$$

for holes. M_n is the avalanche multiplication coefficient for electrons, J_{tn} the electron tunnel current, J_g the MIS depletion region generation current, and J_{rn} the total electron recombination current in the neutral n-type substrate. In the hole current continuity equation, the term $(M_n - 1)$ reflects the production of holes by the avalanche multiplication of electrons that have tunnelled from the

metal, and J_{tp} is the hole tunnel current.

Unsurprisingly, as the work function increases so the switching and holding voltages increase. The increase in the switching voltage is due to the larger oxide potential required to bring the metal Fermi level close to the semiconductor conduction band. For a larger work function it requires a greater value of $\mathcal{E}_s$, and hence a larger potential drop across the MIS depletion region. As the hole multiplication increases, the degree of inversion necessary to compensate for the decrease in the depletion region field is greater for the higher work function devices. Hence the potential drop across the device at the holding point is found to increase.

4.7 Discussion

In this chapter the $I - V$ characteristic of the MISS has been examined for changes in structural parameters. The information presented describes the qualitative behaviour of a large number of devices. Because each structural parameter was varied individually with all others holding their default values, the behaviour of other structures not modelled here can be predicted. In the previous chapter the relative importance of individual current components for the MISS was discussed. Here that discussion was kept to a minimum. Below the effect of parameter changes on device behaviour is summarised.

An increase in the n-type layer doping density produces an increase and then a decrease in the switching voltage. The maximum switching potential is reached for a doping density of $5.10^{15} cm^{-3}$. For the lightly doped devices, switching occurs

by punchthrough, with the oxide potential V_{ox} dominated by hole collection at the IS interface. As the doping density increases, so does the contribution of ionised donors to V_{ox}. This effect reduces the switching voltage until for very heavily doped devices, switching is not seen. The importance of ionised donors can be seen through the value of the hole tunnelling current at the switching and holding points, which is reduced as a proportion of total tunnelling current as the doping density increases.

Changing the work function for the lightly and heavily doped n-type layer devices produces a marked change in behaviour. All the lightly doped devices switch at punchthrough except for the very small work function device ($4.2eV$). This produces a constant switching voltage. However, the switching and holding currents both increase strongly with work function, caused by the need for an increasing oxide potential with work function at the switching and holding points. For the heavily doped device, an increase is seen in the switching voltage and the holding current with work function. Because of the larger work function the oxide potential needs to be greater at the switching point. This is produced mainly by ionised donors so making a wider depletion layer and a greater potential drop. Holding current increases because the oxide potential at the holding point is produced from a hole inversion layer, and this increases with increasing work function, enhancing the hole tunnelling current. The larger work function devices have great enough electric fields in their MIS depletion layers to produce avalanche multiplication. This can be seen in the $I-V$ characteristic as a half bell shape.

For changes in oxide thickness, both the lightly and heavily doped devices

show an increase in switching and holding currents with decreasing oxide thickness. There is an oxide thickness window for $< 100 >$ orientated silicon of $10 - 40\mathring{A}$ outside which switching is not seen. The switching voltage is at at a maximum for oxide thicknesses of $20 - 25\mathring{A}$ for the lightly doped device, and $20 - 30\mathring{A}$ for the heavily doped structure. The switching voltage declines as the oxide thickness increases or decreases outside these ranges.

With changes in n-type layer thickness, the lightly doped device still switches at punchthrough for oxide thicknesses up to $10\mu m$. Between $2\mu m$ and $10\mu m$ the device goes from no switching to a switching voltage of over $60V$. For the heavily doped device only a small change is seen in the switching voltage; a $1V$ difference between n-type layer thicknesses of $2\mu m$ and $15\mu m$. This is because the oxide potential at the switching pont is dominated by the effect of ionised donors, rather than hole collection at the IS interface as in the lightly doped case.

In the MISS model outlined in chapters 3 and 4, the main point to note is that as it is, the one-dimensional model does not adequately describe devices fabricated and tested experimentally. These can be lateral devices, or devices with no isolation of the junctions and top contacts, allowing appreciable current spreading. The model does allow a qualitative description of operation and it enables certain trends in device behaviour to be demonstrated. e.g the increase in the switching and holding currents with doping density, and the bell shaped $I - V$ characteristic for devices displaying appreciable avalanche multiplication. However it would not be expected to give a good quantitative fit with experimental results. Some of these defects are remedied in the next chapter. Finally, in defence of the 1-D model, the quantitative modelling performance improves with

increasing experimental top contact area.

References

1. Wolf, H. F., 'Silicon Semiconductor data', Pergamon Press, (1969).
2. Habib, S. E-D. and Simmons, J. G., 'Theory of Switching in $p-n$ Insulator(Tunnel) Metal Devices Part 2, Avalanche Mode', *Solid-St Electron.*, **23**, pp. 497-505, (1980).
3. Hayashi, Y., 'Switching Phenomena in Thin-Insulator Metal Insulator Semiconductor Diodes', *Appl. Phys Lett.*, **37(4)**, pp. 407-408, (1980).

CHAPTER FIVE

A CIRCULARLY SYMMETRIC QUASI TWO-DIMENSIONAL MODEL OF THE M.I.S.S. DEVICE

5.1 Introduction

In this chapter some of the quantitative differences between the measured current-voltage characteristics of the MISS device, and the theoretical curves determined using the one-dimensional computer model are explained.

From the 1-D model, the calculated values for the switching current density and potential together with the holding current density and potential are less than those found by experiment [1-3]. Also experimentally, the flat-band voltages measured on devices fabricated using silicon dioxide are small, something which is equivalent to a low work function in modelling terms. However, with the 1-D computer model such low work function devices do not produce a switching characteristic, although this has not been found to be the case experimentally.

Generally, fabricated devices have a *pn* junction area which is greater than that of the top contact, and there is certainly a strong area effect on the $I-V$ characteristic, some results of which are shown in the work of Duncan *et al* [1]. In the work of Duncan, for a thick oxide device, as the size of the metal top contact decreases from $25000\mu m^2$ to $1600\mu m^2$, both the switching and holding voltages, together with the switching and holding current densities increase. The

same trend is also seen for a thin oxide. However, with the thin oxide devices the switching characteristic ceases to exist for top contact areas greater than $6400\mu m^2$. In the present work a reasonable quantitative fit for the thick oxide result has been obtained, and a closer fit of theory with experiment for the thin oxide structure has also been achieved [1,2].

5.2 Modelling

The device structure with the pertinent currents being analysed is shown in Fig 5.1. It consists of a radially infinite substrate with a $5\mu m$ thick n-type layer, a tunnelling thickness oxide, and a circular metal top contact of radius r_0. The top contact is assumed to be a disc in the model to allow advantage to be taken of radial symmetry. The modelled structure has a lightly doped n-type layer of $10^{15}cm^{-3}$, with a p-type substrate doping of $10^{19}cm^{-3}$.

The 1-D model has been improved by incorporating current spreading in the n-type layer outside the region immediately below the metal top contact. This is assumed to be a drift current carried by electrons, which flows parallel to the oxide, Fig 5.1. As can be seen, the spreading current $I_{sp}(r)$ at the point r receives a contribution, $I_d(r)$, due to the pn depletion region recombination current in the annulus of width dr, so producing an increasing electron current as the top contact is approached. The total spreading current at the top contact is expressed as $I_{sp}(r_0)$.

Recombination of holes injected into the n-type layer outside the area immediately below the metal top contact is regarded as small enough to be ignored in this

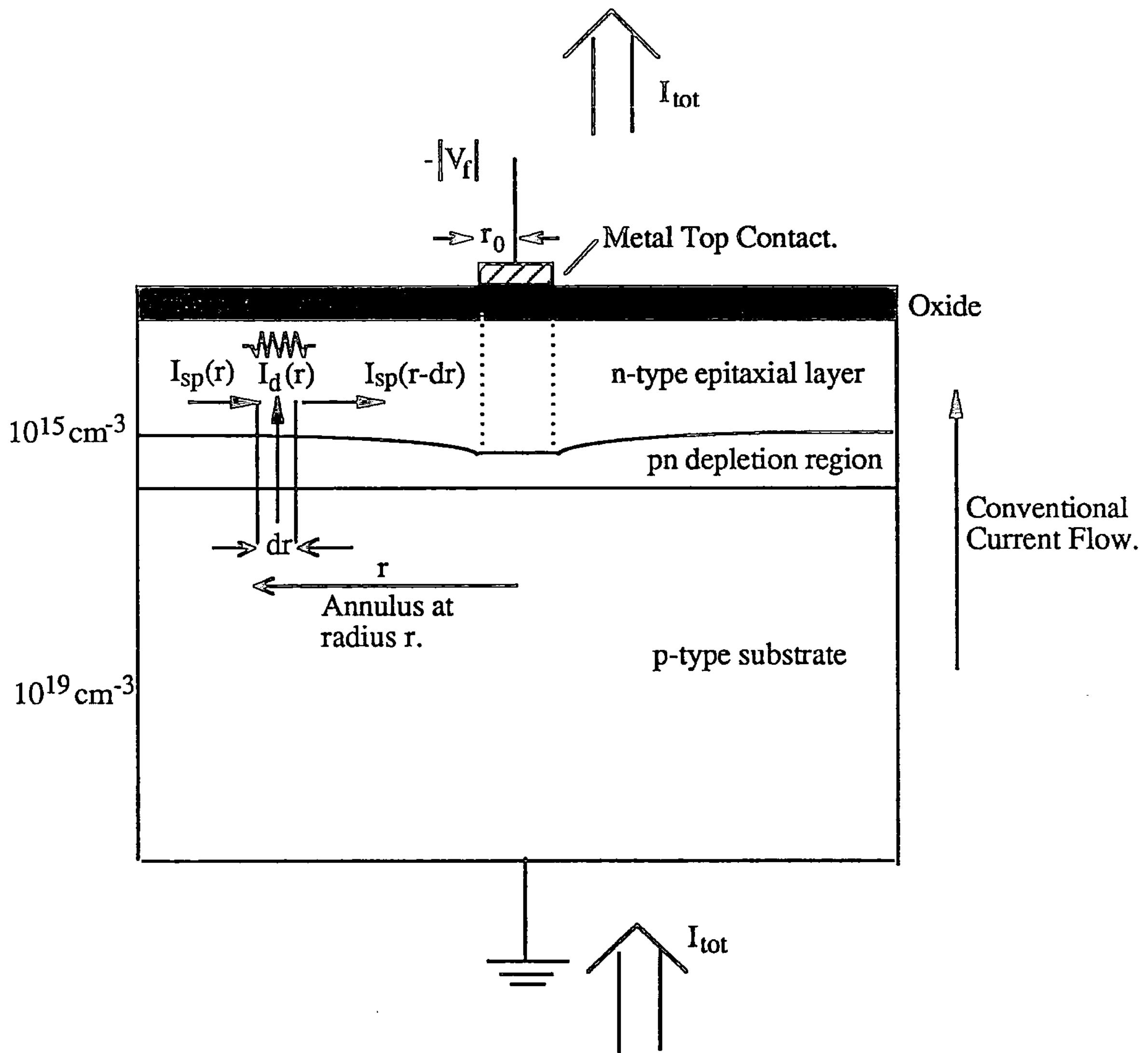

Fig 5.1: Current Flow for the Two Dimensional Device Structure.

first order model. It is at first sight a surprising assumption, but can be justified because of the dominance of the pn depletion region recombination current, J_{rj}, over the total current in the pn region, for a small forward potential V_f. This is clearly demonstrated in Fig 5.2(a) which shows the current densities in a forward biased pn diode with the same doping densities used in the present model, and shows J_{rj} dominating the total current up to a value of $V_f = 0.3V$. By ignoring the hole injected current the calculation is simplified considerably with only the drift current from a single carrier needing to be modelled.

In this circularly symmetric quasi 2-D model, the injected hole current into the MIS depletion region under the top contact takes the same form as in the 1-D case, except current as opposed to current density is used, and an area multiplication factor incorporated to give an expression for the total injected hole current, I_{pj}, of the form

$$I_{pj} = \pi {r_0}^2 J_{pj} \qquad 5.2.1$$

where J_{pj} is the calculated injected hole current density as in the 1-D case. Here I_{pj} is assumed to be unaffected by the much larger pn junction, with holes injected from outside the area immediately below the top contact not arriving at the edge of the MIS depletion region. This is consistent with the previous assumption where all holes injected into the n-type layer outside the top contact area are assumed to recombine, and this hole recombination current is negligible w.r.t the pn depletion region recombination current. This simplifies the model considerably, and though the assumptions are not suitable for thin oxide devices at the holding point, where V_f is found to be greater than $0.4V$, it does produce better results for thicker oxides. Although this approximation can be improved for the thinner

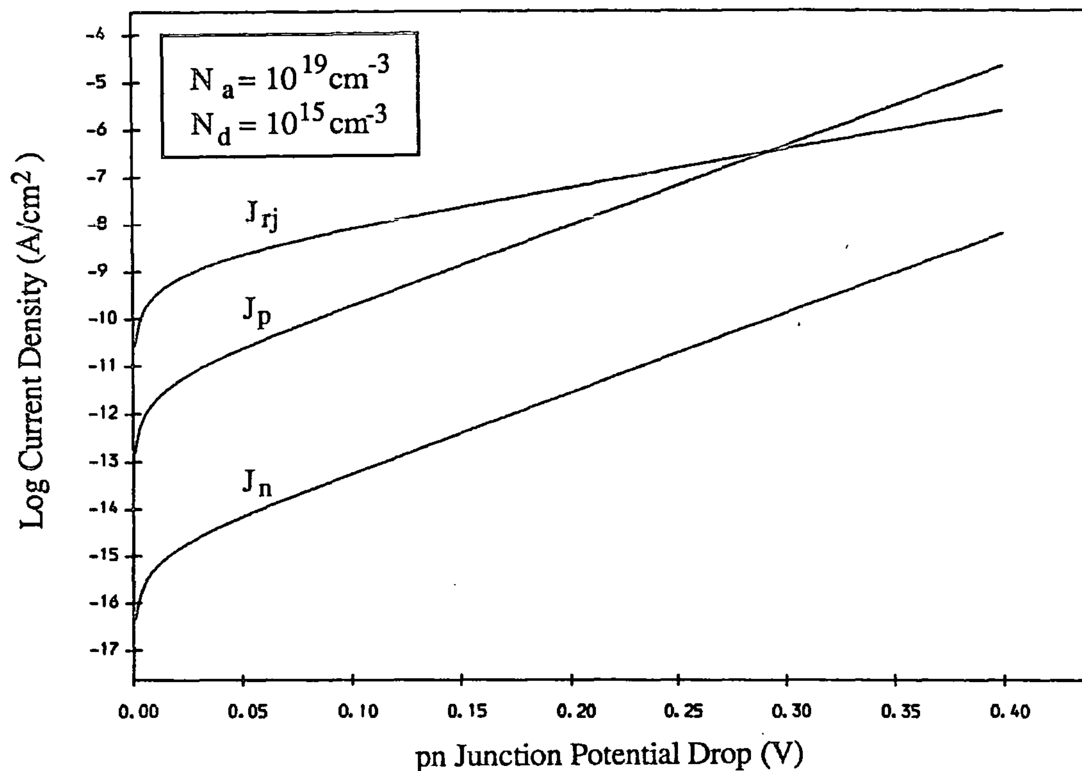

Fig 5.2(a): Depletion Region Recombination plus Electron and Hole Diffusion Currents for a 1-D pn Junction.

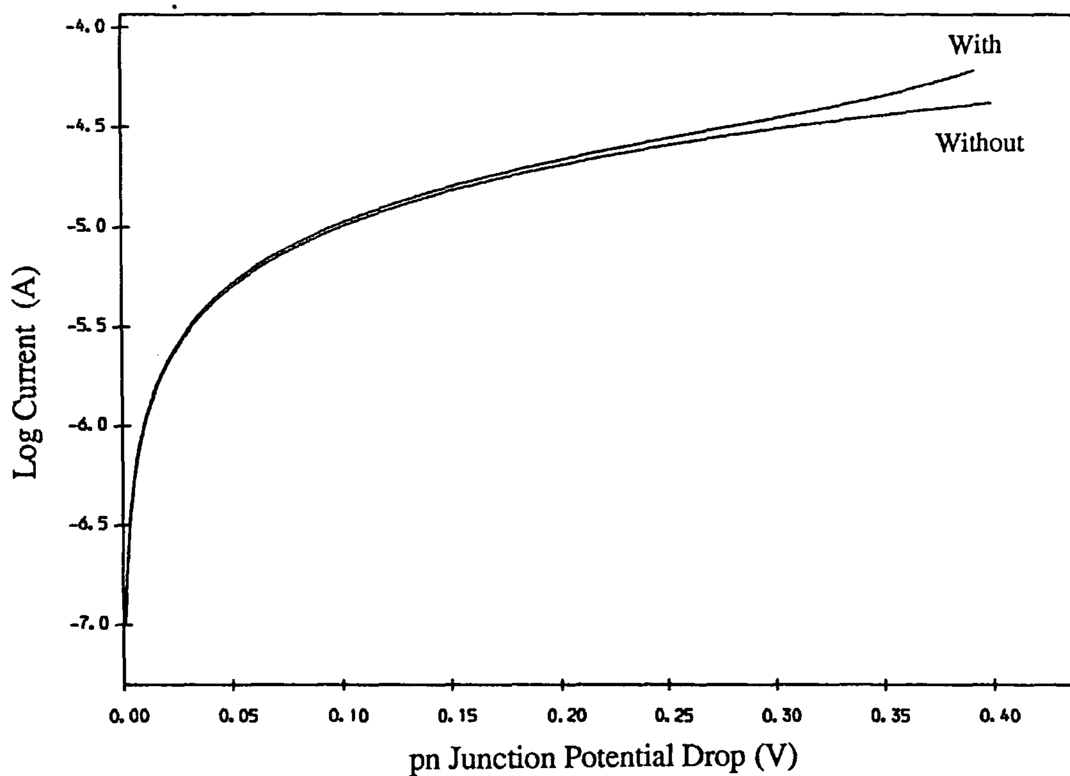

Fig 5.2(b): Total Spreading Recombination Current with/without Hole Recombination in the n-type Layer.Top Contact Radius 2000 μm

oxides, it still produces a much closer quantitative agreement with experiment than the 1-D model.

The surface area of the boundary between the MIS depletion region and the neutral n-type layer is assumed to be equivalent to the area covered by the metal top contact in (5.2.1). This is a reasonable assumption with the n-type layer having a thickness of $5\mu m$ compared with modelled top contact radii of between 250 and $2000\mu m$. Because of the large difference between n-type layer thickness and top contact radius, current collection by the edges of the MIS depletion region outside the area below the top contact would only make a small contribution to the total injected hole current I_{pj}.

5.2.1 Other Assumptions

Other assumptions made in the two-dimensional current spreading model are as follows:

1.) The top contact is assumed to be circular with a radius r_0.

2.) The n-type layer and p-type substrate layer are assumed to be radially infinitely large.

3.) The potential drop V_f across the pn depletion region immediately below the circular top contact is uniform.

4.) The potential drop $V_j(r) = V_f, r \leq r_0$, across the pn depletion region immediately below the radial top contact is taken as the independent variable.

5.) The voltage drop across the pn junction is measured in the neutral n-type layer relative to the neutral substrate which is at ground.

6.) There is a point at radius r_1 where $V_j(r_1)$ and $I_{sp}(r_1)$ both have magnitudes smaller than specified limit values V_{lim} and I_{lim}. $V_j(r_1)$ is the potential drop across the pn junction at this point, $I_{sp}(r_1)$ the current flow radially past this point, and $r_1 > r_0$.

7.) The thickness of the conductive region for electrons in the n-type layer is assumed to be equal to the thickness of the n-type layer itself.

8.) Generation in the MIS depletion region is neglected.

5.2.2 Current Spreading Equation

As can be seen in Fig 5.1, the metal top contact has a negative applied bias w.r.t. the substrate, as required by the MISS to produce a negative impedance characteristic. Classically, the current flow is towards the top contact as shown, and from this it can be seen that

$$V_j(r - dr) < V_j(r) \qquad \text{and} \qquad I_{sp}(r) + I_d(r) = I_{sp}(r - dr) \qquad 5.2.2$$

where $V_j(r)$ is the potential across the pn junction at the point r w.r.t the substrate, $I_{sp}(r)$ is the drift current flow into the annulus at r of width dr, and $I_d(r)$ is the recombination current in this annulus. The resistance as seen by a current $I_{sp}(r)$ flowing from the ring at radius r to $(r - dr)$ is calculated to be

$$R(r) = \frac{\rho dr}{2\pi rt} \qquad 5.2.3$$

where ρ is the resistivity of the n-type layer, and t the n-type layer thickness. The potential drop across the annulus due to the current $I_{sp}(r)$ is given by

$$V_j(r - dr) - V_j(r) = -I_{sp}(r)R(r) \qquad 5.2.4$$

and the current contribution from the annulus is

$$I_d(r) = J(V_j(r))2\pi r dr \qquad 5.2.5$$

where $J(V_j(r))$ is the electron recombination current density in a pn depletion region with a potential drop $V_j(r)$.

The expression for $J(V_j(r))$ is found to be

$$J(V_j(r)) = \frac{qn_i W_{pn}(|V_j|)}{2\tau_p} \frac{(e^{q|V_j|/kT} - 1)}{(e^{q|V_j|/2kT} + 1)} \qquad 5.2.6$$

where the pn depletion width is given by

$$W_{pn}(V_j) = \sqrt{\frac{2\epsilon_s}{q}\left(\frac{N_a + N_d}{N_a N_d}\right)(V_{bi} - V_j(r))} \qquad 5.2.7$$

The modulus of V_j is used in (5.2.6) because the reference potential in the model is taken to be that of the p-type substrate.

Now by combining (5.2.3) and (5.2.4) it can be seen that

$$r\frac{dV_j(r)}{dr} = \frac{\rho}{2\pi t} I_{sp}(r) \qquad 5.2.8$$

and combining (5.2.2) and (5.2.5) gives

$$dI_{sp}(r)/dr = -J(V_j(r))2\pi r \qquad 5.2.9$$

With (5.2.5) differentiated w.r.t. r, and a substitution made for $dI_{sp}(r)/dr$, the second-order differential equation in V_j and r obtained is [4]

$$\frac{d^2V}{dr^2} + \frac{1}{r}\frac{dV}{dr} = \frac{-\rho}{t} J(V_j(r)) \qquad 5.2.10$$

Solving this equation with the boundary conditions

$$V_j(r_0) = V_f \qquad \text{and} \qquad V_j(r_1) < V_{lim}, \quad I_{sp}(r_1) < I_{lim} \qquad 5.2.11$$

where r_1 is undetermined, the total recombination current flow I_{rec} in the depletion layer due to a potential V_f across the pn junction beneath the top contact can be found.

To justify ignoring the hole contribution to the spreading current, a simple approximation can be used to allow the importance of hole recombination outside the region below the metal top contact to be appreciated. This was achieved by adding a hole current expression due to a potential drop V_j to the r.h.s. of (5.2.10) which can be regarded as being due to all holes injected from the substrate recombining at the top surface of the n-type layer.

$$J_p(V_j(r)) = \frac{qD_p {n_i}^2}{N_d(t - W_{pn})}(e^{qV_j(r)/kT} - 1) \qquad 5.2.12$$

The contributions to the total spreading current can be seen in Fig 5.2(b) for the pn recombination current alone, and the sum of the pn recombination current with the hole injected current. The total spreading current is not strongly affected by holes until a value for V_f of $0.4V$ is reached. This shows the accuracy of the electron drift expression used for calculations. By using this hole expression an upper limit is put on the influence of holes on the total electron recombination current in the pn region of the device, although it should not be regarded as an accurate physical description of what actually happens to the holes.

When values for I_{rec} are calculated neglecting hole recombination and using different top contact radii, the recombination currents when plotted against the pn forward voltage beneath the top contact have the form as shown in Fig 5.2(c). The four 2-D curves show a linear increase in the total electron recombination current up to a value for the pn forward voltage potential drop of about $0.4V$. In

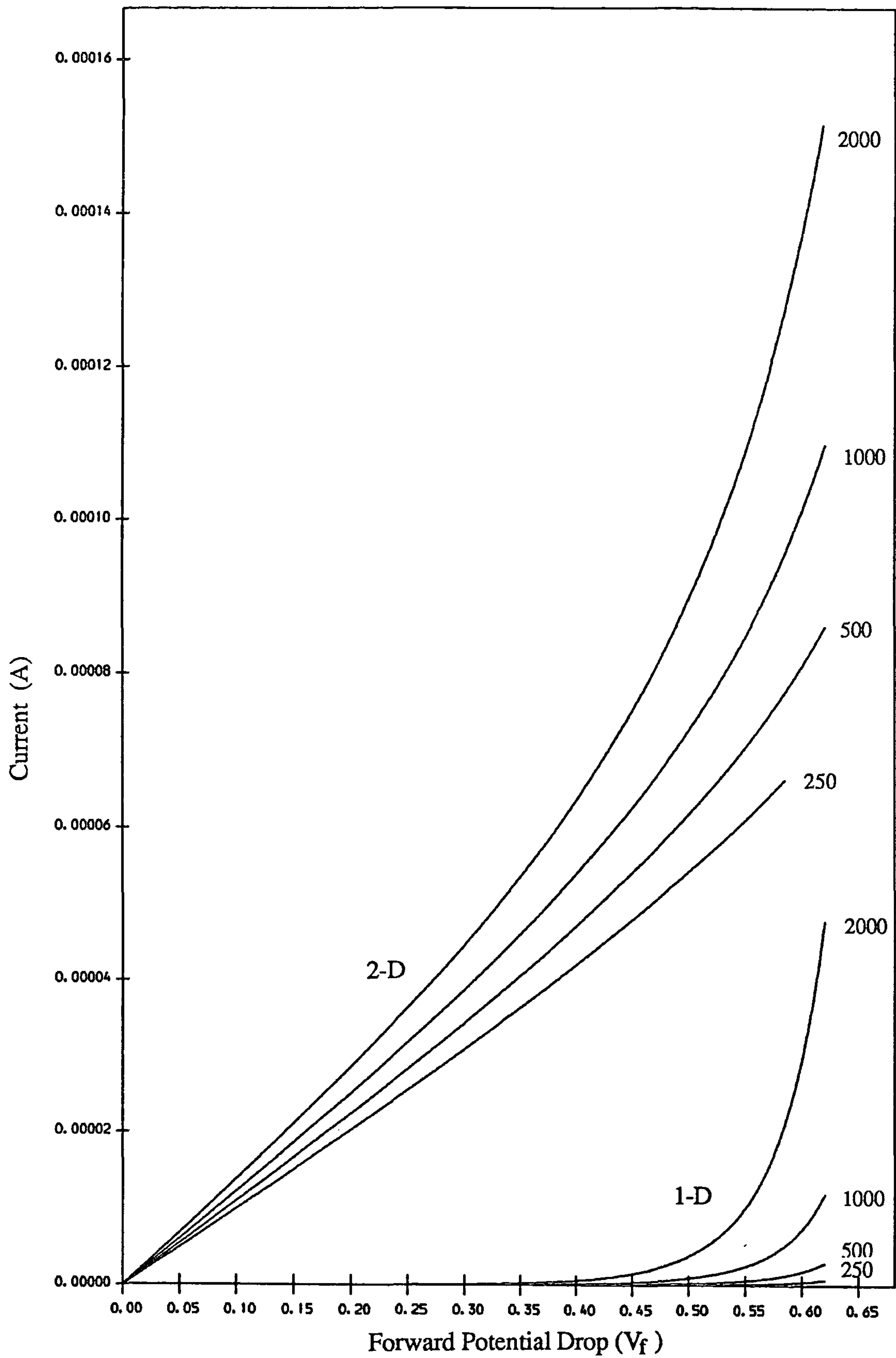

Fig 5.2(c): Total 2-D Spreading Current and 1-D pn Recombination Current against pn Junction Potential Drop for Various Top Contact Radii (μm).

the 1-D case, the total pn depletion recombination current has the form

$$J_{rj} = \frac{qn_iW_{pn}}{\tau_p}\left[\frac{e^{qV_f/kT}-1}{e^{qV_f/2kT}+1}\right] \qquad 5.2.13$$

Values for the expected one-dimensional currents with the same top contact radii and other parameters are also given in Fig 5.2(c). They are much smaller than the 2-D recombination currents for small potential drops across the pn junction. As V_f increases however, differences in the electron recombination current magnitudes between the one and two-dimensional models becomes less marked. Because of this, it is reasonable to assume that devices with the smallest values for V_f at the switching and holding points, and the smallest areas, will display the greatest departures from 1-D behaviour when the 2-D $I - V$ characteristic are calculated. This is borne out by results. As will be seen later, the effect of the spreading current has its most marked effect on the current-voltage curve of the thicker oxide devices with the smallest top contact radii.

5.3 Method of Solution for the Two-Dimensional Model

It can be seen from (5.2.10) and (5.2.11), that by assuming a potential drop V_f across the pn junction beneath the top contact, and a point r_1 at which both the forward voltage across the pn junction and the current flow into the annulus are less than specified limits, a total electron recombination current, I_{rec}, can be calculated for the pn depletion region of the device.

For various values of V_f, the second order differential equation (5.2.10) was solved with the specified boundary conditions, and the results were put into a file to act as a look-up table for the spreading recombination current due to a

particular V_f.

The current continuity equations are similar to the 1-D case, except currents rather than current densities are employed, giving a system of equations that can be written in the form:

$$I_{tp} = \pi r_0^2 J_{tp} = I_{pj} = \pi r_0^2 J_{pj} \qquad 5.3.1$$

for holes and

$$I_{tn} = \pi r_0^2 J_{tn} = I_{rec} = I_{sp}(V_f, r_0) + \pi r_0^2 J_{rj}(V_f) \qquad 5.3.2$$

for electrons. The total potential across the device is given by

$$-qV_{tot} = -q\psi_s - qV_f - qV_{ox} \mp E_g/2 - q\phi_{fn} \mp q\chi_s + q\Phi_m \qquad 5.3.3$$

with all symbols having their usual meanings.

As with the 1-D case, the potential V_f is used as the independent variable in solving the two current continuity equations. This assumes an electron tunnelling current equal to the total recombination current in the pn junction depletion region, and p-type substrate I_{rec}, with the value for $I_{sp}(r_0)$ provided from the look-up table. Use of a look-up table is not a necessary part of the device modelling in 2-D, but it was very quickly found that computational time for solution of (5.2.10) with the boundary conditions (5.2.11) dominated that for the iterative procedures used for solving the two current-continuity equations (5.3.1) and (5.3.2).

This system of equations was solved as in the 1-D case for the two independent variables ξ and $E\psi_s$; the quasi Fermi level splitting at the IS interface, and the energy drop across the MIS depletion region measured from the conduction band of the semiconductor in the neutral n-type layer to the semiconductor conduction

band at the IS interface respectively. With these values calculated, the total current through the device

$$I_{tot} = I_{tn} + I_{tp} = I_{rec} + I_{pj} \qquad 5.3.4$$

together with the total potential drop V_{tot} (5.3.3) could be determined to provide the final $I - V$ characteristic.

Four look-up tables were computed for the two-dimensional analysis, each with a different top contact radius, but with all their other structural parameters in common. The top contact radii used were: $250, 500, 1000$ and $2000\mu m$.

5.4 Results

In the one-dimensional model, a lightly doped MISS with a $5\mu m$ wide n-type layer and an oxide thickness of between 20 and $25\AA$ would behave as a punchthrough device, with a fixed switching potential of $13V$, and a holding voltage of $1V$. For oxide thicknesses greater or smaller than these values, the switching voltage falls off until towards 10 or $40\AA$ switching is not seen, see Fig 4.11. These 1-D model predictions for the switching and holding voltages and current densities, are lower than those found experimentally [1-3]. The 1-D model also predicts the lack of a switching characteristic for metal work functions of less than $4.3eV$. It is these discrepancies between the 1-D model and experimental work that have been remedied in this chapter, with the effect of a large pn junction, (modelled to be infinite), with a much smaller metal top contact area being explored. The effect of area on the $I - V$ characteristic of the MISS is demonstrated through the variation of three parameters: the thickness of the tunnelling oxide for a fixed

top contact radius, the radius of the top contact, and the work function of the metal top contact. By changing these three parameters, it will be seen that the model provides a much better quantitative agreement with experiment; reproducing some of the measured features displayed in experimental MISS current-voltage curves.

In describing the behaviour of the device from the vantage point of the 2-D model, it will be seen that much of the basic qualitative description of device functioning is similar to the 1-D case. It is however necessary to repeat some of this detail to provide a clearer analysis of the important quantitative differences between the two models.

5.4.1 Effect of Oxide Thickness

The effect of oxide thickness is discussed with reference to the $I-V$ characteristics calculated for devices with $2000\mu m$ radii top contacts, and other parameters as described at the start of this results section.

As in the one-dimensional case, total current flow at the switching and holding points increases as the oxide thickness decreases Fig 5.3. There is an increase in both the electron and hole tunnelling currents through the oxide, although as the oxide thickness is altered, the tunnelling current magnitudes change at different rates Fig 5.4 and 5.5. The most obvious difference between the one and two-dimensional models is that the switching and holding currents are greater than if the spreading current I_{sp} had been ignored, and this is seen to be true for all calculated oxide thicknesses.

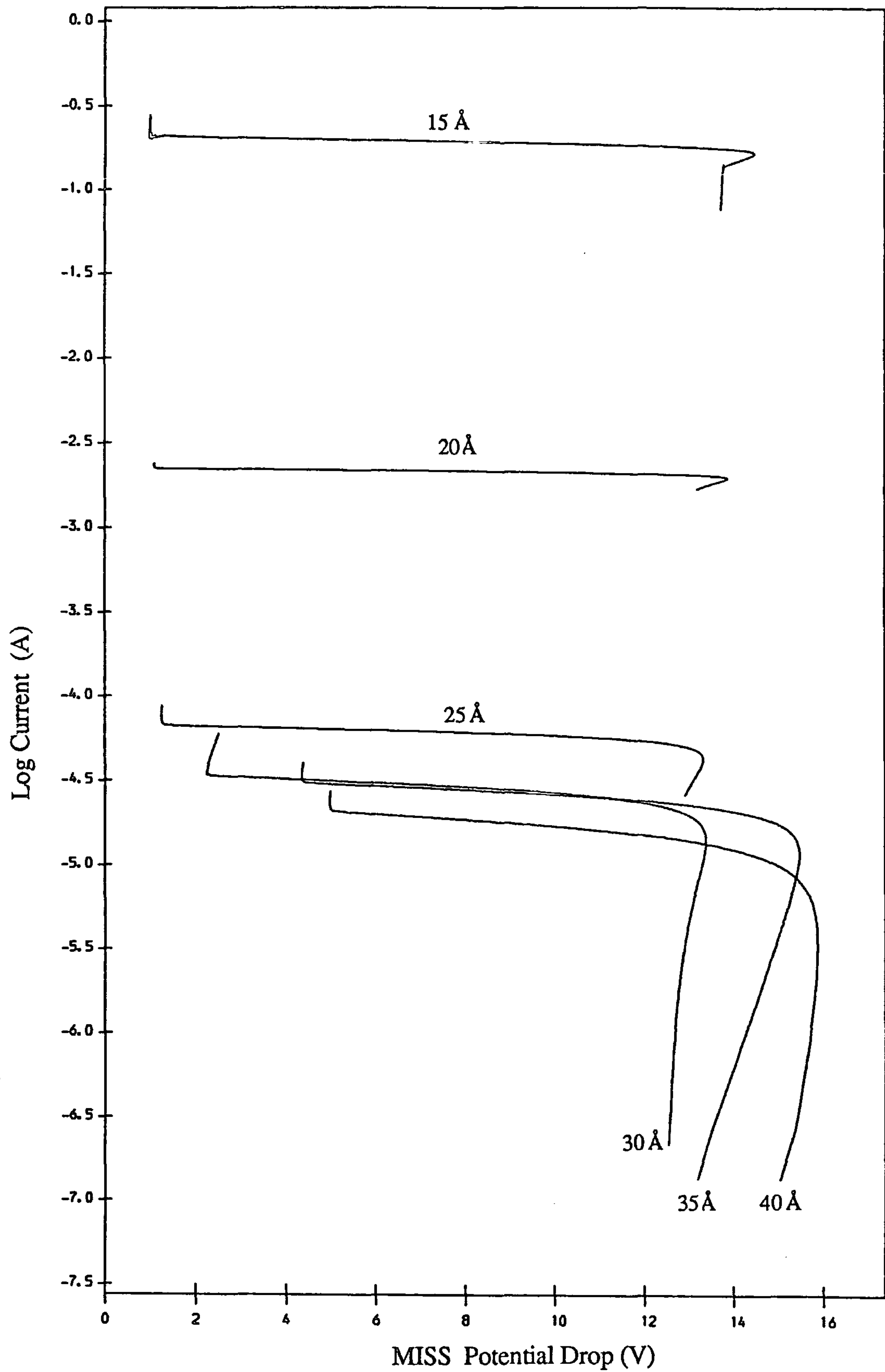

Fig 5.3: I-V Characteristics Using Various Oxide Thicknesses from the 2-D MISS model. Top Contact Radius 2000μm.

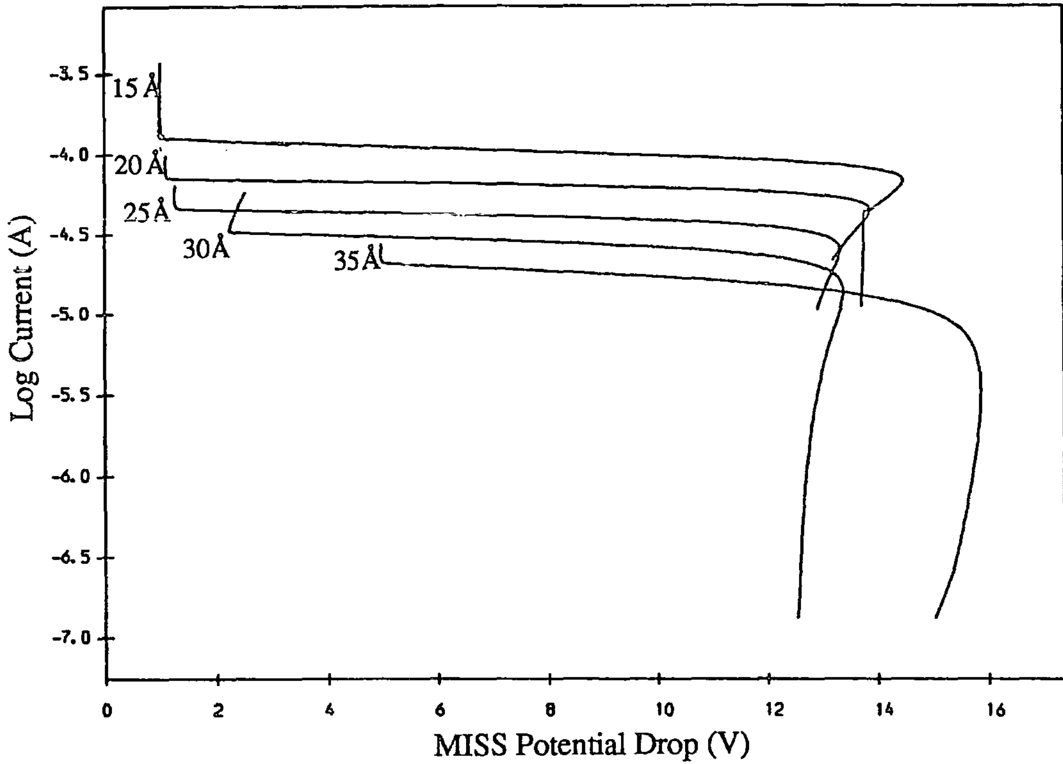

Fig 5.4: Electron Tunnelling Currents Using Various Oxide Thicknesses. Top Contact Radius 2000μm.

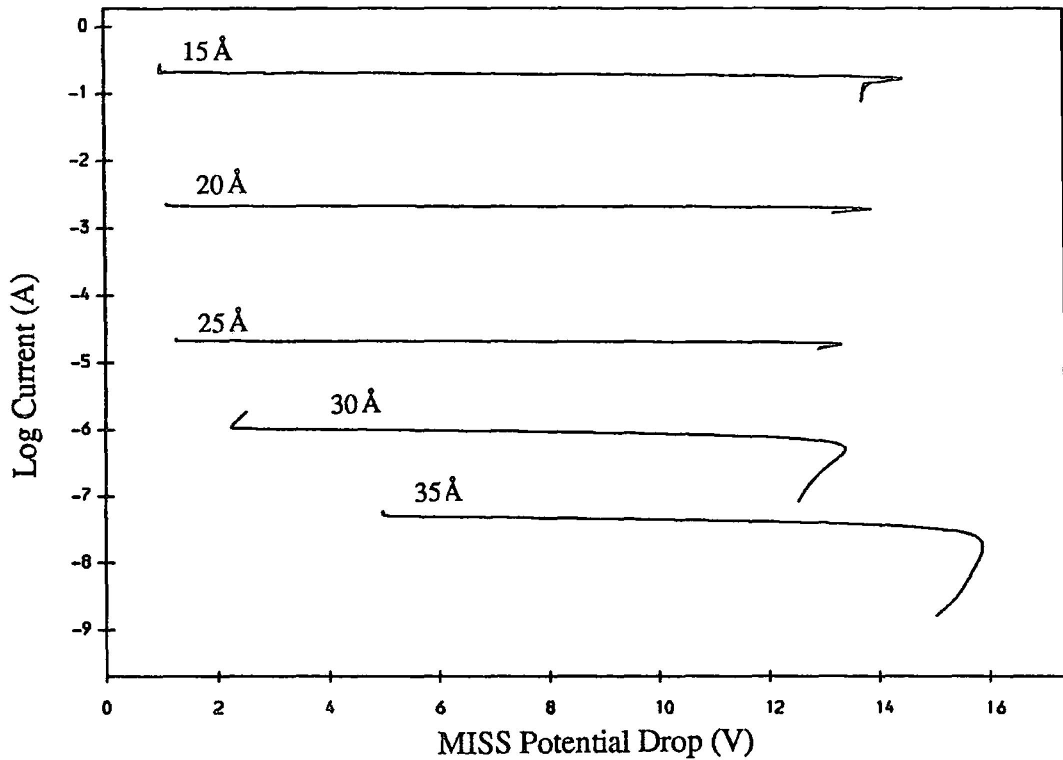

Fig 5.5: Hole Tunnelling Currents Using Various Oxide Thicknesses. Top Contact Radius 2000μm.

For a thick oxide the current through the device at the switching point tends towards a minimum value as the oxide thickness decreases, in contrast to the one-dimensional model. This is due to the almost linear relation between the forward voltage across the *pn* junction and the total electron recombination current, I_{rec}, in the *pn* region of the device. The electron tunnel current dominates the total tunnel current for the thick oxide devices at the switching point.

For the thin oxide devices, the tunnel current tends to be dominated by holes, Fig 5.5. With a thin oxide, hole tunnelling is much easier than for a thicker oxide, and an inversion layer has a proportionally smaller effect on the position of the metal Fermi level relative to the semiconductor conduction band, and therefore on the electron tunnelling current. A greater hole injection current is needed to produce the increase in electron tunnel current and provides the greater hole tunnelling current. This is similar to the 1-D case, except the ratio of the electron recombination current to the hole injected current is much larger.

It can be seen in Fig 5.3 that, as the oxide thickness becomes greater, the switching voltage gradually begins to increase from a relatively stationary value of about $13V$ for the $15\AA$ structure, up to a maximum of $16V$ for the $40\AA$ device, even though switching always occurs by punchthrough. This can be understood because of the increase in the oxide potential drop for the device when a greater electron recombination current needs to be supported from electron tunnelling. The very large difference between the relative recombination currents is demonstrated clearly from Fig 5.2(c) where as V_f decreases the ratio of 2-D to 1-D recombination currents increases rapidly.

For the thin oxide device, the holding voltage is only slightly greater than

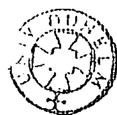

$1V$. As the oxide thickness increases however, the holding voltage also increases, reaching over $4V$ for the $35\mathring{A}$ device. This agrees well with the experimental work of Duncan [2]. One-dimensional theory predicts a holding voltage of about $1V$ for all oxide thicknesses, hence the two dimensional model can be regarded as a much better quantitative description of the experimental situation. This greater holding voltage for the thicker oxide device is again due to the need to support a greater electron recombination current in the *pn* region of the device when compared with the 1-D model.

5.4.2 Effect of Top Contact Radius

It can be seen in Figs 5.6 and 5.7 that the behaviour of the MISS as a function of top contact radius is very dependent upon the thickness of oxide used. For the thin $20\mathring{A}$ oxide device, the switching and holding currents increase strongly with top contact radius, in contrast to the thick $30\mathring{A}$ oxide MISS for which a very slight decrease is seen. This latter result is very interesting as it seems to contradict expectation. For both devices though, as has been described in the previous section, all currents and voltages at the switching and holding points are greater than the values calculated from the 1-D model. Note that in this section, 'thin oxide' refers to the $20\mathring{A}$ device, and 'thick oxide' to the $30\mathring{A}$ structure.

5.4.2.1 The Thin Oxide MISS

In section 5.4.1 it was seen that for the thin oxide device, the tunnelling current

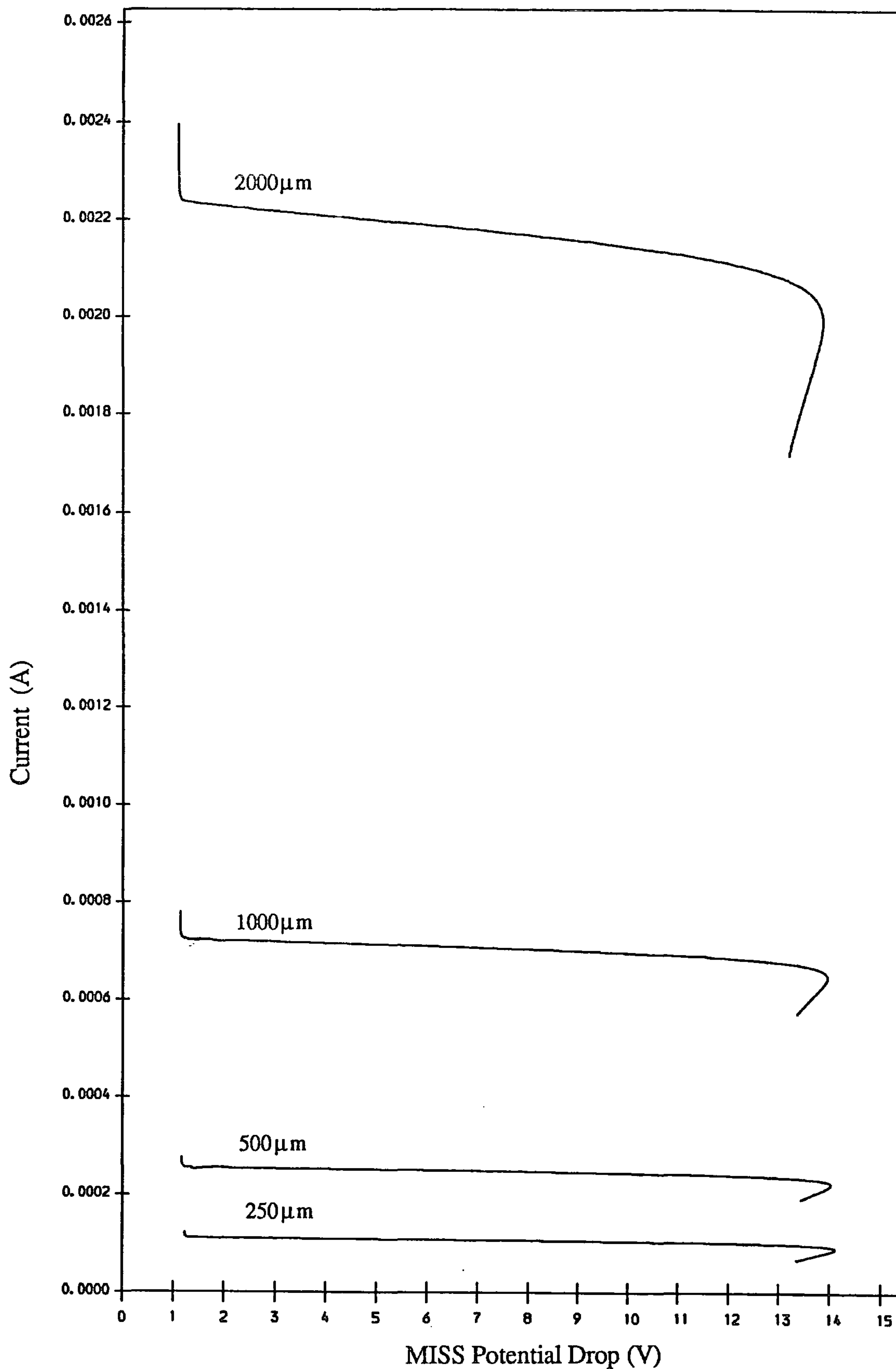

Fig 5.6: Current-Voltage Curves Using Various Top Contact Radii (μm). Oxide Thickness 20Å

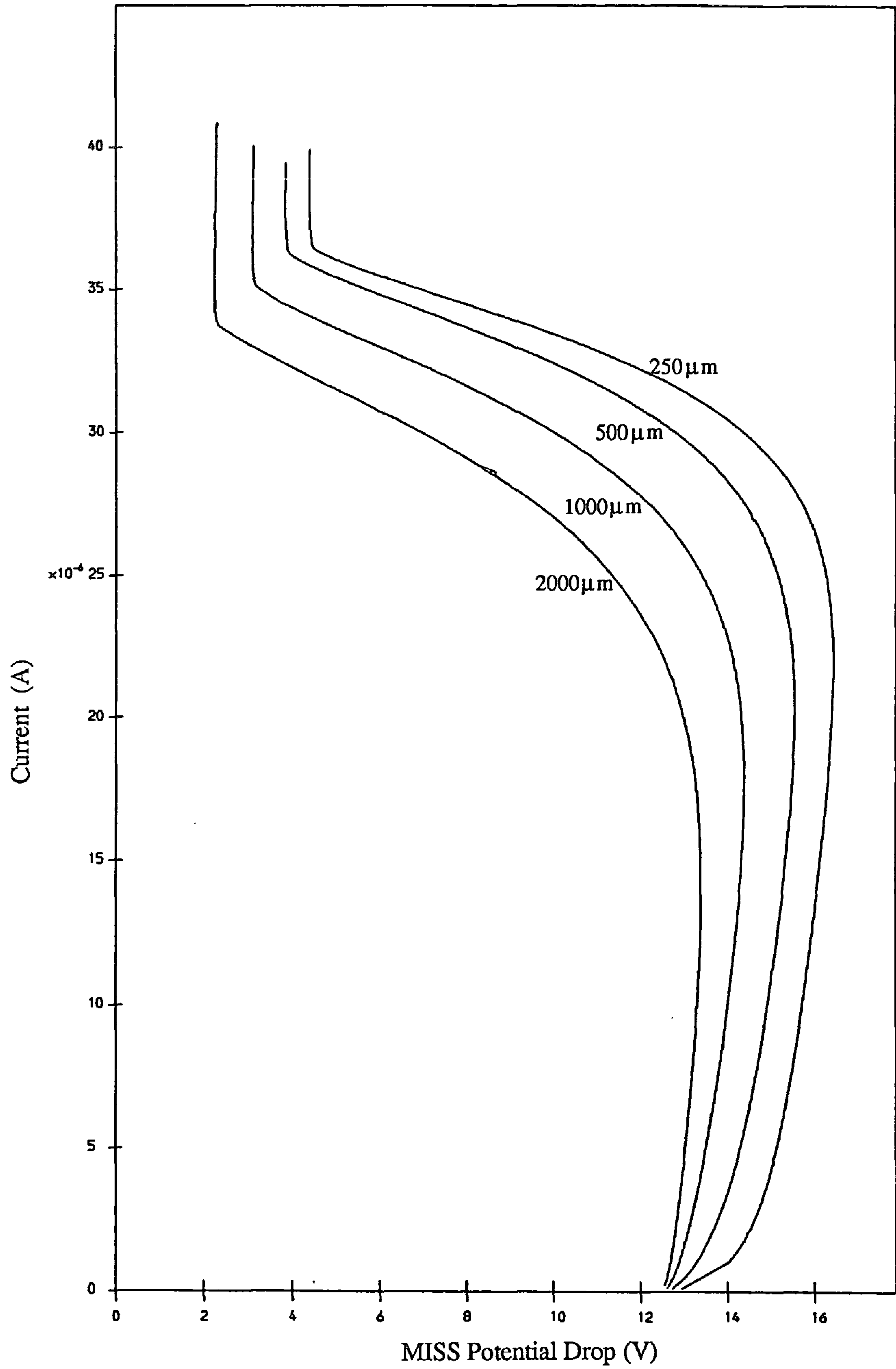

Fig 5.7: Current-Voltage Characteristics Using Various Top Contact Radii (μm). Oxide Thickness 30Å

is dominated by holes at the switching point, throughout the negative impedance region, and at the holding point. With the thin oxide device, as the top contact radius increases so do the values for the switching and holding currents I_S and I_H, Fig 5.6, which is what would be expected for an increase in top contact area.

The thin oxide device needs a large hole current injected towards the IS interface to influence the oxide potential drop, and hence the electron tunnelling current I_{tn}. The thin oxide is very leaky causing holes to tunnel freely, so providing the majority of the total tunnel current. There is a certain minimum inversion charge density required at the IS interface to produce any appreciable electron tunnelling current. This charge density is similar for all device areas, producing a total current through the MISS which is almost linearly proportional to area. These effects are clearly demonstrated in Fig 5.8, where the electron and hole tunnel currents have been plotted for the thin oxide device with varying top contact radii. As the top contact area increases, so the hole tunnel current becomes more dominant. This is demonstrated clearly by examining the ratio $J_{tp}/(J_{tn} + J_{tp})$ at the switching and holding points which can be termed the 'tunnelling efficiency'. For increasing top contact radii the effect of spreading should tend to zero, finally giving the value of the tunnelling efficiency for the one-dimensional model equivalent to an infinite top contact radius. The table below shows that this is the case, with the hole tunnel current becoming almost totally dominant for a top contact to *pn* junction area ratio of 1 : 1

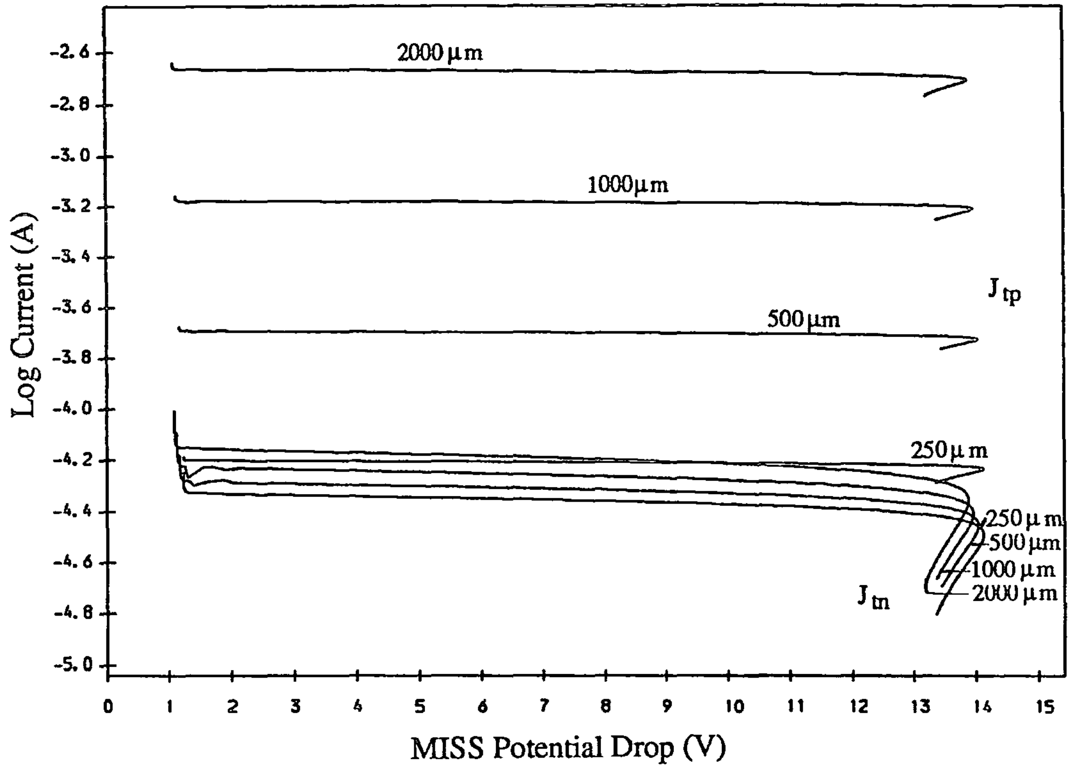

Fig 5.8: Electron and Hole Tunnelling Currents Using Various Top Contact Radii (μm). Oxide 20Å

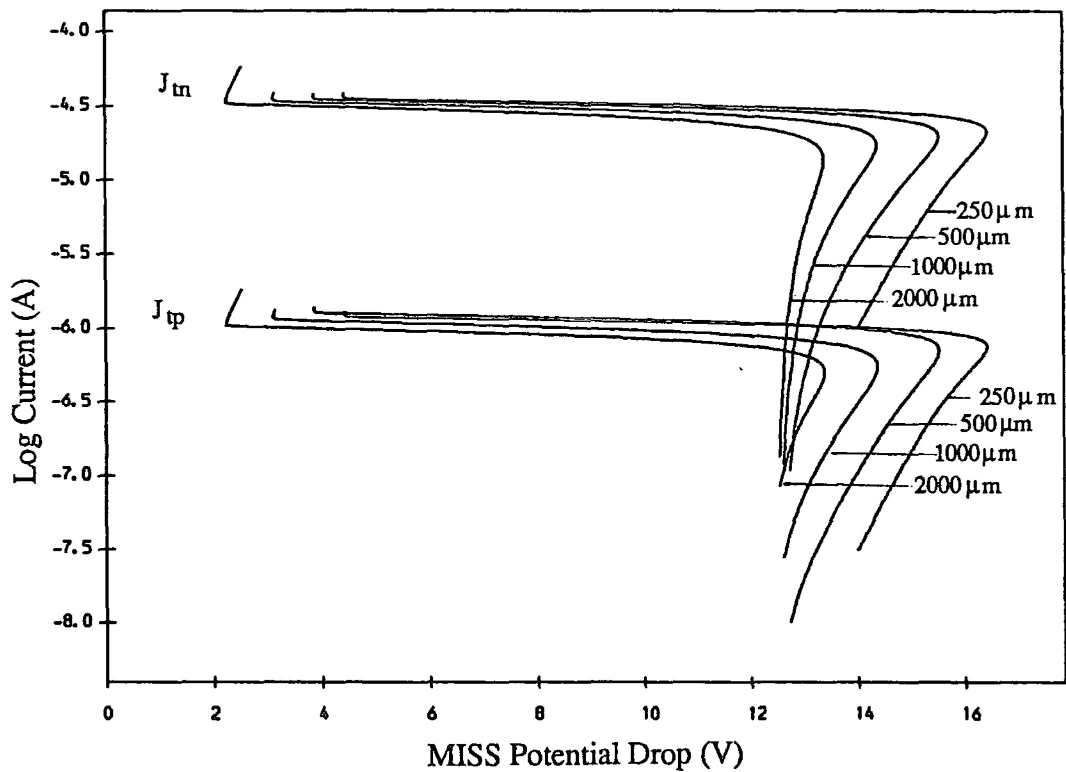

Fig 5.9: Electron and Hole Tunnelling Currents Using Various Top Contact Radii (μm). Oxide 30Å

Top Contact	Tunnelling Efficiency (TE)	
Radius μm	Switching (TE_S)	Holding (TE_H)
250	0.6436	0.5431
500	0.8421	0.7706
1000	0.9400	0.9044
2000	0.9779	0.9624
∞	1.0000	0.9998

5.4.2.2 The Thick Oxide MISS

The thick oxide MISS behaves very differently to the thin oxide structure. As the top contact radius decreases the total current flow at the switching and holding points increases slightly, Fig 5.7. This slight increase corresponds to a very large increase in the current density calculated flowing through the top contact. For all top contact radii, the electron current dominates the total tunnel current from before switching until after the holding point, Fig 5.9. This suprising effect is due to the much greater dominance of spreading current on total electron current in the *pn* region of the device, see Fig 5.2(c). This dominance becomes even more pronounced at a fixed V_f as the top contact radius decreases.

The value for V_f at the switching point increases as the top contact radius decreases. This is because the greater electron tunnel current density needs a stronger inversion layer before switching can take place. The increased electron and hole current densities produced more than compensate for the decrease in the top contact area so producing the the slight rise in switching current.

Overall the total current flow at the switching and holding points and in the

negative impedance region is increased by reducing the top contact radius. This trend is certainly true in the range of top contact radii used - 250 – 2000μm with the current densities at the switching and holding points approaching a minimum for the infinite top contact radius. This is illustrated clearly in the table below.

Radius $r_0(\mu m)$	$V_S(V)$	$J_S(A/cm^2)$	$V_H(V)$	$J_H(A/cm^2)$
250	16.44	1.117E-2	4.423	2.018E-2
500	15.55	2.590E-3	3.864	4.838E-3
1000	14.39	5.653E-4	3.105	1.168E-3
2000	13.39	1.123E-4	2.253	2.789E-4
∞	10.04	1.904E-7	1.092	5.105E-7

5.4.3 Effect of Work Function

As in the one-dimensional case, increasing the metal work function increases the switching and holding currents for both thin and thick oxide devices, Figs 5.10 and 5.11. Fig 4.9 shows the 1-D case for a 25Å oxide. There is however a marked difference in the magnitude of the current changes with work function for the thin and thick oxide devices calculated from the 2-D model, and also switching is seen for work function values for which it is not seen in the 1-D case.

5.4.3.1 The Thin Oxide MISS

For the thin oxide device, the switching and holding currents increase by more than an order of magnitude as the work function changes from 4.2 to 4.8eV. These

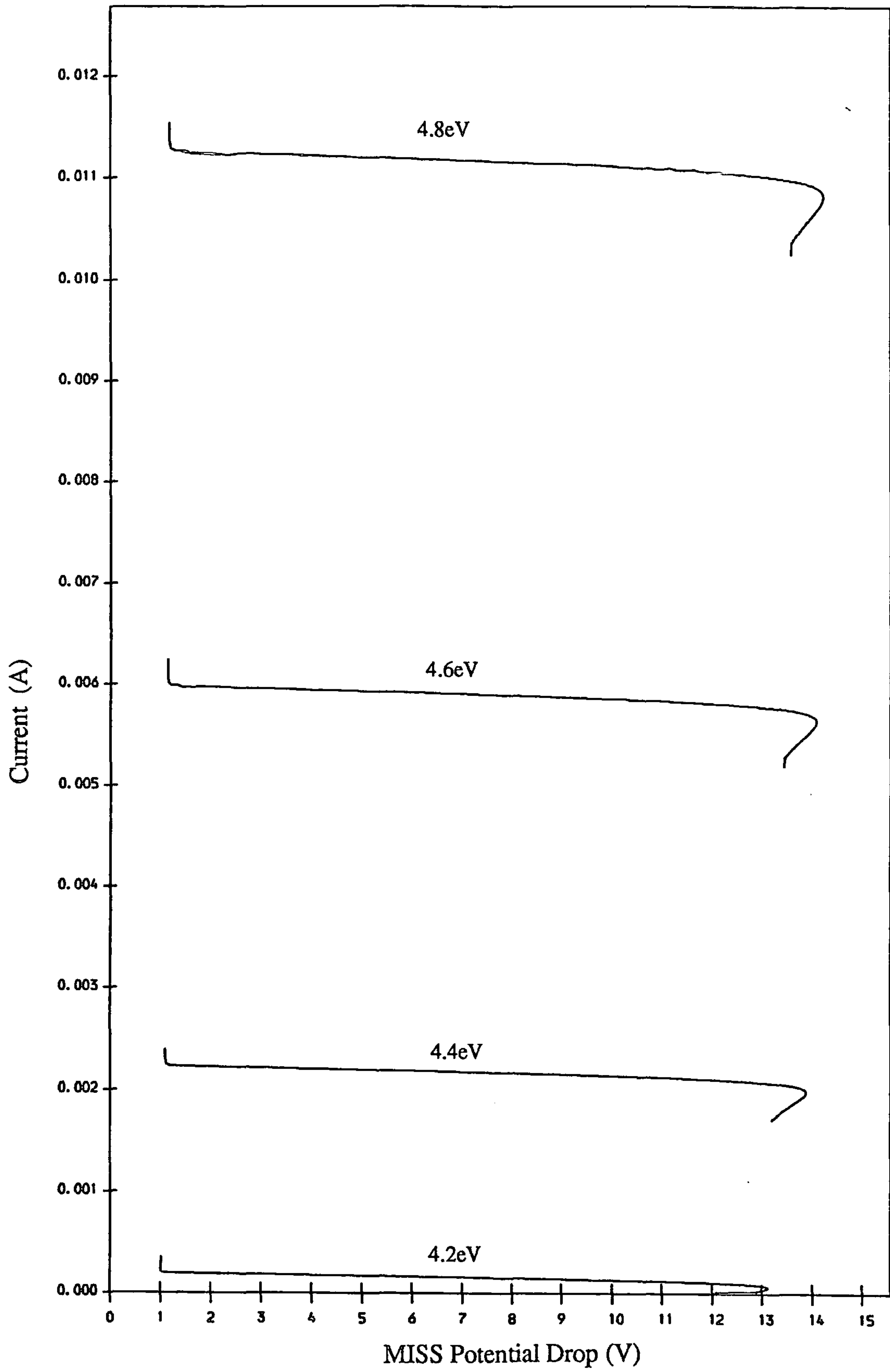

Fig 5.10: Current-Voltage Characterisics Using Various Work Functions. Top Contact 2000μm Oxide 20Å

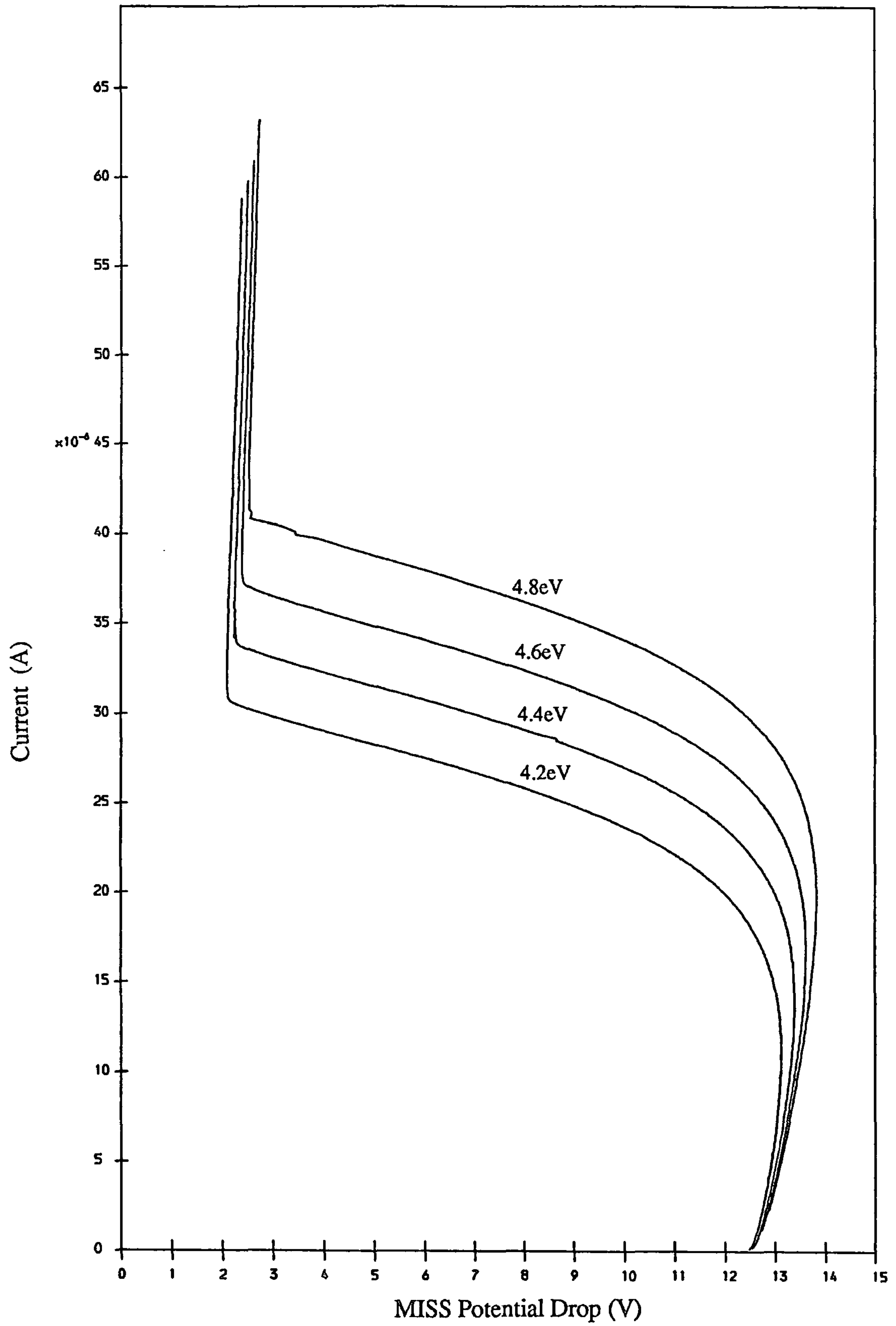

Fig 5.11:Current-Voltage Characterisics Using Various Work Functions. Top Contact 2000μm, Oxide30Å

increases can be understood for similar reasons to the 1-D case with a greater oxide potential drop needed to provide an appreciable electron tunnel current resulting in a higher value for the *pn* junction potential drop, V_f, and hence in all other currents at the switching point.

As can be seen in Fig 5.2(c), the greater V_f, the closer the *pn* recombination current values calculated from the one and two-dimensional models. For the thin oxide MISS this results in a similar qualitative trend with I_S and I_H both doubling as W_f moves from 4.6 to 4.8eV. However, for the 4.2eV device, both the 2-D model and experimental work produce a switching characteristic, something which is not seen with the 1-D model. This is because of the greater electron recombination current in the *pn* depletion region for a fixed V_f in the 2-D model, so producing the need for a greater degree of hole inversion at the IS interface and hence a switching characteristic.

5.4.3.2 The Thick Oxide MISS

For the thick oxide device the switching and holding currents also increase with work function, but not to the same extent as for the thin oxide structure. The tunnelling current through the oxide is dominated by electrons in contrast to the 1-D case, and the thick oxide MISS also produces a switching characteristic for the 4.2eV metal top contact, something that cannot be produced from the 1-D model.

5.5 Discussion

It has been shown in this chapter that the two-dimensional MISS model predicts a greater current density flow at the switching point, through the negative impedance region, and at the holding point than can be calculated from the one-dimensional model. It also shows the device to have a much greater holding voltage for certain device parameters in line with experiment; a result which up until now has remained unexplained. These effects have been shown to be caused by the greater electron recombination current in the *pn* region produced from current spreading. The total electron recombination current I_{rec} is the sum of two contributions: the *pn* recombination current immediately under the top contact I_{rj}, and the spreading current $I_{sp}(V_f, r_0)$ outside the top contact. The ratio $I_{sp}(V_f, r_0)$ relative to I_{rj} decreases with both increasing forward voltage V_f across the *pn* junction, and increasing top contact radius r_0, therefore the divergence between the one and two-dimensional models become less marked as these parameters change in this way.

The basic results from the two-dimensional model can be summarised as follows;

i) Decreasing the oxide thickness for a fixed top contact radius increases the current density at the switching and holding points together with decreasing the switching and holding voltages.

ii) For the thin oxide devices, the current magnitudes increase with the contact radius. With the thick oxide devices the reverse is the case for the top contact radii given.

iii) As the work function is increased the total current flow at the switching and holding points increases, although the effect is much more pronounced for the thin oxide device.

By examining the above results more carefully, it is seen that for the thin oxide devices ($20\mathring{A}$) the total tunnel current is dominated by holes, for the thicker ($30\mathring{A}$) oxide structures it is dominated by electrons. In explaining the results it has been emphasised that it is the oxide voltage which controls the electron tunnel current, and for the lightly doped device this voltage is controlled by the degree of hole collection at the IS interface. The electron current is dependent upon the position of the metal Fermi level relative to the semiconductor conduction band, and when the Fermi level is within a few kT of the conduction band edge, the electron current is large and rising rapidly. This mechanism is the same in all devices, and the oxide potential has to be sufficient to bring it about.

For the region of the device outside the top contact, the two-dimensional model presented here could be improved with the addition of hole recombination in the n-type layer, together with hole recombination at the top surface. Also the contribution of holes injected into the n-type layer from ouside the metal top contact region to the hole injected current into the MIS depletion region could be included. However, difficulties with this more accurate model would immediately arise with the need to deal with two carriers in the spreading region: an electron drift current, and a hole current which would be the sum of both drift and diffusion components. This would obviously make calculation of the spreading currents more difficult so providing another justification for the more simple approximation that has been developed in the text.

References

1. Duncan, K. A., Tonner, P. D., Simmons, J. G. and Faraone, L., ' Characteristics of Metal/Tunnel-Oxide/N/P^+ Silicon Switching Devices-I., Effects of Device Geometry and Fabrication Processes', *Solid-St. Electron.*, **24**, pp. 941-948, (1981).
2. Duncan, K. A., *M. Sc. Thesis*, University of Toronto, (1981).
3. Faraone, L., Simmons, J. G., Hsueh, F-L. and Mishra, U. K., 'Characteristics of Metal/Tunnel-Oxide/N/P^+ Silicon Switching Devices-II., Two Dimensional Effects in Oxide-Isolated Structures' *Solid-St. Electron.*, **25**, pp. 335-344, (1982).
4. Joyce, W. B. and Wemple, S. H., 'Steady-State Junction- Current Distributions in Thin Resistive Films on Semiconductor Junctions', *J. Appl. Phys.*, 41, pp.3818-3830, (1970).

CHAPTER SIX

STEADY STATE NEGATIVE IMPEDANCE

6.1 Introduction

In this thesis the computed current-voltage characteristic for the MISS is produced by taking steady state electron and hole current expressions for the MIS and pn regions of the device, equating, and then solving these equations at the MIS depletion region/neutral n-type layer interface. This provides values for the position of the hole quasi-Fermi level at the IS interface, and the potential drop across the MIS depletion region, so allowing the total current flow and total potential drop across the device to be determined. However, these steady state equations have no explicit time dependence, so very little can be determined about the stability of the device in the negative impedance region. All that can be said is that the computer model can find a unique operating point for a specified total current flow through the device.

As has been explained in chapter two, the accepted method for describing the behaviour of the MISS in the negative impedance region is a regenerative feedback mechanism causing the MISS to switch from its OFF to its ON state. If the device were held in its negative impedance region using a constant current source, the regenerative feedback mechanism would imply oscillatory behaviour. However, it has been found from experimental work in Durham [1], that, with careful use of

measuring apparatus to keep parasitic effects at a minimum, a stable operating point can be found, implying the occurrence of a stable negative impedance region. In this case the regenerative feedback model for device switching is to be regarded as invalid.

This chapter deals with the concept of stable negative impedance [2] for the MISS, and analyses an equivalent circuit model showing that the device can behave as a stable circuit element between the switching and holding points. This is achieved by describing it as displaying both negative differential resistance (NDR), and negative differential capacitance (NDC). These quantities are calculated using the one dimensional MIS diode, and two dimensional MISS models developed in chapters four and five respectively.

The computed values for the small signal NDR, r_{nd}, and small signal NDC, c_{nd}, are presented with emphasis on changes in their magnitudes with variations in the fabrication parameters. These are oxide thickness, work function and top contact area from the 2-D MISS model, and oxide thickness and work function from the MIS diode model. The computed stability of the MISS as a circuit element is also examined using the generated values of r_{nd} and c_{nd} from the 2-D MISS model. In this analysis the measure of stability is the time taken for the MISS to return to the steady state after a delta function perturbation in the supply potential.

6.2 The MISS Device as a Circuit Element

The NDR and NDC are small signal quantities, and their effect in a circuit can be understood by applying standard circuit theory. In this section a brief

description of the circuit theory associated with the device is given, leading to the expression used for stability analysis at the end of the chapter. The more complete theory is outlined in Appendix E.

6.2.1 MISS Circuit Analysis

The circuit examined consists of a supply voltage V_{sup}, in series with a load resistor R, and a parasitic inductance L, see Fig 6.1. The device itself is regarded as behaving in the same way as a negative differential resistance of value $r_{nd}(I_{tot})$, in parallel with a negative differential capacitance of value $c_{nd}(I_{tot})$. It is the small signal response of this type of circuit element that is analysed. The dependence of $c_{nd}(I_{tot})$ and $r_{nd}(I_{tot})$ on the total device current I_{tot} will be dropped, though it must be born in mind that all analysis takes place for a chosen point on the $I-V$ curve, and though R and L remain constant, r_{nd} and c_{nd} change their values depending upon the operating point chosen. The value for R has been picked to ensure the load-line intersects the MISS $I-V$ characteristic at one point only, Fig 6.2.

The NDR of the device is calculated to be

$$r_{nd} = \frac{\Delta V_{tot}}{\Delta I_{tot}} \qquad 6.2.1$$

where I_{tot} is the total current flow, and V_{tot} is the total potential drop. The NDR is calculated by taking the difference between two successive calculated operating points in the steady state model, Δ, so giving (6.2.1).

The NDC is calculated in a similar way. Taking the metal top contact as the top plate of the device when viewed as a capacitor, the total charge stored for a

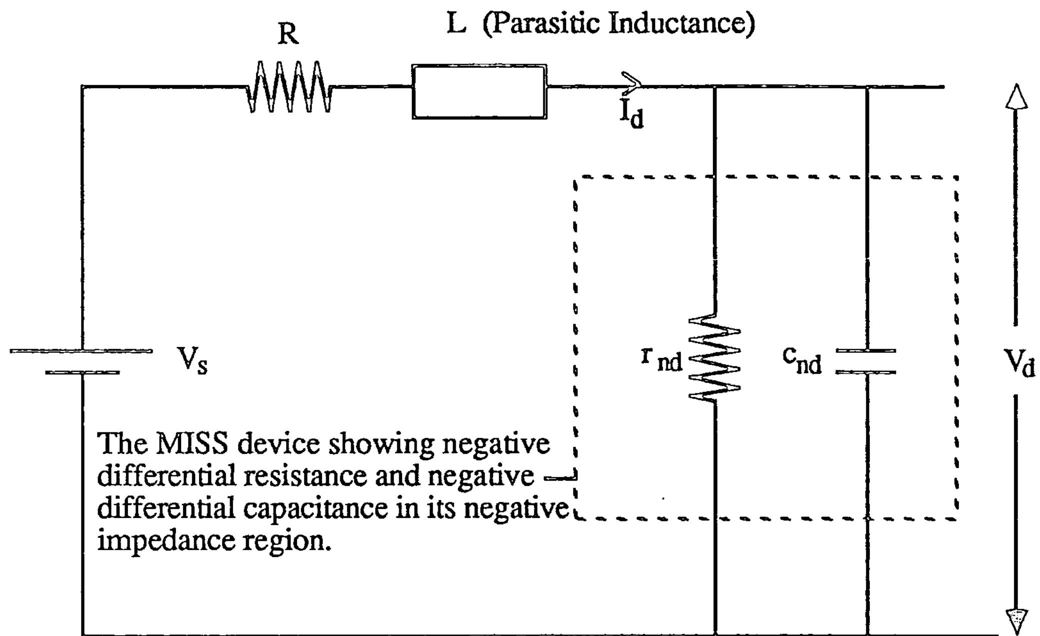

Fig 6.1: The MISS Device as a Circuit Element

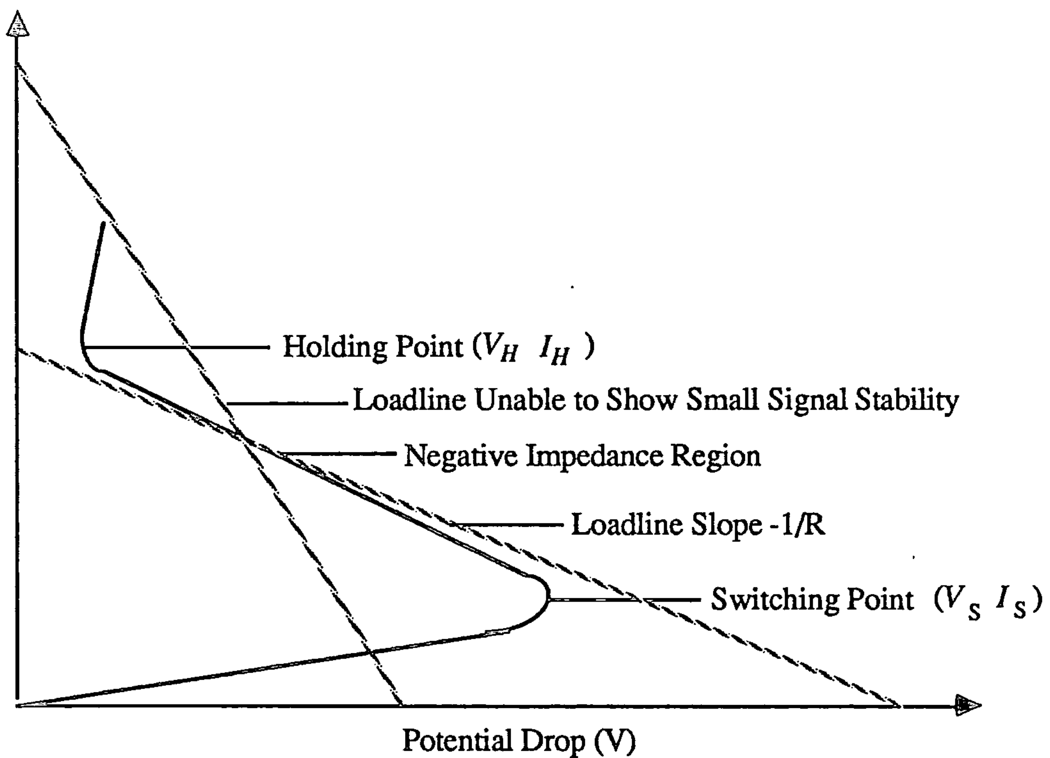

Fig 6.2: The I-V Curve for the MISS Device as a Circuit Element.

particular operating point, Q_{ox}, is determined using electric field continuity across the metal oxide interface. The resulting expression is found to be

$$Q_{ox} = \frac{\epsilon_{ox} V_{ox} A_T}{d_{ox}} \qquad 6.2.2$$

where A_T is the area of the top contact and is given by $A_T = \pi r_0^2$, and other symbols have their previously defined meanings. From this expression the NDC is calculated in the form

$$c_{nd} = \frac{\Delta Q_{ox}}{\Delta V_{tot}} \qquad 6.2.3$$

where, as in the NDR case the Δ appears due to the magnitude of c_{nd} being computed using two successive operating points.

From this expression, it can be seen that throughout the negative impedance region,the differential capacitance of the device is also negative. This is because the potential across the oxide is continuously increasing with current, hence so is the charge stored on the metal top contact. Through the negative impedance region however, the total potential across the device is decreasing, $\Delta V_{tot} < 0$, so making the expression for c_{nd} negative.

The response of the device to an impulse change in the supply potential of magnitude ΔV_{sup} is described in Appendix E. The final form for this response expression is given by

$$\Delta V_{tot}(t) = \frac{r_{nd}}{q}\left[e^{-(p/2r)t}\left(e^{(q/2r)t} - e^{-(q/2r)t}\right)\right]\Delta V_{sup} \qquad 6.2.4$$

where

$$p = r_{nd} c_{nd} R + L$$

$$q = \sqrt{(r_{nd} c_{nd} R + L)^2 - 4 r_{nd} c_{nd} L (r_{nd} + R)}$$

$$r = r_{nd} c_{nd} L \qquad 6.2.5$$

with all other symbols having their previously defined meanings.

6.3 Results

The theoretical data given here for r_{nd} and c_{nd} is only drawn from the 2-D MISS and 1-D MIS diode models in an attempt to produce values that can be achieved in the laboratory.

In the 1-D MISS model, all calculations assume equal active areas of metal top contact to *pn* depletion region. In most cases this produces an unrealistically small electron tunnelling current density through the oxide, and hence a small oxide potential drop. The oxide potential drop is used for the calculation of the charge stored on the metal top contact, which is therefore too small to produce realistic values of NDC.

The MIS diode model described in chapter four produces data for a top contact with an area of $1cm^2$. Because there is no hole injection into the MIS depletion region, and any substrate current is carried solely by electrons, the data can be scaled with area.

This results section is divided into three parts. Firstly,computed values for the NDR and NDC from the 2-D MISS model are given, then the NDR and NDC from the MIS diode model, and finally the stability of the device as a circuit element for different magnitudes of c_{nd} and r_{nd} based upon values calculated from the 2-D MISS model.

6.3.1 Calculated Values for r_{nd} and c_{nd} from the Two Dimensional MISS Model.

This section describes the values of NDR and NDC obtained from the 2-D MISS model through varying the structural parameters. These are oxide thickness, top contact radius, and top contact metal work function.

6.3.1.1 Effect of Oxide Thickness

As can be seen in Fig 6.3, an increase in the oxide thickness of the MISS causes a corresponding increase in the NDR of the device. Fig 6.4 shows the NDC, which in most cases also increases with oxide thickness. The increase in NDR is to be expected, with the device resistance dominated by oxide thickness. However, the standard large signal expression for capacitance predicts the capacitance magnitude to be inversely proportional to oxide thickness, so making the increase in NDC with oxide thickness a suprising result.

In the lightly doped 2-D MISS model, switching occurs at punchthrough producing a similar switching voltage for all devices. In Fig 6.3, it can be seen that except near the switching and holding points, the NDR for each individual oxide thickness is almost constant across the negative impedance region. An approximate expression for the mean NDR can therefore be written in the form

$$\bar{r}_{nd} = \frac{V_H - V_S}{I_H - I_S} \qquad 6.3.1$$

where V_S and V_H are the switching and holding voltages, and I_S and I_H are the switching and holding currents.

With all oxide thicknesses, apart from for the 35Å structure, the value of $V_H - V_S$ is seen to be almost constant, Fig 5.3. Therefore the variations in the NDR of different devices depends predominantly on the difference between the switching and holding currents in expression (6.3.1). This approximate expression for NDR, (6.3.1), enables it to be easily calculated from the large-signal $I - V$ characteristic. It can be seen in Fig 6.3, that as the oxide thickness increases, so does the NDR.

An average expression can also be produced for the NDC by using computed values at the end points of the negative impedance region. As in the NDR case, the NDC curves are almost flat apart from at the switching and holding points, therefore an approximate expression for the mean NDC in the negative impedance region can be written in the form

$$\bar{c}_{nd} = \frac{Q_H - Q_S}{V_H - V_S} = \frac{\epsilon_{ox}}{d_{ox}} \left[\frac{V_{ox_H} - V_{ox_S}}{V_H - V_S} \right] A_T \qquad 6.3.2$$

where Q_H and Q_S are the charges stored on the metal top contact at the holding and switching points, and V_{ox_H} and V_{ox_S} are the oxide potentials at the holding and switching points respectively.

The change in oxide potential is greater for the thicker oxide devices between the switching and holding points, giving a greater value for the negative capacitance. This increase in the oxide potential drop dominates the effect of oxide thickness, d_{ox}, in expression (6.3.2). Only for the 35Å device does the effect of oxide thickness become dominant.

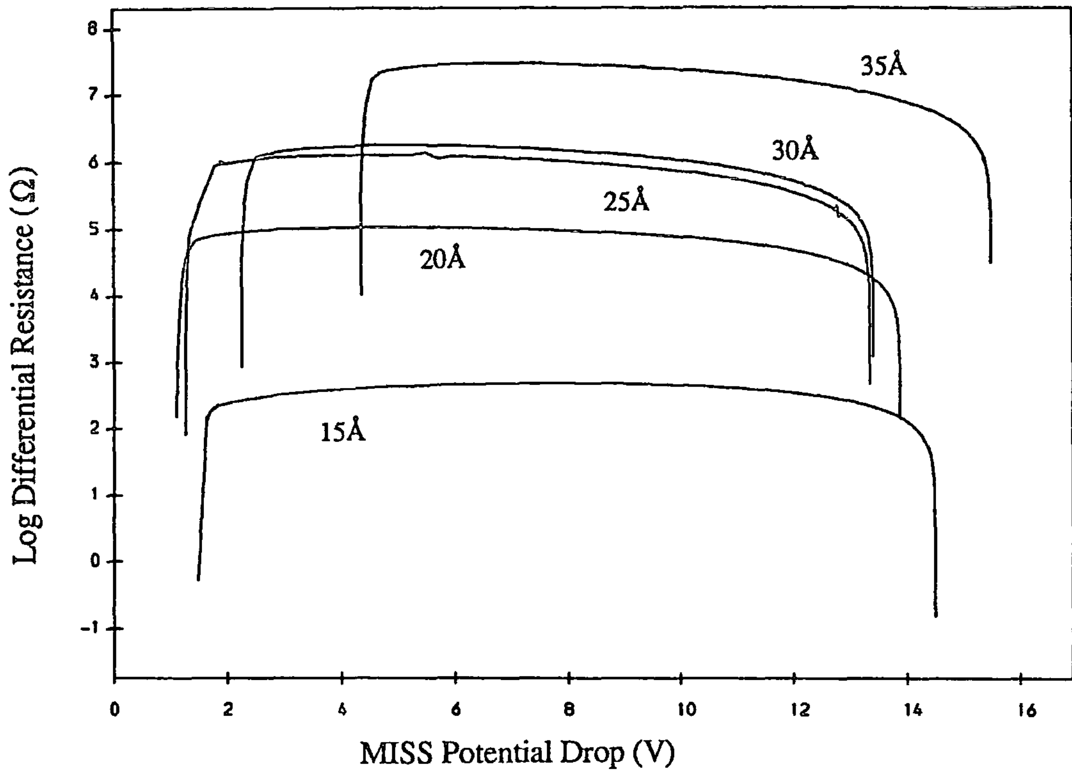

Fig 6.3: NDR Magnitudes for Various Oxide Thicknesses Top Contact Radius 2000μm.

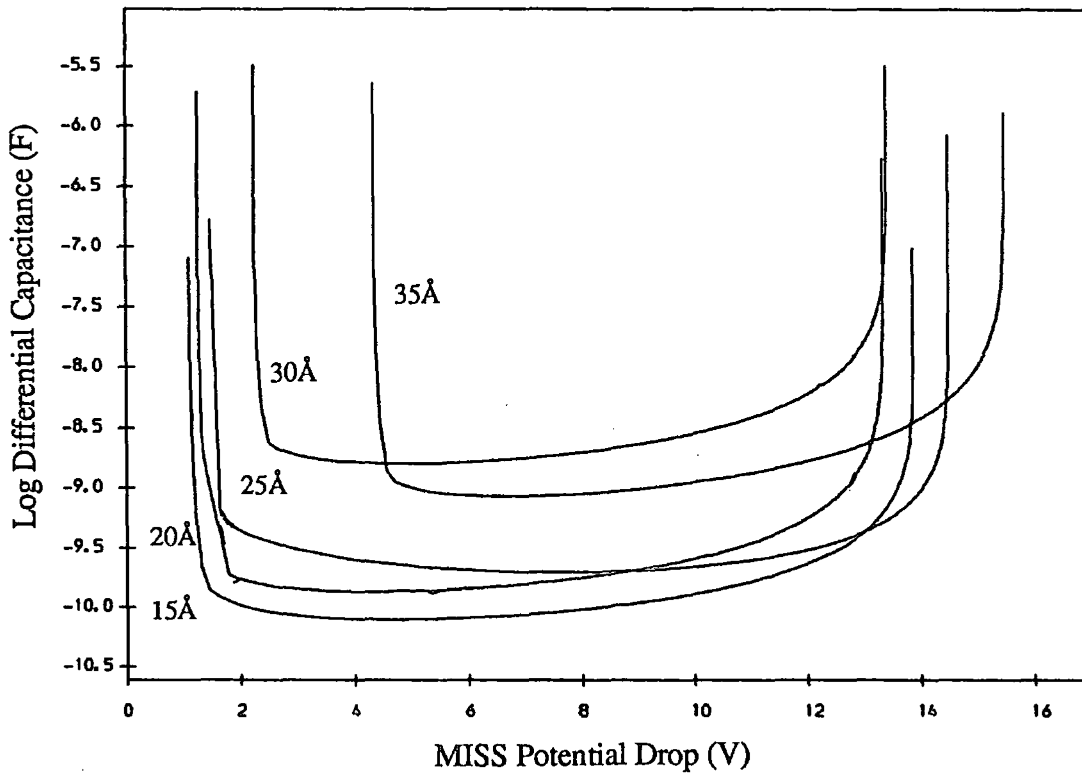

Fig 6.4: NDC Magnitudes for Various Oxide Thicknesses Top Contact Radius 2000μm

6.3.1.2 Effect of Top Contact Radius

Figs 6.5 and 6.6 show the changes in the computed magnitudes of NDR and NDC for top contact radii values ranging between 250 and $2000\mu m$, with the devices having constant top contact oxide thicknesses of $20\AA$. Similarly, Figs. 6.7 and 6.8 show the calculated values for c_{nd} and r_{nd} over the same range of radii for a constant oxide thickness of $30\AA$. With both the $20\AA$ and $30\AA$ MISS devices there is a decrease in NDR with area, and an increase in NDC with area.

As has been demonstrated in chapter five, the current density through the device at a particular operating point in the negative impedance region is approximately inversely proportional to top contact area. Also, the current density in the smaller top contact radii devices increases more rapidly between the switching and holding points than it does for the larger radii devices. This effect is important in understanding how r_{nd} and c_{nd} are affected by area. It can be seen more clearly by writing the expressions for the mean values of negative differential resistance and negative differential capacitance, $\bar{r}_{nd}$ and $\bar{c}_{nd}$ in the forms

$$\bar{r}_{nd} = \frac{V_H - V_S}{I_H - I_S} = \frac{V_H - V_S}{A_T(J_H - J_S)} \qquad 6.3.3$$

and

$$\bar{c}_{nd} = \frac{\epsilon_{ox}}{d_{ox}} \left[\frac{V_{ox_H} - V_{ox_S}}{V_H - V_S} \right] A_T \qquad 6.3.4$$

where J_H and J_S are the current densities at the holding and switching points. With the greater current density for a smaller top contact, it can be seen immediately how the effect of area on the NDR is reduced for both thin and thick oxide devices.

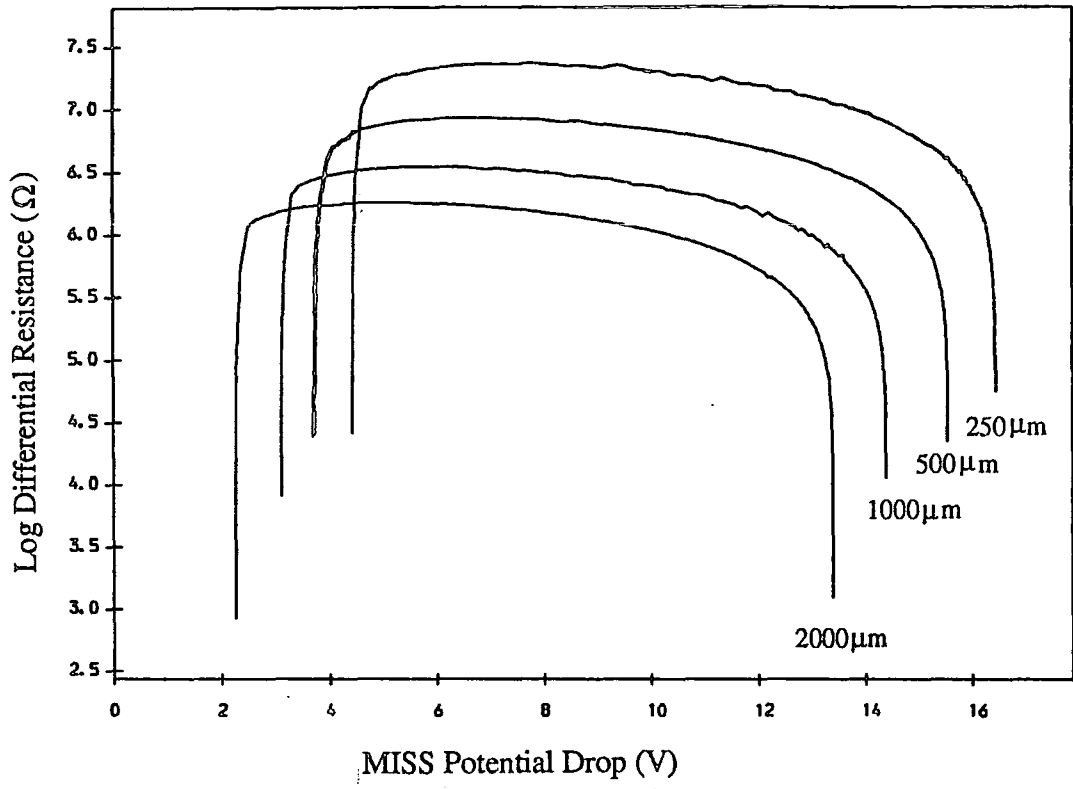

Fig 6.7: NDR Magnitudes for Various Top Contact Radii. Oxide Thickness 30Å

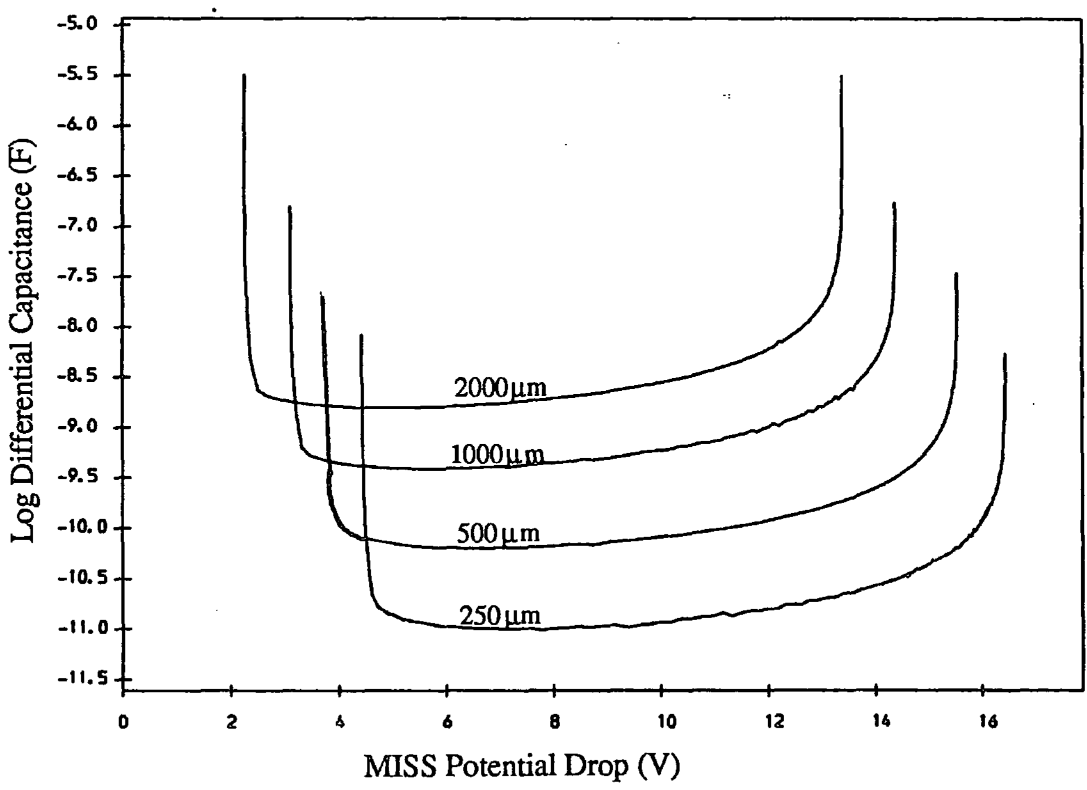

Fig 6.8: NDC Magnitudes for Various Top Contact Radii. Oxide Thickness 30Å

Both curves for the NDC show a much more linear increase with top contact area; the form of this dependence being shown in (6.3.4). The switching and holding voltages for both thin and thick oxides remain almost constant for changes in top contact radius. Also, the difference between the oxide potentials at the switching and holding points for the two thicknesses of oxide remain almost constant. This is especially true for the thin oxide device. With these constant values between the switching and holding points, it can be seen from (6.3.4) that the NDC is dominated by the effect of area.

6.3.1.3 Effect of Work Function

Changing the top contact work function value for a 25Å, 2000μm device, has hardly any effect on the NDR or the NDC. This can be seen clearly in Figs 6.9 and 6.10.

The switching point current increases with increasing work function, Figs 5.10 and 5.11. However, once the switching point is reached, the total change in current flow between the switching and holding points for a varying work function is constant. By examining (6.3.3), it can be seen that with both $I_H - I_S$ and $V_H - V_S$ almost constant for changes in work function, the computed values for the NDR should be similar. This is indeed the case, Fig 6.9.

A similar argument is true for the NDC. In this case, once the switching point is reached, the change in oxide voltage between the switching and holding points, $V_{ox_H} - V_{ox_S}$, for a changing work function remains almost constant. This results in the very similar NDC curves shown in Fig 6.10.

6.3.2 Calculated Values for r_{nd} and c_{nd} from the MIS Diode Model.

In contrast to the 2-D MISS model in which the n-type layer is taken to be lightly doped, the semiconductor is heavily doped for the MIS diode switching device. It was seen in chapter four how the heavily doped n-type layer is necessary to produce a negative impedance characteristic. The results presented here for the MIS diode switching structure show how the device's NDR and NDC are affected by variations in the top contact oxide thickness, and top contact metal work function.

To produce values of NDR and NDC for the MIS diode devices which are more closely comparable with the 2-D results produced above, the results from chapter four have been scaled to produce data from a device with a top contact radius of $2000\mu m$.

6.3.2.1 Effect of Oxide Thickness

From Fig 6.11, it can be seen that the NDR varies strongly with oxide thickness, declining at its maximum negative resistance point by almost four orders of magnitude as the oxide thickness decreases. This is a very large change, and although the actual current voltage curves generated from the MIS diode model do not demonstrate the approximately linear characteristic of the 2-D MISS model, it can be seen that the NDR is greater for the thicker oxide device at all points in the negative impedance region, except close to the switching and holding points. This marked change in NDR between the three devices can be understood from

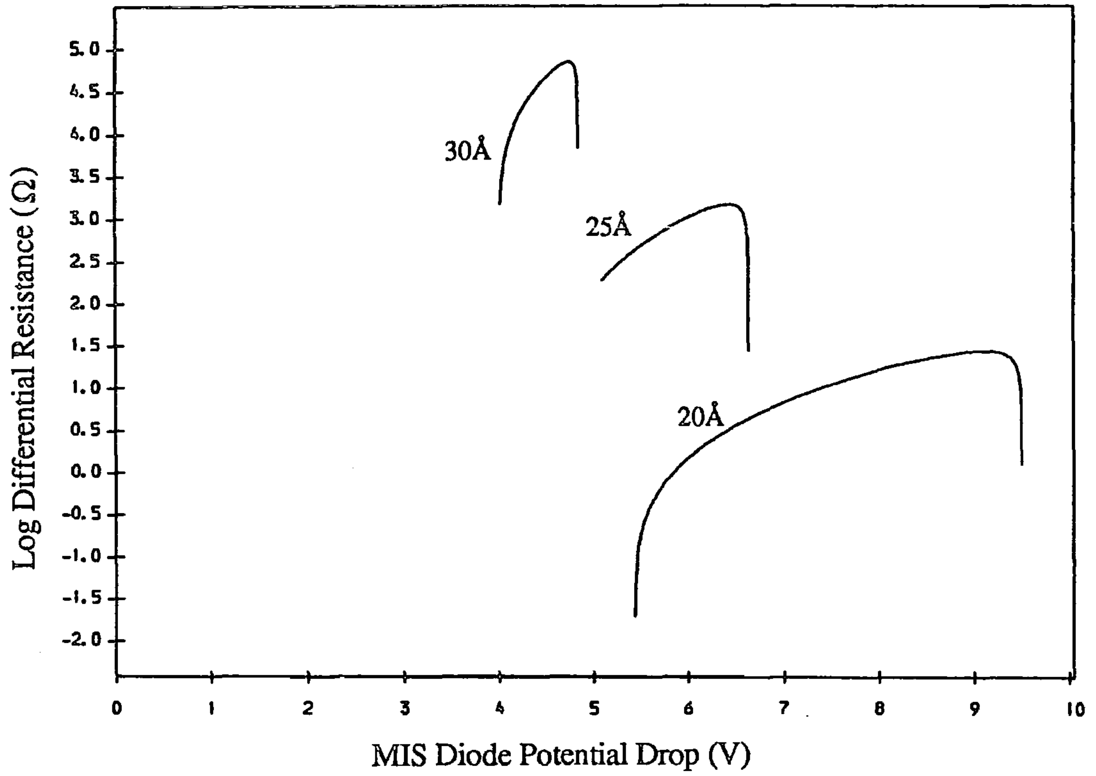

Fig 6.11:NDR Magnitudes for Various Oxide Thicknesses Top Contact Radius 2000 µm.

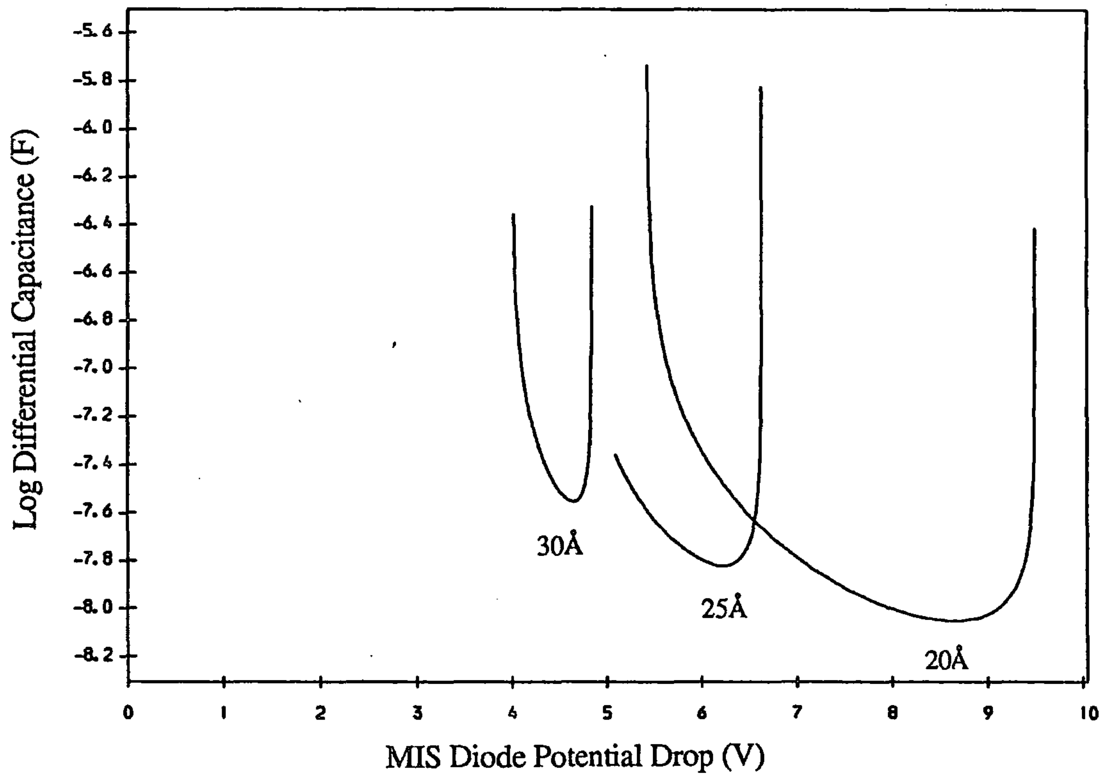

Fig 6.12:NDC Magnitudes for Various Oxide Thicknesses Top Contact Radius 2000µm.

the differences in total current flow. The current is very much smaller for the thicker devices due to greater electron current attenuation from the thicker oxide. A small change in the total potential across the device, ΔV_{tot}, therefore produces a smaller total current change for the thicker oxide structures.

In Fig 6.12 it can be seen that the NDC remains fairly constant with oxide thickness, changing by less than half an order of magnitude between 20 and 30Å. However, the thicker devices do show a greater NDC due to the change in total current flow needing a greater oxide potential drop, and so accounting for the slightly greater calculated NDC. This effect dominates that of oxide thickness.

6.3.2.2 Effect of Work Function

The behaviour of the NDR and NDC for the MIS diode in its negative impedance region as the work function changes is shown in Figs 6.13 and 6.14.

Examining these curves shows that the values of NDR and NDC for the different structures is similar at a constant total device potential. The difference in shape of the three curves is due to the higher work function devices having a much greater switching voltage, so increasing the range of the negative impedance region.

6.3.3 Stability of the Two Dimensional MISS as a Circuit Element

The stability of the 2-D MISS as a circuit element can be determined by a substitution of the computed values for r_{nd} and c_{nd} from the 2-D MISS model

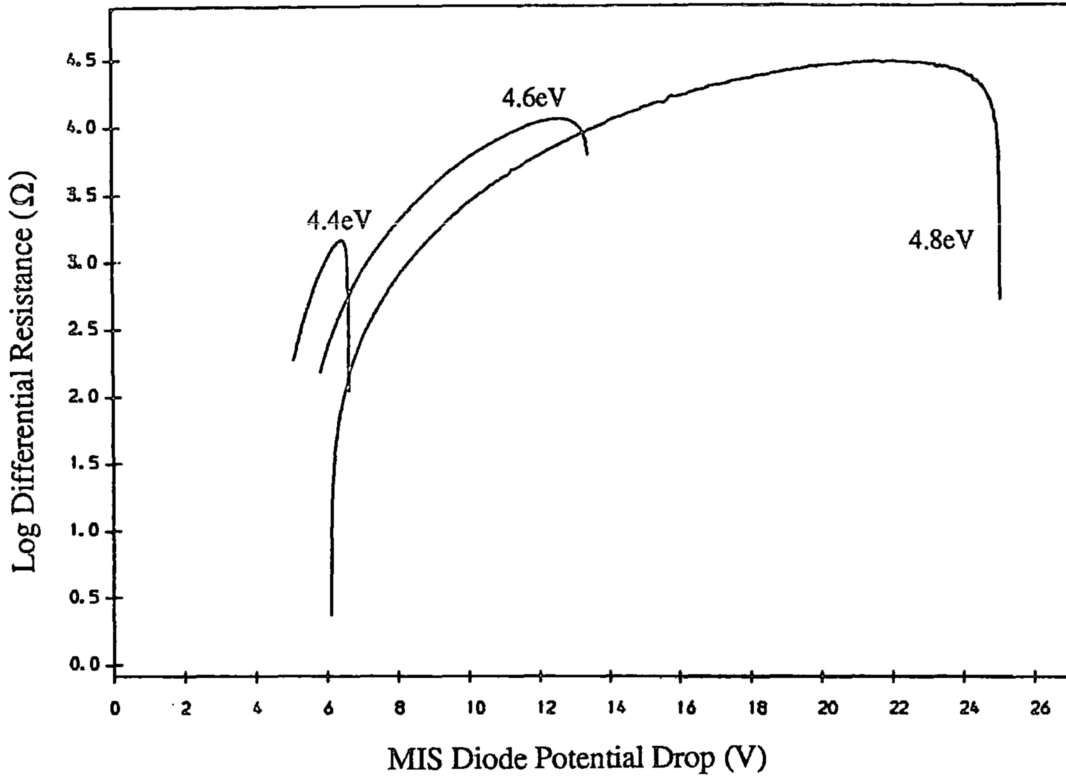

Fig 6.13:NDR Magnitudes for Various Work Functions.
Oxide Thickness 25ÅTop Contact Radius 2000μm.

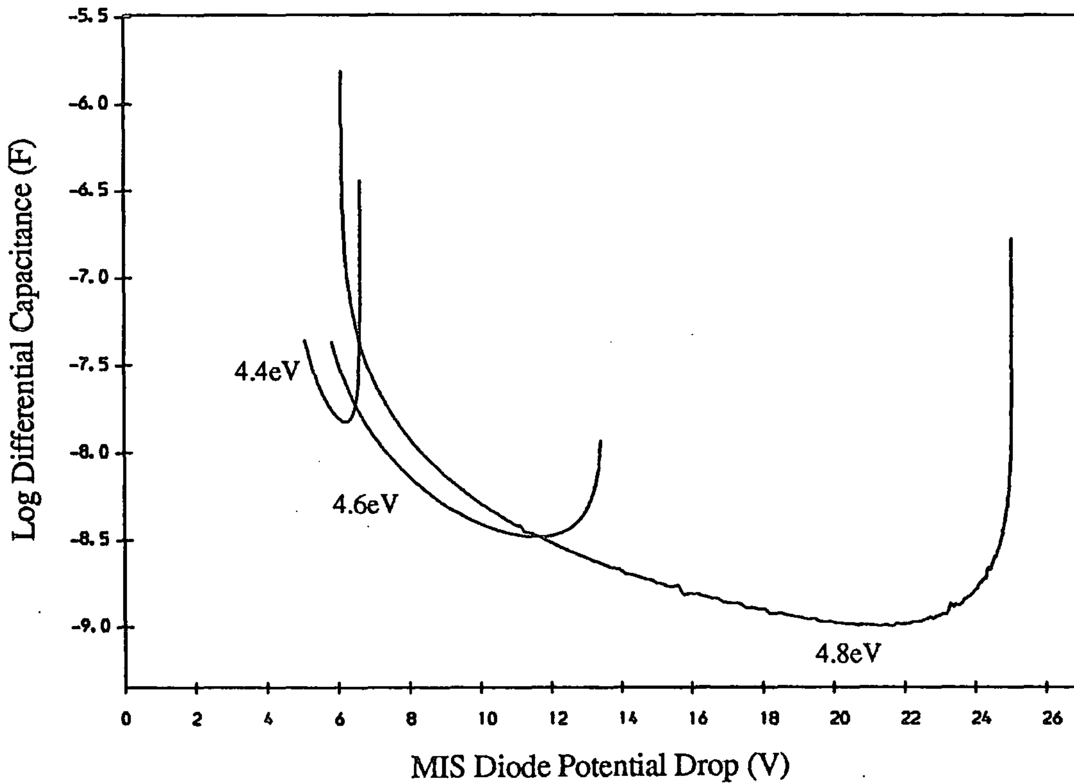

Fig 6.14:NDC Magnitudes for Various Work Functions.
Oxide Thickness 25ÅTop Contact Radius 2000μm.

into the expression for the impulse response of the system (6.2.5). An initial small perturbation to the system ΔV_{sup} is applied, and the time taken for the disturbance in the device potential drop $V_{tot}(t)$, to decline to a suitable small fraction of the initial perturbation is calculated.

A value of $100M\Omega$ for the external resistance R has been chosen to allow the device to have a unique operating point in its negative impedance region, with the load line not intersecting the current voltage curve in either the OFF or ON regions, see Fig 6.2. The parasitic inductance has been given a value of $0.1mH$ [1], to allow solution of the circuit equations.

The time taken for the device to settle back into equilibrium after the application of an external perturbation is dependent upon the magnitudes of the negative differential capacitance c_{nd}, and the negative differential resistance r_{nd}. A program was written to evaluate expression (6.2.5) for the different values of r_{nd} and c_{nd} obtained from the 2-D MISS model. This consisted of a loop providing incremented time intervals at which (6.2.5) was evaluated, and ceasing when $\Delta V_{tot}(t)$ had reached a suitably small value. To show the trends in device stability, an arbitrary perturbation value of $0.01V$ was chosen, together with a limit of $\Delta V_{tot}(t) = 0.001V$ at which equilibrium was assumed to have been reached.

Tables 6.1-6.4 contain the computed NDR, NDC and equilibrium times t_e, for variations in the 2-D MISS structural parameters dealt with in section 6.3.1: oxide thickness, work function, and top contact radius.

Table 6.1 shows the response of t_e to changes in oxide thickness. The swiftest return to equilibrium is for the thin oxide $15\AA$ device. This device also has a relatively small NDR and the second smallest NDC. The longest equilibrium time

calculated was possessed by the thick oxide 35$\AA$ structure. This device also has the second highest NDC. The table shows the equilibrium time to be very sensitive to changes in oxide thickness.

Table 6.2 shows how little the three calculated parameters r_{nd}, c_{nd}, and t_e are affected by changes in the top contact metal work function. As the work function increases there is only a slight decrease in t_e.

Tables 6.3 and 6.4 demonstrate the effect of changes in top contact radii for devices with oxide thicknesses of 20$\AA$ and 30$\AA$ respectively. For the thin oxide device, the NDC increases with top contact radius, and this is accompanied by a drop in the NDR. However, the equilibrium time increases with radius up to $1000\mu m$, at which point it reaches a maximum. With the 30$\AA$ device there is a steady increase in t_e with radius, with the equilibrium time for the 30$\AA$ structure being more than two orders of magnitude greater than that for the 20$\AA$ device.

6.4 Discussion

In this chapter a large number of results have been presented, both for calculated values of NDR and NDC obtained from the 2-D MISS and MIS diode models, together with a simple stability analysis of the 2-D MISS as a circuit element.

For the 2-D MISS model it has been shown that the magnitudes of NDR and NDC can be determined by using large signal values at the switching and holding points, (6.3.3) and (6.3.4), so giving a simple method for determining these values from the computed $I-V$ characteristic. From the 2-D MISS model it can be seen

Equilibrium Times, (t_e), for Different Device Structures

Device Parameters			$r_{dn}(\Omega)$	$c_{dn}(F)$	t_e(s)
Oxide	Contact Radius	Work Function			
$d_{ox} = 15\AA$	$r_T = 2000\mu m$	$W_f = 4.4eV$	$-4.825.10^{2}$	$-1.948.10^{-10}$	$3.710.10^{-7}$
$d_{ox} = 20\AA$	$r_T = 2000\mu m$	$W_f = 4.4eV$	$-1.069.10^{5}$	$-7.831.10^{-11}$	$4.070.10^{-5}$
$d_{ox} = 25\AA$	$r_T = 2000\mu m$	$W_f = 4.4eV$	$-1.284.10^{6}$	$-1.343.10^{-10}$	$7.530.10^{-4}$
$d_{ox} = 30\AA$	$r_T = 2000\mu m$	$W_f = 4.4eV$	$-1.806.10^{6}$	$-1.588.10^{-9}$	$5.380.10^{-3}$
$d_{ox} = 35\AA$	$r_T = 2000\mu m$	$W_f = 4.4eV$	$-2.955.10^{7}$	$-8.348.10^{-10}$	$8.695.10^{-2}$

Table 6.1: Variation of NDR, NDC and t_e with Oxide Thickness.

Device Parameters			$r_{dn}(\Omega)$	$c_{dn}(F)$	t_e(s)
Oxide	Contact Radius	Work Function			
$d_{ox} = 25\AA$	$r_T = 2000\mu m$	$W_f = 4.2eV$	$-1.328.10^{6}$	$-1.415.10^{-10}$	$8.110.10^{-4}$
$d_{ox} = 25\AA$	$r_T = 2000\mu m$	$W_f = 4.4eV$	$-1.284.10^{6}$	$-1.343.10^{-10}$	$7.530.10^{-4}$
$d_{ox} = 25\AA$	$r_T = 2000\mu m$	$W_f = 4.6eV$	$-1.205.10^{6}$	$-1.375.10^{-10}$	$7.190.10^{-4}$
$d_{ox} = 25\AA$	$r_T = 2000\mu m$	$W_f = 4.8eV$	$-1.121.10^{6}$	$-1.419.10^{-10}$	$6.850.10^{-4}$

Table 6.2: Variation of NDR, NDC and t_e with Work Function.

Equilibrium Times, (t_e), for Different Device Structures

Device Parameters			$r_{dn}(\Omega)$	$c_{dn}(F)$	t_e(s)
Oxide	Contact Radius	Work Function			
$d_{ox} = 20\AA$	$r_T = 250\mu m$	$W_f = 4.4eV$	$-1.643.10^6$	$-1.320.10^{-12}$	$1.970.10^{-5}$
$d_{ox} = 20\AA$	$r_T = 500\mu m$	$W_f = 4.4eV$	$-9.395.10^5$	$-4.312.10^{-12}$	$3.170.10^{-5}$
$d_{ox} = 20\AA$	$r_T = 1000\mu m$	$W_f = 4.4eV$	$-3.770.10^5$	$-1.685.10^{-11}$	$4.080.10^{-5}$
$d_{ox} = 20\AA$	$r_T = 2000\mu m$	$W_f = 4.4eV$	$-1.069.10^5$	$-7.831.10^{-11}$	$4.070.10^{-5}$

Table 6.3: Variation of NDR, NDC, and t_e with Top Contact Radii. Oxide Thickness $20\AA$.

Device Parameters			$r_{dn}(\Omega)$	$c_{dn}(F)$	t_e(s)
Oxide	Contact Radius	Work Function			
$d_{ox} = 30\AA$	$r_T = 250\mu m$	$W_f = 4.4eV$	$-2.322.10^7$	$-9.778.10^{-12}$	$2.050.10^{-3}$
$d_{ox} = 30\AA$	$r_T = 500\mu m$	$W_f = 4.4eV$	$-8.553.10^6$	$-6.243.10^{-11}$	$2.970.10^{-3}$
$d_{ox} = 30\AA$	$r_T = 1000\mu m$	$W_f = 4.4eV$	$-3.484.10^6$	$-3.874.10^{-10}$	$4.550.10^{-3}$
$d_{ox} = 30\AA$	$r_T = 2000\mu m$	$W_f = 4.4eV$	$-1.806.10^6$	$-1.588.10^{-9}$	$5.380.10^{-3}$

Table 6.4: Variation of NDR, NDC, and t_e with Top Contact Radii. Oxide thickness $30\AA$.

that the greatest values of NDR are achieved for small top contact radii devices with thick oxides. Small values of NDR are produced using large top contact radii and thin oxides. The NDR value is almost independent of top contact metal work function. For the NDC, large magnitudes are achieved using thicker oxides and large top contact radii, with the computed values again being almost independent of the top contact work function.

From the MIS diode model it can be seen that both the NDR and NDC increase with oxide thickness. For increases in work function, NDR and NDC are seen over a greater voltage range because of the increase in switching voltage.

From the 2-D MISS model, it has been shown that the shortest equilibrium times are achieved for thin oxide structures with small top contact radii and large metal work functions.

References

1. Majlis, B. Y., and Clifton. P., *Private Communication.*

2. Morant, M. J., *Private Communication.*

CHAPTER SEVEN

SUMMARY DISCUSSION AND SUGGESTIONS FOR FURTHER WORK

7.1 Summary and Discussion

In this thesis the MISS has been examined theoretically from three vantage points: as a one-dimensional structure, a two-dimensional structure, and as a circuit element. The one and two dimensional models utilised steady state device equations to generate the $I-V$ characteristics. They were used for the production of results for various fabrication parameters and device geometries. Some aspects of dynamic device operation were also examined. This was achieved by viewing the MISS as a circuit element, and using calculated values for the negative differential resistance and negative differential capacitance obtained from the steady state models. Below is a summary and discussion of some of the more general points raised in this thesis for both steady state and time dependent behaviour. More detailed information and discussion has been given at the end of each chapter.

One-dimensional device operation has been looked at by many investigators, but here the analysis was more comprehensive with the effect of changes in structural parameters, such as work function and oxide thickness on the $I-V$ characteristic determined for a large range of values. Using this careful examination has enabled some of the more accepted ideas associated with device behaviour to

be challenged. This is especially true for the heavily doped n-type layer MISS, where computation showed that ionised donors play a far more important role in determining the switching voltage than avalanche multiplication. This is true for all heavily doped devices except those with thick n-type layers, and/or large work functions. It does however mean that the general mechanism, 'the avalanche mode' [1], offered to describe the switching of these devices in terms of the on-set of avalanche multiplication, is incorrect for most heavily doped n-type layer structures.

For the lightly doped n-type layer device the two active parts of the MISS, the pn region and MIS region, need to be close enough together to allow spacial interaction between them. In this case the MIS depletion region grows towards the pn depletion region enhancing carrier injection. As the n-type layer doping density increases, this effect becomes less important until switching can be seen for a device produced without a hole injecting p-type layer.

It was by using a very thick n-type layer in the 1-D model ($> 1cm$), that a model for the behaviour of the MIS diode switching device was developed. This consisted of a heavily doped ($10^{17}cm^{-3}$), n-type layer, with no hole injecting p-type substrate. The calculated results were consistent with reported experimental work [2], and in quantitative terms provided an excellent model for the behaviour of the MIS diode switching device. This could be understood because of the lack of a hole injected current into the MIS depletion region, making the interaction of the MIS depletion region with the neutral n-type layer only via an electron current. In this case switching was controlled by avalanche multiplication, which also accounted for the high holding voltage since the MIS depletion region needed

to have a minimum width to allow avalanche multiplication to occur.

For the two-dimensional model an infinite substrate was assumed, and the spreading current outside the region below the metal top contact was incorporated in the current continuity equations to produce a better quantitative fit with experiment. This spreading current was assumed to be due to recombination in the *pn* depletion region, and as discussed in chapter five, was shown to produce a good quantitative fit for thick oxides, and a better qualitative fit for the thinner oxides, than did the 1-D model. The most notable triumphs for this simple 2-D model were the prediction of greater total current flows for the device throughout the $I - V$ characteristic, and holding voltages of up to $5V$ for the thicker oxide structures.

The behaviour of the MISS as a circuit element was also examined in an attempt to understand the stability of the device in the negative impedance region. It was found that by choosing an external circuit with a great enough load resistor to intersect the $I - V$ characteristic at one point only, the device could be shown to display stable negative impedance. This was due to the device having both a negative differential capacitance together with the expected negative differential resistance in its negative impedance region.

By describing the device as a circuit element in this way, stability could be analysed without the need for a complete time dependent model of device behaviour. It showed the device to behave as a stable circuit element, and as such the applicability of the regenerative feedback model (RFM) needed to be examined. As discussed previously, the RFM can be regarded as a useful method for visualising switching from the OFF to the ON states, but can supply no quan-

titative information about the device's $I - V$ characteristic. Also, with a load line intersecting the $I - V$ curve in the negative impedance region at one and only one point, the device would be expected to oscillate since the MISS would be in an unstable equilibrium state. This is contrary to what is seen in the laboratory. Therefore the general applicability of the RFM needs to be restricted to the switching of devices and not the actual negative impedance region. This was stated quite clearly by Board [3], but it is a point which has been overlooked by other investigators.

Examining all the results obtained, and seeing how easily the $I - V$ characteristic is affected by excess recombination, the most easily controlled characteristic would appear to be obtained from the MIS switching structure, with no injecting p-type layer. The disadvantage would be its non-linear negative impedance as compared with the lightly doped n-type layer MISS.

7.2 Further Work

The 1-D model can be continuously extended and improved. The MISS has been fabricated using a large variety of semi-insulators and semiconductors, in addition to the silicon, and tunnelling thickness silicon dioxide modelled here. All of these structures could be incorporated in an even more general 1-D model.

However, the greatest limitation on the 1-D model is the assumed geometry; i.e. a 1:1 ratio of top contact area to pn junction area. This was remedied to some extent by the 2-D model, but as was mentioned in chapter five, the 2-D model can be further improved. This improvement can be achieved by incorporating the

electron recombination current in the neutral n-type layer, and the hole current in the neutral region outside the area immediately below the top contact. This would produce a much closer fit with experiment for the thin oxide device, ($< 25\AA$), although it would have little effect on the results that have been presented for the thicker oxide structures, ($> 25\AA$).

As the n-type layer doping density increases, the effect of the MIS depletion region approaching the pn depletion region and so controlling the hole injected current, J_{pj}, becomes less important in determining the switching point. However, for the lightly doped punchthrough devices, this spacial effect is the controlling influence on the switching point, with the oxide electric field being dominated by hole collection at the IS interface. By using this effect, possible novel $I - V$ characteristics could be achieved by fabricating the MISS as a tunnelling thickness oxide grown on the emitter of an npn transistor, with different characteristics produced through variation of the base current. This would have a much lower gain than the MIS emitter transistor because of the lightly doped emitter, but could have a high base-emitter voltage and/ or a fixed collector-emitter voltage.

References

1. Habib, S. E-D. and Simmons, J. G.: ' Theory of Switching in $p-n$ Insulator(Tunnel) Metal Devices Part 2: Avalanche Mode', *Solid-St Electron.*, **23**, pp. 497-505, (1980).

2. Hayashi, Y.: 'Switching Phenomena in Thin-Insulator Metal Insulator Semiconductor Diodes', *Appl. Phys Lett.*, **37(4)**, pp. 407-408, (1980).

3. Board, K.: 'New Unorthodox Semiconductor Devices', *Rep. Prog. Phys.*, **48**, pp. 1595-1635, (1985).

APPENDIX A

TUNNELLING IN THIN SILICON DIOXIDE

A.1 Introduction

The situation being dealt with in this appendix is that of electrons and holes tunnelling between a metal and silicon through a thin layer of silicon dioxide. The basic expressions for carrier tunnelling have been comprehensively dealt with by a number of researchers [2,3]. However, to produce an expression which can be used in device modelling, a number of approximations are generally used. In this appendix an expression is derived which is suitable for computation, and allows the calculation of tunnelling currents for both low and high oxide electric fields. The expressions obtained are for carriers moving to and from $\langle 100 \rangle$ orientated silicon; only the $\langle 100 \rangle$ orientation has been dealt with here because the device modelling throughout the rest of the thesis only uses this orientation.

A.2 Tunnelling Current Expressions

It can be shown that the probability that an electron will make a tunnelling transition from a state 'a' on one side of a barrier to a state 'b' on the other is given by Fermi's Golden Rule [1] to be

$$w_{ab} = \frac{2\pi}{\hbar} |M_{ab}|^2 f_a \rho_b (1 - f_b) \qquad A.2.1$$

where M_{ab} is the matrix element for the transition, ρ_a is the density of states on the 'a' side of the barrier, f_a is the probability of occupation of state 'a', and $(1 - f_b)$ is the probability that a state 'b' is empty.

For an electron, using an independent particle approximation and assuming both the energy E, and transverse momentum k_T are conserved [2], it follows that the total tunnelling current between 'a' and 'b' is given by

$$J = \frac{4\pi q}{\hbar} \sum_{k_T} \int_{-\infty}^{\infty} |M_{ab}|^2 \rho_a \rho_b (f_a - f_b) dE \qquad A.2.2$$

where $|M_{ab}|^2 = |M_{ba}|^2$, and the integration over E is at a fixed transverse wave number k_T. The summation over k_T can be converted to an integral [3] by using

$$\sum_{k_T} = \frac{1}{2\pi} \frac{m_{ti}}{\hbar^2} \int dE_T \qquad A.2.3$$

where m_{ti} is the effective transverse electron mass in the insulator. From expressions (A.2.2) and (A.2.3) the tunnelling current from 'a' to 'b' can be written as

$$J = \frac{2m_{ti}q}{\hbar^3} \int_{-\infty}^{\infty} dE \int |M_{ab}|^2 \rho_a \rho_b (f_a - f_b) dE_T \qquad A.2.4$$

Using the W.K.B. approximation [2,3], the matrix element for the tunnelling transition is calculated to be

$$|M_{ab}|^2 = \frac{1}{\rho_a \rho_b (2\pi)^2} e^{-\eta} \qquad A.2.5$$

where from [5]

$$\eta = \frac{2}{\hbar} \int_{x_a}^{x_b} (P_{ti}^2 - P_i^2)^{1/2} dx \qquad A.2.6$$

P_{ti} and P_i are the transverse and total momenta of the electron in the insulator respectively, and x_b and x_a are the classical turning points.

By setting the state 'a' to be the metal 'm', 'b' to be the semiconductor 's', and substituting for the transition probability M_{ab} gives the situation of interest of conduction between the metal and semiconductor. Equation (A.2.4) can now be written as

$$J = \frac{4\pi m_{ti} q}{h^3} \int_{-\infty}^{\infty} dE \int (f_m - f_s) e^{-\eta} dE_T \qquad A.2.7$$

The limits of the integral (A.2.4) over E_T for electrons tunnelling to and from the silicon conduction band can be determined from the conservation of transverse momentum across the boundary between the silicon and the oxide giving

$$m_{ts} E = m_{ti} E_{ti_{max}} \qquad A.2.8$$

with m_{ts} and m_{ti} the transverse effective masses of electrons in the semiconductor and oxide respectively. The point $E = 0$ is taken as the position of the bottom of the semiconductor conduction band at the semiconductor insulator interface. This gives a final expression for the electron tunnelling current assuming now that all energies are measured relative to the bottom of the silicon conduction band to be

$$J_{tn} = 4\pi q \frac{m_{ti}}{h^3} \int_0^{E_{max}} (f_m - f_s) dE \int_0^{(m_{ts}/m_{ti})E} e^{-\eta(E,E_T)} dE_T. \qquad A.2.9$$

The form for $\eta(E, E_T)$ is determined by utilising the experimental expression due to Franz [4] for the form of P_i in silicon dioxide:

$$\frac{P_i^2}{2m_{ti}} = [E - E_{c_{ox}}(x)][1 + (E - E_{c_{ox}}(x))/E_{g_{ox}}] \qquad A.2.10$$

where $E_{c_{ox}}(x)$ is the oxide conduction band, and $E_{g_{ox}}$ is the oxide band gap. By assuming the transverse momentum of the electron has a parabolic form in the

insulator gives from (A.2.6) the final expression

$$\eta(E,E_T) = 2\left(\frac{2m_{ti}}{\hbar^2}\right)^{1/2} \int_{x_s}^{x_m} \left\{E_T - [E - E_{c_{ox}}(x)][1 + (E - E_{c_{ox}}(x))/E_{g_{ox}}\right\}^{1/2} dx \quad A.2.11$$

This equation is the starting point for the development of tunnelling expressions that deal with a variety of conditions by utilising different approximations.

The integral over E_T, (A.2.9), can be simplified by noting that due to the the form of the $e^{-\eta(E,E_T)}$ term, it is sharply peaked around $E_T = 0$. If $\eta(E,E_T)$ is expanded as a Taylor's series around this value, and the terms after the second are neglected, the expansion takes the form [5]

$$\eta(E,E_T) = \eta(E,0) + E_T \frac{\partial \eta}{\partial E_T}\bigg|_{E_T=0} + \text{2nd order terms} \quad A.2.12$$

This expression when substituted in (A.2.9) and integrated gives

$$J_{tn} = \frac{4\pi q m_{ti}}{h^3} \int_0^{E_{max}} (f_m - f_s) e^{-\eta(E,0)} \left[\left(1 - exp\left(\frac{-\partial\eta}{\partial E_T} E \frac{m_{ts}}{m_{ti}}\right)\right) \Big/ \left(\frac{\partial \eta}{\partial E_T}\right)\right]\bigg|_{E_T=0} dE \quad A.2.13$$

The equation can be further simplified if the metal Fermi level is situated opposite the band gap of the silicon at the silicon insulator interface. The first term from the expanded exponential series in (A.2.12) is used and the value for η is taken at the point $E = 0$, then $e^{-\eta(0,0)}$ is moved outside the integral. The final form for the tunnelling expression is then [5]

$$J_{tn} = \frac{4\pi q m_{ts}}{h^3} e^{-\eta(0,0)} \int_0^{\infty} \frac{E}{1 + exp((E - E_{fm})/kT)} - \frac{E}{1 + exp((E - E_{fn})/kT)} dE \quad A.2.14$$

This expression can be made more tractable by using a change of variable for E/kT giving a final expression for J_{tn} of the form

$$J_{tn} = \frac{4\pi q m_{ts}}{h^3} (kT)^2 e^{-\eta(0,0)} \Big[F_1(E_{fm}/kT) - F_1(E_{fn}/kT)\Big] \quad A.2.15$$

where F_1 is the Fermi integral of order 1.

A similar expression can be demonstrated for holes giving a hole tunnelling expression of the form

$$J_{tp} = \frac{4\pi q m_{th}}{h^3}(kT)^2 e^{-\eta(0,0)}\Big[F_1(-E_{fp}/kT) - F_1(-E_{fm}/kT)\Big] \qquad A.2.16$$

The energy $E = 0$ is taken at the position of the semiconductor valence band at the IS interface for the hole tunnelling expression.

A.3 Tunnelling Attenuation Factor η

To evaluate the tunnelling equations (A.2.13) and (A.2.14), analytic expressions for $\eta(E, E_T)|_{E_T=0}$, $\partial\eta/\partial E_T|_{E_T=0}$, and $\eta(0,0)$ have to be determined. The standard theory has been extended by integrating the expressions for $\eta(E,0)$, and $\partial\eta/\partial E_T|_{E_T=0}$ and then substituting back into (A.2.13) and (A.2.14).

By rearranging expression (A.2.11) replacing $E_{c_{ox}}(x)$ by $E_{v_{ox}}(x) + E_{g_{ox}}$, the form for $\eta(E, E_T)$ can be written as

$$\eta(E, E_T) = 2\Big(\frac{2m_{ti}}{\hbar^2}\Big)^{1/2}\int_{x_s}^{x_m}\Big[E_T - (E - E_{V_{ox}}(x))(1 - (E - E_{V_{ox}}(x))/E_{g_{ox}})\Big]^{1/2} dx \qquad A.3.1$$

where x_m and x_s are the turning points for the metal and semiconductor respectively, $E_{V_{ox}}(x)$ is the position of the oxide valence band at the point x in the oxide and E is the energy of the carrier. By setting $E_T = 0$ it can be seen that

$$\eta(E, 0) = 2\Big(\frac{2m_{ti}}{\hbar^2}\Big)^{1/2}\int_{x_s}^{x_m}\Big[-(E - E_{V_{ox}})(1 - (E - E_{V_{ox}})/E_{g_{ox}})\Big]^{1/2} dx. \qquad A.3.2$$

CASE 1: Carrier Intersects neither the Conduction or Valence Band. (Fig A.1)

Assume for the following discussion that the energy E of the carrier does not intersect either the conduction band or the valence band of the oxide. Other cases will be dealt with later in this appendix.

By taking the potential U_{ox} as being uniformly dropped across the oxide of thickness d_{ox} the barrier assumes a trapezoidal shape for a $|U_{ox}| > 0.0$. The position of the valence band of the insulator at the point x relative to the semiconductor insulator interface is given by

$$E_{V_{ox}}(x) = E_{V_{ox}}(0) + \frac{xU_{ox}}{d_{ox}} = \frac{xU_{ox}}{d_{ox}} \qquad A.3.3$$

because $E_{V_{ox}}(0)$ is now taken as the energy reference level for carriers in the insulator and the point $x = 0$ is taken at the semiconductor insulator interface. For convenience U_{ox} is expressed in $eV's$. Equation (A.3.2) can now be transformed to give

$$\eta(E,0) = 2\Big(\frac{2m_{ti}}{\hbar^2}\Big)^{1/2} \int_{x_s}^{x_m} \Big[-(E - \frac{xU_{ox}}{d_{ox}})(1 - (E - \frac{xU_{ox}}{d_{ox}})/E_{g_{ox}}\Big]^{1/2} dx. \qquad A.3.4$$

The analytic expression for $\eta(E,0)$ can be obtained by integrating (A.3.4) using a sine substitution to give

$$\eta(E,0) = 2\Big(\frac{2m_{ti}}{\hbar^2}\Big)^{1/2} \frac{d_{ox}}{U_{ox}} \frac{E_{g_{ox}}^{3/2}}{8} \Big[y + sin(y)cos(y)\Big]_{y_m}^{y_s} \qquad A.3.5$$

where

$$y_s = sin^{-1}\Big[2\Big(\frac{E}{E_{g_{ox}}}\Big) - 1\Big], \quad y_m = sin^{-1}\Big[2\Big(\frac{E - U_{ox}}{E_{g_{ox}}}\Big) - 1\Big] \qquad A.3.6$$

The discussion above deals with the behaviour of the carrier in the insulator when it does not intersect either the conduction band or valence band of the

insulator. If the carrier violates the conditions above the boundary values y_m and y_s have to be altered accordingly. There are three cases to be dealt with;

CASE 2: Carrier Intersects the Conduction Band Only. (Fig A.2).

For the carrier to intersect the conduction band of the insulator, $E_{g_{ox}} < E$, and $E < (E_{g_{ox}} + U_{ox})$. The effective edge of the barrier as seen by the carrier on the semiconductor side is

$$x_s = \left[\frac{E - E_{g_{ox}}}{U_{ox}}\right] d_{ox} \qquad A.3.7$$

This gives the final form for y_s to be

$$y_s = sin^{-1}\left[\frac{2(E - x_s U_{ox}/d_{ox})}{E_{g_{ox}}} - 1\right] = \frac{\pi}{2} \qquad A.3.8$$

y_m has the same form as in (A.3.6).

CASE 3: Carrier Intersects the Valence Band Only. (Fig A.3).

For the valence band to be intersected, $0 < E < U_{ox}$. On the metal side the effective end to the barrier as seen by the carrier is given by $x_m = (E/U_{ox})d_{ox}$, y_m can then be expressed as

$$y_m = sin^{-1}\left[\frac{2(E - x_m U_{ox}/d_{ox})}{E_{g_{ox}}} - 1\right] = \frac{-\pi}{2} \qquad A.3.9$$

y_s has the same form as in (A.3.6).

CASE 4: Carrier Intersects the Conduction band and Valence Band. (Fig A.4).

This case is not likely to occur in practice because of the high electric fields necessary but is included here for completeness. It does in fact correspond to band to band tunnelling in the oxide. For this to take place $E_{g_{ox}} < E < U_{ox}$ and the expressions for y_s and y_m are the same as for the cases 2 and 3 respectively.

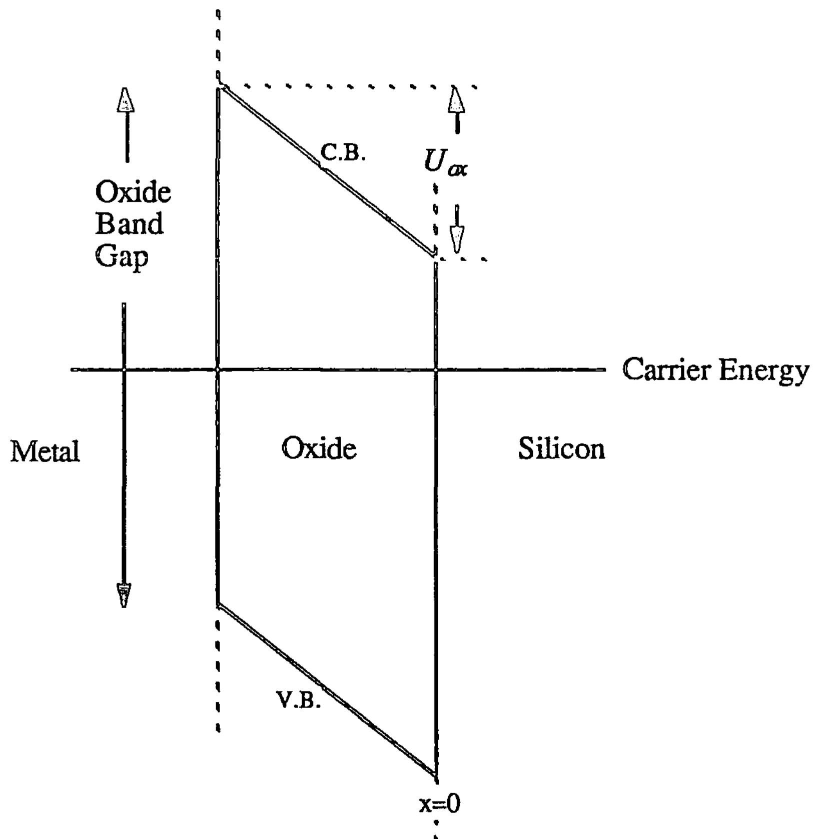

Fig A.1. Case 1: Carrier does not intersect either the conduction or valence band of the oxide.

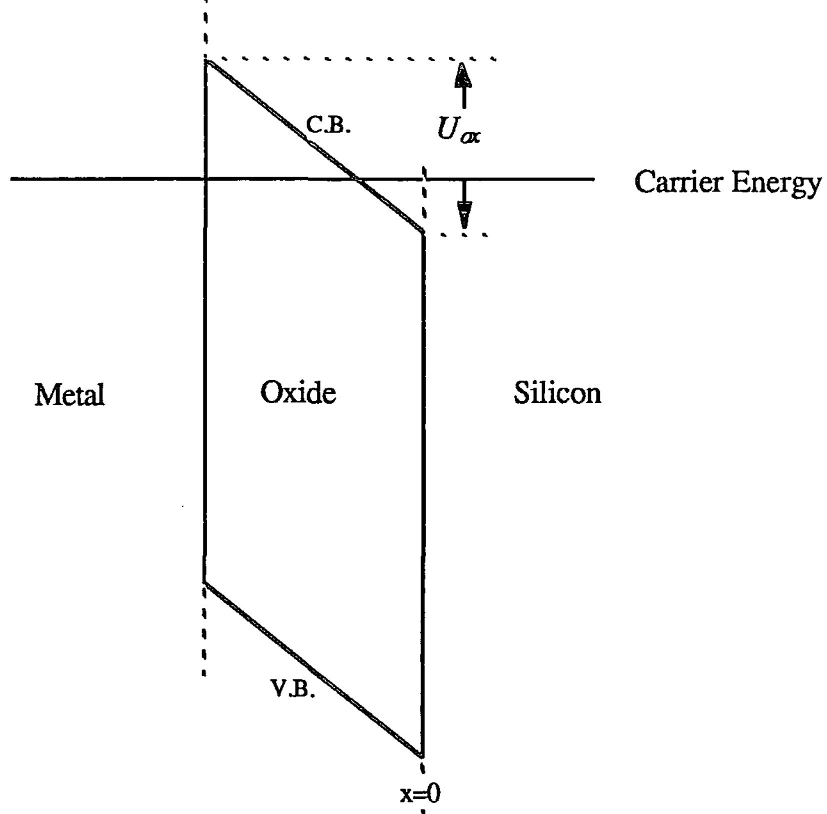

Fig A.2. Case 2: Carrier intersects the conduction band of the oxide.

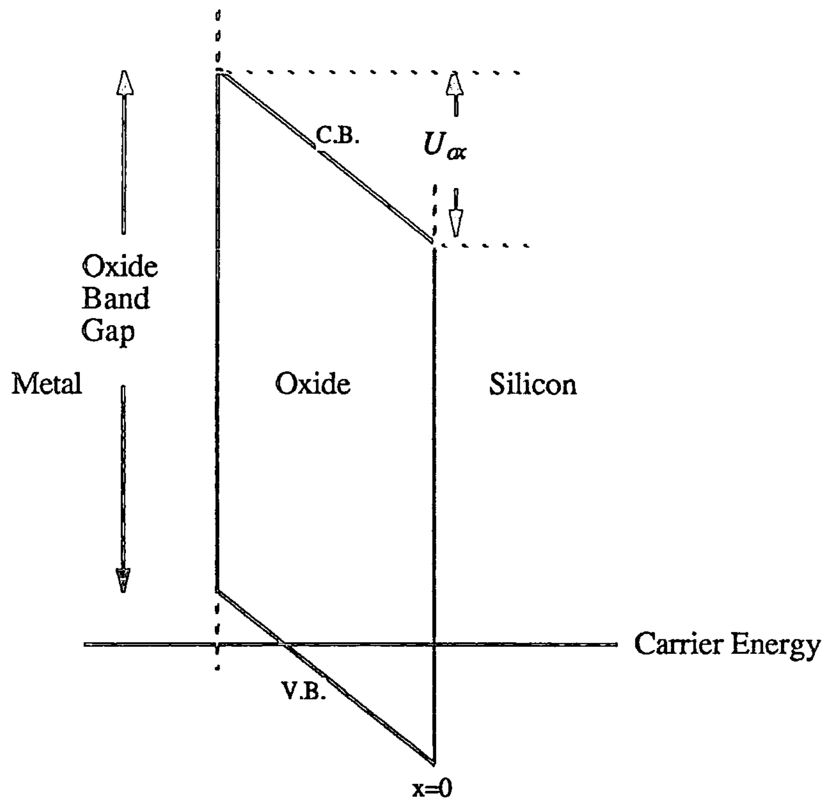

Fig A.3. Case 3: Carrier intersects the valence band of the oxide.

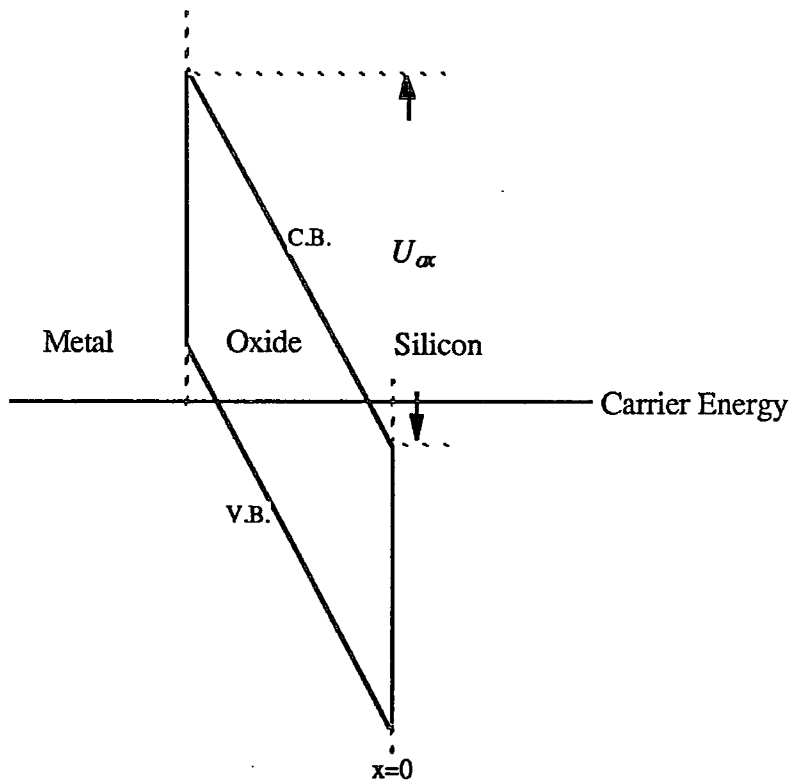

Fig A.4. Case 4: Carrier intersects the conduction band and valence band of the oxide.

To evaluate the integral (A.2.13) an analytic form for $\partial\eta/\partial E_T|_{E_T=0}$ needs to be produced. Using as the starting point

$$\eta(E,E_T) = 2\left(\frac{2m_{ti}}{\hbar^2}\right)^{1/2}\int_{x_s}^{x_m}\Big[E_T - (E - E_{V_{ox}}(x))(1-(E-E_{V_{ox}}(x))/E_{g_{ox}})\Big]^{1/2}dx \qquad A.3.10$$

differentiating under the integral sign and setting $E_T = 0$ gives

$$\left.\frac{\partial\eta}{\partial E_T}\right|_{E_T=0} = \left(\frac{2m_{ti}}{\hbar^2}\right)^{1/2}\int_{x_s}^{x_m}\frac{dx}{\Big[-(E - E_{V_{ox}}(x))(1-(E-E_{V_{ox}}(x))/E_{g_{ox}})\Big]^{1/2}} \qquad A.3.11$$

Again using a sine substitution the final form for $\partial\eta/\partial E_T|_{E_T=0}$ is

$$\left.\frac{\partial\eta}{\partial E_T}\right|_{E_T=0} = \left(\frac{2m_{ti}}{\hbar^2}\right)^{1/2}\sqrt{E_{g_{ox}}}\left(\frac{d_{ox}}{U_{ox}}\right)\Big[y\Big]_{y_s}^{y_m} \qquad A.3.12$$

Here y_m and y_s have the same form as for the cases $A.3.6 - A.3.9$. With these expressions for $\eta(E,E_T)|_{E_T=0}$, and $\partial\eta/\partial E_T|_{E_T=0}$, expression $A.2.13$ can be evaluated.

A.4 A Tunnelling Comparison

The equations (A.2.13) and (A.2.14) derived above can be expressed as

$$J_{tn} = \frac{4\pi q m_{ti}}{h^3}\int_0^{E_{max}}(f_m - f_s)e^{-\eta(E,0)}\left[\left(1 - exp\left(\frac{-\partial\eta}{\partial E_T}E\frac{m_{ts}}{m_{ti}}\right)\right)\Big/\left(\frac{\partial\eta}{\partial E_T}\right)\right]\Bigg|_{E_T=0}dE \qquad A.4.1$$

and

$$J_{tn} = \frac{4\pi q m_{ts}}{h^3}(kT)^2 e^{-\eta(0,0)}\Big[F_1(E_{fm}/kT) - F_1(E_{fn}/kT)\Big] \qquad A.4.2$$

for electrons, where energies are measured from the conduction band of the semi-

conductor at the IS interface, and

$$J_{tp} = \frac{4\pi q m_{ti}}{h^3} \int_0^{E_{max}} (f_{s_h} - f_{m_h}) e^{-\eta(E,0)} \left[\left(1 - exp\left(\frac{-\partial\eta}{\partial E_T} E \frac{m_{th}}{m_{ti}} \right) \right) \Big/ \left(\frac{\partial\eta}{\partial E_T} \right) \right] \Big|_{E_T=0} dE \quad A.4.3$$

and

$$J_{tp} = \frac{4\pi q m_{th}}{h^3} (kT)^2 e^{-\eta(0,0)} \Big[F_1(-E_{fp}/kT) - F_1(-E_{fm}/kT) \Big] \quad A.4.4$$

for holes.

All electron and hole expressions (A.4.1-4) can be used for tunnelling through an oxide with small potential drop, but for a large potential drop where the metal Fermi level is not close to the semiconductor forbidden band, expressions $A.4.1$ and $A.4.3$ need to be used. A comparison of the accuracy of the two expressions is given in Figs A.5 and A.6 for tunnelling of electrons and holes respectively through a $40\AA$ oxide. There is a much greater effect seen for electrons because the semiconductor conduction band to oxide conduction band barrier height is $3.2eV$ compared to the semiconductor valence band to oxide valence band barrier height of $4.68eV$. Hence electron tunnelling into the oxide conduction band occurs for smaller oxide potentials than hole tunnelling into the oxide valence band. In Figs A.7 and A.8 further electron tunnelling current comparisons are made for 20, 30, 40, and $50\AA$ devices with electric field strengths up to $10^7 V/cm$ for both tunnelling expressions. It can be seen that for thicker oxides the new expression (A.4.1) is necessary in contrast to the thin oxide case for which the simpler expression (A.4.2) is adequate.

It can be appreciated from these diagrams that though at low potential drops across the oxide, the currents are similar, for large potentials there is a great difference in results so providing the need for this more accurate approximation.

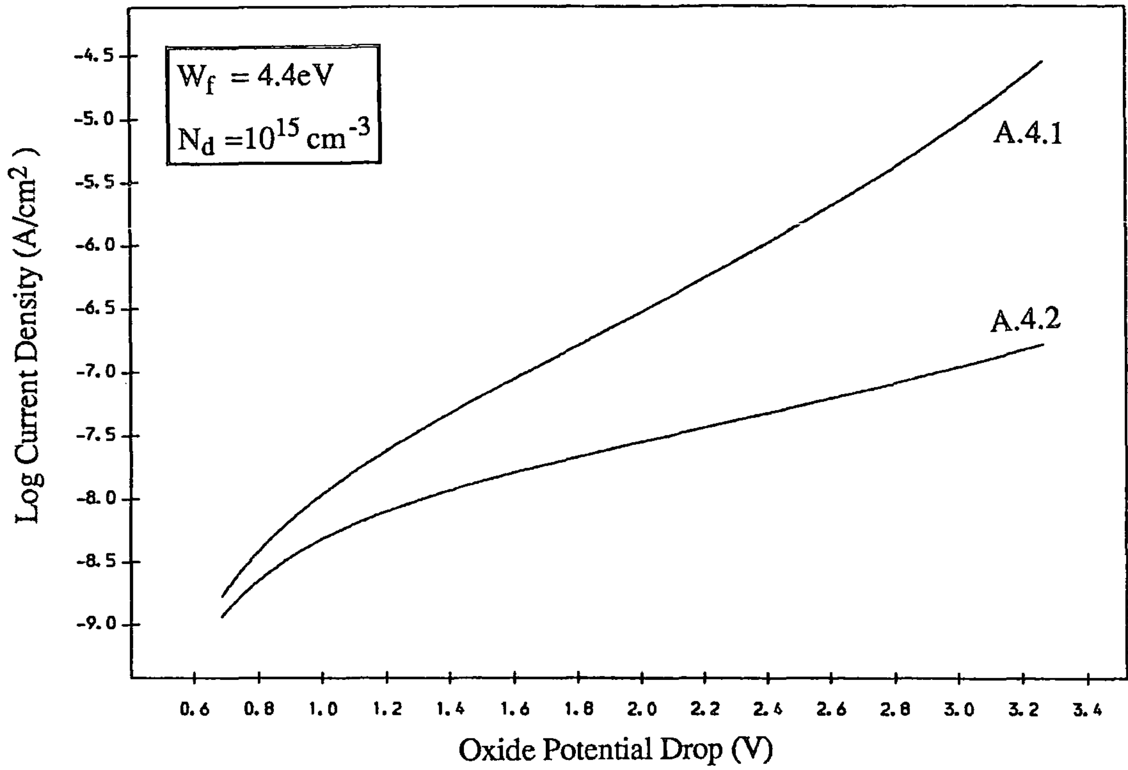

Fig A.5: Electron current flow from a metal to n-type silicon for a 40Å oxide using equations A4.1 and A4.2.

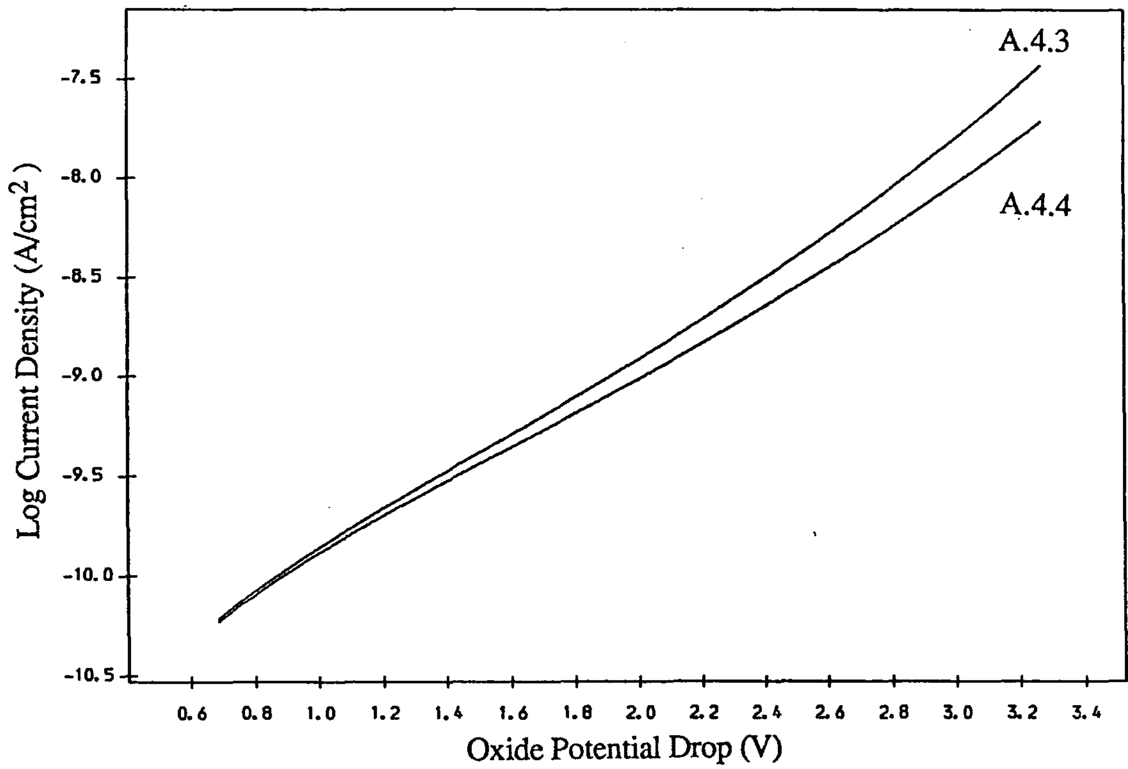

Fig A.6: Hole current flow from a metal to n-type silicon for a 40Å oxide using equations A4.3 and A4.4.

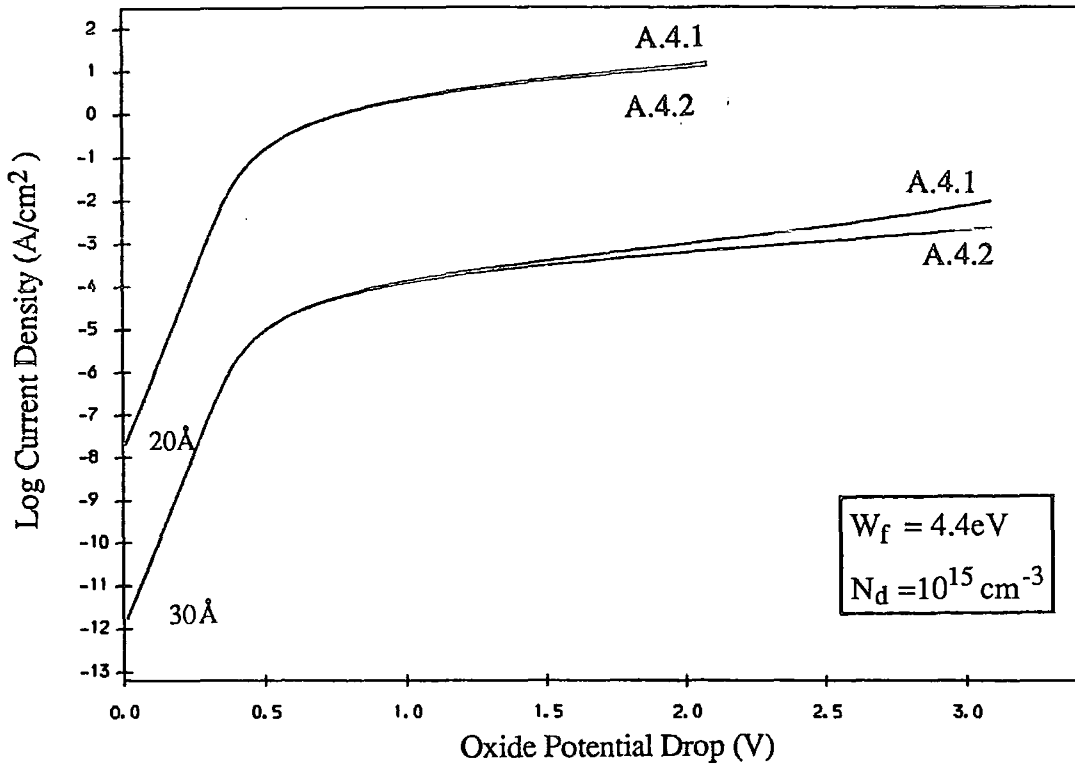

Fig A.7: Electron current flow from a metal to n-type silicon for 20 and 30Å oxides using equations A4.1 and A4.2.

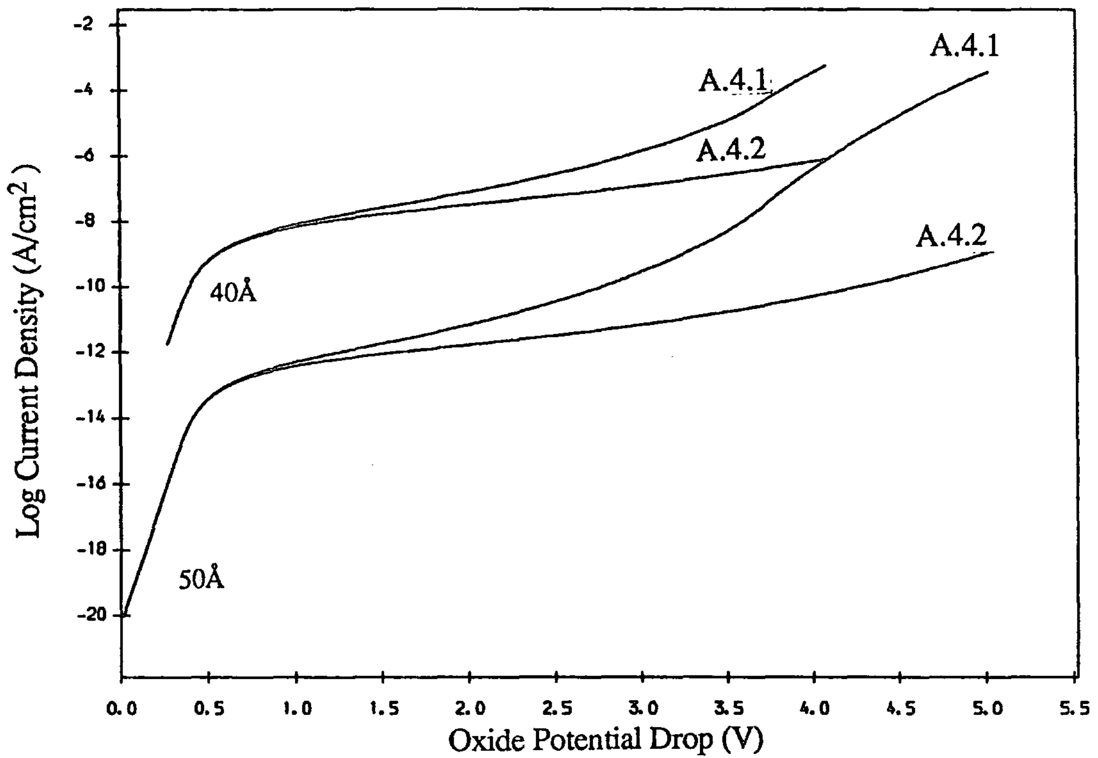

Fig A.8: Electron current flow from a metal to n-type silicon for 40 and 50Å oxides using equations A4.1 and A4.2.

References

1. Merzbacher, E., *Quantum Mechanics*, Wiley, (1970).
2. Harrison, W. A., 'Tunnelling from an Independent Particle Point of View', *Phys. Rev.*, **123**, pp. 85-89, (1961).
3. Gray, P. V., 'Tunnelling from Metal to Semiconductors', *Phys. Rev.*, **140**, pp. A179-A186, (1965).
4. Card, H. C., 'Tunnelling MIS Structures', *Inst. Phys. Conf. Ser.*, **50**, (1979).
5. Green, M. A. and Shewchun, J., 'Current Multiplication in Metal Insulator Semiconductor (MIS) Tunnel Diodes', *Solid St. Electron.*, **17**, pp. 349-365, (1974).

APPENDIX B

ELECTRIC FIELD IN THE MIS DEPLETION REGION

B.1 Introduction

The purpose of this appendix is to provide an analytic expression for the electric field in the MIS depletion region. Initially the general case will be dealt with in which both the quasi Fermi levels and conduction and valence bands vary with position. This takes into account the contribution to the electric field due to current flow. The theory is then modified to deal with the assumptions used in the main body of the text where the quasi Fermi levels are held constant across the MIS depletion region.

B.2 General Theory

The general form for Poisson's equation in an n type semiconductor can be written as

$$\frac{d^2\psi}{dx^2} = -\frac{q}{\epsilon_s}(p - n + N_d) \qquad B.2.1$$

where N_d is the donor dopant density, and p and n are the free electron and hole concentrations respectively. Following [1], using $\mathcal{E} = -d\psi/dx$, (B.2.1) can be written as

$$\mathcal{E}d\mathcal{E} = \frac{q}{\epsilon_s}(n - p - N_d)d\psi \qquad B.2.2.$$

where n and p can be expressed using Fermi-Dirac statistics as

$$n = N_c F_{1/2}\left[\frac{E_{fn} - E_c}{kT}\right] \quad \text{and} \quad p = N_v F_{1/2}\left[\frac{E_v - E_{fp}}{kT}\right] \qquad B.2.3$$

From Sze [1], electron and hole currents can be expressed in terms of quasi Fermi potentials in the form

$$J_n = \mu_n n \frac{dE_{fn}}{dx} \quad \text{and} \quad J_p = \mu_p p \frac{dE_{fp}}{dx} \qquad B.2.4$$

(B.2.2) can be rewritten in the form

$$\mathcal{E} d\mathcal{E} = -\frac{1}{\epsilon_s}(ndE_c - pdE_v + qN_d d\psi) \qquad B.2.5$$

Now

$$d(E_{fn} - E_c) = dE_{fn} - dE_c, \quad \text{and} \quad d(E_v - E_{fp}) = dE_v - dE_{fp} \qquad B.2.6$$

so by rearranging (B.2.4) to provide expressions for ndE_{fn} and pdE_{fp}, and combining with (B.2.5) and (B.2.6) gives an integrable form for the electric field $\mathcal{E}$

$$\mathcal{E} d\mathcal{E} = \frac{1}{\epsilon_s}\left[n(dE_{fn} - dE_c) + p(dE_v - dE_{fp}) - qN_d d\psi - \frac{J_n}{\mu_n}dx + \frac{J_p}{\mu_p}dx\right] \qquad B.2.7$$

The derivative of the Fermi Dirac integral of order j

$$F_j(\eta) = \frac{1}{\Gamma(j+1)} \int_0^\infty \frac{x^j}{1 + exp(x - \eta)} \qquad B.2.8$$

can be expressed as

$$\frac{dF_j(\eta)}{d\eta} = F_{j-1}(\eta) \qquad B.2.9$$

where $\Gamma(j)$ is the gamma function of order j.

Integrating (B.2.7) using this result [2] gives

$$\frac{\mathcal{E}_s^2 - \mathcal{E}_0^2}{2} = \frac{kT}{\epsilon_s}\left\{N_c F_{3/2}\left[\frac{E_{fn}(x) - E_c(x)}{kT}\right]\Bigg|_0^s + N_v F_{3/2}\left[\frac{E_v(x) - E_{fp}(x)}{kT}\right]\Bigg|_0^s\right\}$$

where n and p can be expressed using Fermi-Dirac statistics as

$$n = N_c F_{1/2}\Big[\frac{E_{fn} - E_c}{kT}\Big] \quad \text{and} \quad p = N_v F_{1/2}\Big[\frac{E_v - E_{fp}}{kT}\Big] \qquad B.2.3$$

From Sze [1], electron and hole currents can be expressed in terms of quasi Fermi potentials in the form

$$J_n = \mu_n n \frac{dE_{fn}}{dx} \quad \text{and} \quad J_p = \mu_p p \frac{dE_{fp}}{dx} \qquad B.2.4$$

(B.2.2) can be rewritten in the form

$$\mathcal{E} d\mathcal{E} = -\frac{1}{\epsilon_s}(ndE_c - pdE_v + qN_d d\psi) \qquad B.2.5$$

Now

$$d(E_{fn} - E_c) = dE_{fn} - dE_c, \quad \text{and} \quad d(E_v - E_{fp}) = dE_v - dE_{fp} \qquad B.2.6$$

so by rearranging (B.2.4) to provide expressions for ndE_{fn} and pdE_{fp}, and combining with (B.2.5) and (B.2.6) gives an integrable form for the electric field $\mathcal{E}$

$$\mathcal{E} d\mathcal{E} = \frac{1}{\epsilon_s}\Big[n(dE_{fn} - dE_c) + p(dE_v - dE_{fp}) - qN_d d\psi - \frac{J_n}{\mu_n}dx + \frac{J_p}{\mu_p}dx\Big] \quad B.2.7$$

The derivative of the Fermi Dirac integral of order j

$$F_j(\eta) = \frac{1}{\Gamma(j+1)} \int_0^\infty \frac{x^j}{1 + exp(x - \eta)} \qquad B.2.8$$

can be expressed as

$$\frac{dF_j(\eta)}{d\eta} = F_{j-1}(\eta) \qquad B.2.9$$

where $\Gamma(j)$ is the gamma function of order j.

Integrating (B.2.7) using this result [2] gives

$$\frac{\mathcal{E}_s^2 - \mathcal{E}_0^2}{2} = \frac{kT}{\epsilon_s}\Big\{N_c F_{3/2}\Big[\frac{E_{fn}(x) - E_c(x)}{kT}\Big]\Big|_0^s + N_v F_{3/2}\Big[\frac{E_v(x) - E_{fp}(x)}{kT}\Big]\Big|_0^s\Big\}$$

$$-\frac{q}{\epsilon_s}N_d\psi_s - \int_{x_0}^{x_s} \frac{J_n}{\epsilon_s\mu_n} - \frac{J_p}{\epsilon_s\mu_p}\, dx \qquad B.2.10$$

The contribution to the total electric field due to the free carrier densities from J_n and J_p is plotted in Fig B.1. It can be seen here that for an average potential drop across the depletion region of $5V$, the contribution to the electric field due to currents only becomes significant for carrier densities of about $10^2 A/cm^2$ or greater.

B.3 Further Approximation

Throughout the text, the electron and hole quasi Fermi levels in the MIS depletion region are assumed to be constant. The hole quasi Fermi level being pinned to its value at the oxide semiconductor interface, and the electron quasi Fermi level in the MIS depletion region taking its value from the neutral epitaxial layer level.

Utilising these approximations gives the form of the electric field at the surface to be

$$\frac{\mathcal{E}_s^2 - \mathcal{E}_0^2}{2} = \frac{kT}{\epsilon_s}\left\{N_c F_{3/2}\left[\frac{E_{fn}(0) - E_c(x)}{kT}\right]\Bigg|_0^s + N_v F_{3/2}\left[\frac{E_v(x) - E_{fp}(s)}{kT}\right]\Bigg|_0^s\right\}$$

$$-\frac{q}{\epsilon_s}N_d\psi_s \qquad B.3.1$$

where the limits at for $E_{fn}(0) - E_c(x)$ at $x = s$ and $x = 0$ are given by

$$E_{fn}(0) - E_c(x) = q\phi_n - E_g/2 + E\psi_s \quad x = s$$

$$E_{fn}(0) - E_c(x) = q\phi_n - E_g/2 \qquad x = 0 \qquad B.3.2$$

and for $E_v(x) - E_{fp}(s)$

$$E_v(x) - E_{fp}(s) = E\psi_s - E_g/2 - q\phi_n - \xi \quad x = s$$

$$E_v(x) - E_{fp}(s) = -E_g/2 - q\phi_n - \xi \qquad x = 0 \qquad B.3.3$$

Holding the quasi Fermi levels flat in the MIS depletion region provides an analytic expression which incorporates inversion effects, but does not include the contribution to $\mathcal{E}$ due to current flow. The current integral can be neglected as shown above for for current densities less than $10^2 A/cm^2$. By taking the electric field at the edge of the MIS depletion region to be $\mathcal{E}_0 = 0$, the final expression for the electric field at the oxide-semiconductor interface can be written as

$$\frac{\mathcal{E}_s^2}{2} = \frac{kT}{\epsilon_s}\Big\{N_c F_{3/2}\Big[\frac{E_{fn}(0) - E_c(s)}{kT}\Big] - N_c F_{3/2}\Big[\frac{E_{fn}(0) - E_c(0)}{kT}\Big] +$$

$$N_v F_{3/2}\Big[\frac{E_v(s) - E_{fp}(s)}{kT}\Big] - N_v F_{3/2}\Big[\frac{E_v(0) - E_{fp}(s)}{kT}\Big]\Big\} - \frac{q}{\epsilon_s} N_d \psi_s \qquad B.3.4$$

It is this expression which is used throughout the text.

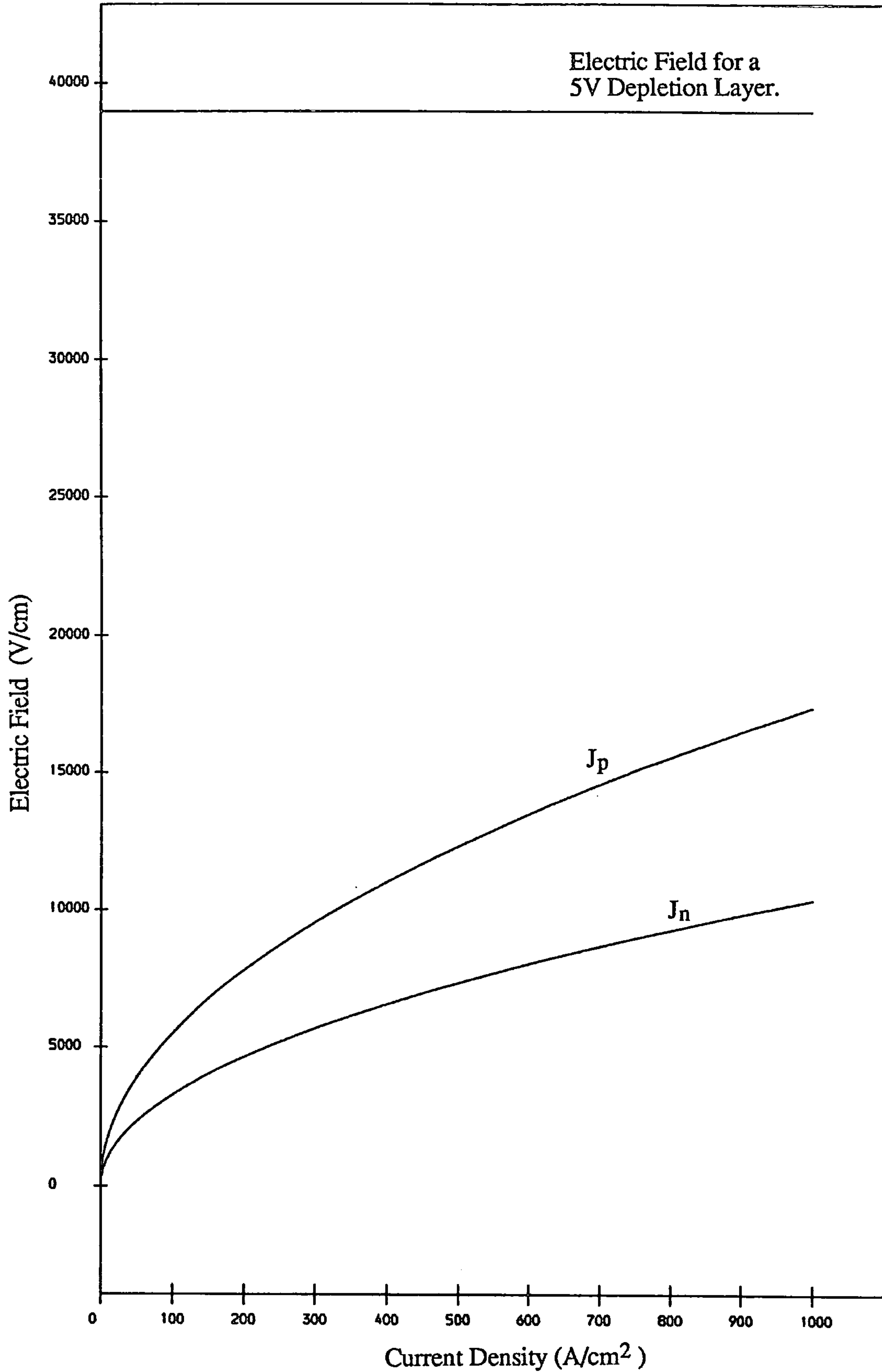

Fig B.1: Electric Field Contributions due to Electron and Hole Currents in a Depletion Region. $N_d = 10^{15}$ cm^{-3} $\psi_s = 5$V.

References

1. Sze, S. M., *The Physics of Semiconductor Devices*, Wiley, (1981).

2. Green, M. A. and Shewchun, J., 'Current Multiplication in Metal Insulator Semiconductor (MIS) Tunnel Diodes', *Solid St. Electron.*, **17**, pp 349-365, (1974).

APPENDIX C

AVALANCHE MULTIPLICATION

C.1 Introduction

The purpose of this appendix is to provide an analytic expression for avalanche multiplication (or impact ionisation) in a heavily doped semiconductor where a high electric field exists.

If the electric field in a depletion region is great enough for impact ionisation to occur, an incident hole current I_p will increase with distance through the depletion region becoming M_pI_p at the opposite edge. A similar process takes place for electrons. It is the purpose of this appendix to provide expressions for M_p and M_n, the electron and hole multiplication factors respectively.

C.2 Multiplication Coefficients

By utilising the differential expression for current gain in an element dx for a hole current I_p with electron and hole avalanche coefficients (ionisation rates) α_p, and α_n for electrons and holes respectively [1]

$$dI_p/dx - (\alpha_p - \alpha_n)I_p = \alpha_n I \qquad C.2.1$$

where carrier I is the total current through the depletion layer, and any generation in the depletion region has been ignored. The current multiplication coefficients,

M_p, and M_n, for holes and electrons respectively can be written [1,2] as

$$1 - \frac{1}{M_p} = \int_0^{W_{mis}} \alpha_p exp\left[\int_0^x (\alpha_n - \alpha_p)dz\right]dx \qquad C.2.2$$

where W_{mis} is the width of the depletion region, and the x axis extends from the edge of the depletion region neutral region interface where $\mathcal{E} = 0$, to the insulator semiconductor interface. A similar expression holds for electrons such that

$$1 - \frac{1}{M_n} = \int_0^{W_{mis}} \alpha_n exp\left[\int_0^y (\alpha_p - \alpha_n)dz\right]dx \qquad C.2.3$$

here the integral over y is in the opposite direction to that for x in the expression (C.2.2).

The ionisation coefficients are functions of electric field and are assumed to obey Chynoweth's Law [3] giving

$$\alpha_p = \alpha_{\infty_p} exp(-b_p/|\mathcal{E}|) \quad \text{and} \quad \alpha_n = \alpha_{\infty_n} exp(-b_n/|\mathcal{E}|) \qquad C.2.4$$

The coefficients for $\alpha_{\infty_{(p,n)}}$, and $b_{(p,n)}$ are as follows:

For electrons $\alpha_{\infty_n} = 7.03 \times 10^5 cm^{-1}$ and $b_n = 1.231 \times 10^6 Vcm^{-1}$

for $1.75 \times 10^5 \leq \mathcal{E} \leq 6.0 \times 10^5 Vcm^{-1}$

For holes $\alpha_{\infty_p} = 1.582 \times 10^6 cm^{-1}$ and $b_p = 2.036 \times 10^6 Vcm^{-1}$

for $1.75 \times 10^5 \leq \mathcal{E} \leq 4.0 \times 10^5 Vcm^{-1}$

and $\alpha_{\infty_p} = 6.71 \times 10^5 cm^{-1}$ and $b_p = 1.693 \times 10^6 Vcm^{-1}$

for $4.0 \times 10^5 \leq \mathcal{E} \leq 6.0 \times 10^5 Vcm^{-1}$

The ratio of ionisation coefficients is considered to be constant throughout the space charge region and equal to the value at maximum electric field $\mathcal{E}_{max}$ in the depletion layer [2]. This ratio γ is given by

$$\gamma = \alpha_p(|\mathcal{E}_{max}|)/\alpha_n(|\mathcal{E}_{max}|) \qquad C.2.5$$

By using the depletion approximation for the electric field within the depletion region

$$\mathcal{E} = \frac{qN_d x}{\epsilon_s} = \Lambda x \qquad C.2.6$$

an analytic expression for the ionisation coefficients can be determined. Hence

$$\alpha_p = \alpha_{\infty_p} exp(-b_p \epsilon_s / qN_d x) = \alpha_{\infty_p} exp(-b_p/\Lambda x) \qquad C.2.7$$

A similar expression holds for the the electron ionisation coefficient.

Expression C.2.2 can be rewritten using C.2.5 as

$$1 - \frac{1}{M_p} = \int_0^{W_{mis}} \gamma\alpha_n exp\left[\int_0^x (1-\gamma)\alpha_n dz\right] dx = \int_0^{W_{mis}} \gamma\alpha_n exp(I) \qquad C.2.8$$

where by substituting $y = b_n/\Lambda z$ gives an expression for I of the form

$$I = \frac{b_n}{\Lambda}(1-\gamma)\alpha_{\infty_n} \int_{b_n/\Lambda x}^{\infty} y^{-2} e^{-y} \qquad C.2.9$$

Integrating this expression gives the final form for I to be

$$I = \frac{b}{\Lambda}(1-\gamma)\alpha_{\infty}\left\{E_1\left(\frac{b}{\Lambda x}\right) - \frac{e^{-b_n/\Lambda x}}{b_n/\Lambda x}\right\} \qquad C.2.10$$

where $E_1(x)$ is the exponential integral

$$E_1(x) = \int_x^{\infty} \frac{e^{-z}}{z} dz \qquad C.2.11$$

with this expression C.2.8 can be numerically integrated to give a final expression for M_p. A similar expression can be shown to hold for M_n. The values for M_p and M_n under certain conditions are illustrated in Fig C.1

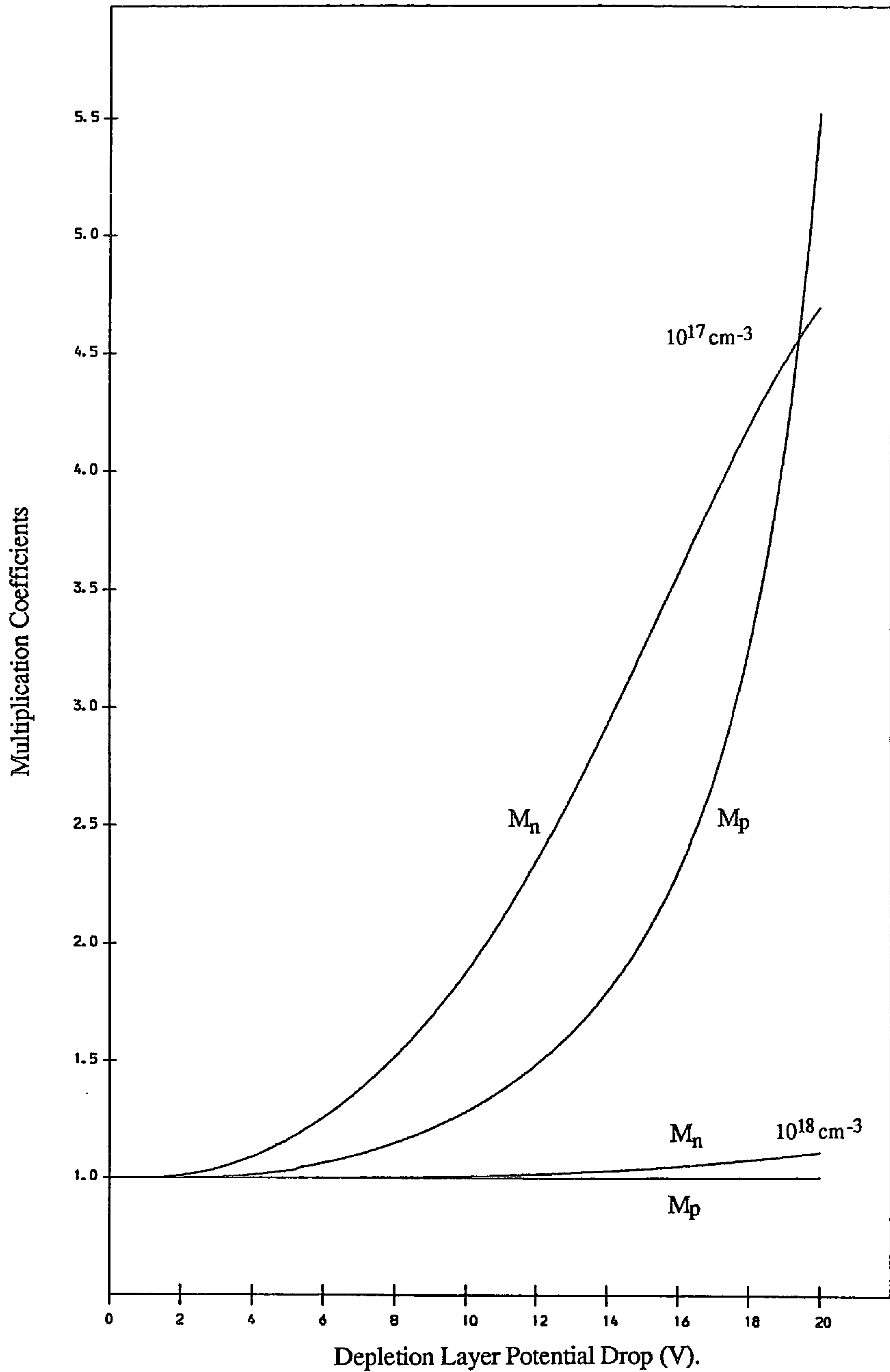

Fig C.1: Electron and Hole Avalanche Multiplication Coefficients for Two Doping Densities.

References

1. Sze, S. M., *The Physics of Semiconductor Devices*, Wiley, (1981).
2. Bulucea, C. D. and Prisecaru, D. C, 'The Calculation of the Avalanche Multiplication Factors in Si $p-n$ Junction Taking Account of Carrier Generation (Thermal or Optical) in the Space Charge Region', *IEEE Trans. Elec. Devices*, ED-**20**, No 8, pp 692-701, (1973).
3. Van Overstraeten, R. and De-Man, H., 'Measurement of Ionization Rates in Diffused Si $p-n$ Junctions', *Solid St. Electron.*, **13**, pp 583-608, (1970).

APPENDIX D

GENERATION CURRENT

D.1 Introduction

The generation current expression developed here has a form similar to that given by Mattos *et al* in their paper on the $MIpn^+$ device [1] and initially derived in the thesis of Fiore De Mattos [2]. The final expression derived here is a reproduction of Mattos's equation, except for an n-type as opposed to a p-type layer.

D.2 The Generation Current Equation

The generation current in the MIS depletion region, J_g, can be determined from the integral

$$q\int_{w_1}^{w_0} U(x)dx \qquad D.1$$

where w_1 and w_0 are the edges of the generation zone of the depletion region, and $U(x)$ is the generation rate at the point x. From Sze [3], the width of a space charge layer in a depletion region for an MIS structure with a band bending ψ_s taking into account the tailing of the carrier distribution is given by

$$W_{mis} = \left(\frac{2\epsilon_s}{q^2 N_d}\right)^{1/2}(q\psi_s - kT)^{1/2} \qquad D.2$$

and with the extrinsic Debye length

$$L_d = \left(\frac{\epsilon_s kT}{q^2 N_d}\right)^{1/2} \quad \text{and} \quad \beta = \frac{q}{kT} \qquad D.3$$

this gives an expression for the depletion width of the form

$$W_{mis} = L_d\sqrt{2}(\beta\psi_s - 1)^{1/2} \qquad D.4$$

It is assumed that for either p or $n \geq n_i$ there is no net generation current.

For the point in the MIS depletion region at which $E_{fn} = E_i$, generation ceases, so reducing the width of the generating region of the MIS structure by

$$W_r = L_d\sqrt{2}(\beta\phi_n - 1)^{1/2} \qquad D.5$$

where ϕ_n is the Fermi potential for electrons in the n type neutral region outside the MIS depletion layer. The width of the generating region is now given by

$$W_g = W_{mis} - W_r = L_d\sqrt{2}\left\{(\beta\psi_s - 1)^{1/2} - (\beta\phi_n - 1)^{1/2}\right\} \qquad D.6$$

The generation rate $U(x)$ at the point x in the depletion region can be expressed in terms of the electron, hole, and intrinsic carrier densities, together with the lifetime τ_0 in the form

$$U(x) = \frac{1}{\tau_0}\frac{n_i^2 - p(x)n(x)}{p(x) + n(x) + 2n_i cosh\left(\frac{E_t - E_i}{kT}\right)} \qquad D.7$$

where the free electron and hole carrier densities are given by

$$n(x) = n_i exp\left(\frac{E_{fn} - E_i(x)}{kT}\right) \quad \text{and} \quad p(x) = n_i exp\left(\frac{E_i(x) - E_{fp}}{kT}\right) \qquad D.8$$

and E_{fn}, E_{fp} and $E_i(x)$ are the electron, hole and intrinsic Fermi levels respectively. The assumption used throughout the text is that the electron and hole

quasi Fermi levels are flat in the MIS depletion region. The most effective trap centres are those with an energy E_t equal to the intrinsic Fermi level in the MIS depletion region.

Taking $E_i(0) = 0$ at the edge of the depletion region, and using the criterion that for generation to occur, $p(x)$ and $n(x) \leq n_i$, the generation region is given by

$$q\phi_n \leq E_i \leq q\phi_n + \xi \qquad D.9$$

where ξ is the quasi Fermi level splitting, and $q\phi_n$ and $q\phi_n + \xi$ are the positions of the electron and hole quasi-Fermi levels in the MIS depletion respectively. From Sze [3], taking the mean value for the intrinsic Fermi level in the MIS depletion region to be

$$E_i = \frac{E_{fp} + E_{fn}}{2} = q\phi_n + \xi/2 \qquad D.10$$

and after a little manipulation of D.7, D.8 and D.10, the generation rate can now be written in the form

$$U(x) = \frac{n_i}{2\tau_0}\left[\frac{1 - e^{-\xi/kT}}{1 + e^{-\xi/2kT}}\right] \qquad D.11$$

By taking into account the two distribution tails for the carriers in the depletion region, the final expression for J_g can be written in the form

$$J_g = \frac{qn_iL_d}{\sqrt{2}\tau_0}\frac{1 - e^{-\xi/kT}}{1 + e^{-\xi/2kT}}\left\{[M(\psi_s, \xi)]^{1/2} - (\beta\phi_n - 1)\right\} \qquad D.12$$

where $M(\psi_s, \xi)$ is the minimum of $(\beta\psi_s - 1)$ and $(\beta(\phi_n + \xi/q) - 1)$

References

1. Fiore De Mattos, A. C. and Sarrabayrouse, G., 'The MISS Device Modelling and Influence of Critical Parameters', *Phys. Stat. Sol.*, 87, pp. 699-707, (1985).

2. Fiore De Mattos, A. C., *Ph.D Thesis.*, (1985).

APPENDIX E

MISS CIRCUIT THEORY

E.1 Introduction

This appendix describes the basic circuit theory necessary to understand the behaviour of the MISS as a circuit element. It is concerned with the functioning of the device when disturbed from an equilibrium point by a small delta function change in the supply potential. The equations are solved to provide an expression for the effect of this delta function change on the potential drop across the device.

E.2 Circuit Analysis

The basic circuit being analysed is drawn in Fig E.1. The external circuit is taken to be a voltage source, in series with a load resistor of value R, and a parasitic inductance L. The device itself is demonstrated in circuit terms to be a dynamic resistance of value r_d in parallel with a dynamic capacitance c_d.

The analysis is performed using Laplace transforms and the initial current and voltage values at $t = 0$ are taken to be constant. This is because we are concerned with the small signal behaviour of the device when the supply potential V_{sup} is perturbed by a small amount ΔV_{sup} i.e. we need to use the dynamic resistance and capacitance values f the $MISS$ to determine the the incremental change in

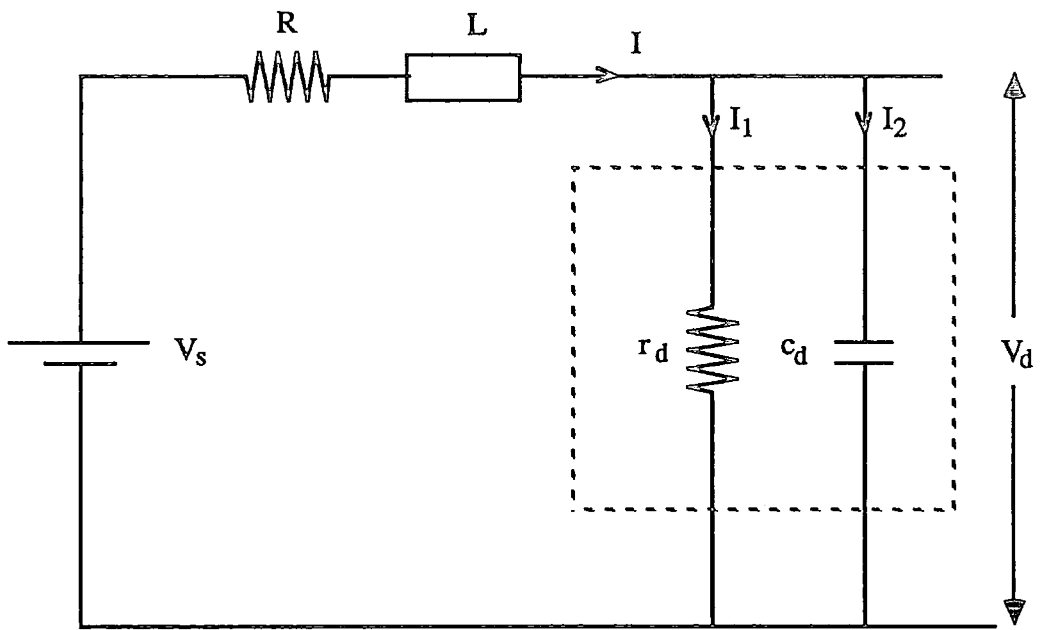

Fig E.1: The MISS Device as a Circuit Element

the device potential ΔV_d. Steady state values in the analysis are only needed to provide the operating point at which the dynamic values of resistance and capacitance for the device are calculated.

The basic equations after Laplace transformation can be expressed as follows; for current continuity

$$I(s) = I_1(s) + I_2(s) \qquad E.1$$

where $I(s)$ is the total current flow through the device, and $I_1(s)$ and $I_2(s)$ are the currents through the dynamic resistance of the device and the dynamic capacitance of the device respectively. See Fig (E.1). The dynamic change in the $MISS$ device potential can now be expressed in terms of the two incremental current changes ΔI_1 and ΔI_2 through the device as

$$\Delta V_d(s) = \Delta I_1(s) r_d \quad \text{and} \quad c_d s \Delta V_d(s) = \Delta I_2(s) \qquad E.2$$

Solving for ΔV_{sup}, and ΔV_d by eliminating current from the set of equations (E.1) and (E.2) gives an expression for the change in device potential due to the perturbation of the supply potential to be

$$\Delta V_d(s) = \frac{r_d}{(1 + s r_d c_d)(R + sL) + r_d} \Delta V_{sup}(s) \qquad E.3$$

Now $\Delta V_{sup}(s)$ can be expressed in terms of the Laplace transform as a delta function multiplied by a scalar, the Laplace transform being a linear operator, hence

$$\Delta V_{sup}(s) = \mathcal{L}[\Delta V_{sup} \delta(t)] = \Delta V_{sup} \mathcal{L}[\delta(t)] = \Delta V_{sup}.1 \qquad E.4$$

Therefore by dividing through by ΔV_{sup}, and setting

$$Y(s) = \frac{\Delta V_d(s)}{\Delta V_{sup}} \qquad E.5$$

with $\mathcal{L}[\delta(t)] = 1$, and letting $H(s)$ be the transfer function for the system, [1] gives

$$Y(s) = H(s) = \frac{r_d}{(1 + s r_d c_d)(R + sL) + r_d} \qquad E.6$$

Therefore in the time domain

$$y(t) = \mathcal{L}^{-1}[Y(s)] = \mathcal{L}^{-1}[H(s)] = h(t) \qquad E.7$$

$y(t)$ is the unit response to a delta function, and $h(t)$ is termed the impulse response of the system.

To provide an expression for the transformation of $H(s)$ into the impulse response function in the time domain the right hand side of (E.3) is broken up into partial fractions, and this expression is then transformed back. By defining the variables p, q, and r as

$$p = r_d c_d R + L \quad q = \sqrt{(r_d c_d R + L)^2 - 4 r_d c_d L(r_d + R)} \quad r = r_d c_d L \qquad E.8$$

The final expression for $h(t)$ can be given in the form

$$h(t) = \frac{r_d}{c_d r_d L}\frac{r}{q}\left[e^{-(p/2r)t}\left(e^{(q/2r)t} - e^{-(q/2r)t}\right)\right] \qquad E.9$$

Knowing the impulse response allows the calculation of a relationship between any input $x(t)$ to the system rather than the unit delta function described, by use of the formula

$$y(t) = \int_0^{\infty} x(\tau)h(t-\tau)d\tau \qquad E.10$$

but for the system analysed in the text only the response to a delta function is required.

References

1. Borrow, L. S., *Elementary Linear Circuit Analysis*, Holt-Saunders, pp. 662, (1981).

APPENDIX F

NUMERICAL CONSTANTS AND EXPRESSIONS

Silicon band gap [1] $E_g - 1.12eV$

Silicon dioxide band gap [1] - $9eV$

Intrinsic carrier concentration [1] $n_i = 1.45 \times 10^{10} cm^{-3}$

Conduction band density of states [1] $N_c = 2.8 \times 10^{19} cm^{-3}$

Valence band density of states [1] $N_v = 1.04 \times 10^{19} cm^{-3}$

Permittivity in a vacuum [1] - $\epsilon_0 = 8.85418 \times 10^{-14} F/cm$

Permittivity of silicon [1] - $\epsilon_s = 1.0536447 \times 10^{-12} F/cm$

Permittivity of silicon dioxide [1] - $\epsilon_{ox} = 3.34 \times 10^{-13} F/cm$

Elementary charge [1] - $q = 1.60218 \times 10^{-19} C$

Boltzmann constant [1] - $k = 1.38066 \times 10^{-23} J/K$

Electron volt [1] - $eV = 1.60218 \times 10^{-19} J$

Angstrom - $\mathring{A} = 10^{-8} cm = 10^{-4} \mu m$

Electron affinity of silicon [1] - 4.05V

Lifetimes for electrons in p-type layers and holes in n-type layers [2]

Doping Density (cm^{-3})	$\tau_n(S)$	$\tau_p(S)$
1×10^{14}	2×10^{-5}	5×10^{-5}
1×10^{15}	1×10^{-5}	4×10^{-5}
1×10^{16}	3×10^{-6}	1×10^{-5}
1×10^{17}	1.5×10^{-6}	2.5×10^{-6}
1×10^{18}	1×10^{-6}	6×10^{-7}
1×10^{19}	1×10^{-6}	3.3×10^{-7}

Expressions used for evaluation of other parameters:

Diffusion coefficient for electrons as a minority carrier in p-type material of doping density N_a at 300K [3]:

$$D_n = 1.6835 + \frac{32.7635}{1 + (N_a/8.5 \times 10^{16})^{0.72}}$$

Diffusion coefficient for holes as a minority carrier in n-type material of doping density N_d at 300K [3]:

$$D_p = 1.2354 + \frac{11.5851}{1 + (N_d/6.3 \times 10^{16})^{0.76}}$$

Electron mobility in p-type silicon [1] $\mu_n = (q/kT)D_n$.

Hole mobility in n-type silicon [1] $\mu_p = (q/kT)D_p$.

Diffusion length for electrons as minority carriers [1] $L_n = \sqrt{D_n\tau_n}$.

Diffusion length for holes as minority carriers [1] $L_p = \sqrt{D_p\tau_p}$

References

1. Sze, S. M., 'Physics of Semiconductor Devices', *John Wiley*, (1981).

2. Wolf, H. F., 'Silicon Semiconductor Data', *Pergamon Press*, (1969).

3. Caughay, D. M., and Thomas, R. E.: 'Carrier Mobilities in Silicon Empirically Related to Doping and Field', *Proceedings IEEE*, 55, pp2192, (1967).

APPENDIX G

MODELLING PROGRAMS

```
Program Onedmiss(readout) ;

VAR MSINK, readout : text ;

VAR i, j : integer ;

VAR Vf, TEMP, dox, phis, xi, elec, hole, dV, OldV, NewV,
    wrout, oldxi, oldphi, TotalJ, TotalV, dxi, dphis : real ;

Procedure TWOEQU(CONST VF, TEMP, DOX, OLDXI, OLDPHI : REAL ;
VAR XI, PHIS, TOTALJ, TOTALV : REAL) ; FORTRAN ;

Procedure pnmiss(VAR Vf,temp,dox,oldxi,oldphi,xi,phis,elec,hole,
wrout, totalj, totalv : real) ; MAIN ;

Procedure pnmiss ;

(*Constants appropriate to the operation of semiconductors
  Electric charge (coulomb), Electron volt (joule),
  Permittivity of free space (F/cm), Boltzmann constant (eV/K),
  PI, Speed of sound (cm/s), Electron rest mass (Kg), Richardsons
  constant for free electrons (A/cm2/K2),Aluminium work function (eV),
  Permittivity of Silicon Dioxide(F/cm), Temperature(K),
  Planck's constant(J-s), Reduced Planck's constant h/2*pi(J-s),
  Energy gap of Silicon Dioxide (eV), Gap from the Si conduction band
  to the SiO2 conduction band (eV),Relative insulator transverse electron
  mass, relative transverse semiconductor electron, longitudinal silicon
  electron mass, semiconductor hole mass. phiAl=4.32197195 *)

CONST q=1.60218E-19 ; eV=1.60218E-19 ; eps0=8.85418E-14 ; Bk=8.61738E-5 ; PI=3.14159 ;
    Cs=3.3E4 ; M0=9.1095E-31 ; Ar=120 ; phiAl=4.4 ; epsox=3.34E-13 ;
    hp=6.62617E-34 ; hpr=1.05458E-34 ; SiOEg=9.0 ; Ebarr=3.20 ; mti=0.42 ;

(* Constants appropriate to silicon
  Energy gap (eV), Effective density of states (cm-3): conduction band,
  valence band, intrinsic carrier concentration (cm-3), intrinsic mobilities:
  electrons, holes (cm/vsec), Dielectric constant, Breakdown field (v/cm),
  q/KT, minority carrier lifetime (s), Saturation drift velocity (cm/s),
  Optical phonon energy (eV), Electron diffusion const.(cm2/sec), Hole diffusion
  const.(cm2/sec), Ntype Si work function (eV), silicon permittivity (F/cm),
  Donor density (cm-3), Acceptor density (cm-3), Silicon electron affinity (V),
  Surface state density (/cm2/eV), Tunnelling exponent for electrons (A-1) ;
  Tunnelling exponent for holes (A-1), Longtitudinal effective mass,
  Transverse effective mass, Light hole effective mass, Heavy hole effective
  mass. *)

Eg=1.12 ; ni=1.45E10 ; Nc=2.8E19 ; Nv=1.04E19 ;
    Ks=11.9 ; BE=3E5 ; torp=4.0E-5 ; torn=1.0E-6 ; Vsat=1E7 ; Ep=6.3E-2 ;
    epss=1.0536447E-12 ; Nd=1E15 ; Na=1E19 ; chiSi=4.05 ; CHIp1=0.948 ;
    CHIn1=0.911 ; ml=0.98 ; mt=0.19 ; mlh=0.16 ; mhh=0.49 ;

VAR Ex, Wmis, Wpn, Wepi, Wneut, Uox, Qss,Es, EUox, Jrec, W, MN, MP,
    EFN, EFP, EFMc, EFMv, EFNW, Jtn, Jtp, phix, Jpj, Jrj, Jg, Jns, v, wout,
    neta, val, C1, C2, error, ans, dnd, newq, Kprime, capac, gain, gainmis,
    Energy, totpn, X, y, chi, dchi, Jsm, chin, chip, Eint, gainpn,
    newjtn, newjtp, Jn, Estat, Edyn, Nd1, diffres, dxi, Qss : real ;

VAR ps, incVf : real ;
    i, j, print : integer ;
    OK : boolean ;
```

```
(* NAG routine definitions *)

Procedure INTFER( CONST DEGREE, NETA : real ;
VAR ANS : real) ; FORTRAN ;

Procedure INTJTN( CONST EFM,EFN,EG,SIOEG,EBARR,DOX,UOX,
BK,TEMP,LIMIT : REAL ; VAR ANS : REAL) ; FORTRAN ;

Procedure INTJTP( CONST EFM,EFP,EG,SIOEG,EBARR,DOX,UOX,
BK,TEMP,LIMIT : REAL ; VAR ANS : REAL) ; FORTRAN ;

Procedure AVAMUL( CONST W,ND : REAL ; VAR MN,MP : REAL) ; FORTRAN ;

Function S15AEF(CONST X : REAL ;VAR IFAIL : INTEGER) : REAL ; FORTRAN ;
Function S15AFF(CONST X : REAL ;VAR IFAIL : INTEGER) : REAL ; FORTRAN ;

Function Beta : real ;
(* Determines q/kT *)

Begin
  beta := 1/(Bk*temp) ;
End ; (*beta*)

Function Dn : real ;
(* Calculates the diffusion length for the electron as a minority carrier
  in a material with an acceptor doping Na *)

VAR x : real ;

Begin
  x := 1.6835 + 32.7635/(1 + exp(0.72*ln(Na/8.5E16))) ;
  Dn := x*exp(-1.5*ln(temp/300)) ;
End;(*Dn*)

Function Dp : real ;
(* Calculates the diffusion length for a hole as a minority carrier
  in a material with a donor doping Na. *)

VAR x : real ;

Begin
  x := 1.2354 + 11.5851/(1 + exp(0.76*ln(Nd/6.3E16))) ;
  Dp := x*exp(-1.5*ln(temp/300)) ;
End;(*Dp*)

Function mun : real ;
(* Calculates the value for the mobility (Sze p.29) *)

VAR x, fHalf, fHmin, degree : real ;

Begin
  mun := Dn*Beta ;
  x := Dn*Beta ;
End;(*mun*)

Function mup : real ;
(* Calculates the value for the mobility (Sze p.29) *)

VAR x : real ;

Begin
  mup := Dp*Beta ;
  x := Dp*Beta ;
End;(*mup*)

Function Arcsin(x:real) : real ;

Begin
  IF (((1-sqr(x))<=0) AND (x<0)) THEN arcsin := -pi/2 ELSE
  IF (((1-sqr(x))<=0) AND (x>0)) THEN arcsin := pi/2
    ELSE arcsin := Arctan(x/(sqrt(1-sqr(x))));
End; (*Arcsin*)
```

```
Function NewIntFermihalf(neta:real) : real ;
(* Calculates the fermi integral of order 1/2 for the value neta, calling the
  FORTRAN routine INTFER. *)

VAR ANS, DEGREE : real ;

Begin
  DEGREE := 1/2 ;
  INTFER(DEGREE,NETA,ANS) ;
  NewIntFermihalf := (2/SQRT(PI))*ANS ;
End; (*NewIntFermhalf*)

Function NewIntFermione(neta:real) : real ;
(* Calculates the fermi integral of order 1 for the value neta, calling the
  FORTRAN routine INTFER. *)

VAR ANS, DEGREE : real ;

Begin
  DEGREE := 1.0 ;
  INTFER(DEGREE,NETA,ANS) ;
  NewIntFermione := ANS ;
End; (*NewIntFermione*)

Function sinh(x : real) : real ;

Begin
  sinh := (exp(x)-exp(-x))/2
End ; (*sinh*)

Function cosh(x : real) : real ;

Begin
  cosh := (exp(x)+exp(-x))/2
End ; (*cosh*)

Function DiffLp : real ;
(* Gives the diffusion length for holes *)

Begin
  Difflp := sqrt(Dp*torp)
End ; (*DiffLp*)

Function DiffLn : real ;

Begin
  Diffln := sqrt(Dn*torn)
End; (*DiffLn*)

Function Phifn : real ;
(* Calculates the fermi potential for N type silicon with donor density
  Nd specified globally *)

Begin
  Phifn := (ln(Nd/ni))/beta
End ; (*Phifn*)

Function PhiSi : real ;
(* Calculates the work function for n type silicon with a dopant density Nd *)

Begin
  PhiSi := Eg/2 + ChiSi - phifn ;
End; (* PhiSi*)

Function Phifp : real ;
(* Calculates the fermi potential for P type silicon with acceptor
  density Na specified globally *)

Begin
  Phifp := (ln(Na/ni))/beta
End ; (*Phifp*)
```

```
Function Vbi : real ;
(* Calculates the built in voltage of p+ n junction due to a dopant densities
  Nd and Na *)

Begin
  Vbi := abs(phifn)+phifp
End (* Vbi*) ;

Function Ldebye : real ;
(* Determines the debye length for a donor density Nd *)

Begin
  Ldebye := sqrt(epss/(beta*q*Nd))
End; (*Ldebye*)

Procedure EFMvalence( Uox : real ; VAR EFMv : real ) ;
(* Calculates the value of the metal fermi level relative to the valence band
  of the semiconductor at the insulator surface *)

VAR EUox : real ;
Begin
  EUox := Uox ;
  EFMv := EUox + chiSi + Eg - phiAl
End ; (*EFMvalence*)

Procedure EFPvalence( xi, phis : real ; VAR EFP : real ) ;
(* Calculates the value of the hole quasi fermi level relative to the valence
  band of the semiconductor at a point in the depletion region with
  band bending phis. *)

VAR Ephis : real ;

Begin
  Ephis := phis ;
  EFP := xi + phifn + Eg/2 - Ephis
End ; (*EFPvalence*)

Procedure EFMconduction( Uox : real ; VAR EFMc : real ) ;
(* Calculates the position of the metal fermi level relative to the conduction
  band of the semiconductor at the insulator surface *)

VAR EUox : real ;

Begin
  EUox := Uox ;
  EFMc := EUox + ChiSi - PhiAl ;
End ; (*EFMconduction*)

Procedure EFNconduction( phis : real ; VAR EFN : real) ;
(* Calculates the value of the electron quasi fermi level relative to the
  conduction band of the semiconductor at a point in the depletion region
  with band bending Phis *)

VAR Ephis : real ;

Begin
  Ephis := phis ;
  EFN := phifn - Eg/2 - Ephis
End ; (*EFNconduction*)

Procedure OldElectunnel(EFMc, EFN, dox, chin : real ; VAR Jtn : real );
(* This procedure determines the electron current tunnelling through an
  oxide layer of width dox with the tunnelling coefficient and total
  expression calculated as in Green's Paper on tunnelling. The electron
  fermi level and metal fermi level are measured relative to the
  semiconductor conduction band at the surface. *)

VAR x, d, NewAr : real ;

Begin
```

```
(* dox is in cm = 1E+8 Angstroms*)
  NewAr := (4*pi*q*m0/hp)*sqr(Bk*q/hp)/10000;
  x := Ar*sqr(Temp)*exp(-CHIn) ; (*d in Angstroms*)
  d := dox*1E+8 ;
  x := mt*NewAr*sqr(Temp)*exp(-CHIn) ; (*d in Angstroms*)
  Jtn := x*(NewIntFermione(EFMc/(Bk*Temp))-NewIntFermione(EFN/(Bk*temp)));
    (*EFN,EFM in eV*)
End ; (*OldElectunnel*)

Procedure NewElectunnel(EFMc, EFN, dox, Uox : real ; VAR Jtn : real );
(* This procedure determines the electron current tunnelling through an
  oxide layer of width dox with the tunnelling coefficient and total
  expression calculated as in Green's Paper on tunnelling. The electron
  fermi level and metal fermi level are measured relative to the
  semiconductor conduction band at the surface. *)

VAR limit, ans, NewAr : real ;

Begin
(* dox is in cm = 1E+8 Angstroms*)
  limit := ebarr + Uox ;
  limit := ebarr + Uox - 1E-20 ;
  INTJTN(EFMc,EFN,EG,SIOEG,EBARR,DOX,UOX,BK,TEMP,LIMIT,ANS) ;
  NewAr := (4*pi*q*mti*m0/hp)*sqr(1/hp)/10000 ;
(* Need q's to convert to eV's*)
  Jtn := q*q*NewAr*ans ;
    (*EFN,EFM in eV*)
End;(*NewElectunnel*)

Procedure NewHoletunnel(EFMv, EFP, dox, Uox : real ; VAR Jtp : real );
(* This procedure determines the electron current tunnelling through an
  oxide layer of width dox with the tunnelling coefficient and total
  expression calculated as in Green's Paper on tunnelling. The electron
  fermi level and metal fermi level are measured relative to the
  semiconductor conduction band at the surface. *)

VAR limit, ans, NewAr : real ;

Begin
(* dox is in cm = 1E+8 Angstroms*)
  limit := SiOEg-Ebarr-Eg ;
  limit := SiOEg-Ebarr-Eg - 1E-50 ;
  INTJTP(EFMv,EFP,EG,SIOEG,EBARR,DOX,UOX,BK,TEMP,LIMIT,ANS) ;
  NewAr := (4*pi*q*mti*m0/hp)*sqr(1/hp)/10000 ;
(* Need q's to convert to eV's*)
  Jtp := q*q*NewAr*ans ;
    (*EFN,EFM in eV*)
End; (*NewHoleTunnel*)

Procedure OldHoletunnel(EFMv, EFP, dox, CHIp : real ; VAR Jtp : real) ;
(* This procedure calculates the hole tunnelling current in the oxide layer
  using the tunnelling expression in Green due to EFP and 8FMv both measured
  relative to the valence band. *)

VAR x, d, y, NewCHIp, NewAr : real ;

Begin
(* dox is in cms = 1E+8 Angstroms *)
  d := 1E+8*dox ;
  NewAr := (4*pi*q*m0/hp)*sqr(Bk*q/hp)/10000;
  x := -0.33*NewAr*sqr(Temp)*exp(-CHIp) ; (*d in Angstroms*)
  Jtp := x*(NewIntFermione(-EFMv/(Bk*Temp))-NewIntFermione(-EFP/(Bk*Temp)));
(*EFP,EFM in eV*)
End ; (*OldHoletunnel*)

Procedure Pndepwidth( Vf : real; VAR Wpn : real) ;
(* Calculates the space charge depletion layer width of a one sided step
```

```
  junction with the lower doped side Nd and forward voltage Vf with the
  width returned as Wpn *)

VAR x : real ;

Begin
  x := ((2*epss*(Vbi-Vf))/q)*(Na+Nd)/(Na*Nd) ;
  Wpn := sqrt(x)
End (*Pndepwidth*) ;

Procedure misdepwidth(phis, xi : real ; VAR Wmis : real );
(* Procedure calculates the width of a MIS depletion layer
  using the depletion approximation and due to a surface potential
  'phis' returning the result as 'Wmis', does not work for accumulation. *)

VAR u,x,Ephis :real ;

Begin
  Ephis := abs(phis) ; (*Ephis in eV*)
  x:= (2*epss)/(q*Nd) ;
  IF Ephis<(2*phifn+xi) THEN u := Ephis
    ELSE IF (2*phifn+xi)<0 THEN u := Ephis ELSE u := 2*phifn + xi ;
  Wmis := sqrt(x*u) ;
End ; (*misdepwidth*)

Procedure Misholecurrent(xi, phis, Vf : real ; VAR Jpj, Jrec : real) ;
(* Calculates the hole current at the MIS/neutral region interface, taking
  Into account recombination in the neutral region. The hole density at the MIS
  edge is given by ni*exp(Ei-Efp)/kT where Ei-Efp=-(phifn+xi) and the hole
  density at the pn junction is given by sqr(ni)/Nd*exp(Beta*Vf). The result is
  returned as Jpj. Using the same variables the recombination current in the
  neutral is calculated with the result returned as Jrec. *)

VAR x, Wpn, Wneut, Wmis, Pjprime, Pmprime, expon, Wn, y : real ;

Begin
  pndepwidth(Vf,Wpn) ;
  misdepwidth(phis, xi, Wmis ) ;
  Wn := Wpn/(1+(Nd/Na)) ;
  Wneut := Wepi - Wmis - Wn ;
  expon := -(phifn+xi)/(Bk*temp) ;
  IF expon>174 THEN expon := 174 ;
  IF expon<-170 THEN expon := -170 ;
  Pmprime := ni*exp(expon) ;
  Pjprime := (sqr(ni)/Nd)*(exp(beta*Vf) - 1) ;
  y := Wneut/Difflp ;
  IF (y>170) THEN y := 170 ;
  x := (q*Dp)/(Difflp*sinh(y)) ;
  Jpj := x*(Pjprime - Pmprime*cosh(y)) ;
  Jrec := x*(Pjprime+Pmprime)*sqr(sinh(y/2)) ;
End ; (*Misholecurrent*)

Procedure Pnrecomb(Wpn, Vf : real ; VAR Jrj : real ) ;
(* Calculates the recombination current in the space charge region of the
  pn junction given the forward potential across the junction along with the
  space charge width Wpn using an expression due to GROVE p187 *)

VAR x : real ;

Begin
  x := (q*ni*Wpn)/(2*torp) ;
  Jrj := x*(exp(beta*Vf)-1)/(exp((beta*Vf)/2)+1)
End (*Pnrecomb*) ;

Procedure Substratecurrent( Vf :real ; VAR Jns : real ) ;
(* Calculates the substrate electron current for a forward bias Vf and
  an acceptor density Na *)
```

```
VAR x : real ;

Begin
  x := (q*Dn*sqr(ni))/(Diffln*Na) ;
  Jns := x*(exp(beta*Vf)-1)
End (*Substratecurrent*) ;

Procedure Generationcurr(phis, xi : real ; VAR Jg : real ) ;
(* Calculates the generation current in the depletion region using a modified
  expression due to Mattos. *)

VAR x, u, Ephis : real ;

Begin
  Ephis := abs(phis) ;
  x := (q*ni*Ldebye)/(torp*sqrt(2)) ;
  IF xi<4 THEN x := x*(1-exp(-xi/(Bk*TEMP)))/(1+exp(-xi/(2*Bk*TEMP))) ;
  IF Ephis<(phifn+xi) THEN u := Ephis ELSE u := phifn+xi ;
  IF (u<(Bk*temp)) THEN Jg := 0 ELSE
    IF xi<0 THEN Jg := 0 ELSE
    Jg := x*(sqrt((u/(Bk*temp))-1) - sqrt((phifn/(Bk*Temp))-1)) ;
End ; (*Generationcurr*)

Procedure Potdropinoxide(Es, dox, Qss : real ; VAR Uox : real ) ;
(* Calculates the potential drop across the oxide of thickness dox due to an
  electric field Es at the surface of the semiconductor/insulator barrier
  along with a surface charge Qss . *)

Begin
  Uox := (dox/epsox)*(epss*Es + Qss) ;
End ; (*Potdropinoxide*)

Procedure PoissonUox(xi,phis,dox : real ; VAR Qss, Uox : real) ;
(* Calculates a full integral of Poissons equation using the expressions
for the fermi integrals of order 3/2. Given values for xi and phis, the value
of Uox is produced. The expression for the electric field does not totally
agree with that of 'Green and Shewchun' because the value for Bk is expressed
in the units of eV/K and hence needs to be multiplied by the value of
q = 1.6E-19 to get it into J/k, this explains the factor of q needed in front
of the fermi integrals. *)

VAR Totalsum, C1, C2, C3, C4, E, Ephis, ANS1, ANS2, ANS3,
    ANS4, DEGREE, Totall : real ;

Begin
  DEGREE := 3/2 ;
  Ephis := phis ;
  C1 := (phifn-Eg/2)/(Bk*Temp) ;
  C2 := (-xi-phifn-Eg/2)/(Bk*temp) ;
  C3 := (Ephis-xi-phifn-Eg/2)/(Bk*Temp) ;
  C4 := (phifn-Eg/2-Ephis)/(Bk*Temp) ;
  INTFER(DEGREE,C1,ANS1) ;
  INTFER(DEGREE,C2,ANS2) ;
  INTFER(DEGREE,C3,ANS3) ;
  INTFER(DEGREE,C4,ANS4) ;
  Totalsum := (4*Nc/(3*sqrt(pi)))*(ANS4-ANS1) ;
  Totalsum := Totalsum + (4*Nv/(3*sqrt(pi)))*(ANS3-ANS2) ;
  IF EPHIS<0 THEN Totalsum := Bk*Temp*Totalsum
    ELSE Totalsum := Nd*Ephis + Bk*Temp*Totalsum ;
  Totalsum := 2*(q/epss)*Totalsum ;
  E := sqrt(abs(Totalsum)) ;
  Interfacecharge(xi,phis,Qss) ;
  Potdropinoxide(E, dox, Qss, Uox ) ;
  newq := epss*E ;
End; (*PoissonUox*)

Procedure OldTunnel( Uox, energy : real ; VAR chi : real) ;
```

```
(* This procedure calculates the tunnelling exponent value for a carrier
with an energy 'energy' above the insulator valence band which has a potential
Uox dropped across it. The potential being positive with a ngative bias on the
metal w.r.t. the silicon. *)

VAR Udox, Uzero, WDox, Wzero, Totalsum, d, Xm, Xs : real ;

Begin
  d := dox*1E+8 ; (* d is in Angstroms. *)
  IF (energy-SiOEg)>0 THEN Xs := dox - ((SiOEg+Uox-energy)/Uox)*dox
    ELSE Xs := 0 ;
  IF (energy-Uox)<0 THEN Xm := (energy/Uox)*dox
    ELSE Xm := dox ;
  Udox := Energy - Xm*Uox/dox ;
  Uzero := Energy - Xs*Uox/dox ;
  Wdox := (2*Udox/SiOEg)-1 ;
  Wzero := (2*Uzero/SiOEg)-1 ;
  Totalsum := Wzero*sqrt(1-sqr(Wzero)) + Arcsin(Wzero) ;
  Totalsum := Totalsum - Wdox*sqrt(1-sqr(Wdox)) - Arcsin(Wdox) ;
  chi := 1.024633*sqrt(0.42)*(d/Uox)*(sqr(SiOEg)/(sqrt(SiOEg)*8))*Totalsum ;
End; (*OldTunnel*)

Procedure Tunnel( Uox, energy : real ; VAR chi : real) ;
(* This procedure calculates the tunnelling exponent value for a carrier
with an energy 'energy' above the insulator valence band which has a potential
Uox dropped across it. The potential being positive with a ngative bias on the
metal w.r.t. the silicon. *)

VAR Udox, Uzero, Mlimit, Slimit, WDox, Wzero, Totalsum, d, Xm, Xs : real ;

Begin
  d := dox*1E+8 ; (* d is in Angstroms. *)
  Udox := Energy - Uox ; Uzero := Energy ;
  Wdox := (2*Udox/SiOEg)-1 ; Wzero := (2*Uzero/SiOEg)-1 ;
  IF (energy-SiOEg)>0 THEN Slimit := PI/2
    ELSE Slimit := Wzero*sqrt(1-sqr(Wzero)) + Arcsin(Wzero) ;
  IF (energy-Uox)<0 THEN Mlimit := -PI/2
    ELSE Mlimit := Wdox*sqrt(1-sqr(Wdox)) + Arcsin(Wdox) ;
  Totalsum := Slimit - Mlimit ;
  chi := 1.024633*sqrt(0.42)*(d/Uox)*(sqr(SiOEg)/(sqrt(SiOEg)*8))*Totalsum ;
End; (*Tunnel*)

Procedure DiffTunnel( Uox, energy : real ; VAR dchi : real) ;
(* This procedure calculates the value for the first differential of the
tunnelling attenuation factor w.r.t. the transverse energy in the insulator
at Et=0. *)

VAR Udox, Uzero, WDox, Wzero, Totalsum, d, Xm, Xs : real ;

Begin
  d := dox*1E+8 ; (* d is in Angstroms. *)
  IF (energy-SiOEg)>0 THEN Xs := ((SiOEg+Uox-energy)/Uox)*dox
    ELSE Xs := 0 ;
  IF (energy-Uox)<0 THEN Xm := (energy/Uox)*dox
    ELSE Xm := dox ;
  Udox := Energy - Xm*Uox/dox ;
  IF UDOX<1E-10 THEN Udox := 1E-10 ;
  Uzero := Energy - Xs*Uox/dox ;
  Wdox := (2*Udox/SiOEg)-1 ;
  Wzero := (2*Uzero/SiOEg)-1 ;
  Totalsum := (1/2)*sqrt(0.4)*sqrt(SiOEg)*(-d/Uox) ;
  dchi := Totalsum*(arcsin(Wdox)-arcsin(Wzero)) ;
End; (*DiffTunnel*)

Procedure JtnandJtpvalue(xi,phis,dox : real ; VAR Qss,Uox,Jtn,Jtp,Jsm : real) ;
(* Calculates the values of Jtn and Jtp for values xi, phis and Uox
```

```
  These values can then be used to determine the values of Jtn and Jtp. *)
VAR EFMc, EFMv, EFP, EFN, chin, chip, energy : real ;

Begin
  PoissonUox(xi,phis,dox,Qss,Uox) ;
  Energy := SiOEg - Ebarr ;
  Tunnel(Uox,energy,chin) ;
  EFMconduction(Uox,EFMc) ;
  EFNconduction(phis,EFN) ;
  OldElectunnel(EFMc,EFN,dox,chin,Jtn) ;
  Energy := SiOEg - Ebarr - Eg ;
  Tunnel(Uox,energy,chip) ;
  EFMvalence(Uox,EFMv) ;
  EFPvalence(xi,phis,EFP) ;
  OldHoletunnel(EFMv,EFP,dox,chip,Jtp);
  IntTunnelCurr(xi,phis,dox,Uox,Jsm) ;
End; (*JtnandJtpvalue*)

Procedure NewJtnandJtpvalue(xi,phis,dox:real;VAR Qss,Uox,Jtn,Jtp,Jsm : real) ;
(* Calculates the values of Jtn and Jtp for values xi, phis and Uox
  These values can then be used to determine the values of Jtn and Jtp. *)

VAR EFMc, EFMv, EFP, EFN : real ;

Begin
  PoissonUox(xi,phis,dox,Qss,Uox) ;
  EFMconduction(Uox,EFMc) ;
  EFNconduction(phis,EFN) ;
  NewElectunnel(EFMc,EFN,dox,Uox,Jtn) ;
  EFMvalence(Uox,EFMv) ;
  EFPvalence(xi,phis,EFP) ;
  NewHoletunnel(EFMv,EFP,dox,Uox,Jtp);
  IntTunnelCurr(xi,phis,dox,Uox,Jsm) ;
End; (*NewJtnandJtpvalue*)

Procedure ValueofJpjandJrj(xi,phis,Vf:real ; VAR Jpj,Jrj,Jrec,Jns,Jg: real);
(* Calculates the value of Jpj and Jrj for particular values of xi, phis
and Vf. It is used in the iterative procedure to balance up the current
contributions. Wepi passed as a global variable. *)

VAR Wpn, Wmis, Jptot, Jntot : real ;

Begin
  pndepwidth(Vf,Wpn) ;
  pnrecomb(Wpn,Vf,Jrj) ;
  misholecurrent(xi,phis,Vf,Jpj,Jrec) ;
  Substratecurrent(Vf,Jns) ;
  Generationcurr(phis,xi,Jg) ;
End; (*ValueofJpjandJrj*)

Procedure Currentchange(xi,phis,vf,dox,incvf,oldxi,oldphi : real ;
VAR gainmis, gainpn, gain : real) ;
(* Procedure to calculate the differential loop current gain of the device
  using dJtn/dJtp and dJpj/d(Jrec+Jrj+Jns). The procedure must be called
  before the procedure Capacitance because capacitance alters the values
  of oldxi, and oldphis. *)

VAR djtn, djtp, djpj, djelec, oldjtn, oldjtp, oldjpj, oldjrec, oldjrj, oldjns,
jtn, jtp, jrj, jpj, jrec, jns, Uox, oldvf, Qss, oldJsm,
jsm : real ;

Begin
  oldvf := vf - incvf ;
  PoissonUox(oldxi,oldphi,dox,Qss,Uox) ;
  Jtnandjtpvalue(oldxi,oldphi,dox,Qss,Uox,oldJtn,oldJtp,oldjsm) ;
  ValueofJpjandJrj(oldxi,oldphi,oldVf,oldJpj,oldJrj,oldJrec,oldJns,Jg) ;
```

```
  PoissonUox(xi,phis,dox,Qss,Uox) ;
  Jtnandjtpvalue(xi,phis,dox,Qss,Uox,Jtn,Jtp,Jsm) ;
  ValueofJpjandJrj(xi,phis,Vf,Jpj,Jrj,Jrec,Jns,Jg) ;
  dJtn := jtn - oldjtn ;
  dJtp := Jtp - oldjtp ;
  dJpj := Jpj - oldJpj ;
  dJelec := Jrec + Jrj + Jns - oldjrec - oldjrj - oldjns ;
  Gainmis := 0 ; Gainpn := 0 ; Gain := 0 ;
  IF ((abs(dJtp)>1E-20) AND (abs(dJelec)>1E-20)) THEN

Begin
    Gainmis := dJtn/dJtp ;
    Gainpn := dJpj/dJelec ;
    Gain := Gainmis*Gainpn ;
    END ;
End ; (*Currentchange*)

Procedure Capacitance(xi,phis,dox,Vf,incvf:real;VAR oldxi,oldphi,capac : real);
(* The procedure calculates the value for the differential capacitance of the
  device using the expression C=dQ/dV where the values for dQ and dV are taken
  from the values of the difference of the non differential quantities *)

VAR newq, newv, oldq, oldv, Qss, Uox : real ;

Begin
  Qss := 0 ;
  PoissonUox(oldxi,oldphi,dox,Qss,Uox) ;
  oldq := (epsox*Uox)/dox ;
  oldv := abs(Uox)+abs(oldphi)+chiSi+Eg/2+Vf-incvf-phiAl-phifn ;
  PoissonUox(xi,phis,dox,Qss,Uox) ;
  newq := (epsox*Uox)/dox ;
  newv := abs(Uox)+abs(phis)+chiSi+Eg/2+Vf-phiAl-phifn ;
  IF (abs(newv-oldv)>1E-20) THEN Capac := (newq - oldq)/(newv - oldv)
    ELSE capac := 0 ;
  oldxi := xi ; oldphi := phis ;
End; (*Capacitance*)

Procedure DifferentialRes(xi,phis,vf,dox,incvf,oldxi,oldphi : real ;
VAR diffres : real) ;

VAR djtn, djtp, djpj, djelec, oldjtn, oldjtp, oldjpj, oldjrec, oldjrj, oldjns,
jtn, jtp, jrj, jpj, jrec, jns, Uox, oldvf, Qss, oldJsm, dJtot, oldv, newv,
jsm : real ;

Begin
  oldvf := vf - incvf ;
  PoissonUox(oldxi,oldphi,dox,Qss,Uox) ;
  oldv := abs(Uox)+abs(oldphi)+chiSi+Eg/2+Vf-incvf-phiAl-phifn ;
  Jtnandjtpvalue(oldxi,oldphi,dox,Qss,Uox,oldJtn,oldJtp,oldjsm) ;
  ValueofJpjandJrj(oldxi,oldphi,oldVf,oldJpj,oldJrj,oldJrec,oldJns,Jg) ;
  PoissonUox(xi,phis,dox,Qss,Uox) ;
  newv := abs(Uox)+abs(phis)+chiSi+Eg/2+Vf-phiAl-phifn ;
  Jtnandjtpvalue(xi,phis,dox,Qss,Uox,Jtn,Jtp,Jsm) ;
  ValueofJpjandJrj(xi,phis,Vf,Jpj,Jrj,Jrec,Jns,Jg) ;
  dJtn := jtn - oldjtn ;
  dJtp := Jtp - oldjtp ;
  dJtot := dJtn+dJtp ;
  IF (abs(djtot)>1E-40) THEN diffres := (newv - oldv)/djtot
    ELSE diffres := 0 ;
End; (*DifferentialRes*)

Procedure IntElecField(Jtn, Jtp : real ; VAR Eint : real) ;
(* Calculates a value for the internal electric field due to
  the diffusive carrier densities.(McKelvey p.330 *)
```

```
VAR sig, b : real ;

Begin
     sig := q*(mun*Nd) ;
     b := mun/mup ;
     Eint := (Jtn+Jtp)/sig - ((b-1)/(Nd*b))*Jtp/(q*Dp*beta) ;
End; (* IntElecField*)

Procedure HoleDensity(xi,phis : real ; VAR Ps : real) ;
(* Determines the hole density at the MIS interface using ni*exp(Ei-Efp)/kT *)

Begin
   IF (abs(beta*(abs(phis)-phifn-xi))>174) THEN Ps := 0 ELSE
     Ps := ni*exp(beta*(abs(phis)-phifn-xi)) ;
End ; (* Holedensity *)

Procedure Avalanche(phis : real ; VAR Mn, Mp : real) ;
(* Calculates the value of the multiplication for holes in a highly doped
piece of silicon using my desperatly clever derived expression *)

VAR W, x, y, Emax : real ;
     i : integer ;

Begin
   x := 0 ; y := 0 ;
   W := sqrt(2*epss*abs(phis)/(q*Nd)) ;
   Emax := q*Nd*W/epss ;
   AVAMUL(W,Nd,x,y) ;
   Mp := 1/(1-y) ; Mn := 1/(1-x) ;
End;(* Avalanche*)

Begin (* MAIN pnmiss *)
(* Initialise variables. When looking at the change in device operation for
changing Vf, put the change in incVf as well as within the main 'newmiss'
program segment *)
   (*incvfhere*)

Wepi := 5E-4 ; incVf := -1E-3 ; Totalj := 0 ; totalV := 0 ;
   NewJtnandJtpvalue(xi,phis,dox,Qss,Uox,Jtn,Jtp,Jsm) ;
   ValueofJpjandJrj(xi,phis,Vf,Jpj,Jrj,Jrec,Jns,Jg) ;
   totalv := abs(Uox)+(phis)+chiSi+Eg/2+Vf-phiAl-phifn ;
   totalj := Jtn + Jtp ;
   Avalanche(phis, Mn, Mp) ;
   Mn := 1 ; Mp := 1 ;
   elec := (Mn*Jtn + (Mp-1)*Jpj + Jg - Jrj - Jrec - Jns);
   Hole := (Jtp - Jg - Mp*Jpj - (Mn-1)*Jtn);
   IF (wrout>0) THEN

Begin
     HoleDensity(xi,phis,Ps) ;
     totalv := abs(Uox)+(phis)+chiSi+Eg/2+Vf-phiAl-phifn ;
     totalj := Jtn + Jtp + Jsm ;
     totpn := Jpj + Jrj + Jrec + Jns ;
     PoissonUox(xi,phis,dox,Qss,Uox) ;
     pndepwidth(Vf,Wpn) ;
     misdepwidth(phis,xi,Wmis) ;
     Currentchange(xi,phis,vf,dox,incvf,oldxi,oldphi,gainmis,gainpn,gain) ;
     DifferentialRes(xi,phis,vf,dox,incvf,oldxi,oldphi,diffres) ;
     Capacitance(xi,phis,dox,Vf,incvf,oldxi,oldphi,capac) ;
     Jtnandjtpvalue(xi,phis,dox,Qss,Uox,Jtn,Jtp,Jsm) ;
     NewJtnandJtpvalue(xi,phis,dox,Qss,Uox,newJtn,newjtp,Jsm) ;
     writeln(output,totalv:10,' ',totalj:10,' ',vf:10,' ',capac:10,' ',
     diffres:10,' ',temp:10,' ',GAINpn:10,' ',GAIN:10,
     ' ',abs(Uox):10,' ',Jtn:10,' ',newjtn:10,' ',Jtp:10,' ',newjtp:10,
     ' ',Jg:10,' ',Jpj:10,' ',jrj:10,' ',
```

```
    jrec:10,' ',jns:10,' ',phis:10,' ',xi:10) ;
  END ;
END ;

(* MAIN PROGRAM *)

Begin
  rewrite(OUTPUT,'UNIT=6,NOCC') ;
  rewrite(msink,'FILE=*MSINK*') ;
  rewrite(readout,'FILE=readout,NOCC') ;
  TEMP := 300 ; dox := 5.0E-7 ; Vf := 3.000E-1 ;
  oldv := -100 ; NewV := -100 ; dv := 0.000 ;
  phis := 3.142E-1 ; xi := 6.333E-2 ;
  oldphi := phis ; oldxi := xi ;
  REPEAT
    TWOEQU(Vf,TEMP,dox,oldxi,oldphi,xi,phis,totalj,totalv) ;
    wrout := 10 ;
    pnmiss(vf,temp,dox,oldxi,oldphi,xi,phis,elec,hole,wrout,totalj,totalv) ;
    vf := vf - 1E-3 ;
    Oldv := NewV ; NewV := totalV ;
    Oldphi := phis ; oldxi := xi ;
    IF (Oldv>-99) THEN dV := (NewV-OldV) ;
  UNTIL (vf<1E-4)
End.
```

```
      SUBROUTINE TWOEQU(VF,TEMP,DOX,OLDXI,OLDPHI,XI,PHIS,TOTALJ,TOTALV)
C
C THIS SUBROUTINE TAKES THE VARIABLES XI AND PHIS, SUBSTITUTES THEM
C INTO A SYSTEM OF TWO NONLINEAR SIMULTANEOUS EQUATIONS AND RETURNS
C THE VALUES OF XI AND PHIS WHERE THESE EQUATIONS ARE BOTH EQUAL TO
ZERO.
      EXTERNAL FCN
      INTEGER N,LWA,IFAIL
      REAL*8 X(2),FVEC(2),XTOL,WA(40),VF,TEMP,DOX,XI,PHIS,VF1,
     $ TEMP1,DOX1,XIOLD,PHIOLD,TOTALJ,TOTALV,TOTJ,TOTV,OLDXI,OLDPHI
      COMMON /BLK1/VF1,TEMP1,DOX1,XIOLD,PHIOLD,TOTJ,TOTV
      VF1=VF
      TEMP1=TEMP
      DOX1=DOX
      XIOLD=OLDXI
      PHIOLD=OLDPHI
      N=2
      IFAIL=0
      X(1)=XI
      X(2)=PHIS
      TOTJ=TOTALJ
      TOTV=TOTALV
      LWA=40
      XTOL=1E-5
      CALL C05NBF(FCN,N,X,FVEC,XTOL,WA,LWA,IFAIL)
      XI=X(1)
      PHIS=X(2)
      TOTALJ=TOTJ
      TOTALV=TOTV
      RETURN
      END
      SUBROUTINE FCN(N,X,FVEC,IFLAG)
      REAL*8 X(2),FVEC(2),VF1,TEMP1,DOX1,XIOLD,PHIOLD,TOTJ,TOTV
      INTEGER N,IFLAG
      COMMON /BLK1/VF1,TEMP1,DOX1,XIOLD,PHIOLD,TOTJ,TOTV
      CALL PNMISS(VF1,TEMP1,DOX1,XIOLD,PHIOLD,X(1),X(2),
     $ FVEC(1),FVEC(2),-5.0,TOTJ,TOTV)
      RETURN
      END

      SUBROUTINE AVAMUL(W,ND,MN,MP)
C
C THIS ROUTINE CALCULATES THE VALUES FOR THE AVALANCHE MULTIPLICATION
C COEFFICIENTS USING EXPRESSIONS FROM HABIB, BULUCEA, AND OVERSTRAETEN
      EXTERNAL AMNINT
      EXTERNAL AMPINT
      INTEGER NPTS, NLIMIT, IFAILA, IFAILB
      REAL*8 S13AAF, ALPHN,ALPHPA,ALPHPB, BN, BPA, BPB, GAMMA, EMAX,
     $ EPSS, Q, DELTA, MN, MP, ND, A,B,C,D, EPSR, RELERR, ANSA, ANSB, W1
      COMMON /AVBLK1/BN,BPA,BPB,ALPHN,ALPHPA,ALPHPB,DELTA,EMAX,W1
      EPSS=1.0536447E-12
      Q=1.60218E-19
      EMAX=Q*ND*W/EPSS
      W1=W
      BN=1.231E6
      BPA=2.036E6
      BPB=1.693E6
```

```
      ALPHN=7.03E5
      ALPHPA=1.582E6
      ALPHPB=6.71E5
      DELTA=Q*ND/EPSS
      A=0.0
      B=W
      C=0.0
      D=W
      NLIMIT=0
      EPSR=1.0E-6
      IFAILA=0
      IFAILB=0

      ANSA=D01AHF(A,B,EPSR,NPTS,RELERR,AMPINT,NLIMIT,IFAILA)

      NLIMIT=0
      EPSR=1.0E-6

      ANSB=D01AHF(C,D,EPSR,NPTS,RELERR,AMNINT,NLIMIT,IFAILB)

      MP=ANSA
      MN=ANSB
      RETURN
      END

      DOUBLE PRECISION FUNCTION AMPINT(X)
      INTEGER IFAIL
      REAL*8 S13AAF,GAMMA,BN,BPA,BPB,ALPHN,ALPHPA,ALPHPB,DELTA,Y,X,
     $ ALPHP,BP,EMAX,EXPINT,Z,X1,X2,W1

      COMMON /AVBLK1/BN,BPA,BPB,ALPHN,ALPHPA,ALPHPB,DELTA,EMAX,W1
      IFAIL=0
      IF(EMAX.LE.4.0E5)ALPHP=ALPHPA
      IF(EMAX.GE.4.0E5)ALPHP=ALPHPB
      IF(EMAX.LE.4.0E5)BP=BPA
      IF(EMAX.GE.4.0E5)BP=BPB
      Y=BP/(DELTA*X)
      GAMMA=(ALPHP/ALPHN)*DEXP(-BP/EMAX)/(DEXP(-BN/EMAX))
      Z=S13AAF(Y,IFAIL)
      EXPINT=Z-DEXP((-Y))/Y
      EXPINT=(BP/DELTA)*(1-GAMMA)*ALPHP*EXPINT
      AMPINT=ALPHP*DEXP((-Y))*DEXP(EXPINT)
      RETURN
      END
      END

      DOUBLE PRECISION FUNCTION AMNINT(X)
      INTEGER IFAIL
      REAL*8 S13AAF,GAMMA,BN,BPA,BPB,ALPHN,ALPHPA,ALPHPB,DELTA,Y,X,
     $ ALPHP,BP,EMAX,EXPINT,Z,X1,X2,UPLIM,LOWLIM,W1

      COMMON /AVBLK1/BN,BPA,BPB,ALPHN,ALPHPA,ALPHPB,DELTA,EMAX,W1
      IFAIL=0
      IF(EMAX.LE.4.0E5)ALPHP=ALPHPA
      IF(EMAX.GE.4.0E5)ALPHP=ALPHPB
      IF(EMAX.LE.4.0E5)BP=BPA
      IF(EMAX.GE.4.0E5)BP=BPB
      GAMMA=(ALPHP/ALPHN)*DEXP(-BP/EMAX)/(DEXP(-BN/EMAX))
      LOWLIM=BN/(DELTA*W1)
      IF((DELTA*(W1-X)/BN).LT.1E-70)UPLIM=1E71
      IF((DELTA*(W1-X)/BN).GE.1E-70)UPLIM=BN/(DELTA*(W1-X))
      Z=S13AAF(LOWLIM,IFAIL)
      EXPINT=(EXP((-LOWLIM))/LOWLIM)-Z
      IF(UPLIM.LT.1E70)Z=S13AAF(UPLIM,IFAIL)
      IF(UPLIM.LT.1E70)EXPINT=EXPINT+Z-(DEXP(-UPLIM)/UPLIM)
      EXPINT=-(BN/DELTA)*(1-GAMMA)*ALPHN*EXPINT
```